UNIVERSITY *of the*
WESTERN CAPE

POROSITY AND PERMEABILITY DISTRIBUTION IN THE DEEP MARINE PLAY OF THE CENTRAL BREDASDORP BASIN, BLOCK 9, OFFSHORE SOUTH AFRICA.

By

OJONGOKPOKO HANSON MBI.

A thesis submitted in fulfilment of the requirements for the degree of Magister Scientae (M.Sc) in Petroleum Geosciences in the Department of Earth Sciences, University of the Western Cape, Bellville, South Africa.

Supervisor: **Professor Paul F. Carey**

November 2006

ABSTRACT

This study describes porosity and permeability distribution in the deep marine play of the central Bredasdorp Basin, Block 9, offshore South Africa using methods that include thin section petrography, X-ray diffraction, and scanning electron microscopy, in order to characterize their porosity and permeability distributions, cementation and clay types that affect the porosity and permeability distribution.

The study includes core samples from nine wells taken from selected depths within the Basin. Seventy three thin sections were described using parameters such as grain size measurement, quantification of porosity and permeability, mineralogy, sorting, grain shape, matrix, cementation, and clay content. Core samples were analyzed using x-ray diffraction for qualitative clay mineralogy and phase analysis. Scanning electron microscope analysis for qualitative assessment of clays and cements. X-ray diffraction (XRD) and scanning electron microscope (SEM) analyses were conducted on fifty-four (54) and thirty-five (35) samples respectively to identify and quantify the clay mineralogy of the sandstones. The SEM micrographs are also useful for estimating the type and distribution of porosity and cements. Analyses of these methods is used in describing the reservoir quality.

Detrital matrix varies in abundance from one well to another. The matrix consists predominantly of clay minerals with lesser amounts of detrital cements. X-ray diffraction analyses suggest these clays largely consist of illite and kaolinite, with minor amounts of chlorite and laumontite. Because these clays are highly illitic, the matrix could exhibit significant swelling if exposed to fresh sea water, thus further reducing the reservoir quality.

The majority of the samples generally have significant cements; in particular quartz cement occurs abundantly in most samples. The high silica cement is possibly caused by the high number of nucleation sites owing to the relatively high abundance of detrital quartz. Carbonate cement, particularly siderite and calcite, occurs in variable amounts in most samples but generally has little effect on reservoir quality in the majority of samples. Authigenic, pore-filling kaolinite occurs in several samples and is probably related to feldspar/glauconite alteration, it degrades reservoir quality. The presence of chlorite locally (plate 4.66A & B) and in minute quantities is attributed to a late stage replacement of lithic grains. Don't put references to plates and figures in abstract.

A high argillaceous content is directly responsible for the low permeability obtained in the core analysis. Pervasive calcite and silica cementation are the main cause of porosity and permeability destruction. Dissolution of pore filling intergranular clays may result in the formation of microporosity and interconnected secondary porosity.

Based on the combination of information derived from thin section petrography, SEM and XRD, diagenetic stages and event sequences are established for the sandstone in the studied area. Reservoir quality deteriorates with depth, as cementation, grain coating and pore infilling authigenic chlorite, illite and kaolinite becomes more abundant.

KEY WORDS

Porosity,

Permeability,

Clays,

Cement,

Reservoir heterogeneity,

Sedimentary rocks,

Deep marine play,

Diagenesis,

Bredasdorp basin,

Block 9.

DECLARATION

I HANSON MBI OJONGOKPOKO declare that **Porosity and Permeability Distribution in the Deep Marine Play of the Central Bredasdorp Basin, Block 9, Offshore South Africa**, is my own work, and has not been submitted before for any degree or examination in any other University, and that all the sources I have used or quoted have been indicated and acknowledged by means of complete references.

Hanson Mbi Ojongokpoko

November 2006

ACKNOWLEDGEMENT

I would like to thank Ms. Johanda Du Toit, and all the staff of the Petroleum Agency of South Africa, for access to all of the pertinent data for this project without which, the science and presentation of this study would not have been a success.

My immense thankfulness to my supervisor, Professor Paul F. Carey, for carefully reading, criticizing and correcting all drafts, and making useful suggestions which are integrated into this study to improve its standard. He provided encouragement, enthusiasm, and was my guide when I entered uncharted territory during this study.

I am highly grateful to Dr. Remy Bucher of iThemba labs for his kind and tireless assistance with respect to X-Ray Diffraction measurements, analysis techniques and software which proved very helpful. His friendly response and timely training program, workshop and lectures added speed to the execution of this thesis.

My deepest appreciation goes to Esme Spicer, of the University of Stellenbosch, Department of Geological Sciences, for her assistance during the sample preparation processes, and also to Dr. Gerald Malgas, of the Physics department, University of the Western Cape, for his assistance on the Scanning Electron Microscope.

I would also like to thank my fellow graduate students who made all of this bearable and enjoyable moment. Special thanks to Unathi Mshumi, Anthony Duah provided editorial support, James Ayuk Ayuk, and everyone else on the ground floor of the Earth Science department (L60). Your support, discussions, advice, and friendship kept me sane. Revise this paragraph, mistakes here.

Finally, I want to express thanks to Mom, Ojongokpoko Mbi Junior, Ayamba Juliet Enoakpa (fiancé), you have always encouraged me with love, patience, and understanding and I owe much of my success to you. Thank you and the rest of my family for all of their support throughout this endeavour.

CONTENTS

List of Figures

List of Tables

LIST OF PLATES

APPENDIX

BASIC TERMINOLOGY

I PETROLEUM RESERVOIR

A subsurface volume of rock "Formation" (a body of sedimentary strata characterized by some degree of internal lithologic homogeneity and distinguishing characteristics in terms of physical properties and chemical composition) that has sufficient porosity and permeability and is located within a favourable geological framework (trap and seal) to permit the accumulation of hydrocarbons in commercial quantityies.

Once a possible hydrocarbon reservoir has been identified, the key physical characteristics of a reservoir that are of interest to a hydrocarbon explorationist are its porosity and permeability. Reservoir assessment encompasses various techniques of determining and analysing properties exhibited by a petroleum reservoir, usually referred to as reservoir characterization (Selley, 1985).

II POROSITY (Ɵ)

This is the fraction of a rock that is occupied by voids (pores) or fraction of the total volume of a rock that is not occupied by framework grains and matrix. It can be expressed as a fraction or percentage of pore volume in a volume of rock. Porosity in sedimentary rocks can be primary or secondary. Primary (original) porosity refers to the porosity remaining after the sediments have been compacted but without considering changes resulting from subsequent chemical action or flow of water through the sediments. Affected by factors such as, particle shericity and angularity, Packing and sorting. Secondary (induced) porosity on the other hand

is the additional porosity resulting from fractures, vugs, solution channels, diagenesis, and dolomitization. The three common types of secondary porosity are: fracture porosity, shrinkage porosity and dissolution porosity (Selley, 1985).

III PERMEABILITY (K)

This is a measure of the ability of a rock to transmit a fluid through its connected pores; it is therefore influenced by pore throat radii. It is measured in Darcies, usually in millidarcies (mD).

The magnitude of permeability can be affected by factors such as; the shape and size of the pore system, lithology, sorting, cementation, fracturing and solution.

The major controls on permeability include: the higher the porosity, the higher the permeability, except for clay; the smaller the grains, the smaller the pores and the pore throats, the lower the permeability; the smaller the grain size, the larger the exposed surface area to the flowing fluid, which leads to larger friction between the fluid and the rock, and hence lower permeability; and permeability is highly variable but a cut-off of 1mD is generally applied for reservoir rocks (Selley, 1985).

IV CORE SAMPLES

Cylindrical sections of rock, taken as samples from a formation, penetrated by a hollow core bit and brought to the surface for analysis purposes. Core samples provide a full sample of rocks penetrated. It is used both for qualitative and quantitative analysis, which is a laboratory analysis of recovered reservoir formation samples for the purpose of measuring porosity,

permeability, grain size, and other properties of the rock and contained fluids. It is also used to calibrate wireline logs, (Schlumberger 2005)

V WELL LOGS

A record of the measured or computed physical characteristics of the rock section encountered in a well formation, plotted as a continuous function of depth. Well logs are a group of the most useful and important tools available to petroleum geologists. They are used to identify and correlate underground rocks, determine their mineralogy, generate their physical properties and the nature of the fluids they contain (Serra, 1984).

For the purpose of this study, only gamma ray and resistivity logs are/will be used for correlation of adjacent wells. are mentioned.

VI GAMMA RAY LOG (GR)

The gamma ray log is a record of a formation, designed to measure the natural radioactivity. The radiation emanates from naturally occurring elements such as Uranium, Thorium and Potassium. In sediments the log mainly reflects clay content because clay contains the radioisotopes of potassium, uranium, and thorium. Amongst the sediments, shales have by far the strongest radiation (Rider, 2000). Shale-free sandstones and carbonates have low concentrations of radioactive materials and give low gamma ray readings. High gamma ray may often not imply shaliness, but a reflection of radioactive sands such as potassium rich feldspathic, glauconitic, or micaceous sandstones. Quantitatively, the gamma ray log is important for identifying lithologies, calculating the shaliness of a formation, and correlating between adjacent boreholes.

VII RESISTIVITY LOG

The essential target of resistivity logging is the true resistivity of the formation and its saturation in hydrocarbons. The resistivity log is used to give the volume of oil in a particular reservoir, or to define the water saturation (Rider, 2000). Examples of resistivity tools include: Normal Devices, Lateral Logs, Laterolog, Microlaterolog, Microlog, Proximity Log, and Spherically Focused Logs.

1. CHAPTER ONE

1.1 INTRODUCTION

It is anticipated that deep marine plays are likely to hold hydrocarbon resources which are presently in high demand. To ensure effective hydrocarbon recovery, detailed characterization of the sand-rich intervals in the Bredasdorp Basin deep-marine play with respect to controls on their porosity and permeability distribution is required. Knowledge of porosity and permeability heterogeneity is essential to exploration geologists, production geologists and reservoir engineers for accurate evaluation of economic resources. A higher porosity and permeability coupled with other favourable conditions (trap and seal) for hydrocarbon accumulation within a reservoir zone implies greater probability of producing a commercially viable resource.

Sandstone reservoirs are commonly heterogeneous; consequently, they may require special methods and techniques for description and evaluation. Reservoir characterization is the study of the reservoir rocks, their petrophysical properties, the fluids they contain – or the manner in which they influence the movement of fluids in the subsurface. This study focuses on the description of core samples and the pore network of reservoir intervals located in Bredasdorp central basin wells, South Africa (Figure 1.0 and Table 1.0). Porosity and permeability relationships, wireline log signals, and thin sections have been examined to determine how the porosity and permeability influence reservoir quality.

The reservoir sandstone is composed mainly of fine- to coarse-grained sandstones with thin intercalations of siltstones, claystones and shales.

In carrying out this research the samples are used to characterize reservoir zones through petrophysical analyses, thin section petrography, scanning electron microscope (SEM) and X-Ray diffraction (XRD). Detailed thin section petrographic analyses are performed on seventy-three (73) samples to determine the texture (size, packing and sorting). X-ray diffraction (XRD) and scanning electron microscope (SEM) analyses are conducted on fifty-four (54) and thirty-five (35) samples respectively to identify and quantify the clay mineralogy of the sandstones. The SEM micrographs are also useful for estimating the type and distribution of porosity and cements.

1.2 AIM AND OBJECTIVES

1.2.1 AIM

The aim of this study is to assess the characteristics of previously defined reservoir zones and lithologies associated with favourable porosities and permeabilities by integrating basic core analysis, wireline logs, thin section petrography, scanning electron microscopy (SEM) and X-Ray Diffraction (XRD) analyses to characterise their porosity and permeability distributions, cementation and clay types that affect the porosity and permeability distribution.

1.2.2 OBJECTIVES

The primary objectives are as follows:

i. Characterisation of different sand units within reservoir zones.
ii. Assessment of the impact of clay and cement composition on porosity and permeability distribution.
iii. Development of a comprehensive understanding of porosity and permeability relationships within the study area.
iv. Complete well log correlation of all wells within the studied area, leading to the identification of clean sands regions with favourable porosity and permeability.
v. X-Ray Diffraction for phase identification and to confirm clay mineralogy.
vi. Analysis of pore systems in cores through the use of thin section petrography
vii. Establishing the nature and the distribution of microporosity in clays present within the reservoir zones using scanning electron microscope (SEM).

1.3 E & P HISTORY ON BREDASDORP BASIN (BLOCK 9)

The Bredasdorp Basin has been the focus of seismic and drilling activity since 1980. Exploration drilling was active from 1981 to 1991 and about 181 exploration wells have been drilled in this area. Exploration has led to the discovery of several oil and gas fields, and the commercial production of oil and gas. Presently exploration in South Africa is managed by the Petroleum Agencyof South Africa (PASA), responsible for soliciting bids for offshore acreage of the southern and western coasts of South Africa (PASA brochure 2004/5)

Extensive exploration for more than thirty years has revealed no onshore hydrocarbons. Block 9 is located offshore South Africa within the Bredasdorp Basin. SOEKOR (Southern Oil Exploration Corporation), the State owned Oil and gas Exploration Company, (now PetroSA, Petroleum South Africa) discovered gas and oil deposits offshore in Block 9 in the Bredasdorp Basin. In Block 9, a total of 165 wells have been drilled, thirty-two of these wells are classified as oil and/or gas discoveries, even are oil. The discoveries are relatively small and the economic viability is still being assessed. In the Bredasdorp basin, the F-A gas and condensate fields, discovered in 1980 by Soekor are being exploited by Mossgas. Production from these fields started in 1992 and an average of 194 million cubic feet of gas and 9,500 barrels of condensate are being produced per a day. A pipeline of 91km conveys gas and condensate to the Mossgas Synfuels plant at Mossel Bay, where petrol, diesel and kerosene are produced. The EM and Satellite gas fields situated 120km south west of the Mossel Bay, in the Bredasdorp basin (Block9) were discovered in 1984 in early Cretaceous sands (PASA brochure 2004/5).

1.4 STUDY AREA

The Bredasdorp Basin is situated off the south coast of South Africa, southeast of Cape Town and west-southwest of Port Elizabeth. The Bredasdorp Basin is the most south-westerly of the Southern African offshore basins. The Basin is formed as a result of extensional episodes during the initial stages of rifting during in Jurassic period. The Bredasdorp Basin is delimited in the north by the Infanta Arch and to the south by the Agulhas Arch (Figure1.0). These arches are basement highs comprising Cape Supergroup sediments, granite and Precambrian metamorphic rock.

The research is focussed on reservoir zones encountered by the nine central basin wells. The wells are located within the Bredasdorp Basin and include: E-BA1, E-CA1, E-AA1, E-AD1, E-AR1, E-BB1, E-BB2, E-AO1, and E-AO2, from 9A-13A deep marine channel play located within the Bredasdorp Basin. Well locations are shown below, (Table 1.0) and (Figure1.0).

Table 1.0: Names and locations of wells

Well Name	Location,	Depth (m)
E-BA1	125km SSW of Mossel Bay Seismic Ref., line E56-069 (shot point 610) Lat., 35^0 09' 29. 67" S Long., 21^0 28' 31. 19" E	3130.5
E-AR1	120km SSW of Mossel Bay Seismic Ref., line E87-074, (shot point 353) Lat., 35^0 12' 13. 67" S Long., 21^0 32' 41. 86" E	3458
E-CA1	120km SW of Mossel Bay Seismic Ref., line 893D, Track 540 CDP 720 Lat., 35^0 09' 20. 09" S Long., 21^0 33' 34. 96" E	3288
E-AA1	120km SSW of Mossel Bay Seismic Ref., line E80-17 (shot point 1620) Lat., 35^0 11' 8.8" S Long., 21^0 35' 36. 18" E	3925
E-AD1	120km SW of Mossel Bay Seismic Ref., line E80-019, (shot point 970) Lat., 35^0 11' 50. 08" S Long., 21^0 38' 58. 25" E	3862
E-BB1	100km South of Stillbaai Seismic Ref., At intersection of Inline 570 and Crossline 1941 of 3D seismic grid Lat., 35^0 14' 51. 32" S Long., 21^0 41' 41. 08" E	3321
E-BB2	120km South of Stillbaai Seismic Ref., line E93-027 Lat., 35^0 23'83"31 S Long., 21^0 68'02"17 E	3100
E-AO1	124km SSW of Mossel Bay Seismic Ref., line E87-214 (shot point 894) Lat., 35^0 14' 15. 66" S Long., 21^0 45' 41. 89" E	3351
E-AO2	125km SSW of Mossel Bay Seismic Ref., line E89-061 (shot point 550) Lat., 35^0 15' 12. 77" S Long., 21^0 46' 27. 53" E	3183

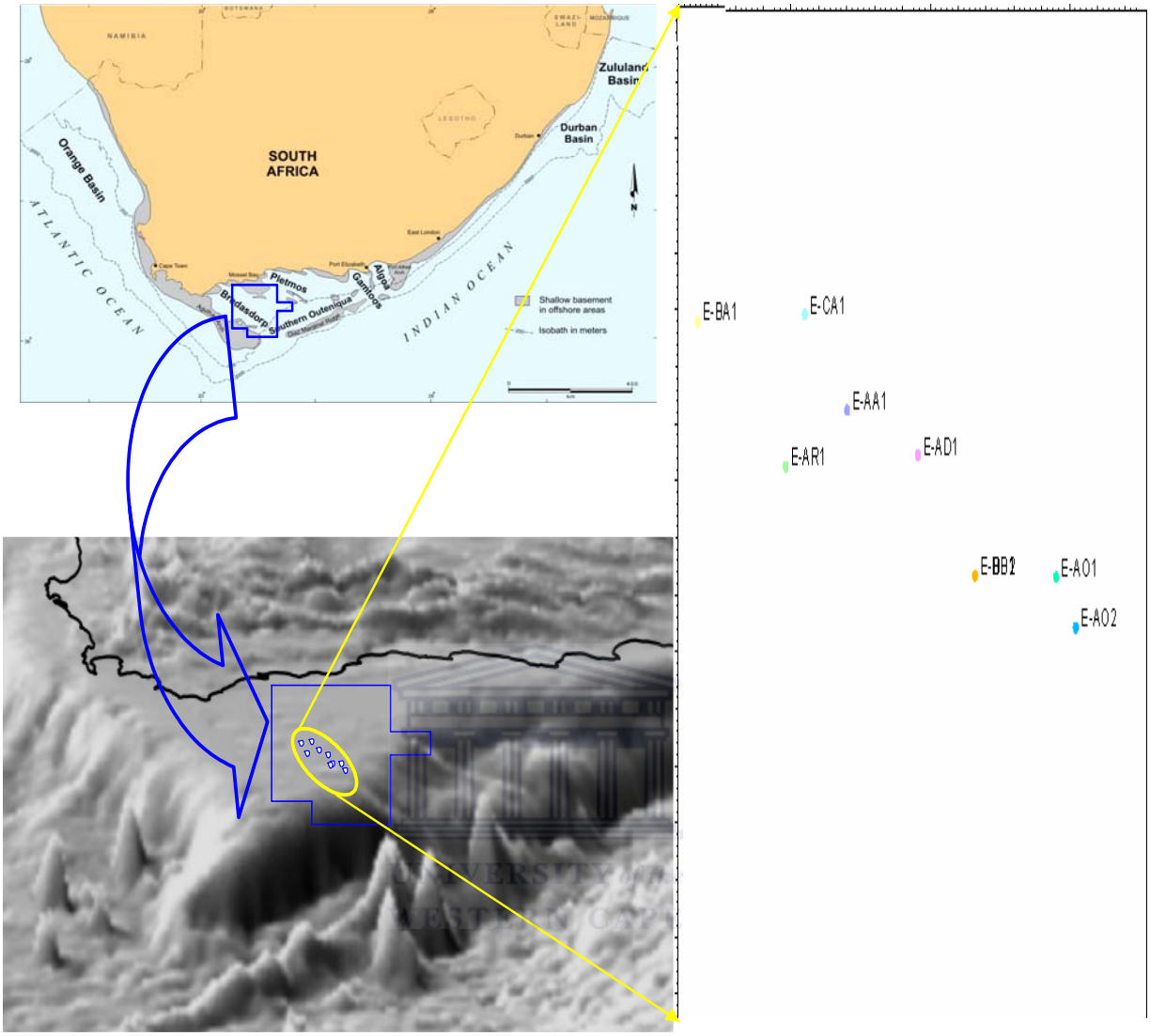

Figure1.0: Location Map of the Bredasdorp Basin and well positions

Offshore South Africa.

(Modified from; Petroleum Agency S A, Brochure, 2003/4)

1.5 GEOLOGICAL BACKGROUND OF THE BREDASDORP BASIN

The rapidly growing South African upstream petroleum sector is playing an important role in the evolution of the South African oil industry. The Bredasdorp Basin which is the subject of this study has a number of economic to marginal economic discoveries of oil, gas and condensate (e.g Oribi and Oryx fields). Estimated ultimate recoverable reserves of the Oribi and Oryx fields are 23 and 7 million barrels (MMbbl) respectively, and Sable field 25 MMbbl (Petroleum Agency S A, Brochure, 2003/4).

Wells drilled offshore had gas shows and tested good gas flow rates and provided good evidence for a gas province. South Africa's prospects for natural gas production increased recently, with the discovery of offshore reserves. Exploration is being carried out in the Bredasdorp Basin, with the aim of assessing the extent of these available reserves, and determining their economic potential.

South Africa's offshore basins can be divided into three distinct tectonostratigraphic zones:

The Western offshore comprises a broad passive margin basin related to the opening of the South Atlantic in the Early Cretaceous, known as the Orange Basin which is the largest offshore basin (Petroleum Agency S A, Brochure, 2004/5).

Figure1.1: The Western offshore of South Africa

(Modified from; Petroleum Agency SA, Brochure, 2004/5).

The Eastern offshore is a narrow passive margin that was formed as a result of the break-up of Africa, Madagascar and Antarctica in the Jurassic. Very limited deposition has occurred here. Two offshore basins are known, the Durban and Zululand basins. (Petroleum Agency S A, Brochure, 2004/5).

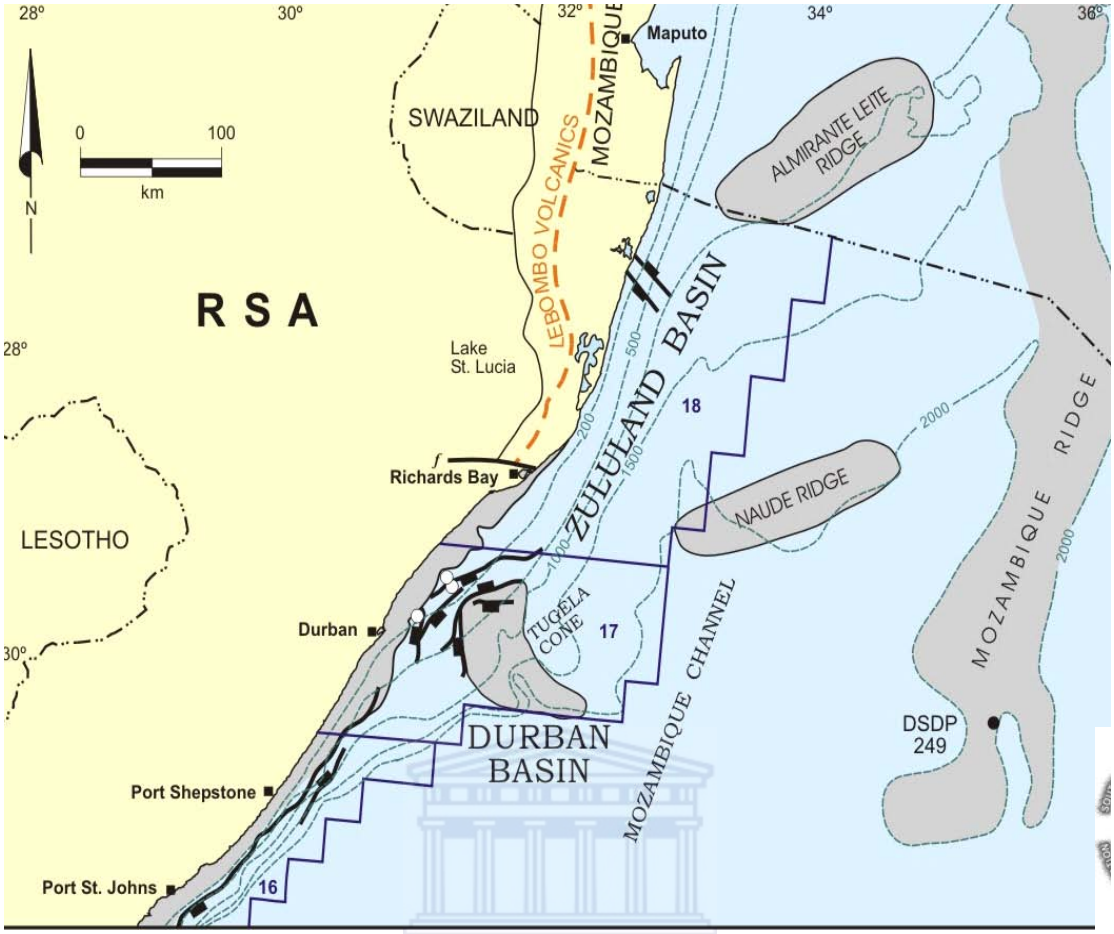

Figure 1.2: The Eastern offshore of South Africa

(Modified from; Petroleum Agency SA, Brochure, 2004/5).

The Southern offshore region is a large composite intracratonic rift basin, known as the Outeniqua Basin, shows a history of strong strike-slip movement during the Late Jurassic-Early Cretaceous break-up and separation of Gondwana.

The Outeniqua Basin comprises of rift sub-basin, from east to west, the Algoa, Gamtoos, Pletmos, Infanta and the Bredasdorp basins. Each of these basins comprises a rift half-graben overlain by variable thicknesses of drift sediments and the deepwater extensions of these basins merge into the Southern Outeniqua Basin.

1.6 REGIONAL GEOLOGY OF THE BREDASDORP BASIN

The Bredasdorp Basin is dominated to the north by the east-west branch of the Permo-Triassic Cape Fold Belt (CFB) and to the southeast by the lower-Cretaceous Agulhas Falkland Fracture Zone (AFFZ). The CFB is a northern verging fold and thrust belt whereas the AFFZ is a dextral transform fault formed during the separation of Africa and South America and it forms a boundary between continental and oceanic crusts. The basin formation is closely related to the break-up of Gondwanaland (Figure 1.3a and 1.3b) and subsequent development purely related to thermal subsidence in response to a single rifting event. The Syn-rift sedimentary sequence is composed of fluvial and shallow-marine sediments whereas the post-rift sequence is dominated by deep-marine sediments (De Wit and Ransome, 1992)

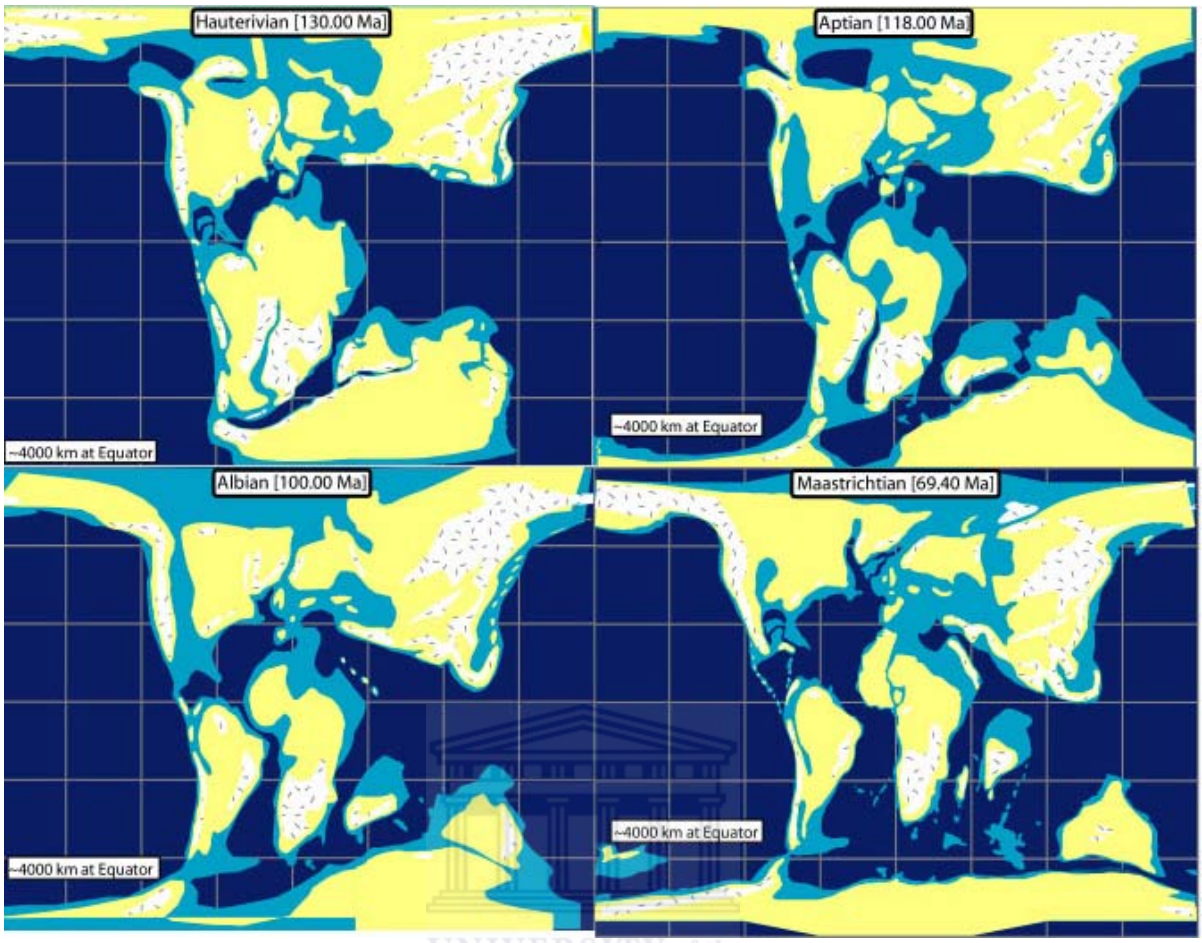

Figure1. 3a: Showing the break up of Super Continent Pangea and the development of the region around the Outeniqua Basin in the Cretaceous period

(Modified from; www.Pubs.usgs.gov/of/2003)

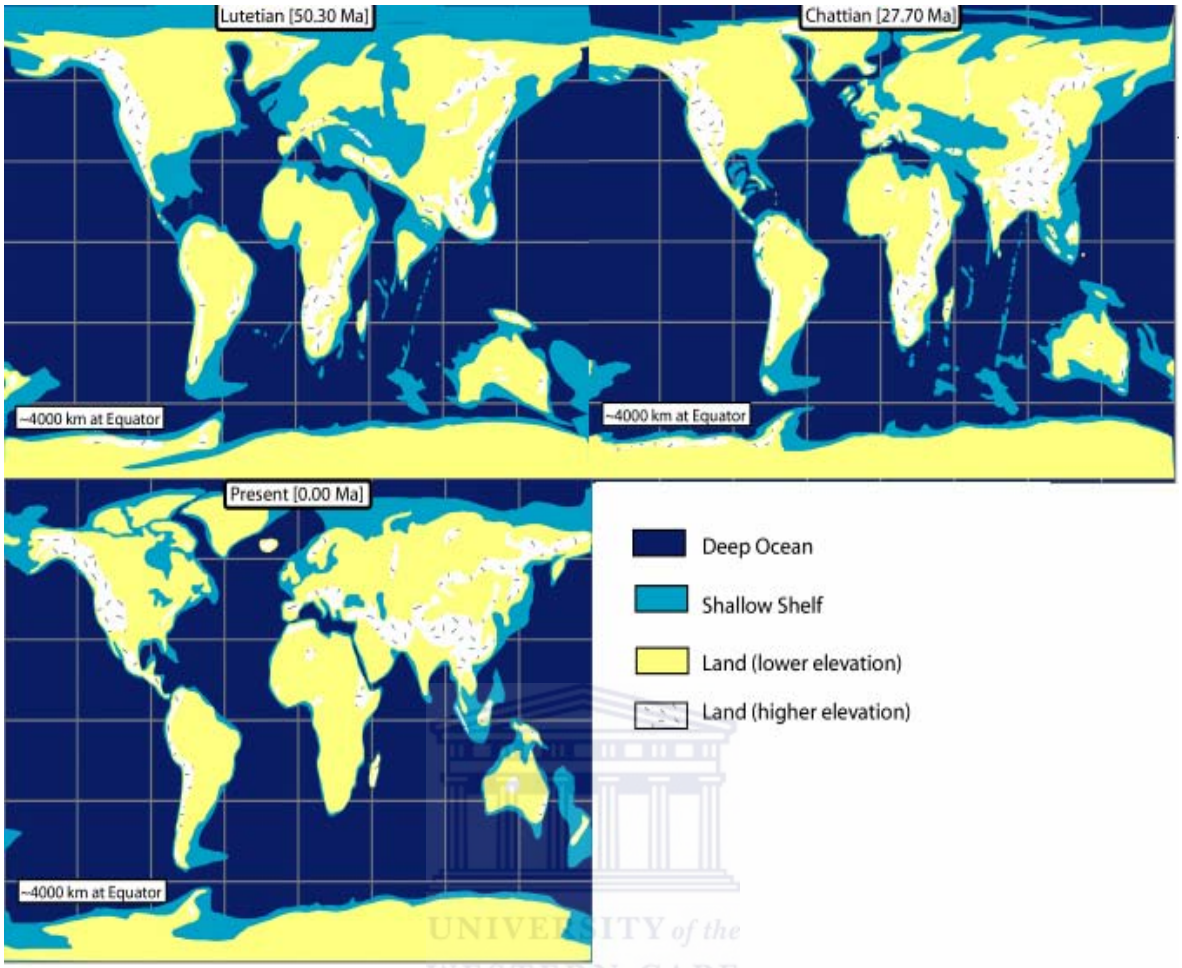

Figure1. 3b: Showing the break up of Super Continent Pangea and the development of the region around the Outeniqua Basin in the Cenozoic period

(Modified from; www.Pubs.usgs.gov/of/2003)

A regionally correlatable Late-Valanginian unconformity 1At1 separates the syn-rift and post-rift sequence (Figure 1.5). The rift-drift, drift-onset or break-up unconformity corresponds to the 1At1 unconformity. The rift phase on the south coast ended during this period, but was followed by three phases of inversion related to continued dextral shearing, which ended in the Mid-Albian (14At1). The Late-Valanginian drift-onset unconformity on the south coast was contemporaneous with the earliest oceanic crust in the south Atlantic (De Wit and Ransome, 1992)

In the Bredasdorp Basin, three distinct post-rift positive inversion events were intervening, (De Wit and Ransome, 1992), in chronological order, starting with the oldest:

Pre-1At1 inversion; the basement-syn-rift contact defines a sharp discontinuity and the syn-rift sediments are folded above (Figure 1.5). This interface is interpreted to be a fault plane along which compressional reactivation of a pre-existing normal (rift) fault took place. An indication of the timing of the end of deformation can be obtained from the onlap relationships of a second phase of syn-rift sediments against the fold structure. This was followed by a period of erosion resulting in the formation of the drift-onset unconformity, 1At1, which clearly erodes the top off the antiform in the syn-rift sequence (Figure 1.5). Another type of response of the syn-rift sequence to pre-1At1 compression shows a half-graben in which the syn-rift sequence has been folded by compressional reactivation of the half-graben forming fault. (De Wit and Ransome, 1992)

Post-1At1 inversion; this involves the deformation of the Late-Valanginian drift-onset unconformity, 1At1. The 1At1 unconformity and the over- and underlying stratas, responded to compression by either folding or low-angle reverse faulting. The initial graben forming normal faults were reactivated to produce a faulted drift-onset unconformity (1At1). Post-1At1 compression resulted in folding and tilting of the syn-rift sequence. The 1At1

unconformity is displaced in a reverse sense along a northwestward verging thrust fault and folding can be recognized in the post-rift sequence as late as Hauterivian times. (De Wit and Ransome, 1992)

Mid-Albian inversion; the final positive inversion event that can be recognized in the Bredasdorp basin occurred during Albian times, which exhibits a clear fault plane reflection in basement and reverse displacement of the 1At1 unconformity. The reverse movement on the fault also caused asymmetric folding in the post-rift sequence of at least Albian age as is the deformation of the mid-Albian 14At1 unconformity (De Wit and Ransome, 1992).

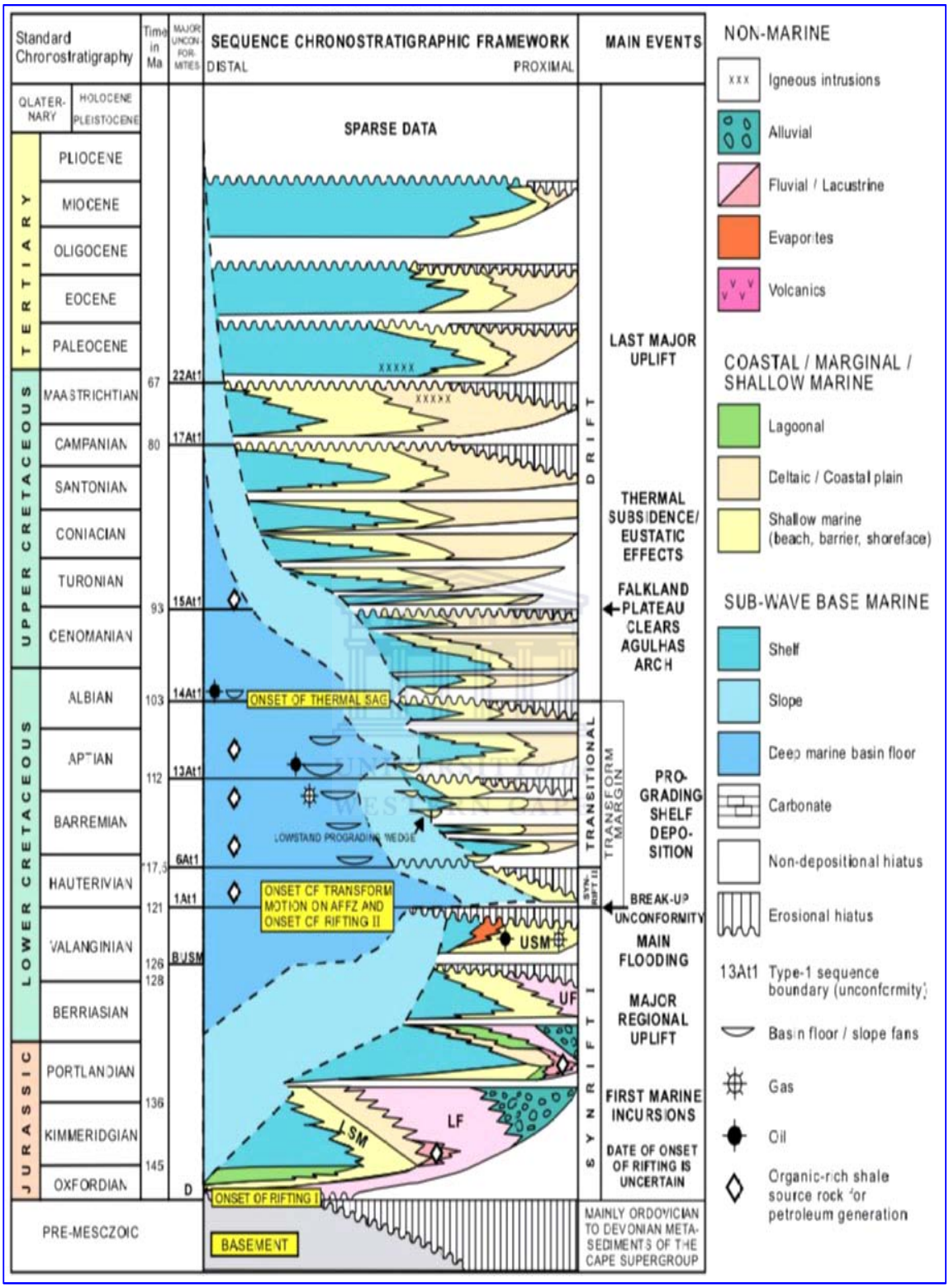

Figure 1.4: Chronostratigaphy of the Bredasdorp Sub-Basin

(Petroleum Agency SA, Brochure, 2004/5)

1.7 STRUCTURAL DEVELOPMENT OF THE BREDASDORP BASIN

The Bredasdorp basin has no onshore equivalent, although it does lie between two anticlinally dominated basement highs at Cape Infanta and Cape Agulhas.

Dingle et al, (1983) described the Bredasdorp Basin as a wide basement depression and its cross-section is asymmetric (Figure 1.5). To them the Bredasdorp Basin is best described as a graben.

The Southern boundary of the Bredasdorp Basin formed as a result of faulted and gently northward tilting flank of the Agulhas Arch can be traced as a major subsurface feature to the southeast of Cape Agulhas. The upper division of the arch is exposed of post-Paleozoic rocks, and is composed of Table Mountain Group quartzite and Bokkeveld shales over a granite core. The floor is relatively flat, except the western part, and dips generally to the North West such that the deepest parts of the basin lie close to its northern margin (Dingle et al, (1983).

In the northern part of the Bredasdorp Basin the Basement descends rapidly through several small boundary faults from the Infanta Arch. The northern edge linearity which is broken by small, deep grabens, form embayments onto the Infanta Arch, and at least three horsts which project southeast and southwards into the Basin. These horsts stand above the general level of the basin floor and are bounded by short curved faults. These horsts have been targets for oil exploration drilling.

The western portion of the Bredasdorp basin does not extend onshore, but breaks up into small, narrow, northwest-southeast horsts and graben, which extend to the coast linking Cape Agulhas and Cape Infanta (Dingle et al, (1983).

1.7.1 Rift Phase (Mid-Jurassic – Valaginian).

Extension-driven subsidence and synrift basin fill characterized rift phase. Isostatic uplift on both flanks of the half graben resulted in erosional truncation of the late-rift sediments. Extreme marginal uplift and erosion of the northern flank removed the entire synrift sequence in places (Petroleum Agency SA, Brochure, 2004/5).

1.7.2 Early Drift Phase (Hauterivian – Early Barremian).

Before onset of rapid thermal subsidence, continued uplift resulted in erosional truncation on the southern flank. Rapid subsidence and deposition of deep water sequence (source rocks) occurred within the graben (Petroleum Agency SA, Brochure, 2004/5).

1.7.3 Drift Phase (Barremian – Turonian).

Regional subsidence driven by thermal cooling and sediment loading, with continued minor movement on the Arniston Fault. In early Palaeozoic oil prone source in the half graben reached the main stage of generation.

Continued minor subsidence until early Tertiary when alkaline intrusives affected the southern flank, resulting in uplift and erosion (Turonian – Present Day) (Petroleum Agency SA, Brochure, 2004/5).

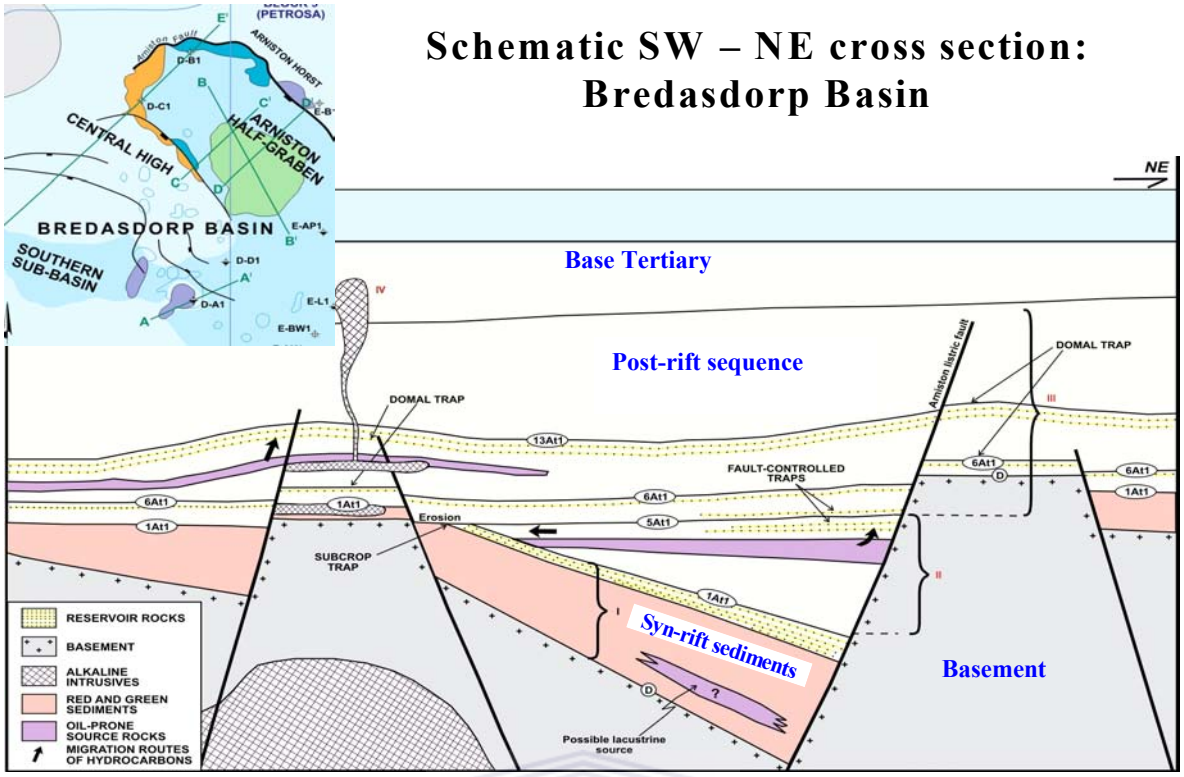

Figure 1.5: Schematic cross section of Bredasdorp Basin showing inverted graben

(Modified from; Petroleum Agency SA, Brochure, 2004/5).

1.8 STRATIGRAPHY AND SEDIMENTARY GEOLOGY

Oil and gas exploration in the offshore South African rift basins within structural synrift plays yielded limited success. In 1987, after the first oil discovery in post rift sediments in the Bredasdorp Basin, sequence-stratigraphic concepts were applied to the lower Cretaceous post rift sequences to permit correlation of depositional system tracts and related facies throughout the Basin. The interaction of rift tectonics, thermal cooling and indirect eustatic variations in global sea level produced a distinguishing series of cyclical depositional sequences. Within resolution limits of regional seismic profiles, about 10 cyclic sequences and mega sequences, deposited between the mid-Valanginian and lower Santonian can be recognized (Broad, 2000).

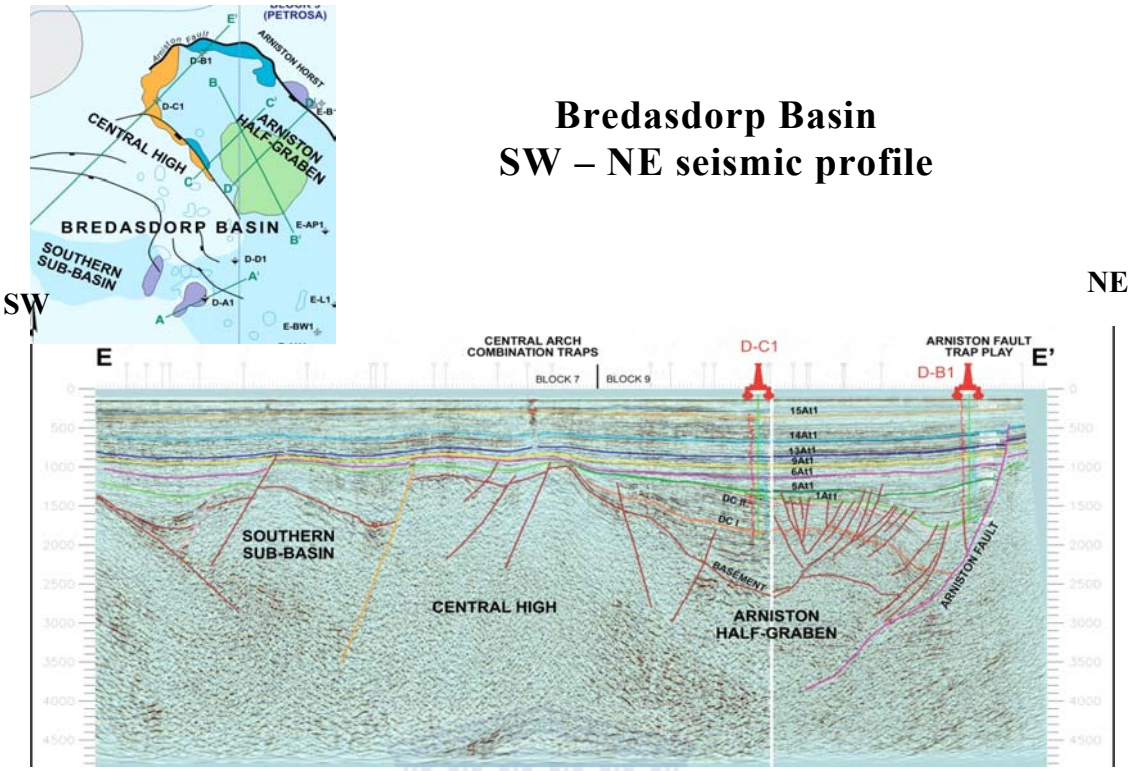

Figure 1.6: Seismic Profile showing sequence deposited between Mid-Valanginian and Lower Santonian.

(Modified from Petroleum Agency SA, Brochure, 2004/5)

The basin fill consists of cyclic sequences deposited in response to relative changes in sea level. Cyclic sequence concepts were applied to delineate hydrocarbon plays, a process that does not depend upon a global system. However, once the sequences were identified, mapped, and placed within a chronostratigraphic framework (Figure 1.4) using age dating, these cycles were compiled with Exxon's global system. Thus, although processes of global cyclicity as proposed by Exxon can be observed in the Bredasdorp Basin, local tectonics has overprinted this global effect to produce a unique sedimentation history (Broad, 2000).

Various elements of low-stand systems tracts within these sequences appear to contain potential reservoirs. High erosional (type1) unconformity, exhibiting incised valleys and canyons (Figure1.7a), provide surfaces on which:

- Mounded and sheet-like submarine/basin floor fans,
- Submarine channel fill and associated mounds and fans, and
- Prograding deltaic/coastal low stand wedges were deposited.

These fans, channel fill, and wedges are top sealed and sourced by transgressive shales and marine condensed sections, deposited at a time of regional transgression of the shoreline. In discovery wells and various reservoir-quality sandstones occurring at predicted stratigraphic levels support the application of the sequence-stratigraphic concepts to hydrocarbon exploration. A seismic-stratigraphic study of Cretaceous strata in the Bredasdorp Basin has evaluated potential stratigraphic hydrocarbon plays in a classic post-rift Basin where structural traps are rare (Broad, 2000).

In a terrigenous clastic Basin such as the Bredasdorp, low stand system tracts are interpreted as being composed of basin floor turbidite fans, channels and/or sheets. These features formed contemporaneously with the erosion of incised valleys and submarine canyons, followed by channelized slope fans and deltaic / coastal low stand wedges that prograded during a relative sea level rise (Figure1.7b). Subsequent flooding of the shelf as relative sea level rises accelerated, resulted in poorly defined transgressive system tracts. With the relative sea level at a highstand, extensively developed deltaic/coastal systems prograded basinward exhibiting well-defined clinoforms.(Figure1.7c) The major hydrocarbon plays in the low stand tracts occur as mounded basin-floor turbidite fans, channel fills, draped sheets and are found in the up-dip pinch-out of deltaic/coastal sandstones (Broad, 2000).

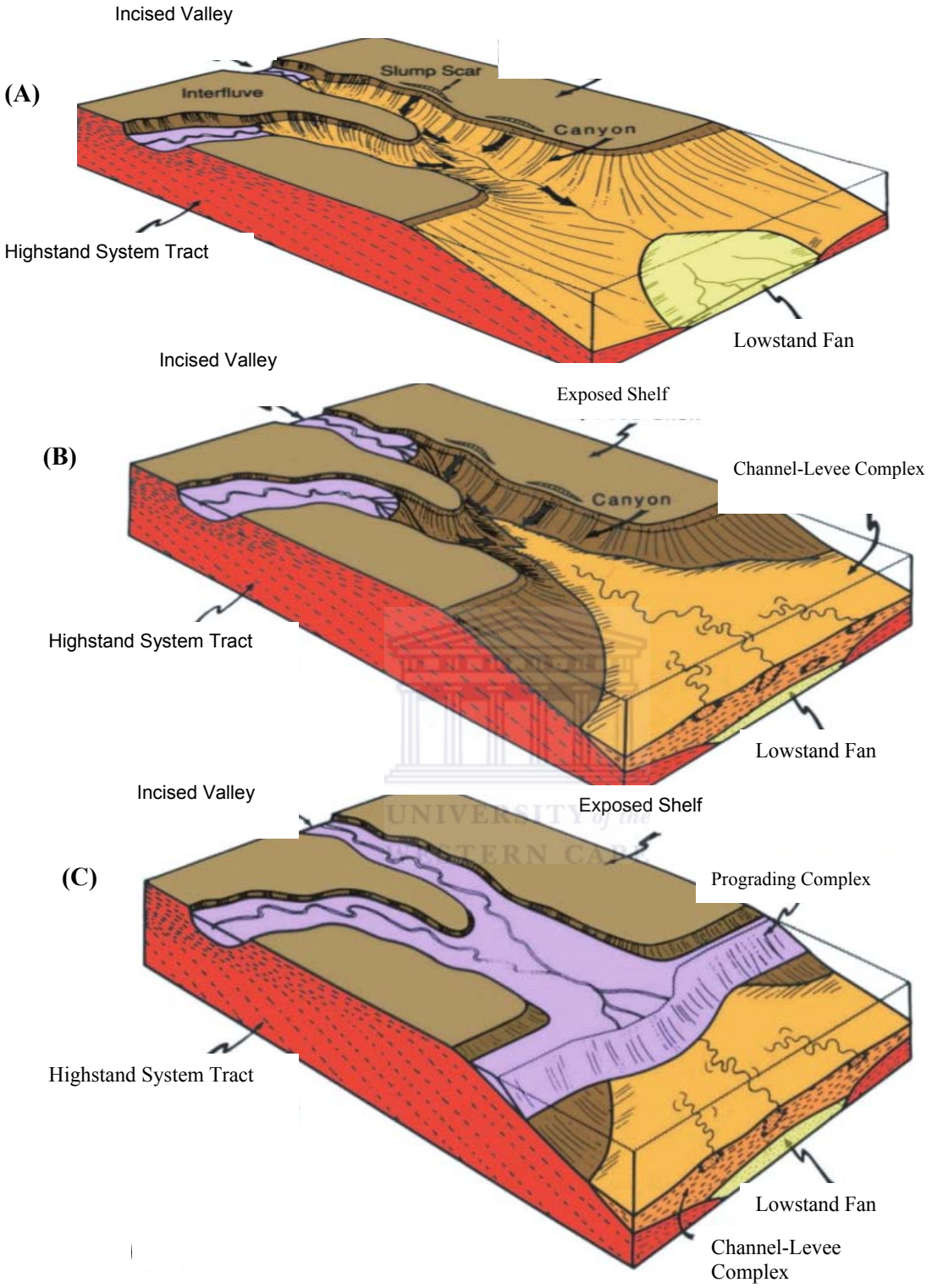

Figure 1.7: Basin floor fan on canyon floor (a), Channel-Levee complex on basin floor fan (b), Prograding complex terminates canyon filling episode (c)

(Modified from: Broad, 2000)

1.9 GENERAL OVERVIEW OF DEEP-MARINE DEPOSITIONAL ENVIRONMENTS

Clastic rocks accumulate in a variety of depositional settings that have become better known largely through the exploration for more hydrocarbon reserves and their exploitation. Clastic rocks are commonly the product of processes that are active in their depositional setting. Water depth, winds, waves, currents, temperature, water chemistry, and biologic action all affect the character of the clastic formed. Diagenesis plays a major role in forming and modifying the facies that are found in the subsurface.

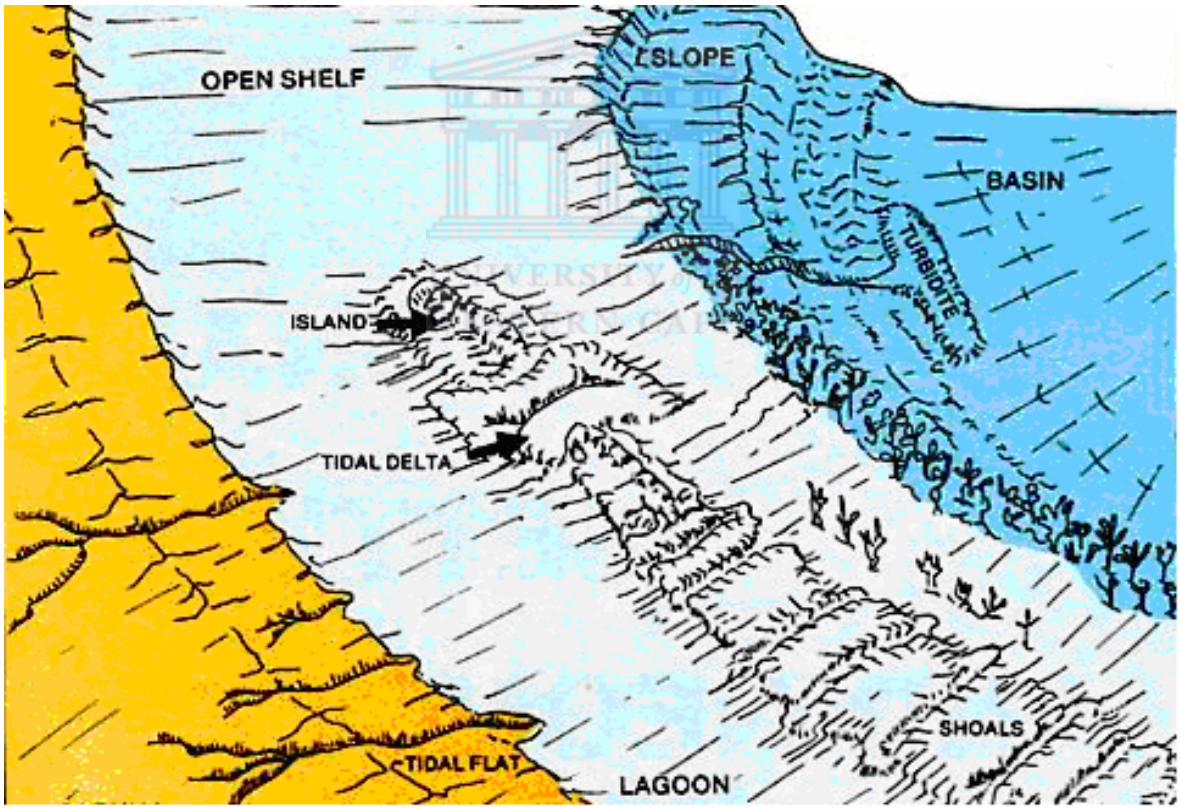

Figure 1.8: Deep marine depositional environment

(USC Sequence stratigraphy Web, April 4, 2006)

In the Bredasdorp Basin sandstone reservoirs are characterized by a range of stacked and amalgamated channel fills and lobes. They originated from the materials eroded from pre-existing highstand shelf sandstones and transported into the central basin by turbidity currents. Turbidites are sediments transported and redeposited by turbidity currents. The turbidites form fan-shaped wedges which in cross-section are composed of evenly-bedded sheets. Bedding varies from thin to almost massive. These sediments, transported from shallow platform and upper slope (Figure 1.8), may include reef debris, oolites, lime mud or broken limestone blocks, as these could be seen in some of the cores. Earthquakes, sea level changes or slope failure may initiate transportation (Turner et al., 2000).

Channelized reservoirs are numerous in the western and southwestern play areas, reflecting their proximity to the base of the slope relative to the eastern area where fan lobes predominates. Channelized reservoirs are not directly affected by faulting though there is evidence to suggest that deep-seated basement structures related to synrift faulting influenced palaeo channel trend with the Aptian and Albian sequences. Generally, sandstone reservoirs are present in both synrift and drift sections (Frewin, et al., 2000).

Proximal turbidites are characterized by the lower part of the Bouma graded bed sequence in which a lime mud matrix supports the grains. The basal layers of turbidites may be unsorted and may include ripups from the substrate. Bedding is irregular and discontinuous because the sediment is deposited as channel fills and levees on submarine fans. Sediment composition and grain size are extremely variable and may include a wide range of shallow water bioturbation mixed with pelagic skeletons (Mc Aloon, et al., 2000).

Distal turbidites are characterized by the upper part of the Bouma graded bed sequence. Bedding is regular, planar, and commonly the turbidites are interbedded with claystone/siltstone. These turbidite sediments are deposited at the margins of submarine fans some distance from their source (Mc Aloon, et al., 2000).

Turbidites could have significant source potential because of their origin in shallow water areas of high organic productivity. In addition, their porous facies may act as reservoirs or as conduits for migrating oil.

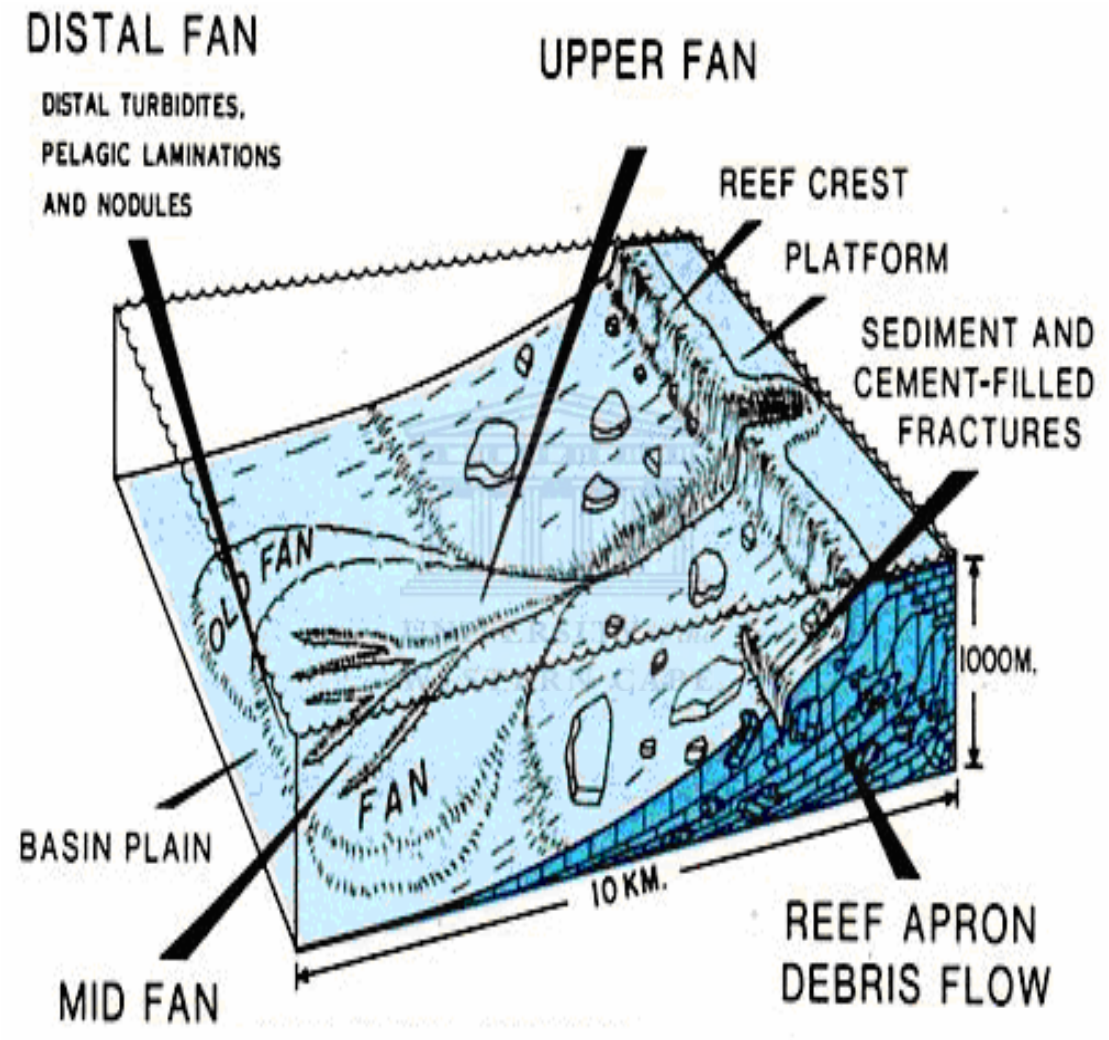

Figure 1.9: Generalised deep marine fan.

(*USC Sequence stratigraphy Web, April 4, 2006)*

1.10 PETROLEUM SYSTEMS OF THE BREDASDORP BASIN

The elements necessary for oil and gas accumulation in sufficient quantities to be worth producing are; organic-rich source rock, porous and permeable reservoir rock to store the accumulated oil and gas and a system of trap and seal to prevent the oil and gas from leaking away.

1.10.1 SOURCE ROCKS AND MATURITY

In the Bredasdorp Basin deep marine oil and gas source rocks are developed in the transitional rift-drift sequence (lower Valanginian to mid-Aptian, 1A – 13A sequences), where the 13A (Mid-Aptian) source is probably the main source for the gas condensate fields. The synrift source rocks are mature over large parts of the basin and the younger source intervals are mature in the west and south of the Bredasdorp Basin. (Petroleum Agency SA, Brochure, 2003)

1.10.2 RESERVOIRS, SEALS AND TRAPS

In the synrift and the drift sections, sandstone reservoirs are present. Synrift reservoirs are shallow marine to fluvial whereas the drift sandstones are deep marine turbidite deposits. The main seals are the drift marine shales, potential synrift seals do exist. The synrift traps are mostly tilted blocks and include structural as well as truncational traps. In the drift sections mainly low relief closures are developed, including drape anticlines, stratigraphic pinch-out traps and inversion closures. (Petroleum agency SA, Brochure, 2003)

1.10.3 PROSPECTIVITY

Hydrocarbons are prospectively rated high in the basin, which contains the entire proven hydrocarbons in South Africa. A number of oil and gas accumulations has been discovered and some under appraisal and further exploration and investigation in the basin is expected to yield continued success, including the present study of porosity and permeability distribution in the deep marine play of the central Bredasdorp Basin, Block 9, offshore South Africa (Petroleum agency SA, Brochure, 2003).

Prospectivity of the Bredasdorp Basin:

- The "kitchen" area is large
- Migration distance is short
- Traps are abundant
- Effective seals are evident
- Oil and gas finds, proven oil and gas potential are undrilled to the east
- Hydrocarbon potential excellent.

2. CHAPTER TWO

2.1 METHODOLOGY

This section lists the available data within the study area and outlines the various methods employed to characterize the reservoir zones. The flow chart (Figure 2.0) below illustrates steps taken in carrying out this research. The method starts with the review of previous studies and literature search in analogous oil and gas fields. The data collection section has the list of all the data collected from the Petroleum Agency SA, which is used in this study. They are carefully arranged, and prepared for easy access (Data Development). Well log correlation and delineation of reservoir sand units together with reservoir studies using thin section petrography, SEM and XRD are carried out to characterise the reservoir quality.

2.2 PREVIOUS WORK

Given the nature of this research, this section begins with an overview of several significant geological, stratigraphic and structural characteristics as well as the hydrocarbon potential of reservoir rocks studies conducted on the Bredasdorp Basin and associated formations from surface exposures and through subsurface studies. The Bredasdorp Basin is characterized by deep marine sedimentation. Sedimentary processes such as bulk emplacement, debris flow, turbidity current and slumping have put together its sequence and reservoir geometry. Accumulation of terriginous materials (land derived) on the continental slope and continental rise are deposited into the deep sea by slumping (movement of sediment piles as a mass) or by turbidity currents which is the rapid movement of large slurries (mixture of sediment and

water) down slope. Turbidity currents are driven by gravity and can move far into the sea. Sediment deposition is accelerated by sea-level falls during which the coast is at the shelf break causing rivers to empty sediment directly on the slope.

According to Turner (2000), the sea-level fall during early Aptian and mid-Albian, resulted in material eroded from pre-existing highstand shelf sandstones and transported into the central basin by turbidity currents from the west-southwest flank. He also pointed out that sandstone reservoirs in the Bredasdorp Basin consist of stacked and amalgamated channels and lobes. Fan lobes have a coarsening-upward pattern, whereas channelised reservoirs are fining upward.

McAloon *et al*., (2000) presented a pre-developmental characterisation of a marginal deep-marine channel-lobe system reservoir. By using core, well log and dip data, it is concluded that the massive, amalgamated deep-marine sandstones, which make up the larger part of the E-BD reservoir, represent extensive mass-flow deposits. Additionally, the distribution of these deposits has been controlled by a significant erosional feature on a regional unconformity, which basically represented a major easterly-trending valley on basin floor. It is analogous to a submarine canyon extending through the E-BD area and acting as a conduit for sand sourced from the shelf to the west.

Frewin *et al.*, (2000) discussed the geologic characterisation of a deep-marine channel-lobe system: The Oribi and Oryx oil fields; both being reservoir accumulations within the same turbidite system in the Cretaceous drift succession of the Bredasdorp Basin.

Based on the seismic recognition of multiple unconformities within the drift successions, stratigraphic naming reflects a sequence stratigraphic approach. According to Brown et al, (1996); sequences defined by significant unconformities recognized on seismic sections, were assigned numbers (1 to 22). Third and higher order sequences; composite sequences and sequence sets recognized subsequently were designated by letters (A, B, C etc). Unconformities are designated by the sequence overlying them (1A, 4B etc) and by their nature chart, (Petroleum Agency SA, brochure, 2004/05).

Turner *et al*., (2000) focussing on sequences 13A and 14A addressed the fact that reservoirs in the Bredasdorp Basin principally within Block 9 generally consist of stacked, deep-marine channel/lobe sandstones of Aptian age. The work had the objective of predicting and delineating additional hydrocarbon reservoirs, based on geological modelling of the Aptian and Albian sequences within Block 9.

Generally, for an overview of natural gas resources and petroleum exploration offshore South Africa, the reader is directed to the Petroleum Agency SA brochure (2003/4/5), Jikelo, (2000), McLachlan, *et al.* (2000) and Wood (1995).

These studies have helped to provide information for improved understanding of the stratigraphic architecture and geological development utilized for the present research.

2.3 EQUIPMENt

2.3.1 THIN SECTION PETROGRAPHY

- Nikon petrographic microscope
- Nikon digital camera

2.3.2 XRD

Karlsruhe: D8 ADVANCE powder diffractometer (BRUKER-Axs) equipped with a copper X-ray source (50kV, 35mA) and a position sensitive detector (Vantec-1).

Diffracplus BASICS 4.0 #1 software (XRD Evaluation and Quantification programs).

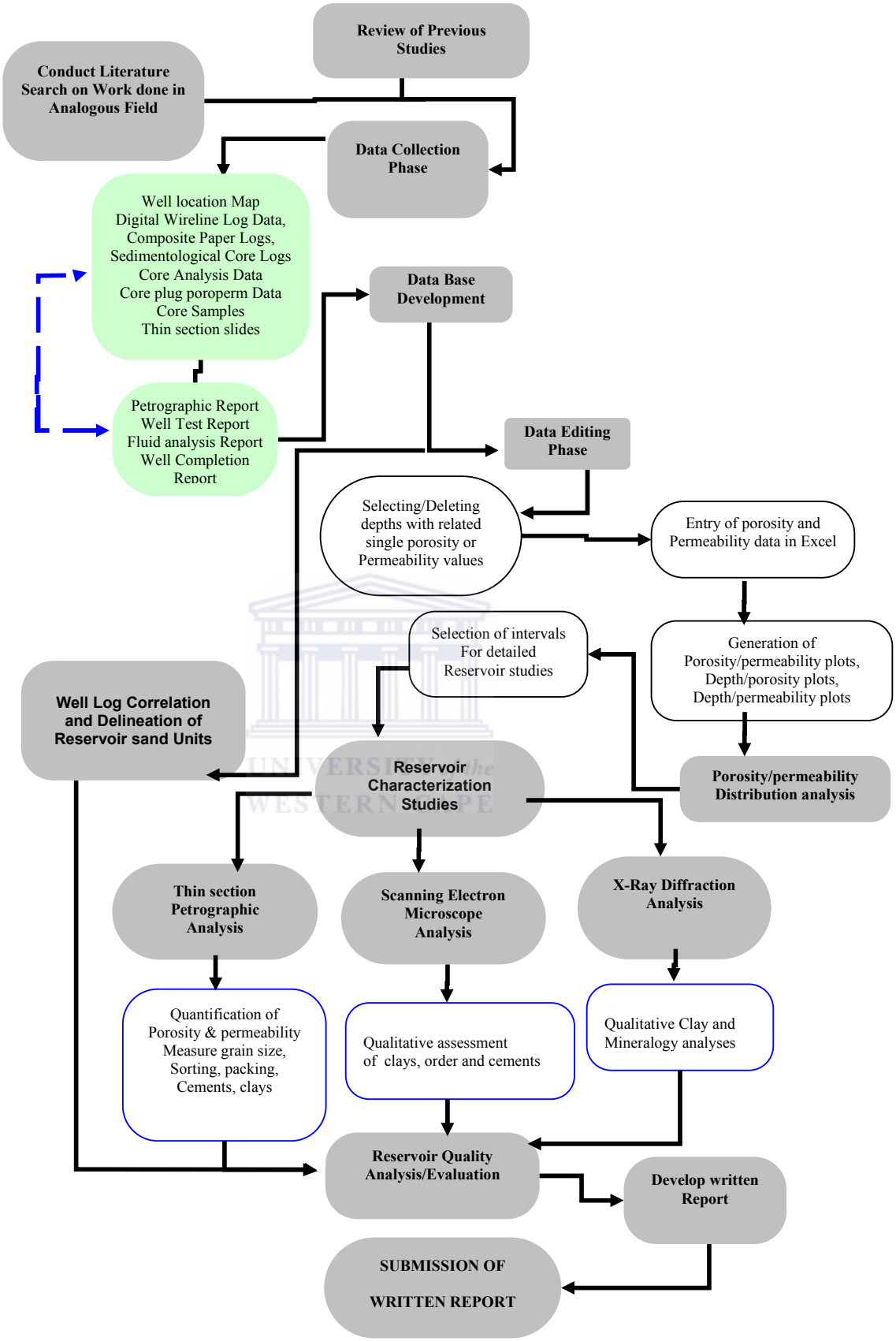

Figure 2.0: METHODOLOGY FLOW CHART

2.4 SOURCES OF DATA

Sources of information include core samples, core analyses results, well completion data, well location map, wireline log data, composite paper logs, petrographic reports, well test reports, formation pressure data, and fluid analysis reports. The cores used in this study are located at the Petroleum Agency South Africa core library. The Petroleum Agency South Africa (PASA) provided all the data use for this study. Due to the fact that this area is an **active** area, petroleum reserve and production data was not provided.

2.5 SAMPLE TYPE AND SAMPLE PREPARATION

A study of 73 thin sections covering virtually all 9 wells was done to determine relationships between pore characteristics and reservoir quality as well as pore size, shape, and abundance are useful indicators of relative quality in reservoir flow units. Some thin sections are stained with blue-epoxy resin to facilitate the recognition of porosity or pore spaces and are studied under plane- and cross polarized light. Thin sections used in this study were collected from the Petroleum Agency South Africa (PASA) and were examined using a Nikon petrographic microscope.

Core samples for clay mineral XRD analyses were disaggregated in a mortar and pestle, after which the mortar and pestle were cleaned of obvious contaminants from sample to sample using methylated spirits/ethylene. A split of each sample was transferred for pulverization using a McCrone micronizing mill. Sample preparation was conducted at the Geology Department, University of Stellenbosch. The resultant powder was then used for measurements conducted at iThemba labs, Somerset West.

A split of samples that were X-rayed were also examined with a scanning electron microscope (SEM) to aid in the identification of authigenic components, particularly clay minerals, and to better visualize pore geometries. This work was performed at the Physics Department of the University of the Western Cape.

2.6 THIN SECTION PETROGRAPHY

Thin section petrography provides detailed petrographic descriptions of thin section samples from selected depths. These depths are chosen from three regions of the porosity and permeability scattered plots (i.e. good, moderate and poor poroperm areas). Petrographic observation and optical photomicrographs are performed on a Nikon petrographic microscope; most descriptions are done at 4 or 10 magnification.

Images viewed through the microscope are focused for viewing and subsequent capture by the Nikon digital camera and then transferred to a disc and saved as, .tif image files for later analyses. Magnification, light source, light intensity, and light polarity are standardized so that measurement techniques are comparable on all thin sections sampled.

Thin sections are examined to identify visible porosity types, grain sizes, sorting, cements, clays clasts or laminae and matrix. The porosity and permeability values stated for each image was determined and tabulated for each of the wells from core analyses done by PASA (petrographic and well completion reports).

2.7 SCANNING ELECTRON MICROSCOPE (SEM)

The assessment of cement and clay and their distribution within the reservoir sandstone units is carried out using scanning electron microscope. SEM analysis is used in the identification

of authigenic clays filling pore spaces, cementation, and any other diagenetic products, such as dissolution or replacement of grains within the samples. Identification of cement type and abundance will allow for more accurate prediction of permeability and porosity distribution.

2.8 X-RAY DIFFRACTION (XRD)

X-ray diffraction analyses of the samples were performed using a D8 ADVANCE powder diffractometer equipped with a copper X-ray source, tube (50kV, 35mA) and a Vantec-1, position sensitive X-ray detector. The samples were analyzed using over an angular range of ten to ninety degrees two theta at a step size of 0.0074 degree with a speed of 0.02 sec/point.
In order to assess the exact clay mineralogy in these samples, X-ray diffraction (XRD) analysis was used. The data is interpreted and presented in annotated XRD traces (graphs). This analysis may prove extremely useful when reservoir properties are being studied, for instance when possible reservoir impairment by swelling clay minerals is concerned.

Using thin section petrography, x-ray diffraction, scanning electron microscopy analysis, reservoir quality assessment will be described, and the present study can be use as a tool for other parts of the basin for future research.

2.9 COMPUTER METHODOLOGY

The Microsoft Excel application and other graphics programs were used to generate the charts and/or graphs used in figures. Graphical distributions of results from thin-section petrographic analyses and well-log and core-porosity and core-permeability data are plotted using

Microsoft Excel program. X- Ray analyses is performed using Diffracplus BASICS 4.0 #1 software (XRD Evaluation and Quantification programs).

2.10 PETROPHYSICAL ANALYSIS

The deep marine reservoir sandstone intervals are correlated by linking well-log traces for nine wells leading to the identification of clean sands regions with favourable porosity and permeability. Traces include gamma and resistivity logs response. Boundaries between reservoir-grade sandstone beds, shaly and siltstone formation are differentiated using wireline logs. These boundaries are also characterized by a rapid decrease in core and well-log porosity. In this study less attention is paid to the petrophysical characterization, because a research has been carried out on this aspect on the same wells.

2.11 WELL LOG CORRELATION AND DELINEATION OF RESERVOIR SAND UNITS

Petrophysical wireline logs are used to correlate reservoir zones. The well-log correlation of boreholes in the study area is done along the NW – SE direction. The sandstone (reservoir units) and shale sequences of various thicknesses across the wells are correlated over a distance of about 30km. The eight wells include: E-BA1, E-AR1, E-CA1, E-AA1, E-AD1, E-BB1, E-AO1, and E-AO2. During the initial qualitative interpretation using gamma ray and resistivity logs, major sandstone units (Top and Base) are identified (Figure 2.1). Nevertheless, the correlation work is concentrated on the shale section. This is a general practice in wireline log correlation, the reason being that the low-energy environments normally result in fine-grained deposits of considerable lateral extent. Therefore, shale sections are used to provide the first-pass correlation between the wells as they also show

specific resistivity characteristic over large areas than sandstone units. These features are observed during the correlating process of the well logs. Shale units with thin intercalation of sands separating Top sand unit from the Base sand unit can be recognised across all the wells in the correlation section, with thickness ranges from 260m in E-BA1 to about 110m in E-AO2 (Figure 2.1). Core samples taken within this interval has been reported in the geological well completion report to contain good quality source rocks (McAloon, 2000). A comparable shale unit is observed beneath the base sand unit which seems noticeable below 2910m depth in E-BA1 and is correlated across all the wells (Figure 2.1). The shale units follow the general dipping trend across the wells. However, lack of adequate data within these intervals limit their being studied in details.

The main sand unit in the shallower part (above 2390m depth in E-BA1, (Figure 2.1)) of the correlation section shows a fairly uniform thickness and characteristics across the wireline logs section distinct from the deeper sand unit (above 2790m depth in E-BA1, (Figure 2.1)) which varies from well to well. However, the resistivity logs fairly display similar trends. These behaviours could be explained from the fact that; firstly, geologic province like the Bredasdorp Basin generally display low dipping structures towards shallower depth. Secondly, geologic structures tend to be less complicated towards the shallower part as a result of faults terminating upward which in turn make their effect on stratigraphic units being correlated less prominent particularly at the upper part of the correlated section.

A comparable example is shown in the schematic SW-NE cross section within the Bredasdorp Basin shown in (Figure 1.5) where the stratigraphic units tend to be less affected by fault structure at shallower depth. The lateral discontinuity of geologic units observed could be due to stratigraphic variation or fault cut. Generally, the thickness of these sequences increases and the sandstone interval gradually tends to be more serrated basin ward (South-Eastward). This is evident beyond well E-AO1 for both Top and Base sandstones sequences.

LOG CORRELATION OF BOREHOLES AND DELINEATION OF THE TOP AND BASE SAND UNITS.

Figure 2.1: Well Log Correlation and Delineation of Reservoir sand units.

Table 2.0: Identified Reservoir Sands (Zones) Depths Within The Boreholes.

RESERVOIR ZONES		WELLS: E-BA1	E-AR1	E-CA1	E-AA1	E-AD1	E-BB1	E-BB2	E-AO1	E-AO2
	DEPTH (m)									
TOP SAND (ZONE 1)										
	From:	2412	2470	2490	2453	2494	2552	2537	2555	2555
	To:	2459	2523	2520	2531	2592	2617	2587	2636	2627
BASE SAND (ZONE 2)										
	From:	2812	2828	2776	2813	2824	2864	2845	2893	2907
	To:	2869	2945	3002	3007	3016	3073	3043	3270	3129

3. CHAPTER THREE

3.1 POROSITY AND PERMEABILITY DISTRIBUTION

Because of poor sorting (more clay and mud) finer grained sandstones exhibit lower initial porosity and permeability.

Sandstone framework components constitute an extremely important pre-burial control on reservoir quality potential. Composition and abundance of principal framework grains have a great impact on diagenetic processes controlling porosity reduction, preservation and enhancement with burial. In tight reservoir intervals the framework has a profound effect on reservoir porosity and permeability characteristics.

Characterization of reservoirs is challenging due to the various scales of heterogeneity that exist. The analysis of heterogeneity is primarily concerned with the distribution and connectivity of reservoir sand bodies. Heterogeneity also affects reservoir performance. The architecture of reservoirs is often difficult to characterize due to the relatively limited lateral extent of depositional elements and bounding surfaces. Associated shale drapes can influence reservoir behaviour because they are potential baffles and barriers to fluid flow. Also, facies variations, such as the vertical change from cross-bedded to ripple-laminated sandstone, produce a fining-upward trend in grain size and a corresponding decrease in porosity and permeability.

3.2 RESERVOIR FRAMEWORK

Heterogeneity in sandstone reservoirs is controlled by the following factors;

1. The geometry of sandstone bodies (lens-shaped, tabular, etc.). Lens shape reservoir interval, has different fluid flow and petroleum production characteristics than, for

example, a tabular reservoir. Production is concentrated along the thickest intervals of stacked reservoir sandstones.

2. Faulting and fracturing of the reservoir intervals; this influences oil trapping and retention, as well as influencing fluid flow at well scales.

3. Mudstone and other low-permeability baffles that direct flow of fluids through the rocks.

4. Vertical and lateral distribution of facies and interbedding characteristics of the sandstone, mudstone, and other rock types, Connectivity and vertical- and lateral-continuity of oil-productive facies influences how much petroleum can be produced from individual wells. They also govern how effective will be techniques of water-flood and other methods of secondary and tertiary oil recovery.

5. Sedimentary structures (e.g. cross-bedding, burrowing).

6. Laminae, (such as thin mudstone, claystone and siltstone layers and calcite-cemented intervals), and

7. Influence of diagenetic history on porosity/permeability preservation, destruction, and enhancement. Diagenetic and depositional processes strongly influence porosity and permeability destruction, preservation, and creation; these are of course critical to migration of oil into the basin and its subsequent recovery (Lori, 1995).

3.3 CEMENT COMPOSITION

Depositional grain size and the presence or absence of diagenetic cement controls reservoir quality. Porosity distribution and porosity types are related to rock texture and fabric. The distribution as well as abundance of diagenetic cement has important consequences for porosity and permeability heterogeneity within the reservoir units. The relationship of hydrocarbon emplacement and cement precipitation has a major control on reservoir quality.

Hydrocarbon emplacement also causes a distinctive pattern of porosity and permeability heterogeneity in the reservoir units (Lori, 1995).

3.4 POROSITY – PERMEABILITY DISTRIBUTION FOR WELLS

Porosity-permeability relations vary from borehole to borehole. Porosity and permeability data used were measured from core plugs by the Petroleum Agency South Africa. The data represented at the appendices gives the permeability and porosity values used for the plots. Permeability measured in millidarcies is plotted on a logarithmic scale (y-axis) versus porosity measured as a percent is plotted on a linear scale (x-axis), and permeability is very closely related to porosity. Boyle's law or Gas expansion porosity and Klinkenberg corrected permeability have been used in all cases.

Boyle's law and gas expansion porosities are porosity measurement methods obtained from modal analysis, and modal analysis is a suitable method for determining porosities of samples, especially well cuttings. The measurement of effective porosity of reservoir rocks can be made by determining the volume of sand grains in a core sample by a procedure depending on Boyle's law or procedure that measure the void volume.

3.4.1 Porosity-permeability distribution for well E-BA1.

Porosity and permeability range from very poor to moderate. Porosity is secondary after leaching of cement and detrital grains, and is reduced mainly overgrowth cements and clays. Probably, the presence of clays (e.g. Kaolinite) has reduced much of the secondary porosity to microporosity, resulting in poor permeabilities (Figure 3.0).

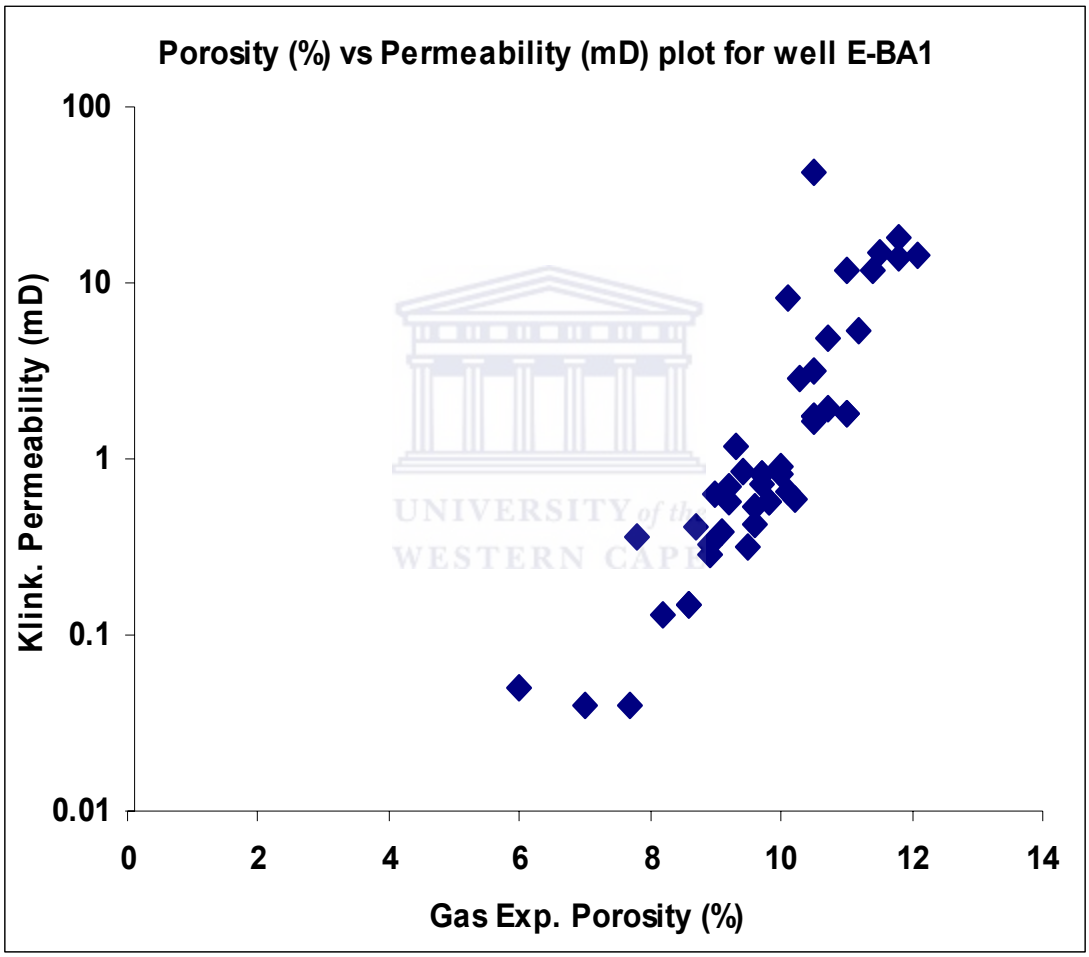

Figure 3.0: Porosity-permeability scatter plot for well E-BA1.

Appendix 1, list all porosity and permeability values for well E-BA1 included in this plot.

3.4.2 Porosity-permeability distribution for well E-CA1.

Poroperms in Figure 3.1 are poor, due to overgrowth cementation and authigenic clays which produce microporosity and reduce permeabilities. The area with good poroperms, overgrowths are not abundant enough to significantly affect poroperm characteristics, hence poroperms are preserved. The points that are plotted on line 0.01 in the figure have permeability values of 0.01.

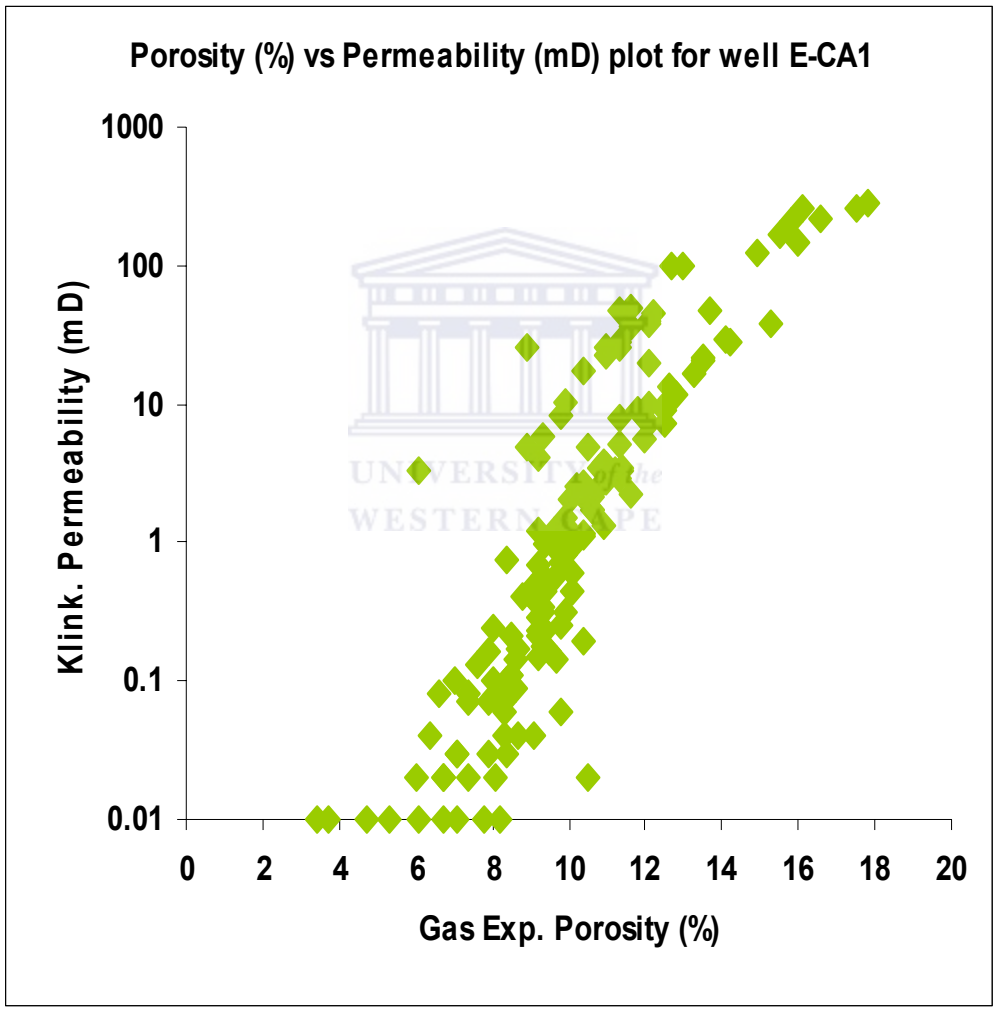

Figure 3.1: Porosity-permeability scatter plot for well E-CA1.

Appendix 2, lists all porosity and permeability values for well E-CA1 include in this plot.

3.4.3 Porosity-permeability distribution for well E-AA1.

In Figure 3.2, microporosity and local development of secondary porosity characterised this well and are attributed to the formation of authigenic, pore-filling kaolinite and partial dissolution of lithic clasts. An improvement in permeability is attributed to dissolution of pore-filling kaolinite (plate 4.61, SEM, E-AA1, 3075.92m). The points that are plotted on line 0.01 in the figure have permeability values of 0.01.

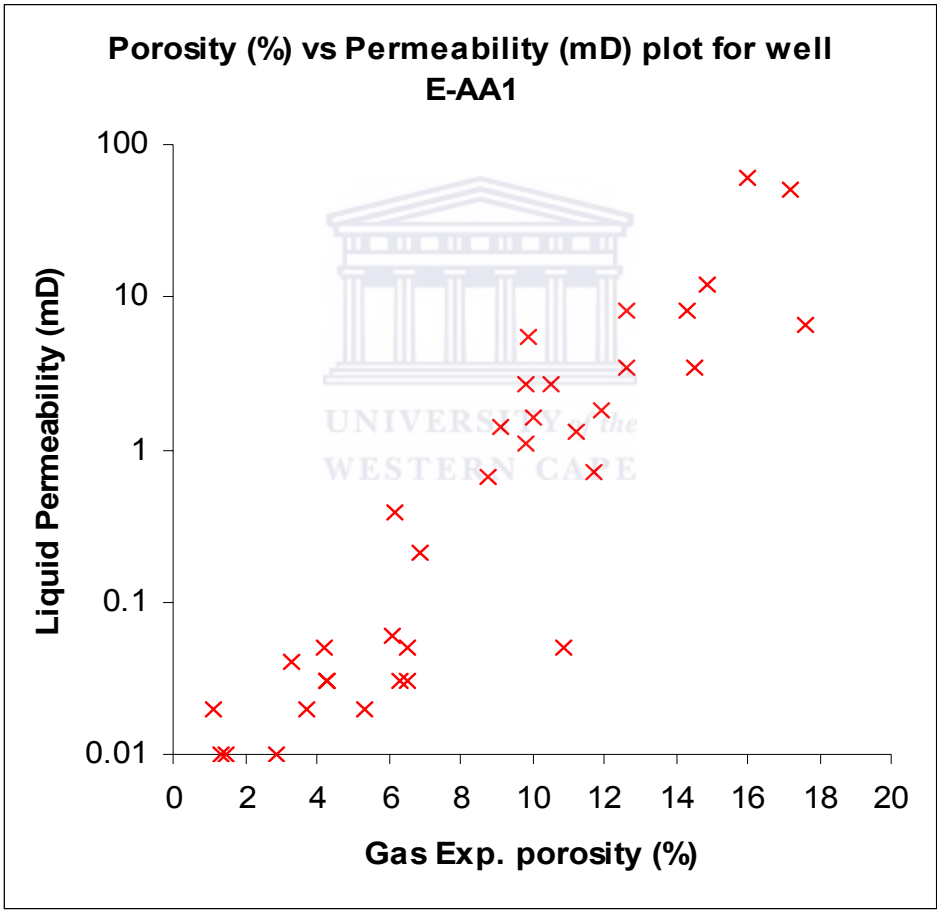

Figure 3.2: Porosity-permeability scatter plot for well E-AA1.

Appendix 3, lists all porosity and permeability values for well E-AA1 included in this plot

3.4.4 Porosity-permeability distribution for well E-AD1.

Figure 3.3, has good permeability and good secondary porosity. Poor permeability values are associated with the presence of microporosity and porosity is further reduced by calcareous cement and silica overgrowths. In addition poor porosity and permeability values are attributed to the fine to silty nature of the sandstone (e.g. plate 4.46 a&b, E-AD1, 2868.75-2869.00).

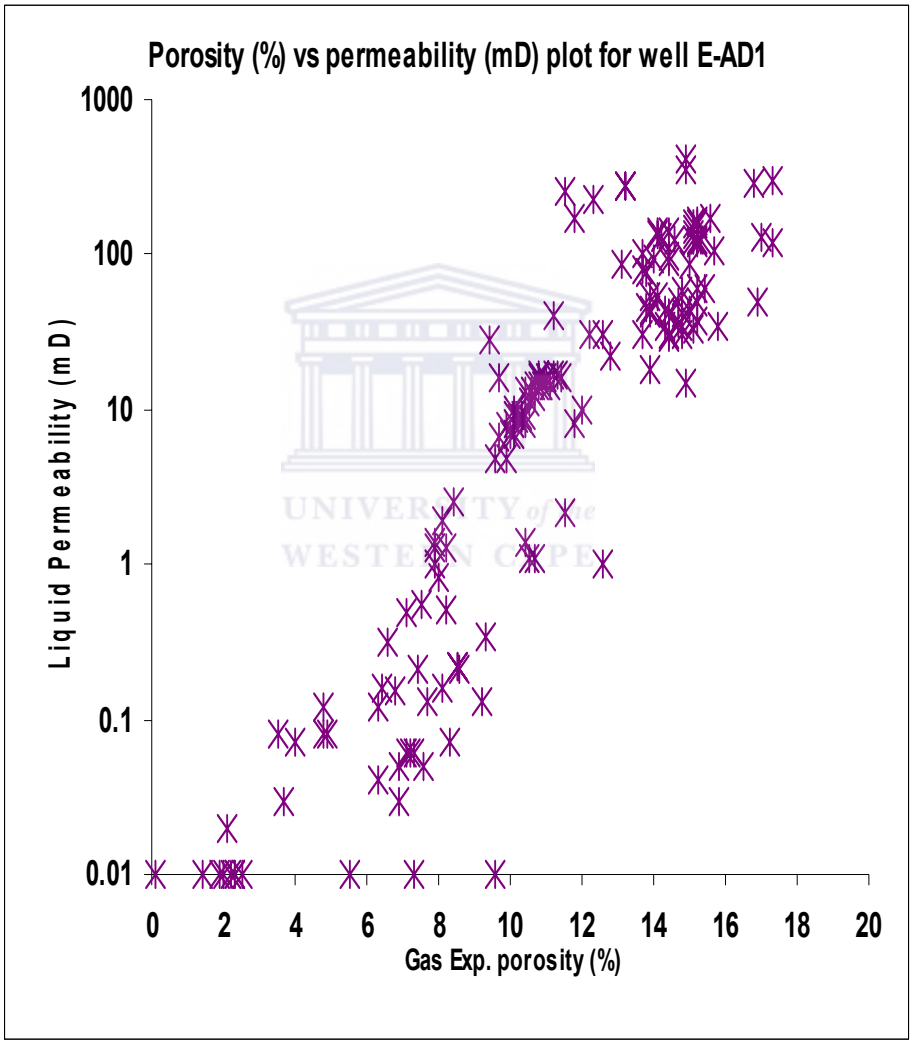

Figure 3.3: Porosity-permeability scatter plot for well E-AD1.

Appendix 4, lists all porosity and permeability values for well E-AD1 included in this plot

3.4.5 Porosity-permeability distribution for well E-BB1.

Poroperm characteristics are good, with 8.4-14.4% porosity and 0.10-39mD permeability. Porosity is secondary after dissolution of intergranular cement. The reduction in porosity and permeability could be as a result of overgrowths, vug filling and fibrous clays. Another significant porosity reducing effect could be the development of pseudomatrix infilling intergranular porosity.

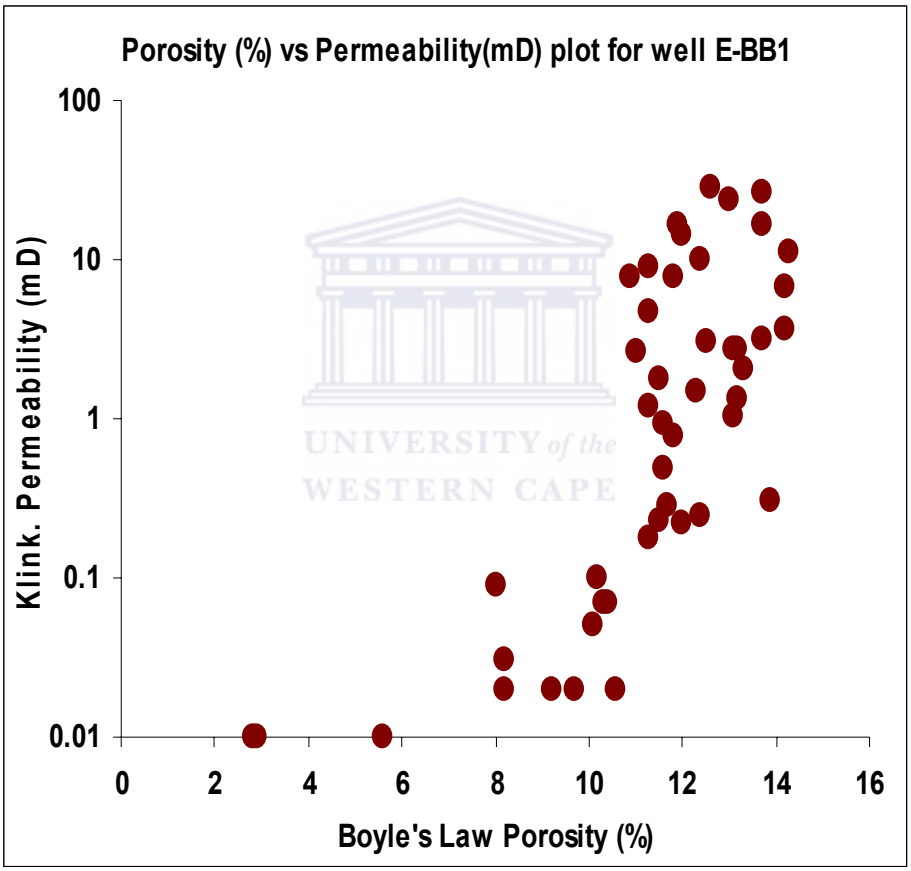

Figure 3.4: Porosity-permeability scatter plot for well E-BB1.

Appendix 5, lists all porosity and permeability values for well E-BB1 included in this plot

3.4.6 Porosity-permeability distribution for well E-BB2.

Porosity and permeability characteristics are very good to excellent, and this shows that the sandstone intersected in this well is clean.

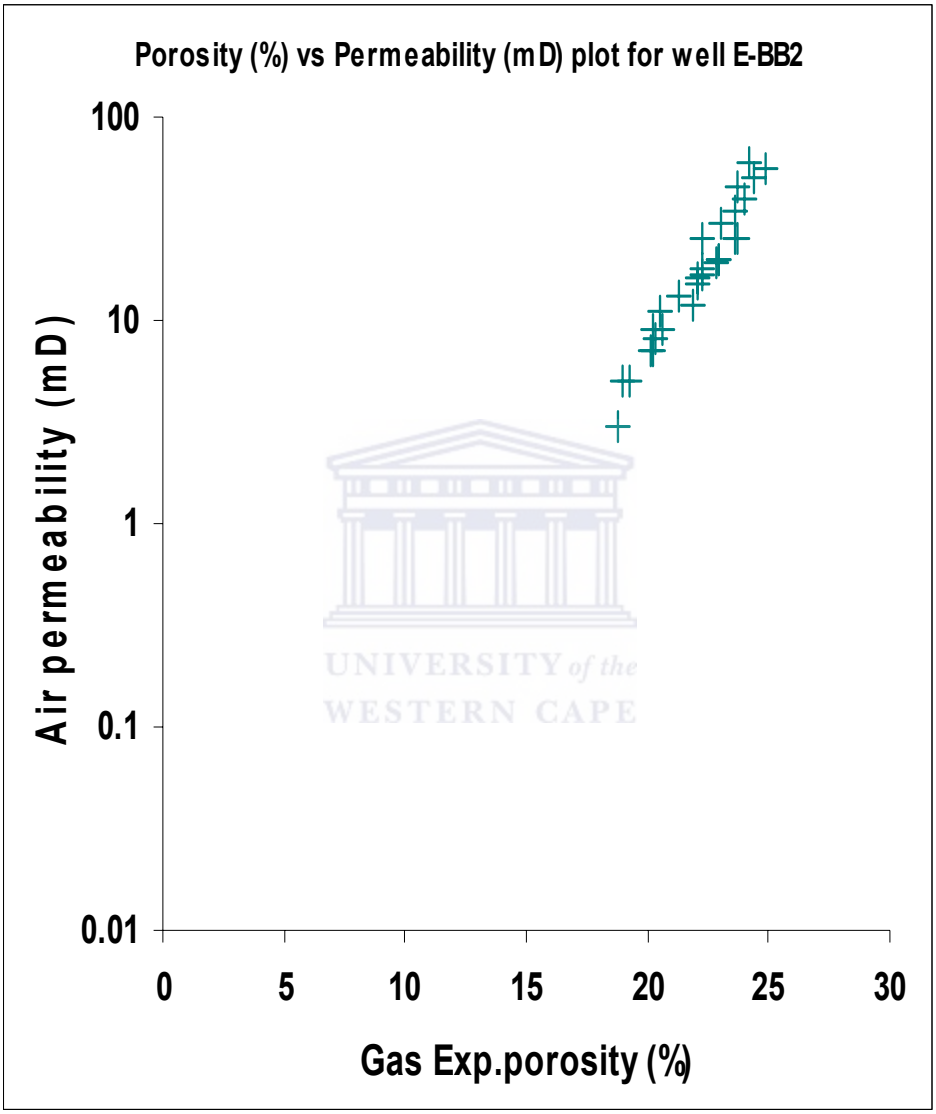

Figure 3.5: Porosity-permeability scatter plot for well E-BB2.

Appendix 6, lists all porosity and permeability values for well E-BB2 included in this plot

3.4.7 Porosity-permeability distribution for well E-AO1

Porosity and permeability are good, but tend to deteriorate as cementation become abundant; the preserved porosity is secondary which is reduced to microporosity in poor poroperm region.

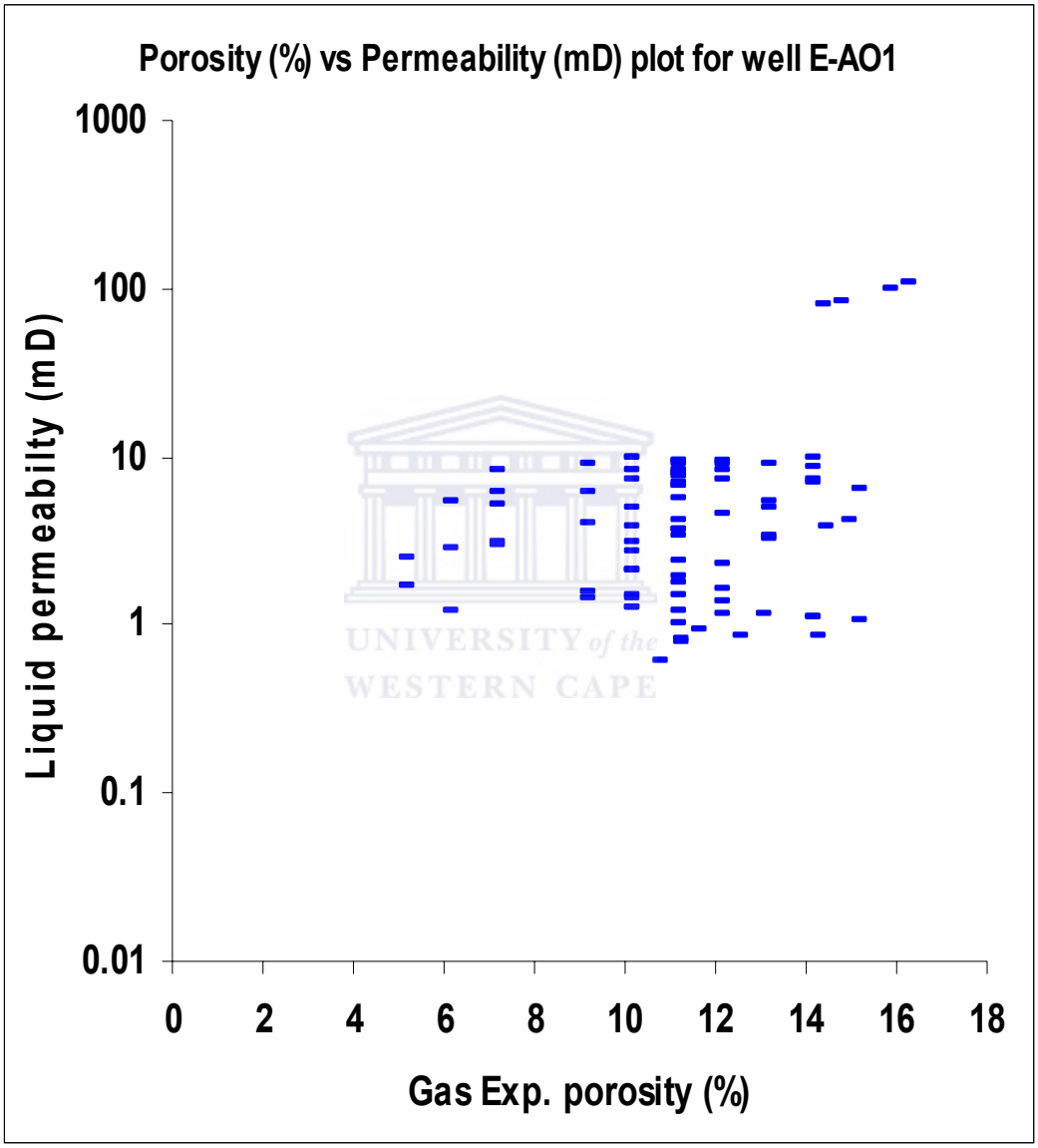

Figure 3.6: Porosity-permeability scatter plot for well E-AO1.

Appendix 7, lists all porosity and permeability values for well E-AO1 include in this plot

3.4.8 Porosity-permeability distribution for well E-AO2

Poroperms are poor due to extensive cementation, and the presence of detrital clays. Secondary porosity is developed to a minor extent and poroperms are better due to the absence of pseudomatrix.

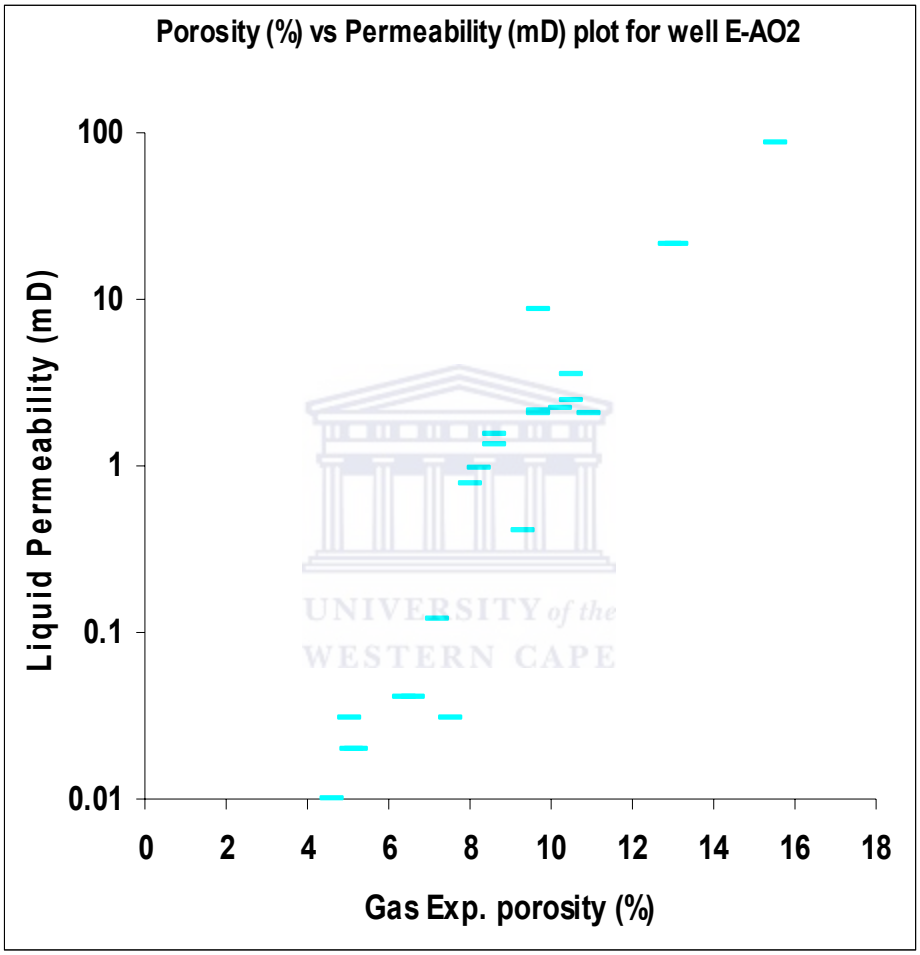

Figure 3.7: Porosity-permeability scatter plot for well E-AO2.

Appendix 8, lists all porosity and permeability values for well E-AO2 include in this plot

3.4.9 Porosity-permeability distribution for well E-AR1

Porosity and permeability are poor; due to clays and quartz cementation that reduces secondary porosity to microporosity. Porosity is secondary after cement and grain dissolution, resulting in good to excellent permeability values. The points that are plotted on line 0.01 in the figure have permeability values of 0.01.

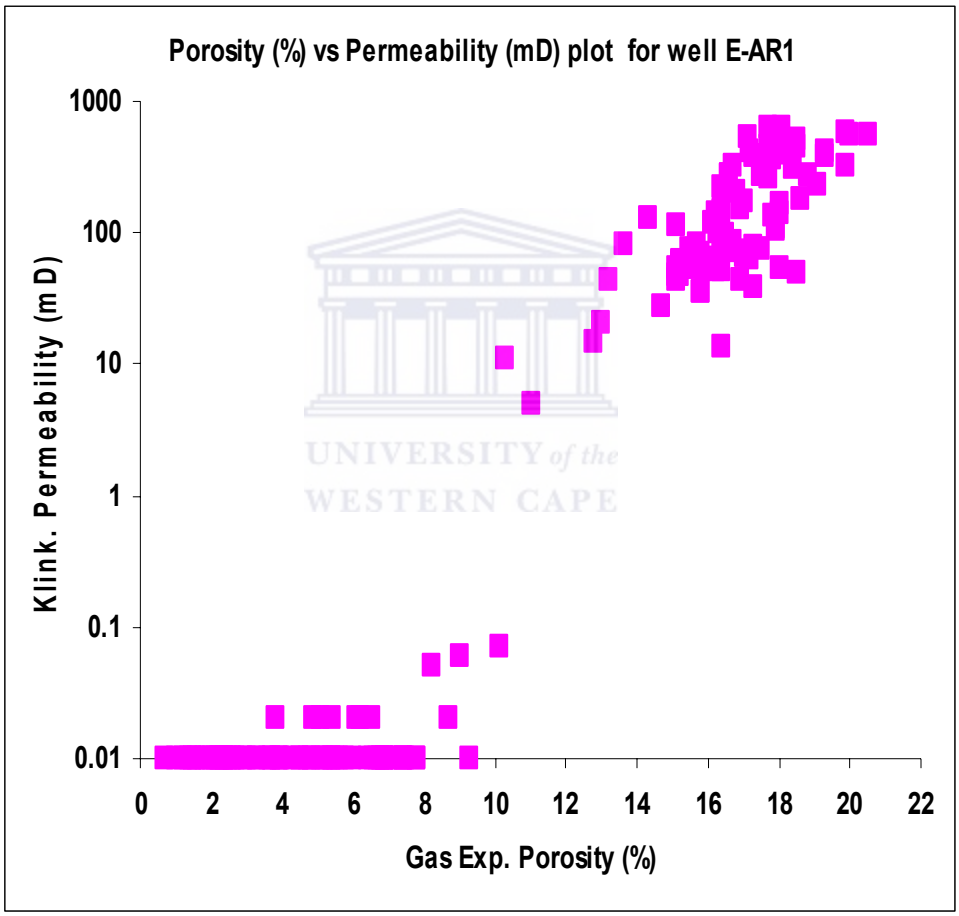

Figure 3.8: Porosity-permeability scatter plot for well E-AR1.

Appendix 9, lists all porosity and permeability values for well E-AR1 included in this plot

3.4.10 Top sand porosity-permeability distribution across the wells.

Three wells, E-BA1, E-CA1, and E-AO2 intervals are not represented here because this area was not cored. From the well completion report, this reservoir interval had immature sand bodies.

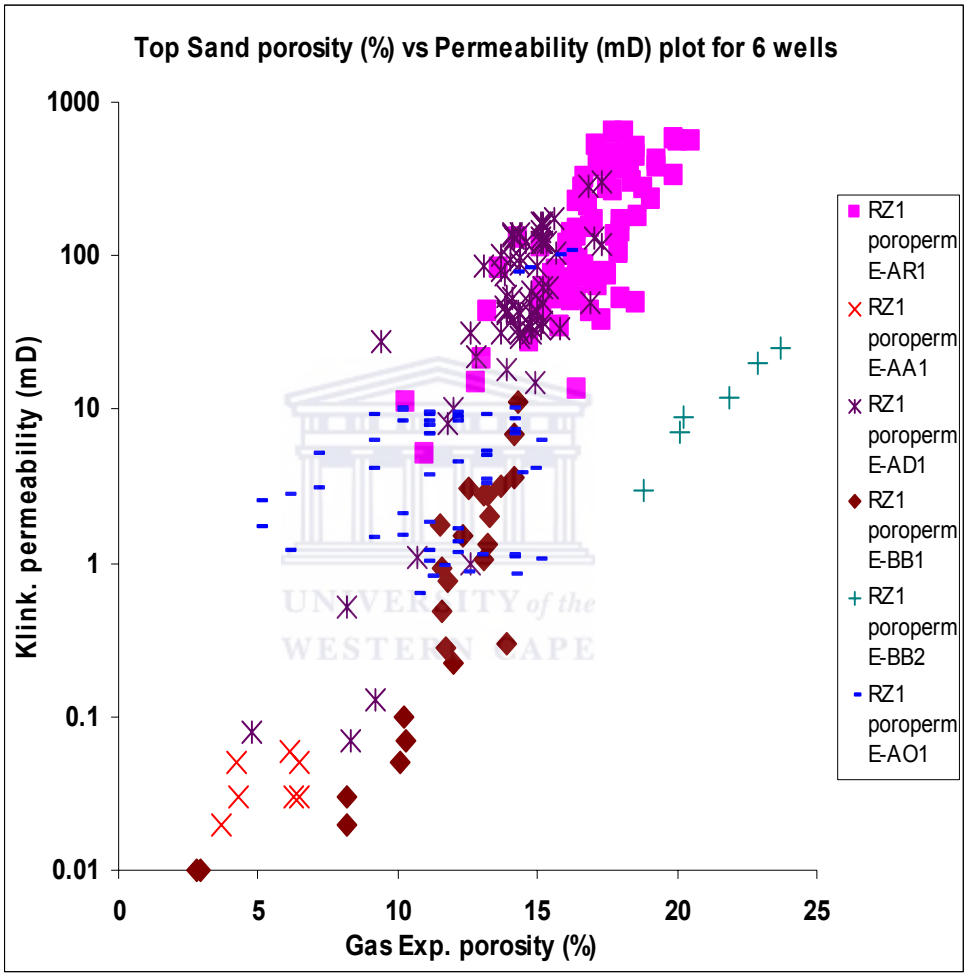

Figure 3.9: Top sand porosity-permeability scatter plot.

3.4.11 Base sand porosity-permeability distribution across the wells.

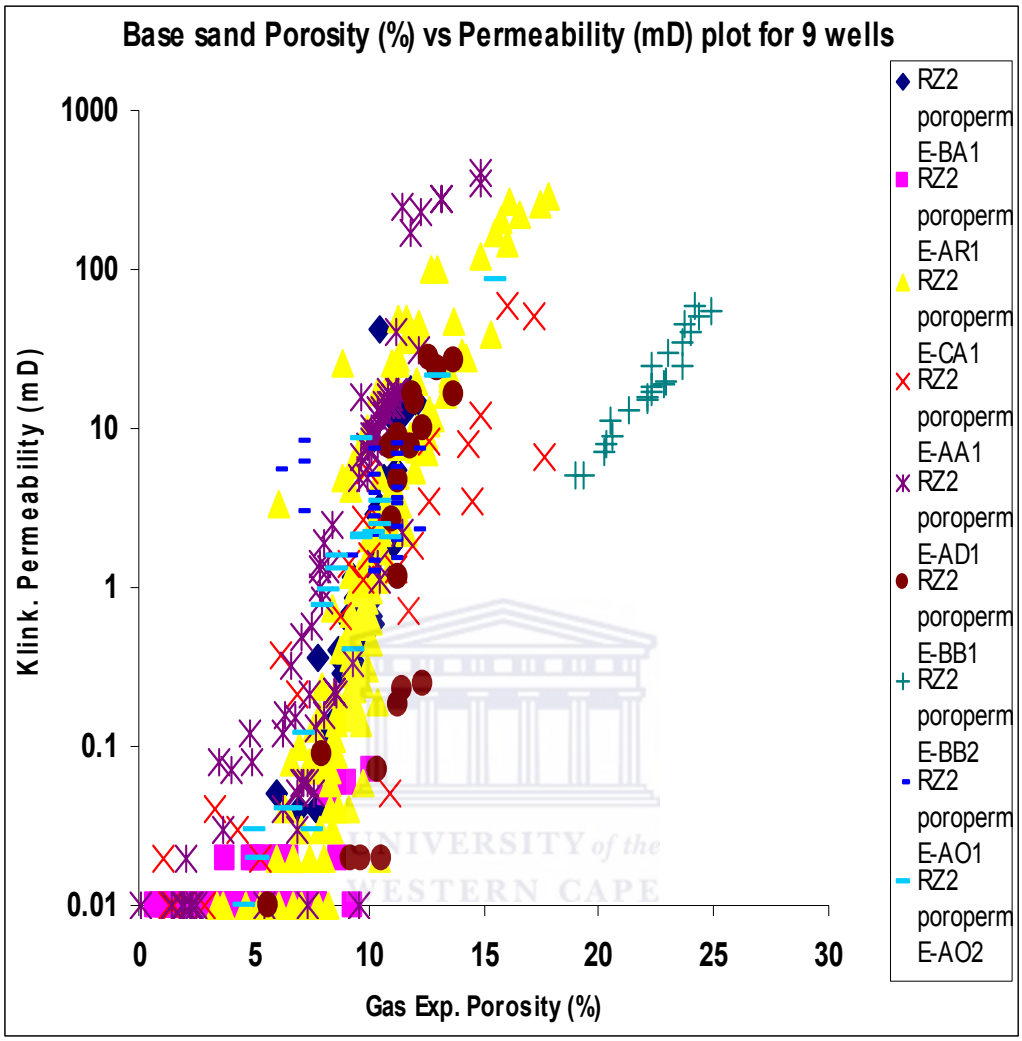

Figure 3.10: Base sand porosity-permeability scatter plot.

3.4.12 Top and Base sands porosity-permeability distribution across the wells

Using an arbitary cut-off of 10% porosity and 1mD permeability, a large proportion of wells have good to excellent reservoir quality. Excellent means porosity values greater than 20% and permeability of 100-1000mD, good implies 15-20% porosity and permeability of 10-100mD. Moderate implies 10-15% porosity and 1-10mD permeability and poor porosity below 10% and permeability below 1mD. The Top sand interval has high reservoir quality whereas the majority of low reservoir quality is from the Base sand interval.

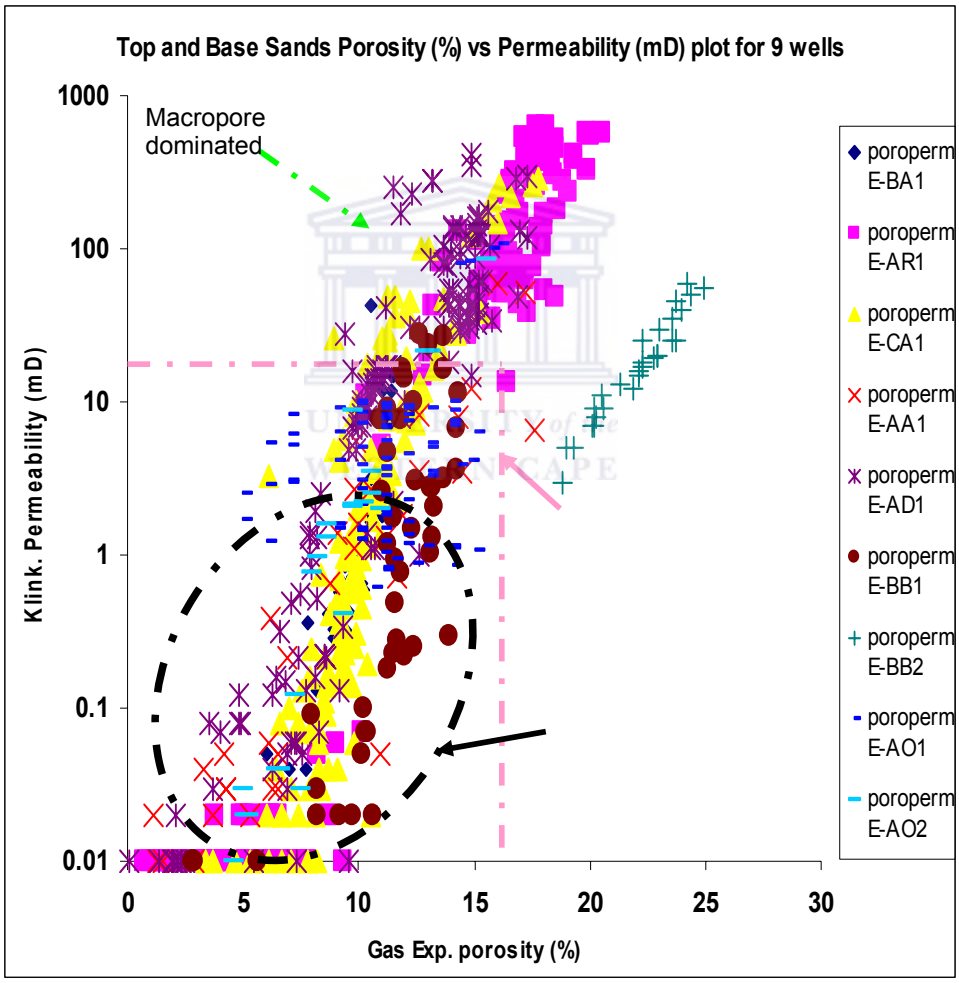

Figure 3.11: Top and Base sands porosity-permeability scatter plot.

3.4.13 Top and Base sands porosity-depth trend across the wells

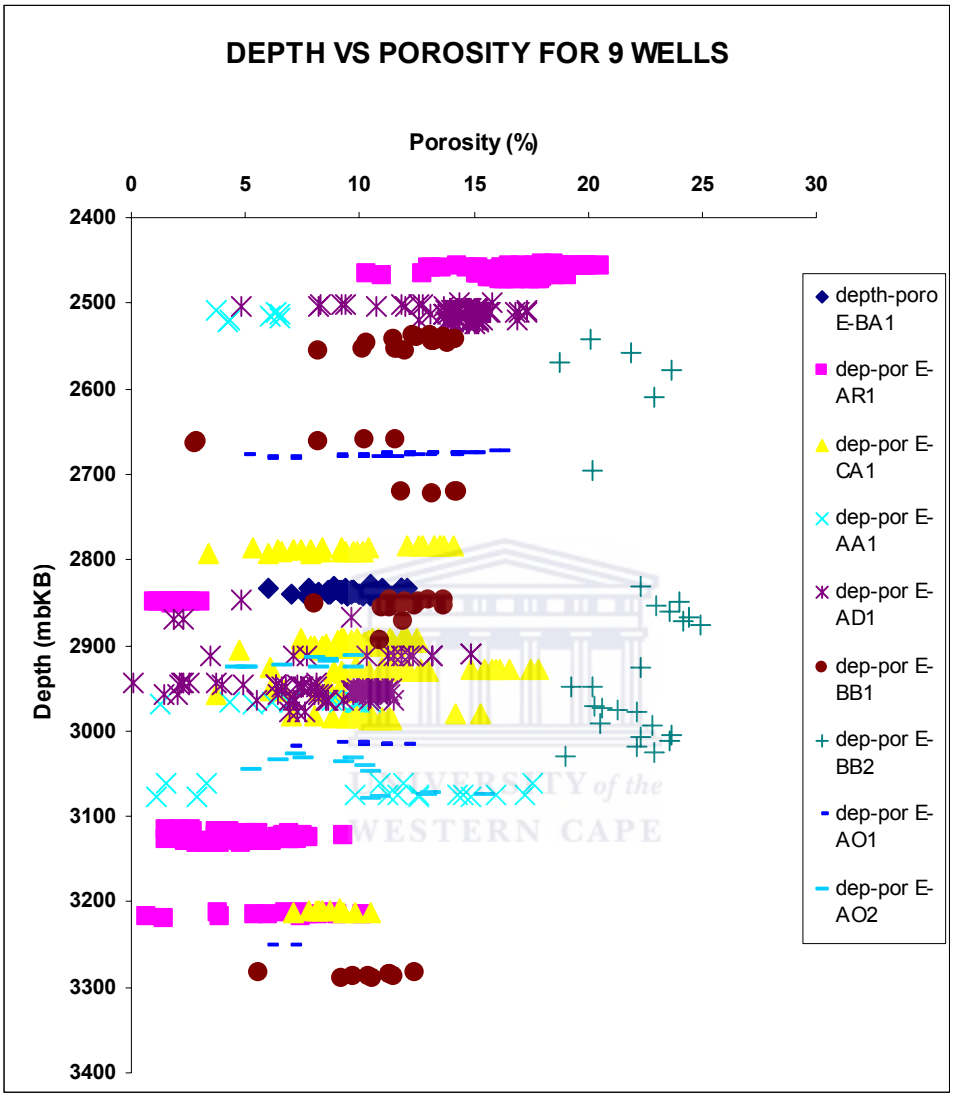

Figure 3.12: Top and Base sands porosity-depth trend (scatter plot).

3.4.14 Top and Base sands permeability-depth trend across the wells

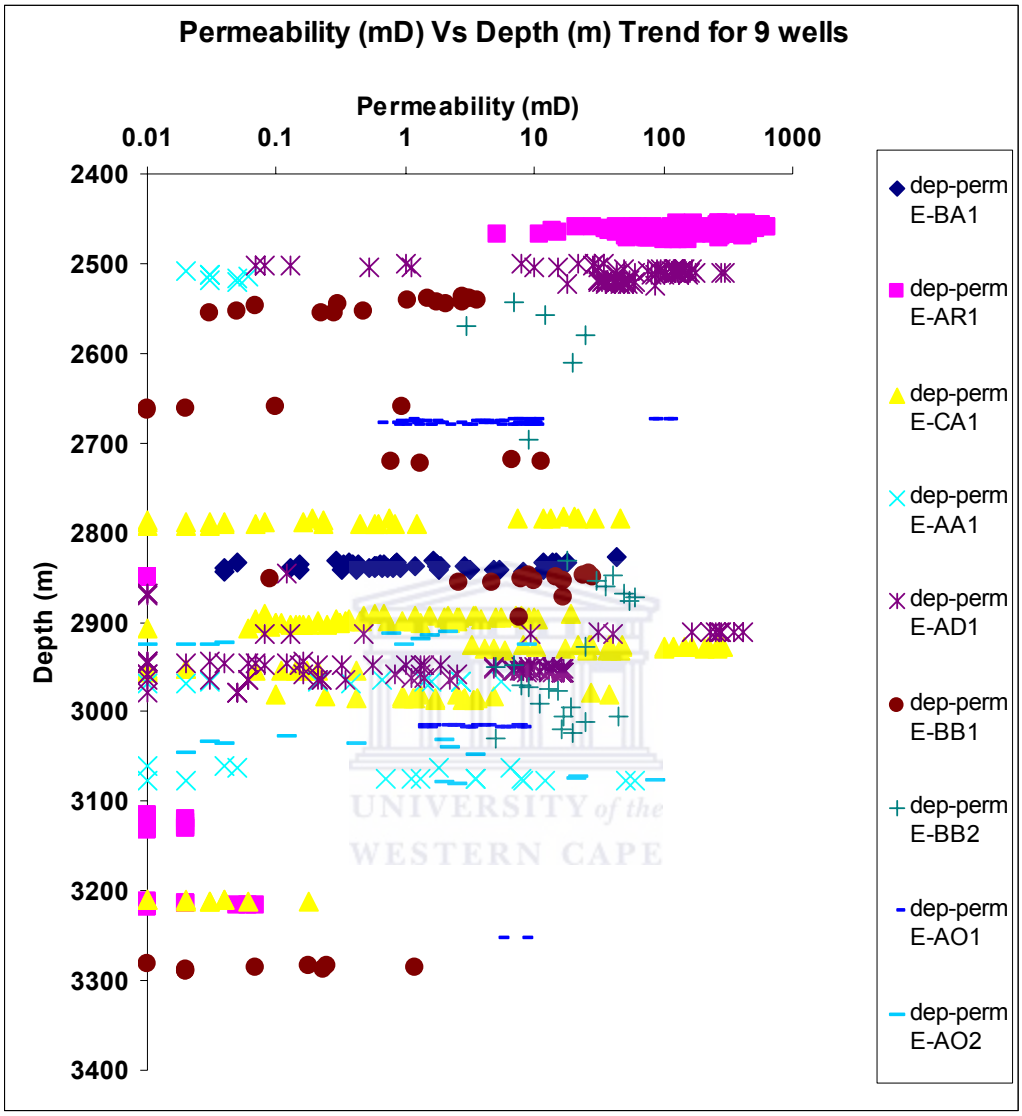

Figure 3.13: Top and Base sands permeability-depth trend (scatter plot).

In order to illustrate the porosity-permeability trend, data for sandstones reservoir intervals (Top and Base Sands) for all the wells are plotted together (Figure 3.11). Using an economic cut-off of 10% porosity and 1mD permeability (suitable for liquid hydrocarbons), a large proportion of wells has good to excellent reservoir qualities. The Top sand interval has high reservoir quality whereas the majority of low reservoir quality is from the Base sand interval. Using a lower porosity-permeability cut-off of 7% porosity and 0.1mD permeability, the Base sand could be an effective gas reservoir.

There is a fairly systematic relationship between reservoir quality (porosity-permeability) and depth (Figure 3.12 and 3.13). The plots show a slight reduction of porosity and permeability with depth. According to Atkins and McBride, (1992) the decrease in porosity with depth may not be uniform. The controlling factor could be porosity gradient, geothermal gradient, and decrease in sorting in sandstone reservoirs. Generally, porosity and permeability decrease with depth, but depth is not the only factor to consider in the decrease of either porosity or permeability. This could be due to a number of factors. Compaction and cementation causes decrease in sediment porosity and permeability. Examination of thin section indicates that, although compaction due to increasing depth of burial may be a factor, the degree of compaction is greatly influence by lithology, especially the presence and quantity of labile rock fragments (Dutton and Diggs, 1992). The decrease in porosity and permeability could be indicative of the presence of overgrowth cementation, grain rimming cements, pore filling cements and grain rimming clays. On the other hand, an increase in porosity with depth could be due to creation of secondary porosity, entrapment of hydrocarbons, and a relatively early overpressure. It should be noted that the reservoir quality is drastically reduced below depth of 2800 mbkb, (i.e. Base reservoir) probably because of increase in compaction and cementation with burial depth.

4. CHAPTER FOUR

4.1 RESERVOIR CHARACTERIZATION STUDIES

4.1.1 PETROGRAPHIC ANALYSIS

Petrography is the detailed study of the grains that compose a rock, the geologic history and implications of the sandstone grains, the cements that bind the rock.

Understanding of depositional facies and associated reservoir quality can only be gleaned by "looking at the rocks," preferably core studies supplemented with thin section petrography. In the absence of core data, well cuttings can be thin sectioned and provide useful data as well. Enhanced petrography often results in a firmer understanding of stratigraphic controls on porosity development and distribution. When properly tied to log data, a more rigorous stratigraphy-facies framework can be developed to define play relationships and more efficiently exploit the reservoir (Dravis, 1985)

The aim of carrying out petrographic studies includes:

- Recognition of relict grains
- Determination of primary depositional texture
- Documentation of the origin of porosity
- Recognition of microporosity invisible in normal thin sections.
- Delineation of relict diagenetic fabrics, such as healed fractures.
- Establishment of a facies control on reservoir quality (relationship of preserved porosity to relict texture)
- Timing of diagenetic alteration

- Timing of secondary porosity evolution and its implications for fluid migration
- Easier identification of associated diagenetic minerals.

This chapter is divided into three parts as follows:

PART ONE:

4.1.1 THIN SECTION PETROGRAPHY

Thin section petrography forms an important part of this study. It comprises mineralogical description of the rock components, porosity types present and assessing grain size and sorting, using thin sections. This includes photomicrographs of the samples, or comprehensive petrographical sample descriptions.

PART TWO:

4.1.2 SCANNING ELECTRON MICROSCOPE (SEM)

Scanning electron microscopy technique is used to further assess the petrography of these samples, especially in describing the morphology of clay-minerals.

PART THREE:

4.1.3 X-RAY DIFFRACTION (XRD)

In order to assess the exact mineralogy in these samples, X-ray diffraction (XRD) analyses, are performed. The data is interpreted and presented in annotated XRD traces (graphs). This analysis may prove extremely useful when reservoir properties are being studied, for instance when possible reservoir impairment by swelling clay minerals is concerned.

PART ONE

4.1.1.1 THIN SECTION PETROGRAPHIC DESCRIPTION

Thin section description includes; a complete description of the mineral constituents of the core samples, texture, sorting (grain size and range), porosity types and the type and abundance of pore filling cements or alteration products. Thin sections contain framework mineralogy composed mainly of quartz, lithic fragments and glauconite. Lithic fragments/clasts are composed essentially of shale, carbonaceous, shelly and calcareous particles. Isolated patches of calcareous material are present as cementing material. Authigenic mineralogy includes quartz cement, which occur as overgrowths on detrital grains, carbonate cement and clay minerals (an appreciable amount of clayey authigenic and detrital matrix and illite, kaolinite and chlorite flakes are important to mention). The samples show overgrowth of quartz grains and grain dissolution alterations and siltstone bands. Calcite cementing materials is also present between quartz grains. Some samples showed ferruginous cement. Quartz grains are monocrystalline and 15% of the grains show a polycrystalline structure. Quartz is constituted of subangular to subrounded framework grains having low to medium sphericity with calcite/dolomite cement. Minor minerals include pyrite, dolomite, siderite, calcite, feldspar, mica (mica occurs as flakes) and laumontite. The minor minerals present are dependant on depth and well, as will be detailed below. Texturally, the grain size is coarse to fine quartz with normal extinction and most grains are, angular to round in shape with moderate compaction. The finer grain shows more angularity than the coarser grains. They are well sorted to moderately sorted, at places and occasionally poorly sorted. The contact type is classified into four classes, point, long, concavo-convex, and sutured. Matrix of from less than 5% to over 15% is present and composed of very fine and fine quartz grains admixed with argillaceous material and clay clasts. This is seen specifically in the poor

poroperm areas. The sections are in general, very poor in heavy minerals, i.e. the sandstones are mineralogically immature.

The following section provides detailed petrographic descriptions of thin section samples from selected depths. These depths were chosen from three regions of the porosity and permeability distribution scattered plots seen in chapter three, (i.e. good, moderate and poor poroperm areas). Good implies 15-20% porosity and permeability of 10-100mD. Moderate implies 10-15% porosity and 1-10mD permeability and poor porosity below 10% and permeability below 1mD. Petrographic observation and optical photomicrographs were performed on a Nikon petrographic microscope; most descriptions were done at 4X or 10X magnification.

4.1.1.1.1 THIN SECTION PETROGRAPHIC DESCRIPTION FOR WELL E-AA1

4.1.1.1.1.1 PLATE 4.0 (A & B): E-AA1, 2520.98-21.24, X4 MAG.

This specimen is chosen from the poor region of the poroperm cross-plot (Figure 3.11), with porosity (4.2%) and permeability (0.05mD). The sample is moderately sorted; tight packing, no visible porosity type and fine grain size (0.01-0.25mm). A high argillaceous content is directly responsible for the low permeability obtained in the core analysis. Generally, the sample is glauconitic as can be seen by the clear green colour in (4.0A), a high organic content (dark) and some pyrite (pale brassy yellow). The framework grains consist mainly of quartz grains (gray to white in XPL). Minor calcite cementation occurs throughout (4.0B) with high order pink and green interference colours and the detrital clay content is high (tiny yellowish or brown crystal) filling the space between the framework grains.

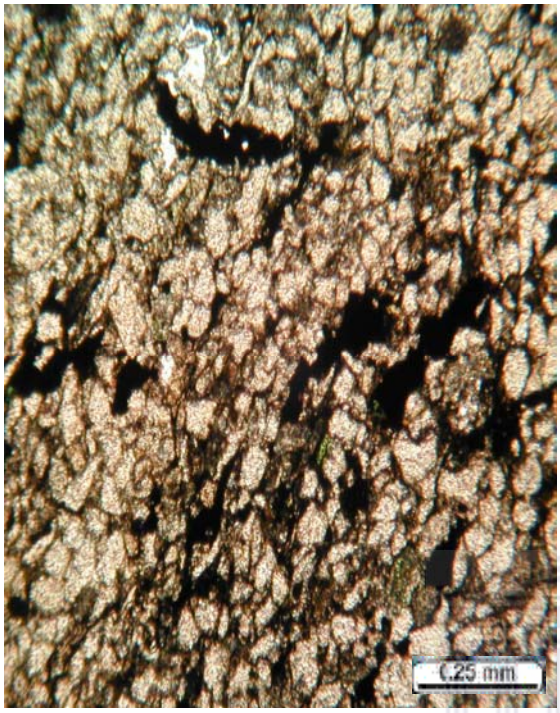

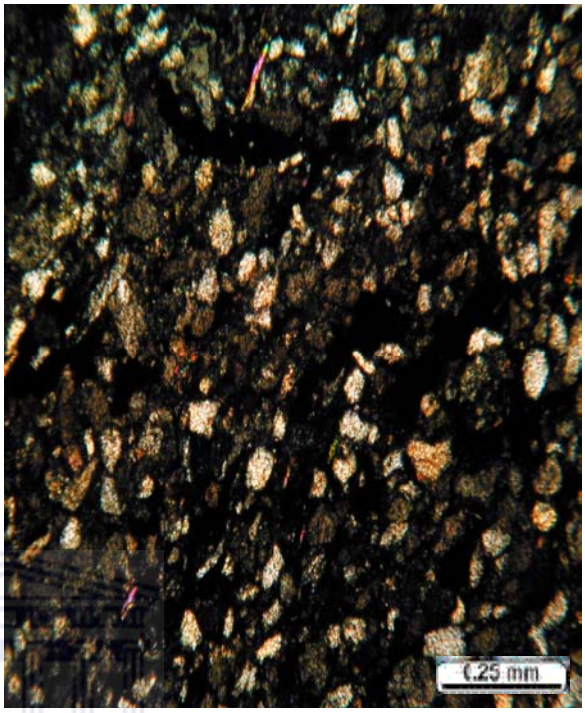

Plate 4.0 (A): PPL

Plate 4.0 (B): XPL

PLATE 4.0 (A & B): E-AA1, 2520.98-21.24, X4 MAG.

4.1.1.1.1.2 PLATE 4.1 (A & B): E-AA1, 2966.92-67.24, X4 MAG.

This interval is fine to coarse grained (0.10-2.5mm) and poorly sorted, subrounded to rounded grains with tight packing, with porosity (6.9%) and permeability (0.21mD). It is glauconitic, shelly and contains pyrite. Calcite cementation is present throughout, indicated by floating clasts and is attributed to precipitation of CaCO3 at fluid interface and/or the dissolution of shelly material incorporated in the sediments. Silica cementation can also be observed. Vugs are partially infilled with dolomite crystals and the centre infilled with clays may imply dissolution of features such as pellets, shells or burrows. Microporosity is the porosity type observed. Pervasive calcite and silica cementation are the main cause of porosity and permeability destruction.

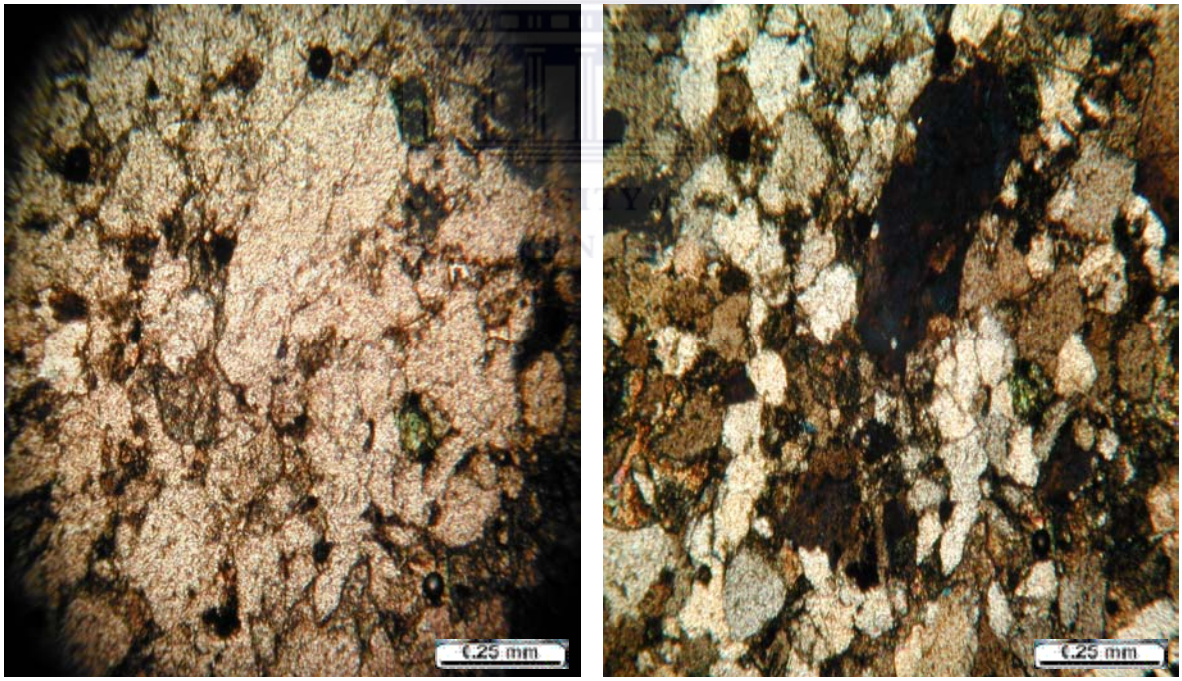

Plate 4.1 (A): PPL Plate 4.1 (B): XPL

PLATE 4.1 (A & B): E-AA1, 2966.92-67.24, X4 MAG.

4.1.1.1.1.3 PLATE 4.2 (A & B): E-AA1, 3061.95-67.24, X4 MAG.

This interval is chosen from the moderate area of the poro-perm cross plot. Grain size is very fine to medium (0.125-0.5mm), sorted, with subrounded to angular grains and slightly loosely packed grains and porosity (11.9%) and permeability (1.80mD) from core analysis. Glauconite and pyrite occur throughout. The framework grain is made-up of quartz grain and sedimentary fragments. There are abundant lithic clasts and argillaceous lamellae, as this may indicate immaturity. Calcite and silica cements are present and occur in patches. Dissolution of pore filling intergranular clays may result in the formation of microporosity and interconnected secondary porosity.

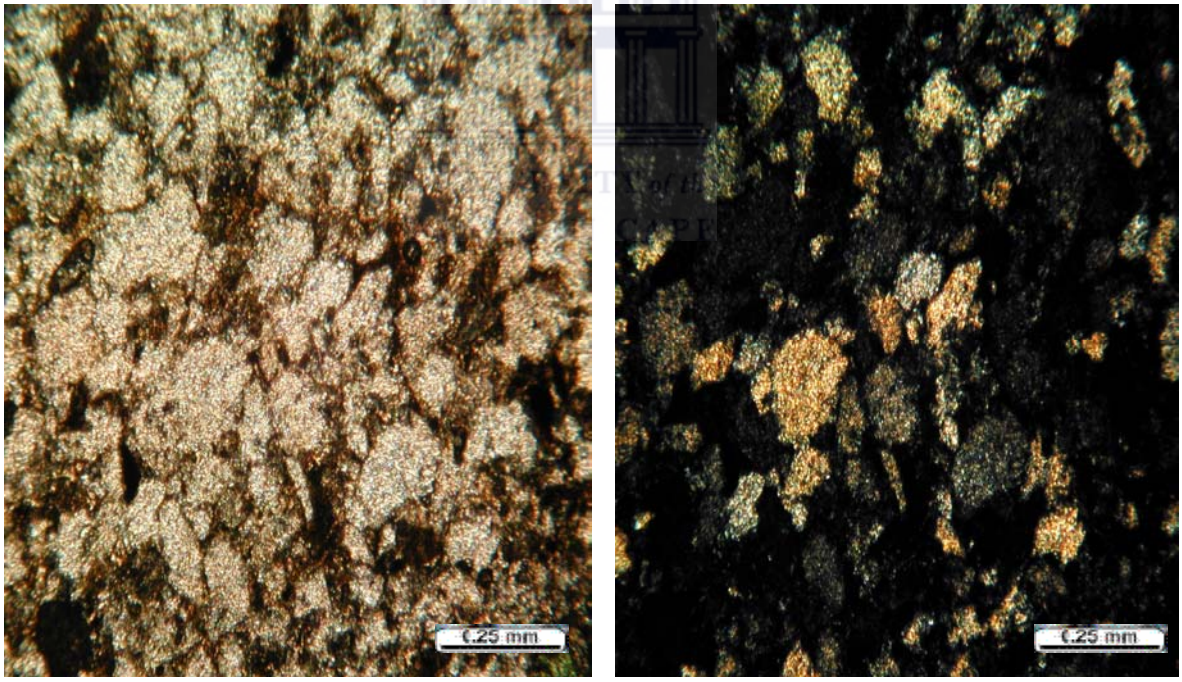

Plate 4.2 (A): PPL Plate 4.2 (B): XPL

PLATE 4.2 (A & B): E-AA1, 3061.95-67.24, X4 MAG.

4.1.1.1.1.4 PLATE 4.3 (A& B): E-AA1, 3074.26-.45, X4 MAG.

Texturally, the grain size ranges from very fine to fine sand grains (0.0625-0.25mm), moderately sorted. A moderately poroperm area with porosity (11.2%) and permeability (1.3mD). This sample is characterized by abundant lithic clasts, argillaceous lamellae and it is very glauconitic and pyritized. The very fine grain size, argillaceous lamina and silica contribute significantly to the low permeability. However, it must be noted that silica overgrowths do not totally occlude pore space and the main cause of poor permeability in the sample is fine grained size.

Plate 4.3 (A): PPL

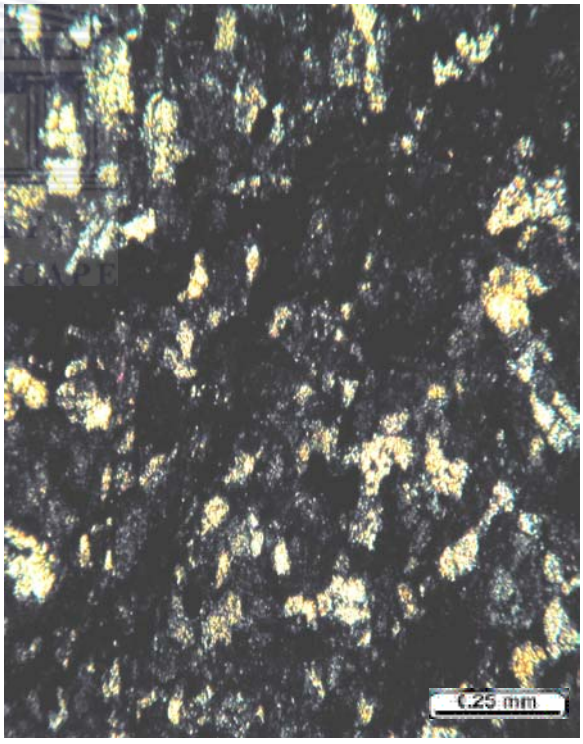

Plate 4.3 (B): XPL

PLATE 4.3 (A& B): E-AA1, 3074.26-.45, X4 MAG.

4.1.1.1.1.5 PLATE 4.4 (A & B): E-AA1, 3075.92-6.11, X4 MAG.

The grain sizes range from very fine to fine (0.0625-0.25) and occasionally medium grain (0.5) and it is moderately sorted, with a permeability of 63 mD and porosity of 16%. The grain shape rounded to subangular. It is very lithic, argillaceous with presence of glauconite and pyrite. Dolomite and siderite appear to replace glauconite but calcite and silica occur as cement. Note the absence of clays in the sample which results in a noticeable improvement in permeability. Abundant lithic grains have resulted in the formation of a pseudomatrix during burial and compaction and in the formation of secondary porosity by grain dissolution. There are small colourless crystals in the pores; they have parallel extinction (because crystallographic axes and indicatrix axes coincide). The high porosity is probably due to these pores, possibly secondary porosity.

Plate 4.4 (A): PPL

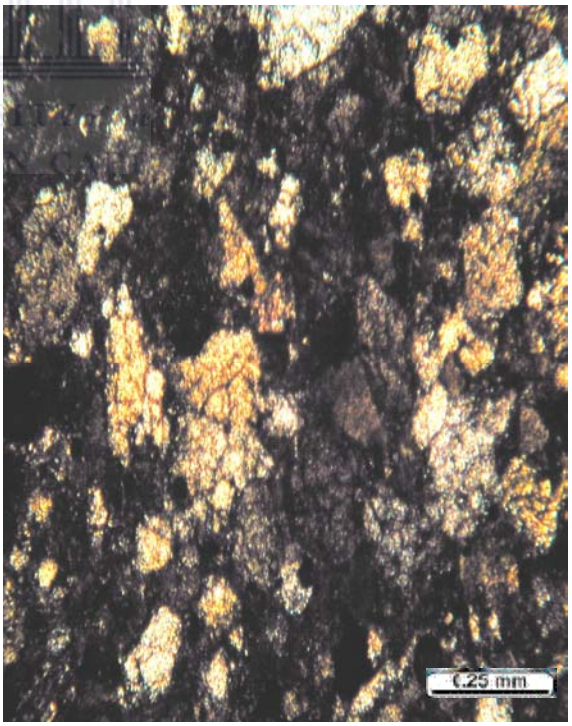

Plate 4.4 (B): XPL

PLATE 4.4 (A & B): E-AA1, 3075.92-6.11, X4 MAG.

4.1.1.1.1.6 PLATE 4.5 (A & B): E-AA1, 3076.91-7.08, X4 MAG.

This section chosen from the poor poroperm region (Figure3.11) with porosity (1.1%) and permeability (0.02mD). It is composed of fine to medium grains (0.25-0.5), well sorted, and tightly packed with rounded to subangular grains. It appears to be very clayey-little texture. The small grains are illite-with lath morphology and high birefringence, but might be carbonate cement, the field is dark under crossed polars, suggesting silica and not carbonate. In reflected light, the pyrite is framboidal, also seems to be replacement of amorphous grains. Glauconite (patchy) and detrital grains (quartz) also appear under reflected light. Calcite, typically of early cementation, occurs patchily and is responsible for the extremely low permeability. Local horizons, cemented by iron rich carbonate, contribute to the extremely low porosity and permeability values. The fracture visible may act as a component of principal flow barrier or baffles.

Plate 4.5 (A): PPL

Plate 4.5 (B): XPL

PLATE 4.5 (A & B): E-AA1, 3076.91-7.08, X4 MAG.

4.1.1.1.2 THIN SECTION PETROGRAPHIC DESCRIPTION FOR WELL E-CA1

4.1.1.1.2.1 PLATE 4.6 (A & B): E-CA, 2784.03, X10 MAG.

This section is clean predominantly fine grained (0.0625-0.25), well sorted, loose packing and grains are round - subrounded. Glauconitic, felspathic and lithic, with clays and metaquartzite clasts. Mica and carbonaceous material are fairly common, and shell fragments are locally preserved. Traces of pyrite overgrowths are developed throughout and the glauconite and clay clasts are commonly deformed to form pseudomatrix. The sample is pervasively cemented by ferroan dolomite, possibly as a result of edge-effect diagenesis. The euhedral lath in the centre is calcite (plate 4.6B XPL).

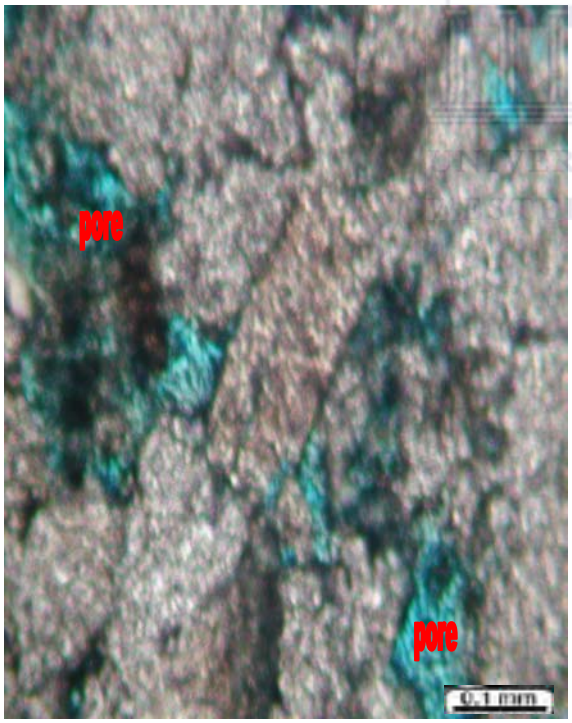

Plate 4.6 (A) PPL

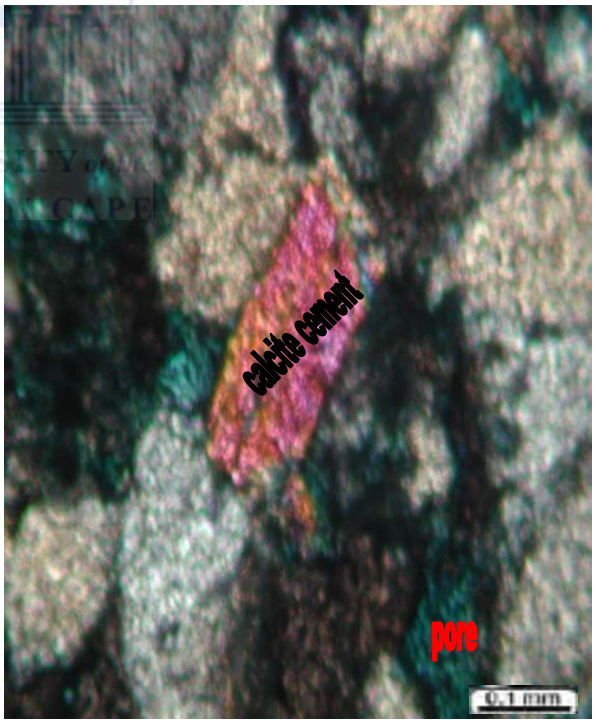

Plate 4.6 (B) XPL

PLATE 4.6 (A & B): E-CA, 2784.03, X10 MAG.

4.1.1.1.2.2 PLATE 4.7 (A & B): E-CA1, 2901.13, X4 MAG.

The sample is clean, moderately sorted and fine to medium grained (0.125-0.5mm). It is glauconitic, lithic to very lithic with clay clasts, feldspathic and slightly carbonaceous and micaceous. Carbonate material is concentrated in stylolitised streaks at the centre (a stylolite is a surface or contact, that is marked by an irregular, interlocking penetration of two sides. These are thought to be formed diagenetically by differential movement under pressure, accompanied by solution).Porosity is secondary, after dissolution of intergranular cement and detrital grains. Quartz overgrowth is the main pore filling phase, with abundant kaolinite and illite. Pseudomatrix is commonly developed by compaction of glauconite and clay clasts. Traces of pyrite, feldspar overgrowths and siderite are also developed.

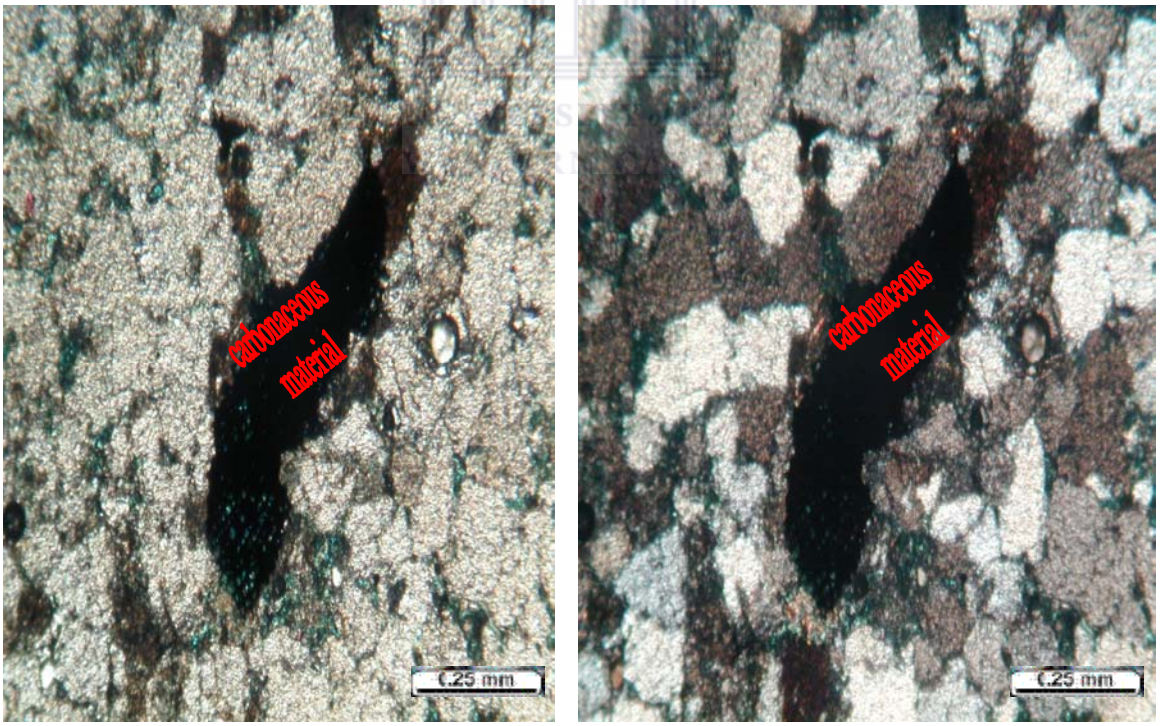

Plate 4.7 (A) PPL Plate 4.7 (B) XPL

PLATE 4.7 (A & B): E-CA1, 2901.13, X4 MAG.

4.1.1.1.2.3 PLATE 4.8 (A & B), E-CA1, 2927.08, X4 MAG.

The specimen is moderately sorted, and medium grained, lithic and glauconitic, with slightly tighter packing. The porosity characteristics of this sample are fair to moderate (average 9.9% and 10.15mD). Minor (3%) amount of mica and carbonaceous material are present. Very minor (1.5%) amount of authigenic feldspar and pyrite are also developed. Quartz overgrowth and ferroan dolomite are the most abundant pore filling cements.

Plate 4.8 (A) PPL

Plate 4.8 (B) XPL

PLATE 4.8 (A & B), E-CA1, 2927.08, X4 MAG.

4.1.1.1.2.4 PLATE 4.9 (A & B), E-CA1, 2928.05, X4 MAG.

The section comprises argillaceous, poorly sorted, very fine to fine grained. Kaolinite is the most abundant authigenic clay mineral, occurring as common pore filing aggregates. Illite is common as grain alteration product throughout. Microporosity is associated with these authigenic clays, and locally, oil staining of kaolinite aggregates is visible ((A), top RHS). Alterations of glauconite clasts "G" are present (B). It is a very lithic, feldspathic, and slightly carbonaceous and micaceous.

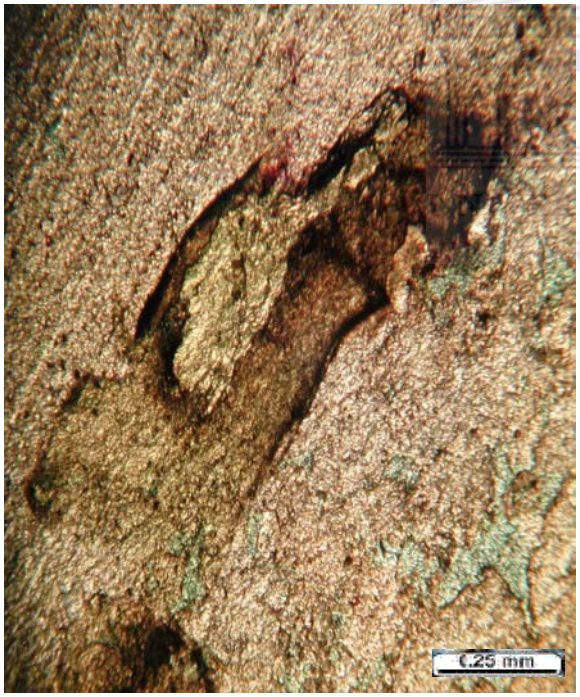

Plate 4.9 (A) PPL

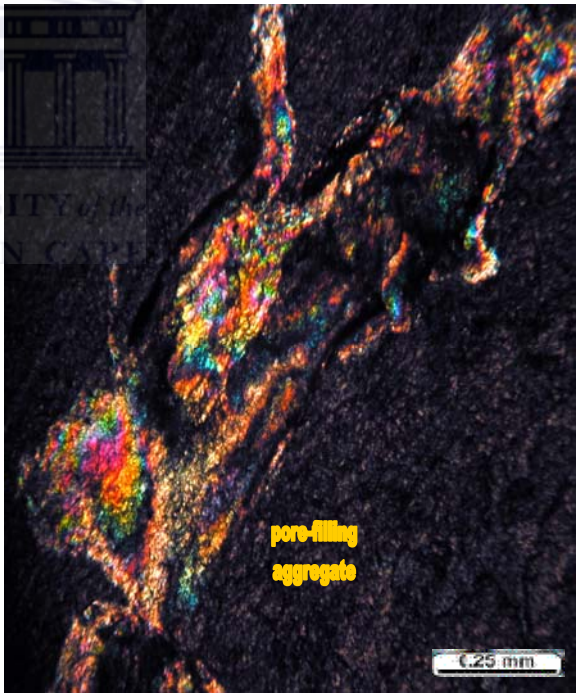

Plate 4.9 (B) XPL.

PLATE 4.9 (A & B), E-CA1, 2928.05, X4 MAG.

4.1.1.1.2.5 PLATE 4.10 (A & B), E-CA1, 2930.04, X10 MAG.

The section comprises of moderately sorted, fine to coarse grained, slightly loose packing and slightly carbonaceous and micaceous. The dark regions are probably hydrocarbons with much lower content. There small colourless crystal in the pores, they have parallel extinction. Poroperm characteristics are poor, due to quartz overgrowth cementation and detrital clays, producing microporosity and reducing permeability. Pseudomatrix and feldspar overgrowth are present throughout, but are not abundant enough to significantly affect poroperm characteristics.

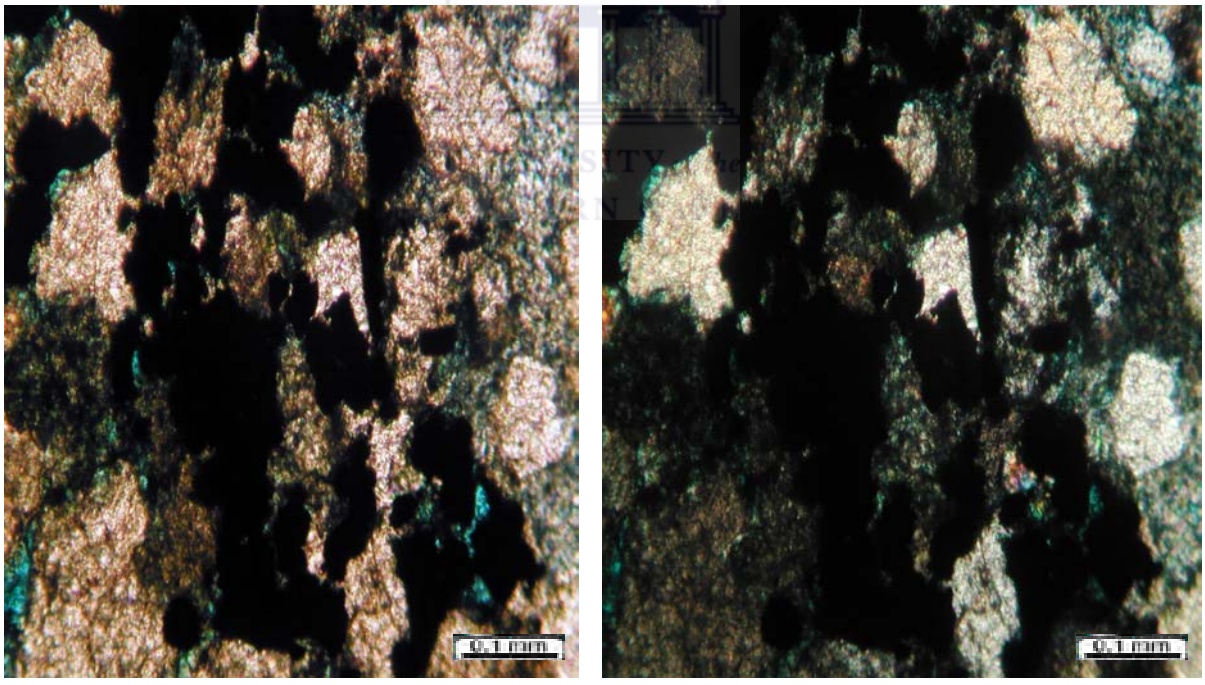

Plate 4.10 (A) PPL Plate 4.10 (B) XPL

PLATE 4.10 (A & B), E-CA1, 2930.04, X10 MAG.

4.1.1.1.2.6 PLATE 4.11 (A & B), E-CA1, 2981.01, X10 MAG.

This sample is predominantly medium grained and moderately sorted. Slightly loose packing, glauconitic and lithic. Minor amounts of mica and carbonaceous material are present. The pyrite appears to be spherical but not framboidal. The matrix between the grains contains opaque iron oxide and some calcite (B, XPL), the latter shows high-order interference colours of pink and green. Cementation extensively reduces intergranular porosity and permeability. Microporosity associated with authigenic clays may have significant permeability reducing effect.

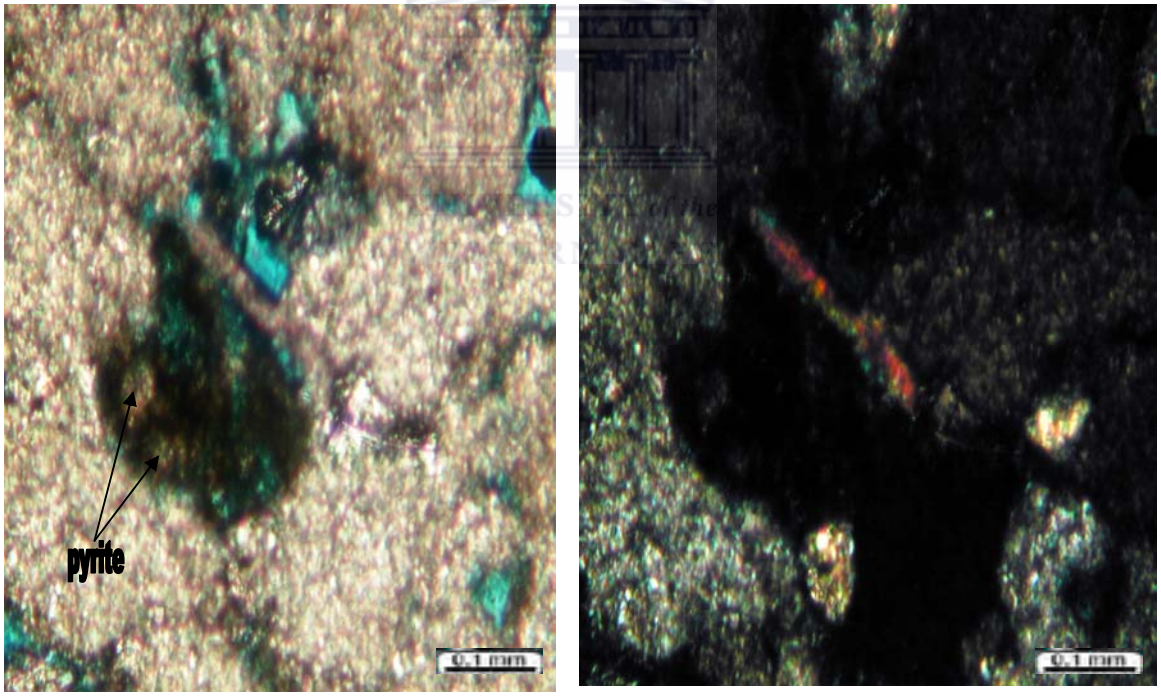

Plate 4.11 (A) PPL Plate 4.11 (B) XPL.

PLATE 4.11 (A & B), E-CA1, 2981.01, X10 MAG.

4.1.1.1.2.7 PLATE 4.12 (A & B), E-CA1, 2982.95, X10 MAG.

A very fine to medium grained, poorly sorted, tight packing and lithic, composed of 50 % quartz and 30-40% of rock particles, both compacted and partially dissolved rock fragments. Some porosity is microporosity due to partial dissolution of rock fragments. The sample also contains glaucinite which may be altered to pseudomatrix, which probably affect porosity and permeability. Authigenic cements include silica overgrowths and intergranular cement. The shape of original detrital particles is not visible where overgrowths are present. Calcite cement postdates the quartz overgrowth and infill pores.

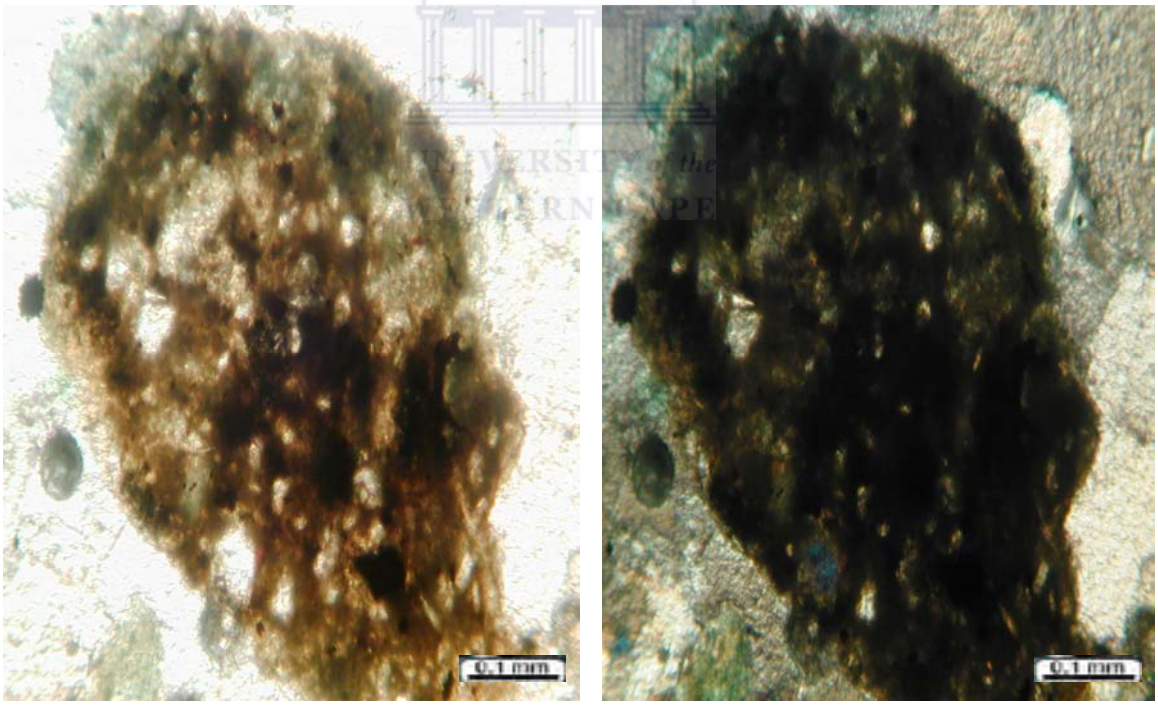

Plate 4.12 (A) PPL Plate 4.12 (B) XPL

PLATE 4.12 (A & B), E-CA1, 2982.95, X10 MAG.

4.1.1.1.2.8 PLATE 4.13 (A & B), E-CA1, 3211.89, X4 MAG.

A predominantly argillaceous, poorly sorted, tight packing, consisting of rounded – subrounded quart grains, silty to fine grained. Quartz grains form nearly one-third of the framework. Minor amount of lithic clasts, shell debris and glaucinite, and carbonaceous laminations are present in places. The latter are pervasively cemented by quartz overgrowths, illite, ferroan dolomite and calcite. Porosity characteristics are very poor, average 9.8% porosity and 0.06mD permeability, mainly due to the presence of intergranular detrital clays, and to a lesser extent quartz cementation and pseudomatrix development. Argillaceous content could probably be the predominant cause of poor poroperm characteristics, in addition to pseudomatrix that may affect poroperm slightly. Minor ferroan (Fe-rich variety) dolomite, ferroan calcite and pyrite are present.

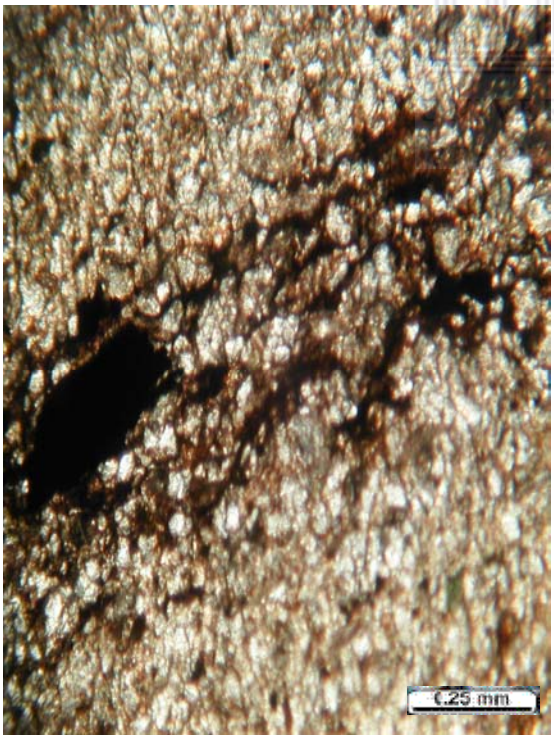

Plate 4.13 (A) PPL

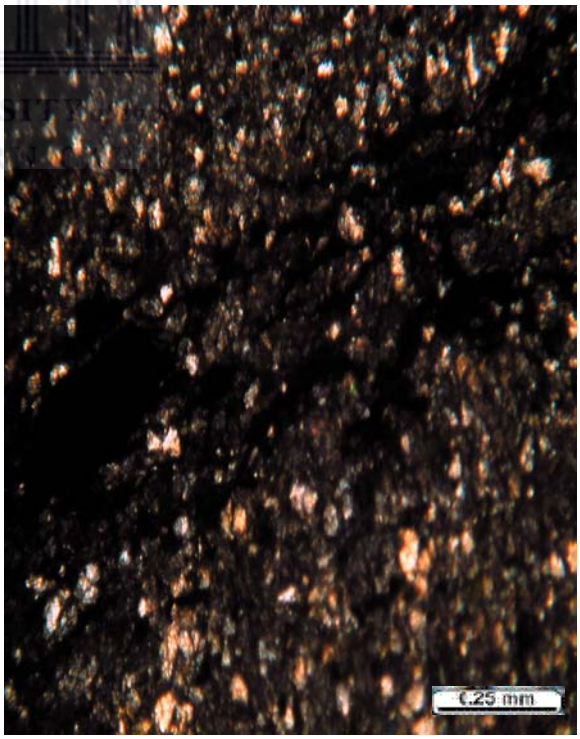

Plate 4.13 (B) XPL.

PLATE 4.13 (A & B), E-CA1, 3211.89, X4 MAG.

4.1.1.1.3 THIN SECTION PETROGRAPHIC DESCRIPTION FOR WELL E-AR1

4.1.1.1.3.1 PLATE 4.14 (A & B), E-AR1, 2455.96-2456.03, X4 MAG.

A moderately sorted, fine to medium grained, comprising of loose packing and rounded grains. It is glauconitic, lithic, with carbonaceous material present. Clay lamellae are present. This section is porous and the pores are interconnected. The porosity type observed is secondary, after grain and cement dissolution. Cementing material include calcite cement and quartz overgrowths, that slightly affects poroperm. Poroperm characteristics are very good, with porosity of 16.6% and permeability of 272mD.

Plate 4.14 (A) PPL

Plate 4.14 (B) XPL.

PLATE 4.14 (A & B), E-AR1, 2455.96-2456.03, X4 MAG.

4.1.1.1.3.2 PLATE 4.15 (A & B), E-AR1, 2456.59-.71, X4 MAG.

A well sorted, medium to coarse grained, comprising of very loose packing and rounded grains. It is glauconitic, slightly lithic and feldspathic. Pores are highly interconnected, with secondary porosity. Quartz overgrowths and calcite cement present do not completely occlude the pores. Poroperm characteristics are very good, comprising of 19.3% porosity and permeability of 417mD.

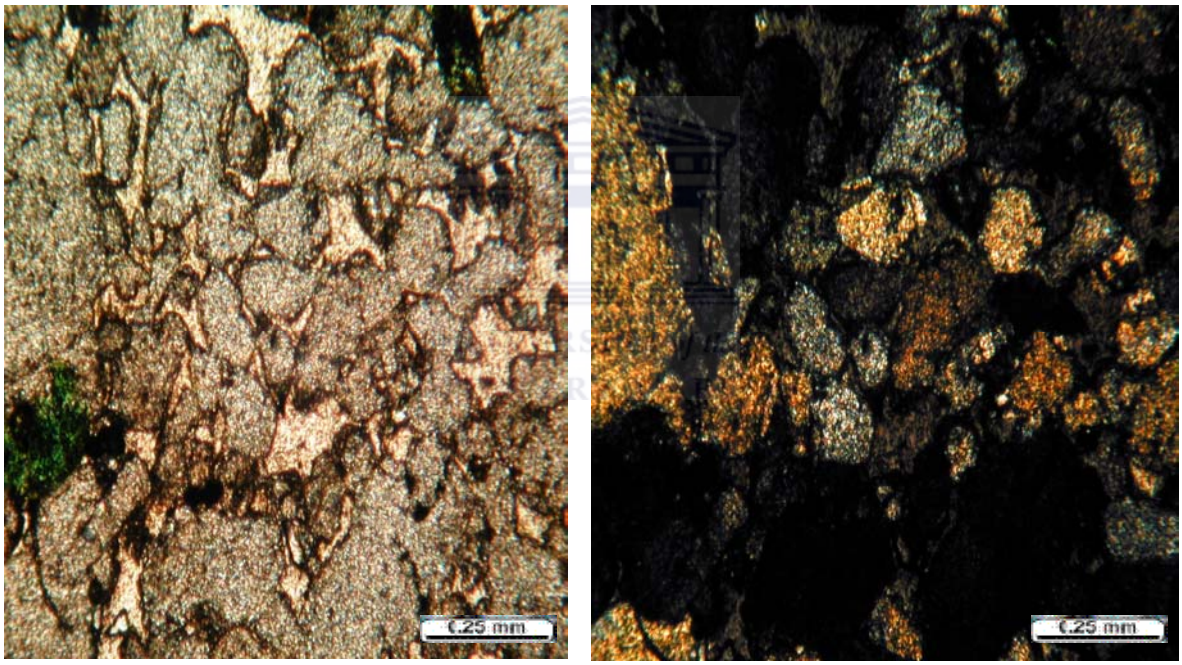

Plate 4.15 (A) PPL Plate 4.15 (B) XPL

PLATE 4.15 (A & B), E-AR1, 2456.59-.71, X4 MAG.

4.1.1.1.3.3 PLATE 4.16 (A & B), E-AR1, 2459.31-.43, X4 MAG.

Moderately sorted, very fine to medium grained section, comprising of slightly loose packing, with subrounded to subangular grains. Poroperms are moderate, with 13% porosity and permeability of 25mD. Porosity types are secondary and microporosity, after detrital cement and grain dissolution. Grain dissolution and alteration is visible. Secondary porosity probably developed, after the leaching of early carbonate cement, but could have also been reduced by extensive quartz overgrowth cementation. Ferroan dolomite that may have developed as an alteration/grain solution product could also have significant porosity and permeability reducing effects. Grain alteration might have produced minor amounts of illite, chlorite and kaolinite, which can slightly affect porosity and permeability.

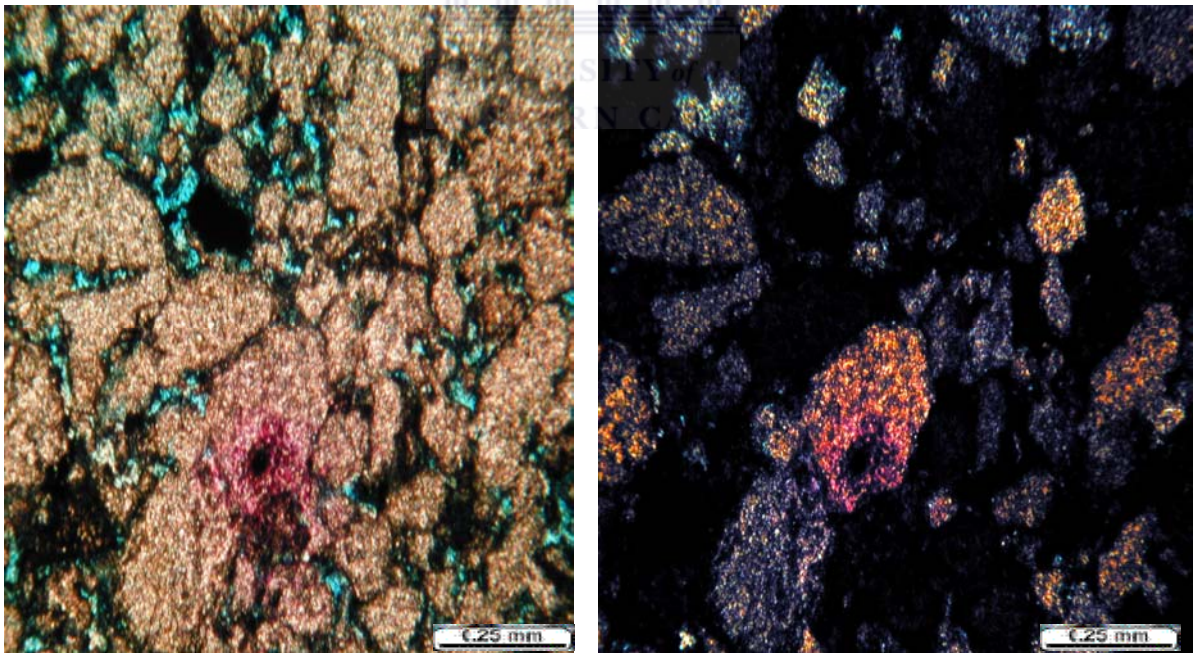

Plate 4.16 (A) PPL Plate 4.16 (B) XPL

PLATE 4.16 (A & B), E-AR1, 2459.31-.43, X4 MAG.

4.1.1.1.3.4 PLATE 4.17 (A & B), E-AR1, 2465.30, X4 MAG.

A slightly argillaceous, fine to medium grained, moderately sorted, with rounded grains. It is lithic, carbonaceous, slightly glauconitic and pyritised. Poroperm characteristics are moderate to good, with porosity of 16% and permeability of 64mD. Porosity deteriorates due to increased amounts of quartz overgrowths, ferroan calcite cement, pseudomatrix and the presence of detrital clays (possibly kaolinite). Isolated secondary porosity present has been reduced to microporosity by clays.

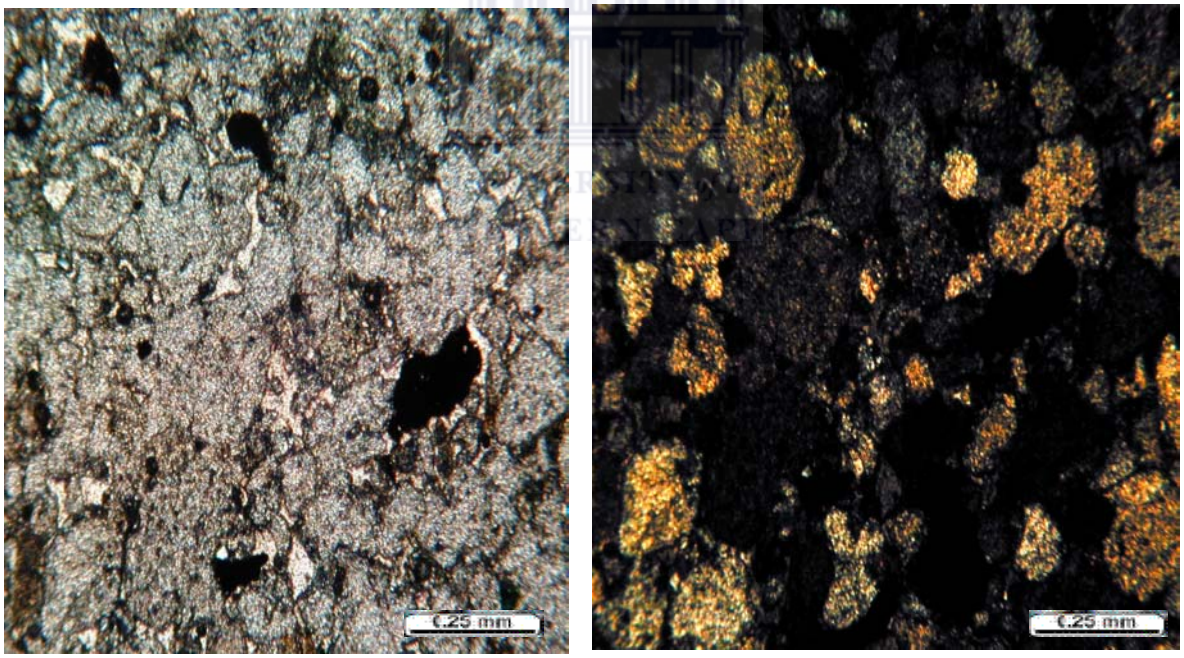

Plate 4.17 (A) PPL Plate 4.17 (B) XPL

PLATE 4.17 (A & B), E-AR1, 2465.30, X4 MAG.

4.1.1.1.3.5 PLATE 4.18: E-AR1, 3212.95-3213.19, X4 MAG.

Poorly sorted, argillaceous, lithic, contains glauconite and shell fragments. It has moderate but poorly interconnected secondary porosity, isolated by quartz cements and pseudomatrix, and commonly reduced to microporosity by authigenic kaolinite and illite/chlorite. Poroperms are poor, 8.7% porosity and 0.04mD permeability.

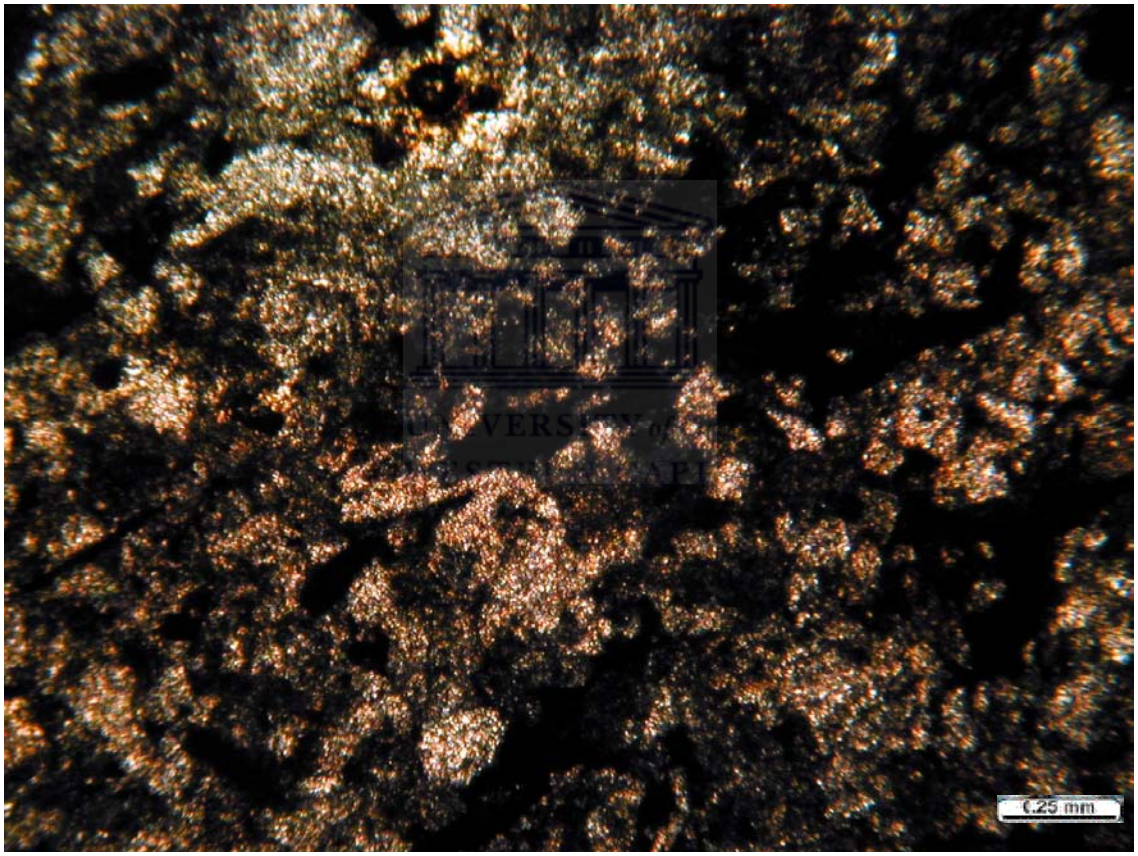

Plate 4.18: PPL

PLATE 4.18: E-AR1, 3212.95-3213.19, X4 MAG.

4.1.1.1.3.6 PLATE 4.19 XPL, E-AR1, 3215.28-.45, X4 MAG.

It is slightly argillaceous, poorly sorted and very fine to fine grained. Glauconite, Carbonaceous material and litho— clasts are all common. Lithic grains include clay lamellae/clasts. Chloritised micas are also present. Poroperm characteristics are poor, with porosity of 7.8% and permeability of 0.01mD, due to extensive cementation by quartz overgrowths and dolomite. Detrital clays and authigenic illite also reduce porosity and permeability to a lesser extent. Only minor secondary porosity was observed.

Plate 4.19 XPL

PLATE 4.19 XPL, E-AR1, 3215.28-.45, X4 MAG.

4.1.1.1.4 THIN SECTION PETROGRAPHIC DESCRIPTION FOR WELL E-BA1

4.1.1.1.4.1 PLATE 4.20 (A & B), E-BA1, 2828.00-.12, X4 MAG.

A fine to medium grained, moderately to well sorted, loose packing with rounded grains, glauconitic, and locally shelly and carbonaceous. Stylolitised carbonaceous streaks are present in places. The vugs are filled with clays that slightly affect porosity and permeability. The pores are connected, hence, increase in permeability. Secondary porosity developed by dissolution of early diagenetic cement and detrital grains. Quartz overgrowth and dolomite euhedral are the most abundant pore filling cements. Kaolinite is abundant and reduces secondary porosity to microporosity. Dark brown oil residue is visible in places. Mud clasts are found in pores. It has a clay-to-mud matrix with very fine grains of quartz. A pore, to the immediate left of the clasts is observed with a gas bubble probably from the mounting medium. The mud clasts are seen being partially dissolved, as in the immediate left of the pore in (A). Most of the view in XPL is dark brown to black as most quartz grains are extinct and pore with the mud stays black.

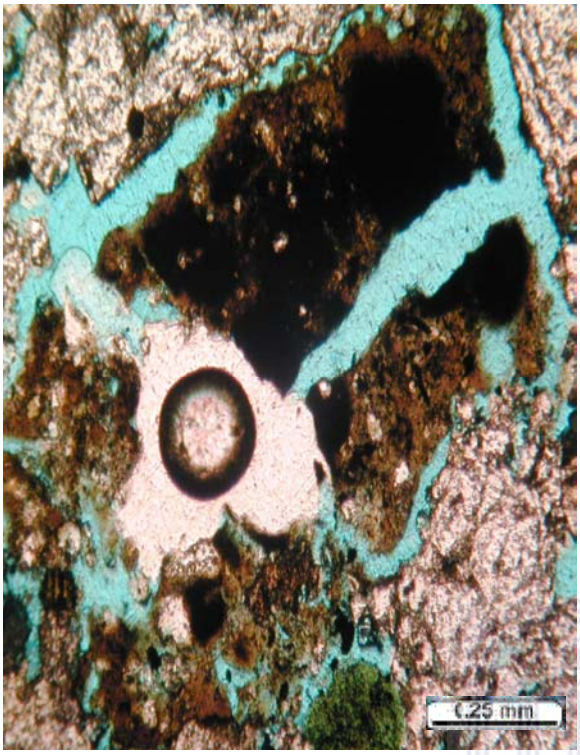

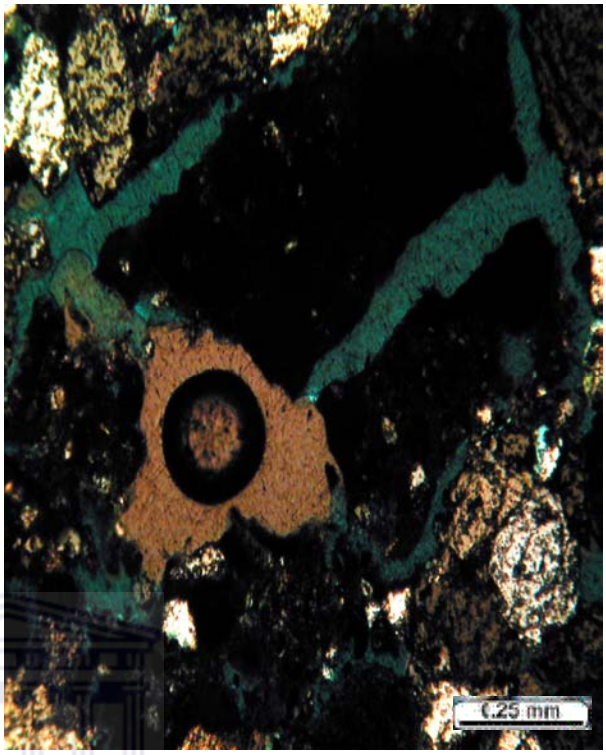

Plate 4.20 (A) PPL Plate 4.20 (B) XPL

PLATE 4.20 (A & B), E-BA1, 2828.00-.12, X4 MAG.

4.1.1.1.4.2 PLATE 4.21 (A & B), E-BA1, 2833.89-.98, X4 MAG.

A moderately sorted, silty to fine grained, with tight packing, consisting of subangular to angular grains. Glauconitic, lithic, pyritised, micaceous, with clay clast and argillaceous laminae. Poroperm characteristics are poor due to pervasive quartz cementation, the development of pseudomatrix, and the presence of argillaceous laminae.

Plate 4.21 (A) PPL

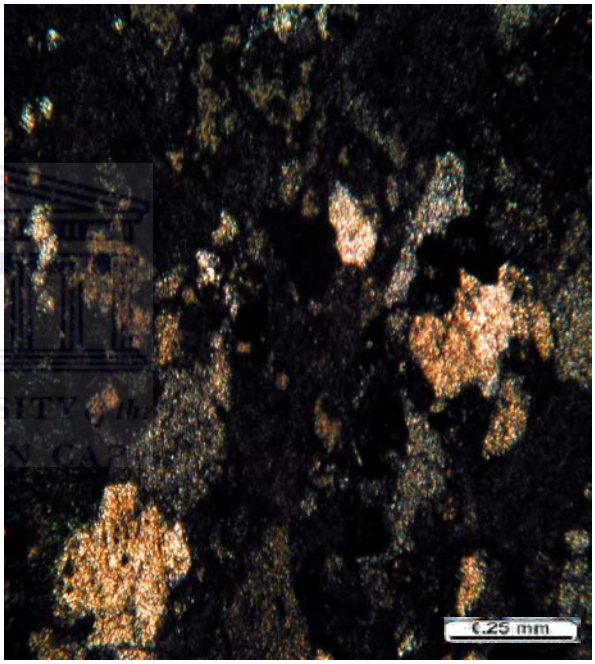

Plate 4.21 (B) XPL.

PLATE 4.21 (A & B), E-BA1, 2833.89-.98, X4 MAG.

4.1.1.1.4.3 PLATE 4.22 (A & B), E-BA1, 2834.08-.17, X4 MAG.

A very lithic, glauconitic, consisting of fine to coarse grained, moderately sorted, with round to subrounded grains, and slightly tight packing. Carbonaceous, with minor amount of poikilotopic calcite and pyrite develop in most areas. Calcite/ dolomite cementation has occurred, resulting in more drastic reduction of porosity and permeability. Porosity is patchily secondary porosity and microporosity. The vugs are filling clay (kaolinte), quartz overgrowth and dolomite and calcite are the main cause of permeability and porosity reduction.

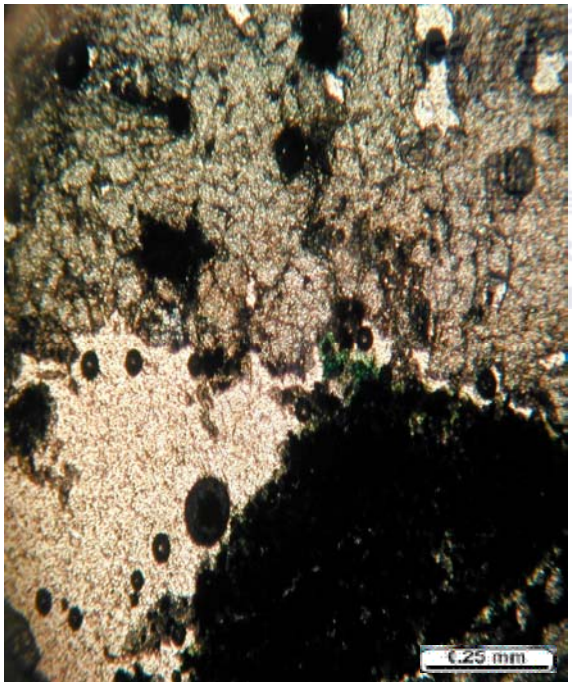

Plate 4.22 (A) PPL

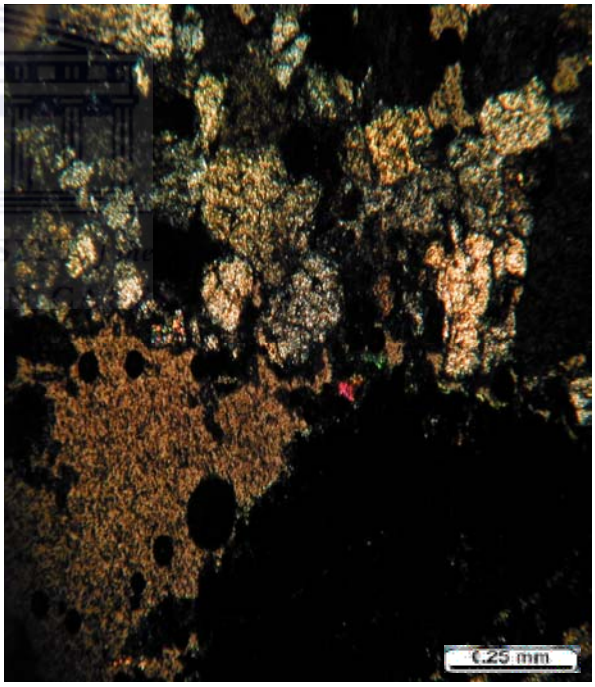

Plate 4.22 (B) XPL

PLATE 4.22 (A & B), E-BA1, 2834.08-.17, X4 MAG.

4.1.1.1.4.4 PLATE 4.23 (A & B), E-BA1, 2839.00-.15, X4 MAG.

This section is moderately sorted, very fine to medium, occasionally coarse grains, with slightly loose packing, rounded grains and pores slightly connected. The section contains both quartz and dolomite cements. The quartz cement is in the form of overgrowths on detrital grains, evident by the euhedral terminations seen on some grains. Quartz lamination/granular seam visible could also act as components of principal flow barriers or baffles. Quartz overgrowth and dolomite cement are the main cause of porosity and permeability reduction. Permeability is most significantly lower probably as a result of the more extensive development of microporous kaolinite.

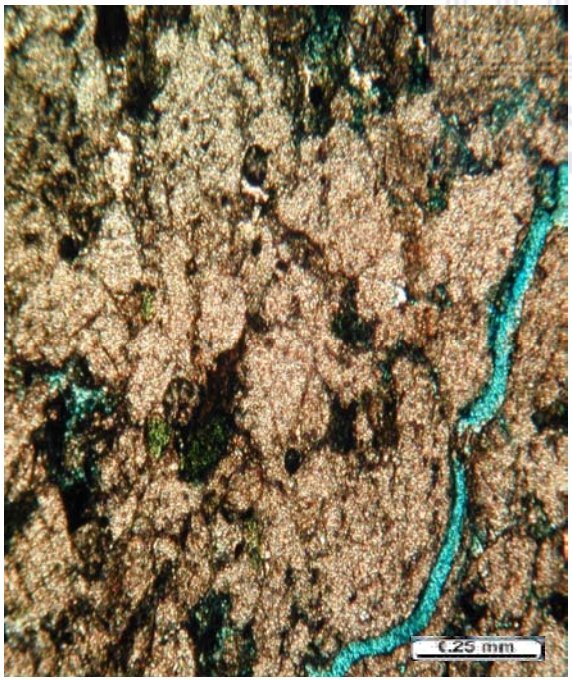

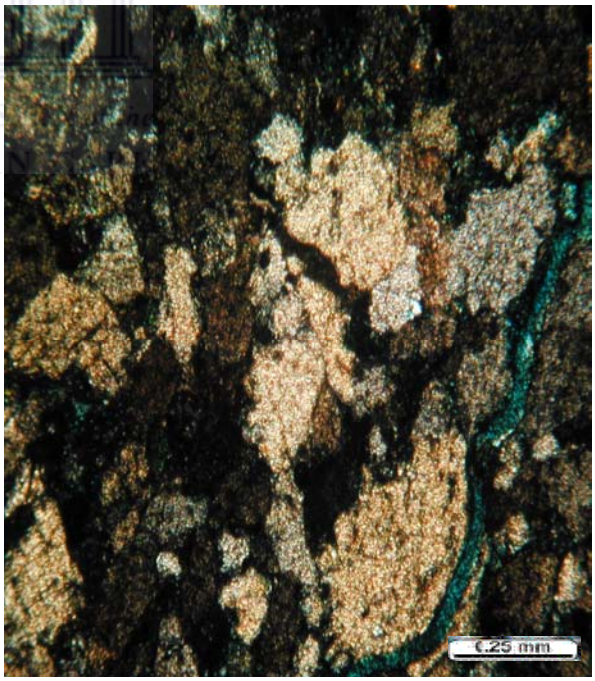

Plate 4.23 (A) PPL Plate 4.23 (B) XPL

PLATE 4.23 (A & B), E-BA1, 2839.00-.15, X4 MAG.

4.1.1.1.4.5 PLATE 4.24 (A & B), E-BA1, 2842.96-2843.09, X4 MAG.

A fine to coarse grained, moderately sorted, comprising of loose packing, rounded to subrounded grains with partially connected pores. It is glauconitic, slightly lithic and feldspathic, and locally contains micas and carbonaceous material. Residual dark brown oil spots are visible in places. Quartz overgrowth and dolomite affects porosity and permeability and kaolinite slightly affects porosity and permeability probably because the pores are not completely occluded.

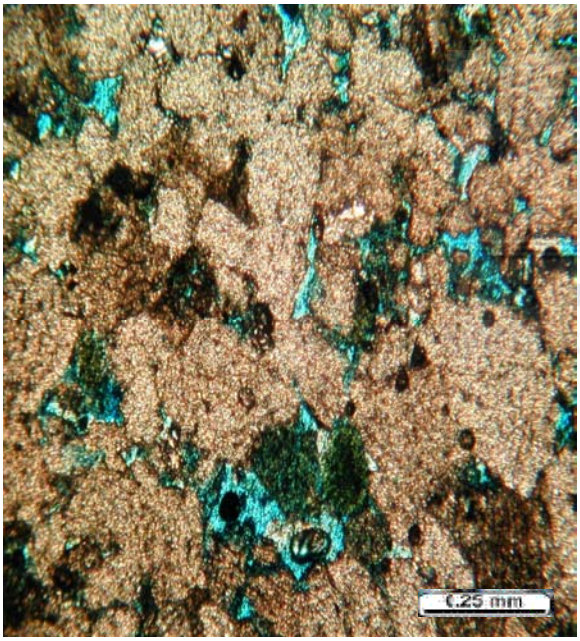

Plate 4.24 (A) PPL

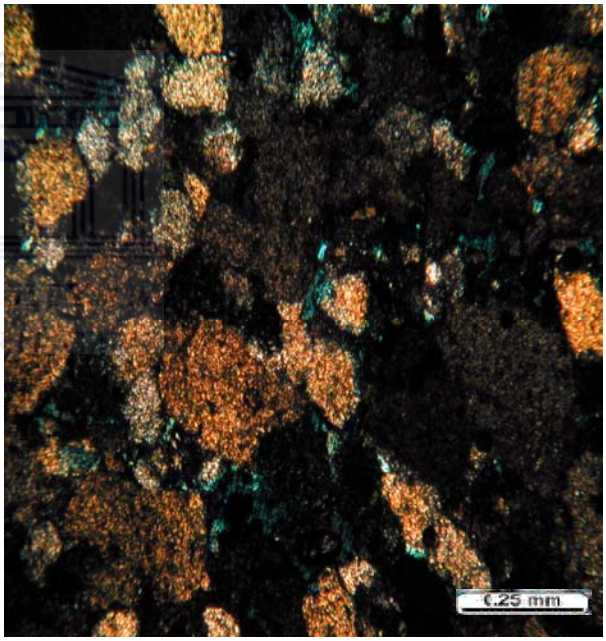

Plate 4.24 (B) XPL

PLATE 4.24 (A & B), E-BA1, 2842.96-2843.09, X4 MAG.

4.1.1.1.5 THIN SECTION PETROGRAPHIC DESCRIPTION FOR WELL E-AO1

4.1.1.1.5.1 PLATE 4.25 (A & B), E-AO1, 2674.00-.10, X4 MAG.

A clean, very fine to medium grained, shelly, glauconitic section, moderately sorted, comprising of rounded to subrounded grains, with loose packing of grains. Porosity and permeability are very good, with 16.1% porosity and permeability of 106.44mD. Quartz and calcite/dolomite cements appear in minor amounts at this depth. Preserved porosity is secondary, after cement and grain dissolution. There is alteration of glauconite, and there is also minimal amount of pore filling cements and clays.

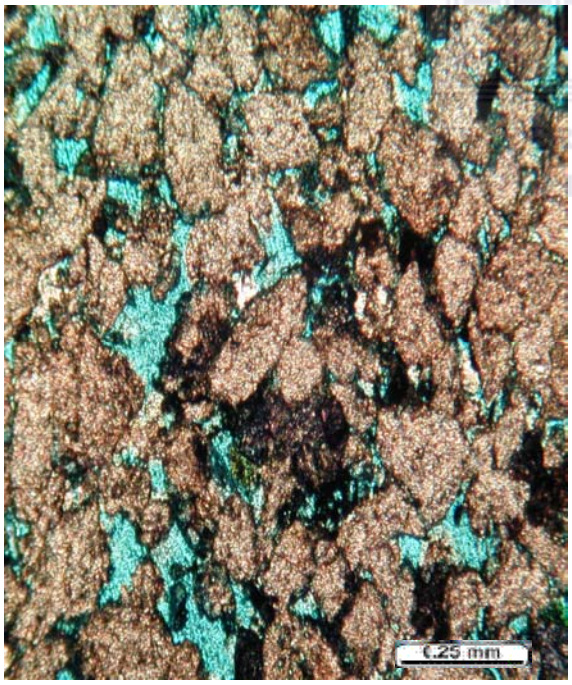

Plate 4.25 (A) PPL

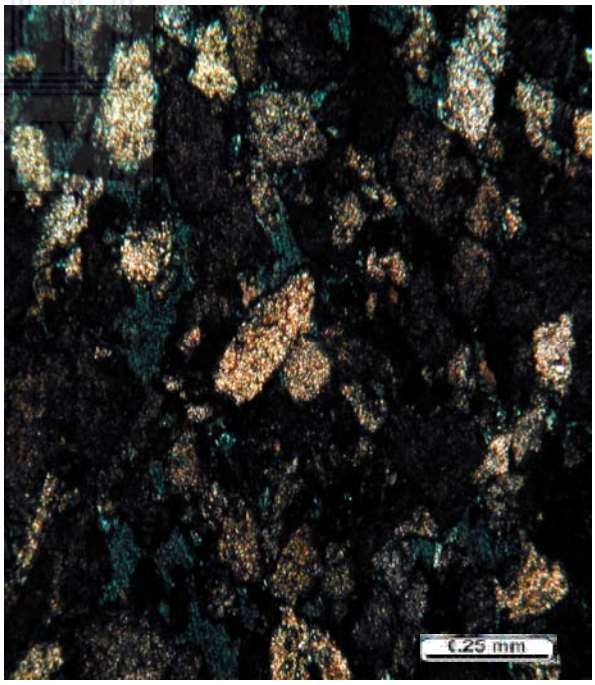

Plate 4.25 (B) XPL

PLATE 4.25 (A & B), E-AO1, 2674.00-.10, X4 MAG.

4.1.1.1.5.2 PLATE 4.26 (A & B), E-AO1, 3016.25-.45, X4 MAG.

Very fine to medium grained, Iithic, glauconitic sample. Sorting is poor to moderate, with 11-12% porosity and permeability of 6.76-7.43mD. Porosity is secondary, after grain and, to a lesser degree, cement dissolution. Quartz overgrowths and calcite and dolomite cement infill most primary porosity resulting in the secondary pores being poorly interconnected. Kaolinite and illite are the only clay minerals present. Kaolinite infill secondary vugs and illite is developed by grain alteration and, to a lesser extent, as grain coatings. Fe-rich carbonate cements and pyrite are the only potentially reactive minerals observed.

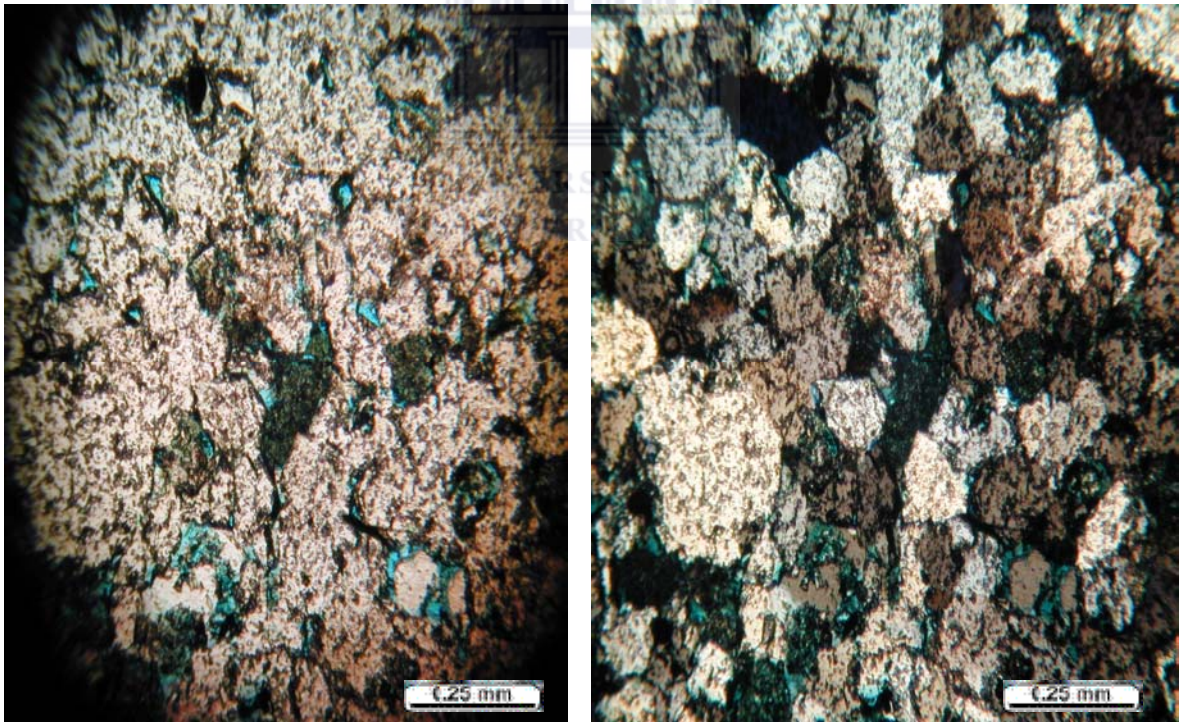

Plate 4.26 (A) PPL Plate 4.26 (B) XPL

PLATE 4.26 (A & B), E-AO1, 3016.25-.45, X4 MAG.

4.1.1.1.5.3 PLATE 4.27 (A & B), E-AO1, 3017.26-.46, X4 MAG.

The sample is poorly to moderately sorted, comprising of very fine to fine grains, clean, Iithic and glauconitic, with porosity of 7-10% and permeability of 1.49-2.94mD. Porosity and permeability are generally poor due to extensive quartz and, locally, calcite cementation, and pseudomatrix development. Porosity is secondary after cement and grain dissolution. Late developed kaolinite reduces secondary pores to microporosity in places.

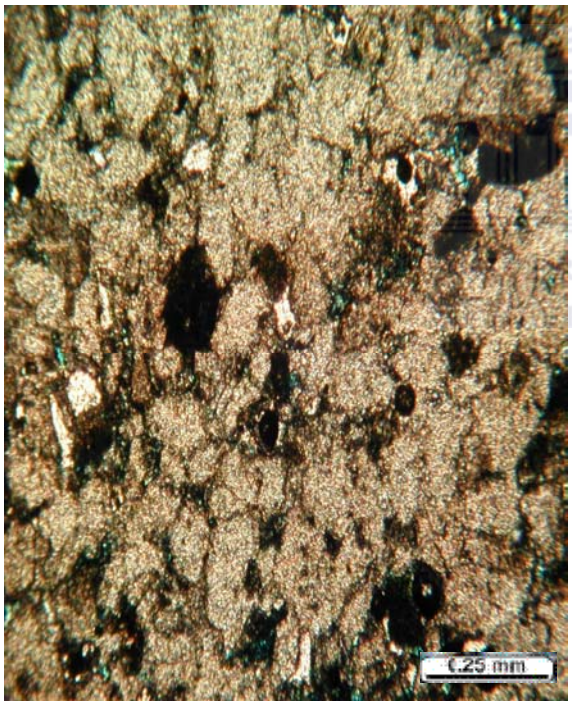

Plate 4.27 (A) PPL

Plate 4.27 (B) XPL

PLATE 4.27 (A & B), E-AO1, 3017.26-.46, X4 MAG.

4.1.1.1.5.4 PLATE 4.28 (A & B), E-AO1, 3252.00-.25, X4 MAG.

The sample is poorly sorted, silty to coarse grained, lithic, and commonly argillaceous. Porosity and permeability are poor, mostly due to clays. Detrital clays (where present) and pseudomatrix are the main clay types, but authigenic kaolinite and chlorite are developed in minor amounts. In clean sandstones quartz cementation has extensively reduced primary porosities. Most of the porosity observed is isolated and secondary, after grain dissolution, and is commonly reduced to microporosity by clays. Argillaceous, poorly sorted lithic sandstone, composed of detrital clays and pseudomatrix, of illite composition, infill all intergranular areas. Porosity and permeability are very poor due to the clay-rich nature of the sandstone,

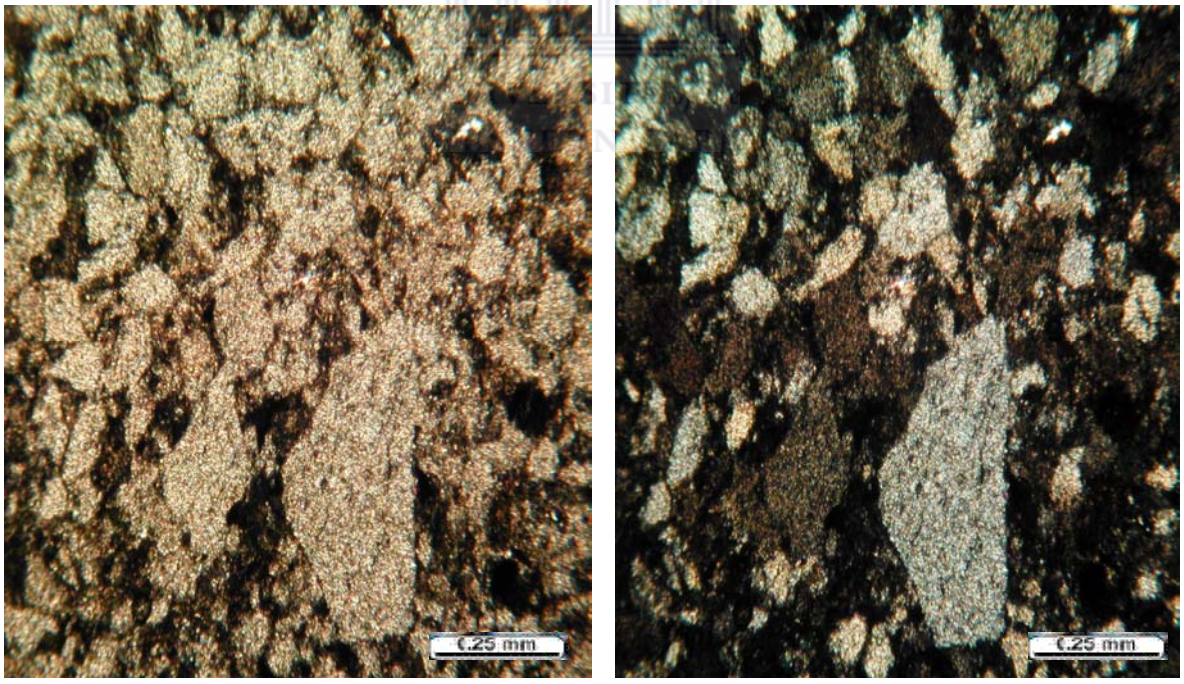

Plate 4.28 (A) PPL Plate 4.28 (B) XPL

PLATE 4.28 (A & B), E-AO1, 3252.00-.25, X4 MAG.

4.1.1.1.6 THIN SECTION PETROGRAPHIC DESCRIPTION FOR WELL E-BB1

4.1.1.1.6.1 PLATE 4.29 (A & B), E-BB1, 2544.05, X4 MAG.

This section comprises clean, well sorted, very fine to fine grained, and loose packing, with rounded to angular grains. It is very lithic, glauconitic, micaceous and slightly shelly and carbonaceous. Moderate secondary porosity is developed by cement and grain dissolution, with 13.2 % porosity, and 2.7mD permeability recorded by core analysis. Porosity is significantly reduced by quartz overgrowths and compaction of claystone clasts to pseudomatrix. Laser amounts of etched ferroan calcite cement are also preserved. Permeability may probably been restricted by the development of authigenic clay (fibrous illite), thus producing microporosity.

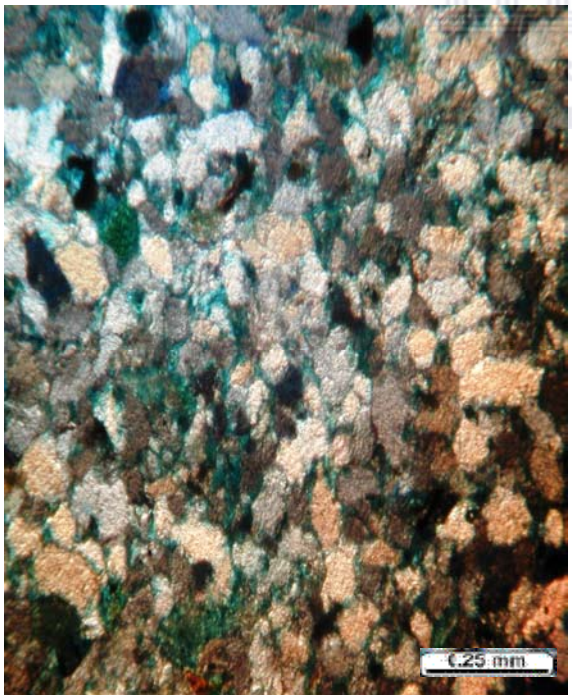

Plate 4.29 (A) PPL

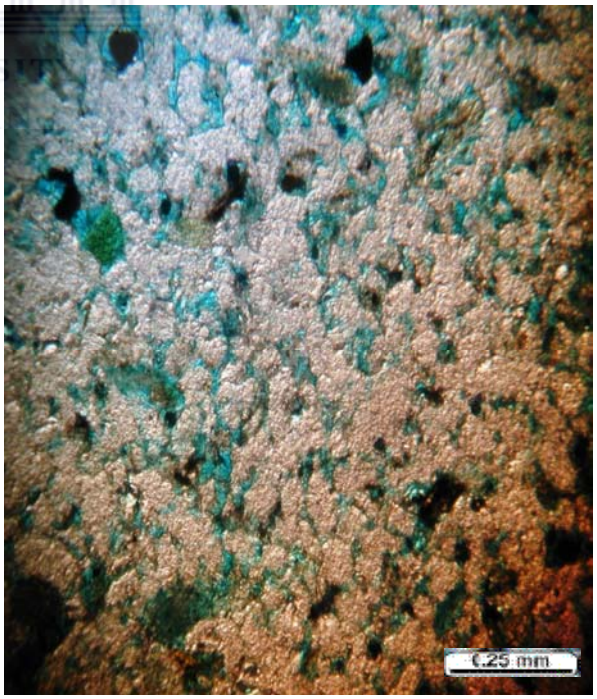

Plate 4.29 (B) XPL

PLATE 4.29 (A & B), E-BB1, 2544.05, X4 MAG.

4.1.1.1.6.2 PLATE 4.30 (A & B), E-BB1, 2552.51, X10 MAG.

A clean, well sorted, and very fine to fine grained and tight packing, with rounded to angular grains. It is lithic to very lithic (with clay clasts), glauconitic, micaceous, slightly carbonaceous and feldspathic. Carbonaceous streaks are stylolitised in places. Seen are remains of bivalve, echinoderm and foraminifera. Secondary porosity is patchily developed, probably after dissolution of calcite cement and quartz overgrowths also reduce porosity. Minor amounts of ferroan calcite, illite, pseudomatrix and trace of kaolinite occur in places. The average permeability is 0.05mD from core analysis result; this could be due to a resultant microporosity development and probably increase in abundance of fibrous illite, which is primarily responsible for this permeability.

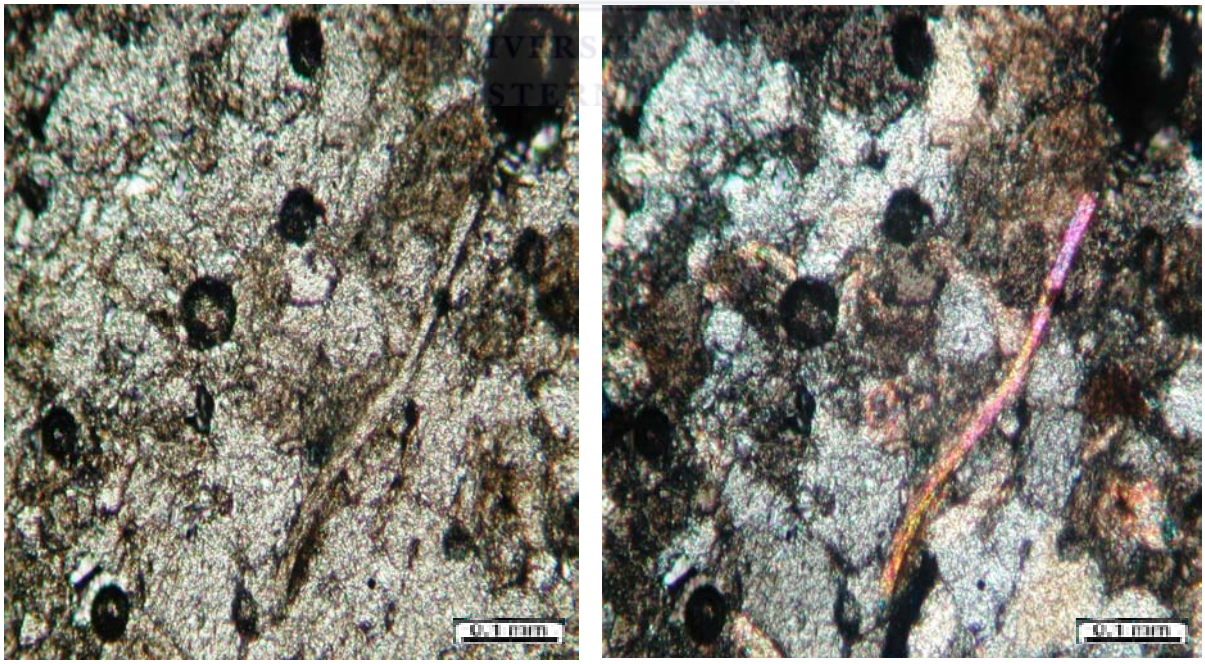

Plate 4.30 (A) PPL Plate 4.30 (B) XPL

PLATE 4.30 (A & B), E-BB1, 2552.51, X10 MAG.

4.1.1.1.6.3 PLATE 4.31 (A & B), E-BB1, 2659.05, X4 MAG.

A moderately to well sorted, fine to medium grained, with loose packing and rounded to angular grain shape. It is glauconitic, lithic and shelly, with bivalve and echinoderm fragments. Minor feldspar, mica and carbonaceous material are also present. Grain and cement dissolution may result in the development of secondary porosity, which may also be reduced by pore filling quartz overgrowths and calcite cement. The calcite is etched, suggesting that it may be the precursor to secondary porosity. Grain alteration, may result to the development of fibrous illite, which may probably has reduced secondary porosity to microporosity, hence, resulting in reduced permeability. Generally, the poor porosity and permeability may be due pervasive calcite cementation, quartz overgrowths and probably fibrous authigenic illite.

Plate 4.31 (A) PPL

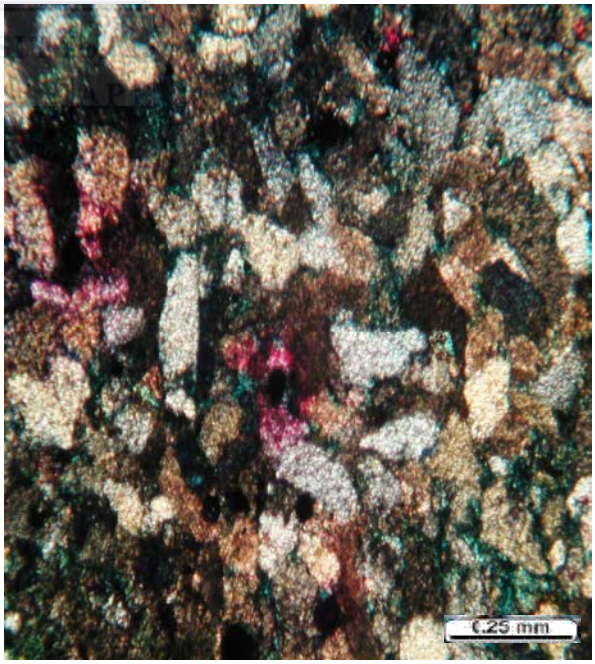

Plate 4.31 (B) XPL

PLATE 4.31 (A & B), E-BB1, 2659.05, X4 MAG.

4.1.1.1.6.4 PLATE 4.32 (A & B), E-BB1, 2660.05, X10 MAG.

A well sorted, very fine to fine, comprising of rounded to subangular grains, with tight packing. It is glauconitic, with lithic clasts, micaceous, and slightly carbonaceous and feldspathic. Shelly fragments of bivalve and foraminifera are abundant. Grain dissolution and alteration is visible. Secondary porosity probably developed, after the leaching of early carbonate cement, but could have also been reduced by extensive quartz overgrowth cementation. Ferroan dolomite that may have developed as an alteration/grain solution product could also have significant porosity and permeability reducing effects. Grain alteration might have produced minor amounts of illite, chlorite and kaolinite, which can slightly affect porosity and permeability.

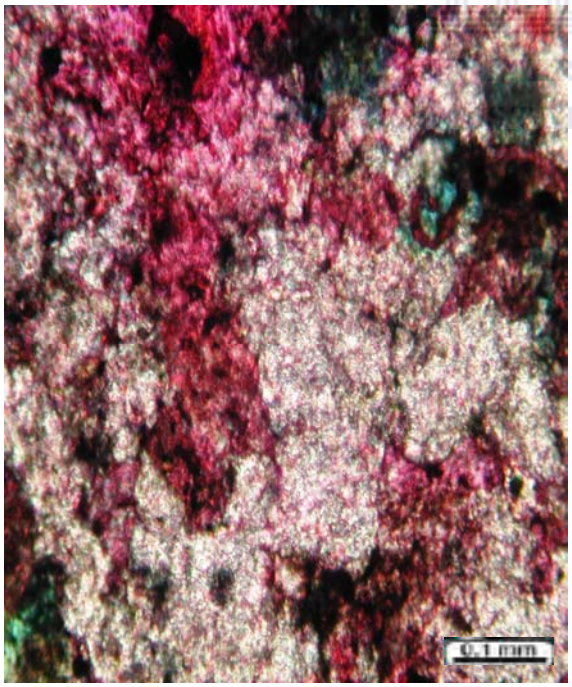

Plate 4.32 (A) PPL

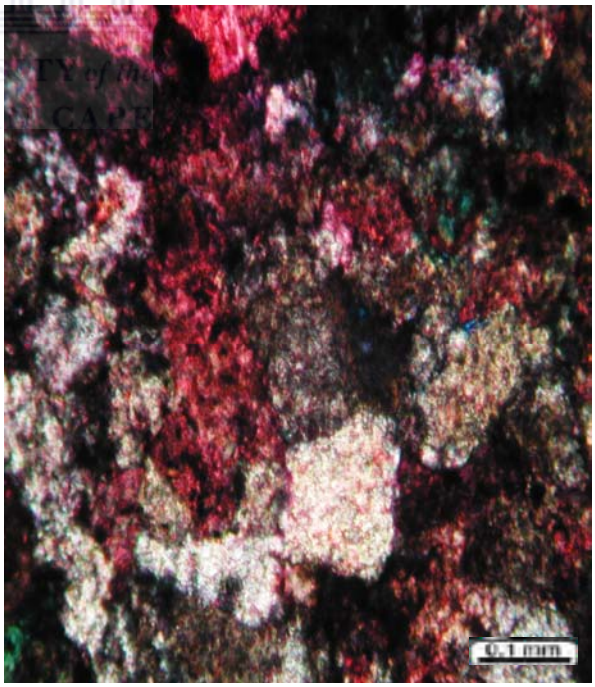

Plate 4.32 (B) XPL

PLATE 4.32 (A & B), E-BB1, 2660.05, X10 MAG.

4.1.1.1.6.5 PLATE 4.33 (A & B), E-BB1, 2849.00-.11, X10 MAG.

A clean, moderately sorted, medium grained, with loose packing and comprising of rounded to angular grains. It contains common to abundant metaquartzite and claystone clasts, is carbonaceous, slightly feldspathic and pyritised and locally minor amounts of mica and glauconite. The vugs are filled by clays. Poroperm characteristics are generally good, with 12% porosity and 28.08mD permeability recorded from core analysis result. Porosity is secondary after dissolution of early intergranular cement, probably calcite. Quartz overgrowths, vug filling clays, probably kaolinite and fibrous illite must have reduced porosity and permeability. Minor amounts of ferroan dolomite, pyrite siderite are also preserved. The most important process of compaction is pressure solution and/or grain solution, which has occurred along carbonaceous streaks, resulting in more extensive quartz and kaolinite cementation.

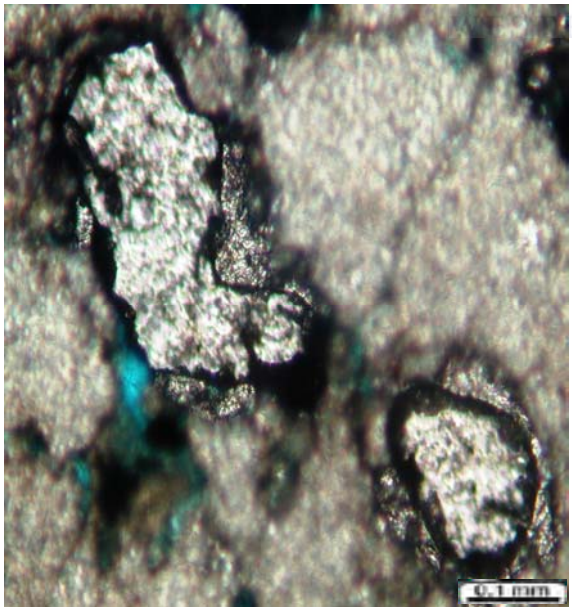

Plate 4.33 (A) PPL

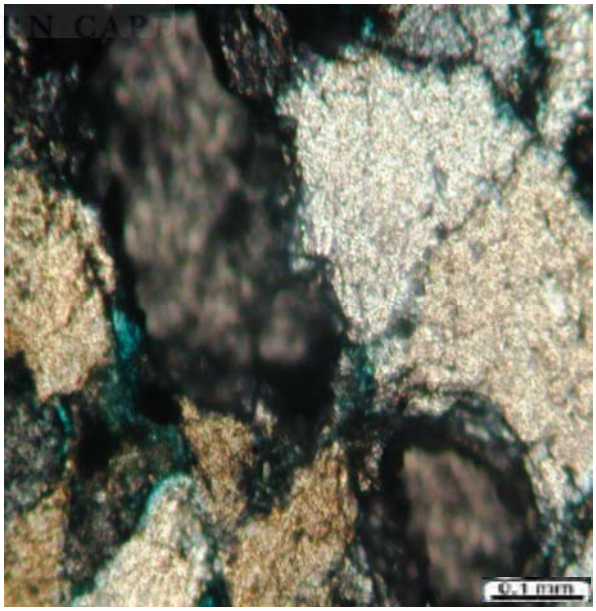

Plate 4.33 (B) XPL

PLATE 4.33 (A & B), E-BB1, 2849.00-.11, X10 MAG.

4.1.1.1.6.6 PLATE 4.34 (A & B), E-BB1, 2856.00, X10 MAG.

A very fine to fine grained, well sorted, with slightly loose packing and rounded to subrounded grains. It is glauconitic, comprising of lithic clasts, carbonaceous and feldspathic, and slightly micaceous. Poroperm characteristics range from very poor to moderate. Secondary porosity is developed by leaching of calcite cement and detrital grains. Quartz overgrowths, ferroan dolomite and illite are the main authigenic phases affecting porosity and permeability, though calcite cements are preserved. Pseudomatrix, from compaction of clay and glauconite clasts, has also contributed to porosity reduction.

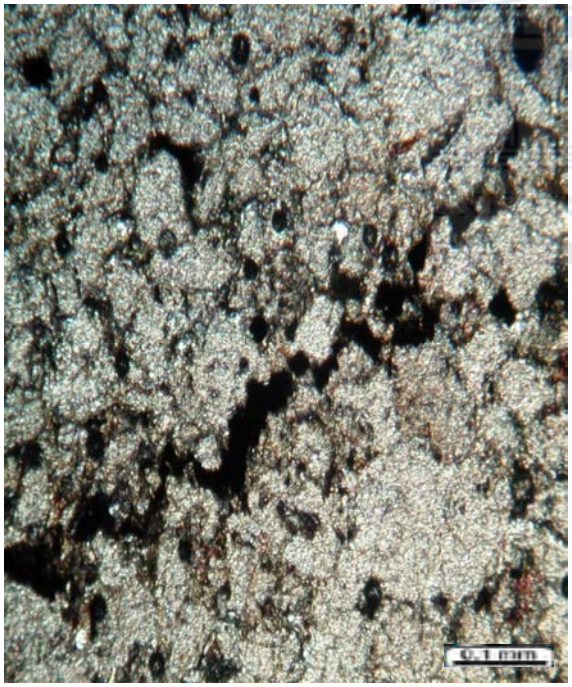

Plate 4.34 (A) PPL

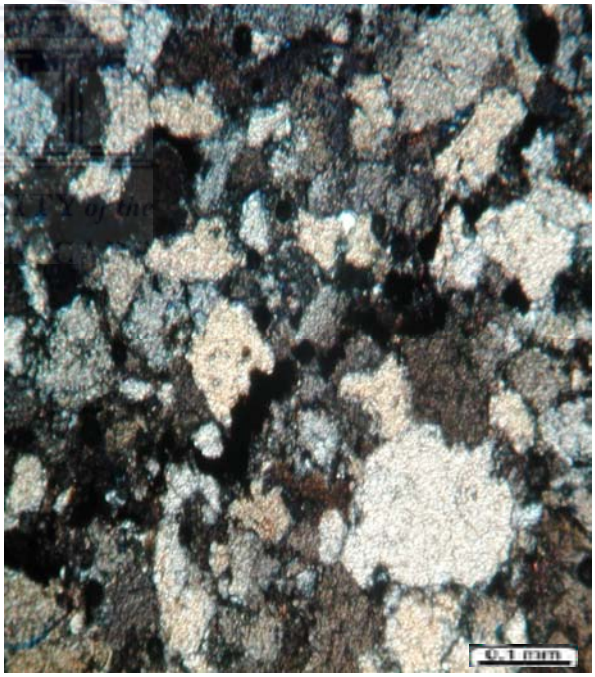

Plate 4.34 (B) XPL

PLATE 4.34 (A & B), E-BB1, 2856.00, X10 MAG.

4.1.1.1.6.7 PLATE 4.35 (A & B), E-BB1, 2872.05, X4 MAG.

A moderately sorted and medium grained. It is lithic, with metaquartzite and claystone clasts, carbonaceous, glauconitic and slightly feldspathic and micaceous. The grains are rounded, with slightly loose packing. Poroperms are good, with 11.9% porosity and 16.5mD permeability, with secondary porosity developed by leaching of early calcite cement. Quartz overgrowths, kaolinite and illite from grain dissolution/alteration are the main permeability restricting phases. Minor amounts of ferroan dolomite, pyrite and locally, siderite are also developed.

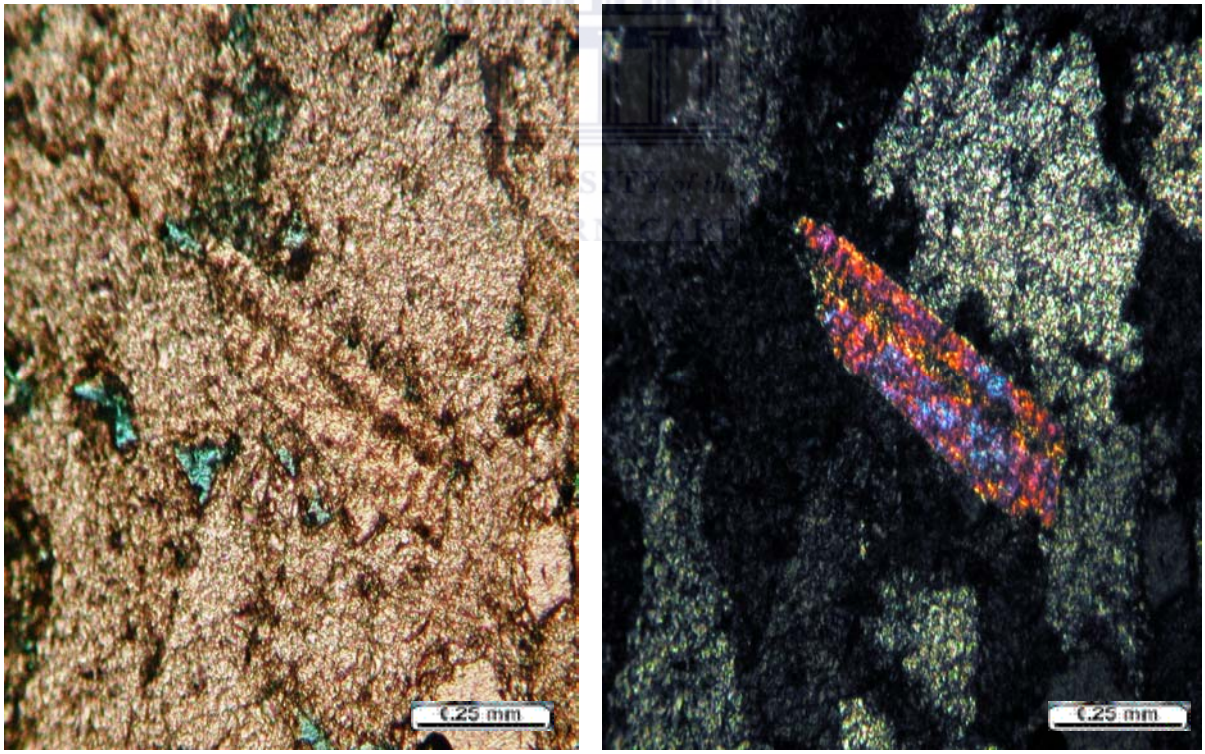

Plate 4.35 (A) PPL Plate 4.35 (B) XPL

PLATE 4.35 (A & B), E-BB1, 2872.05, X4 MAG.

4.1.1.1.7 THIN SECTION PETROGRAPHIC DESCRIPTION FOR WELL E-AO2

4.1.1.1.7.1 PLATE 4.36 (A & B), E-AO2, 2919.00, X10 MAG.

A clean fine to medium grained, moderately sorted, with slightly loose packing comprising of rounded to angular grains. It is glauconitic, carbonaceous, slightly feldspathic, lithic, with cement and grain dissolution preserved. Lithic clasts are altered to illite. Poroperm characteristics are poor to moderate, with 8.6% of porosity and permeability of 1.32mD, due to extensive dolomite and quartz cementation, and the presence of detrital clays. This section is slightly porous and secondary porosity is developed to a minor extent, and is commonly infilled by authigenic illite.

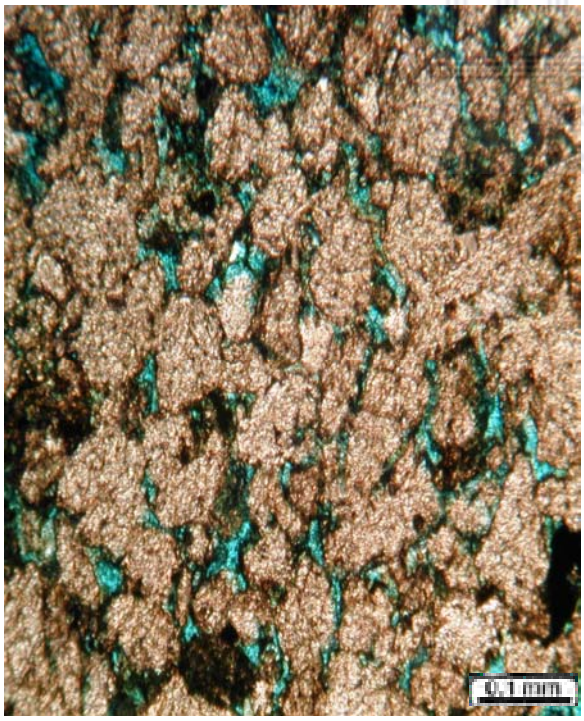

Plate 4.36 (A) PPL

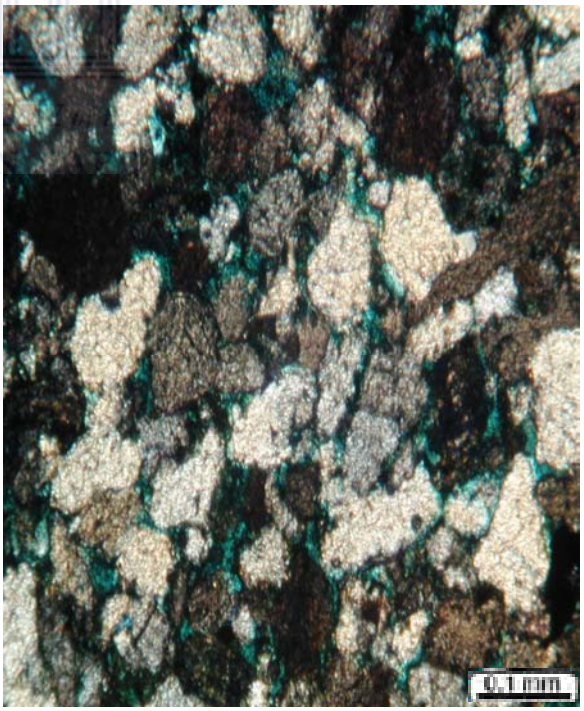

Plate 4.36 (B) XPL

PLATE 4.36 (A & B), E-AO2, 2919.00, X10 MAG.

4.1.1.1.7.2 PLATE 4.37 (A & B), E-AO2, 2926.41-.55, X4 MAG.

A moderately sorted and fine to coarse grained. High amounts of lithic grains, minor glauconite, pyrite, mica and feldspar are present throughout, carbonaceous material and reddish—brown intergranular clays are present. Poroperm characteristics are poor (5.0%, porosity and 0.03mD permeability). Porosity is secondary, after cement and grain dissolution, but is restricted by extensive quartz and lesser dolomite cementation. Kaolinite and illite commonly infill secondary pores, particularly grain dissolution pores, reducing them to microporosity. The decrease in porosity and permeability is due to more abundant quartz overgrowth and dolomite cements and the presence of intergranular clays.

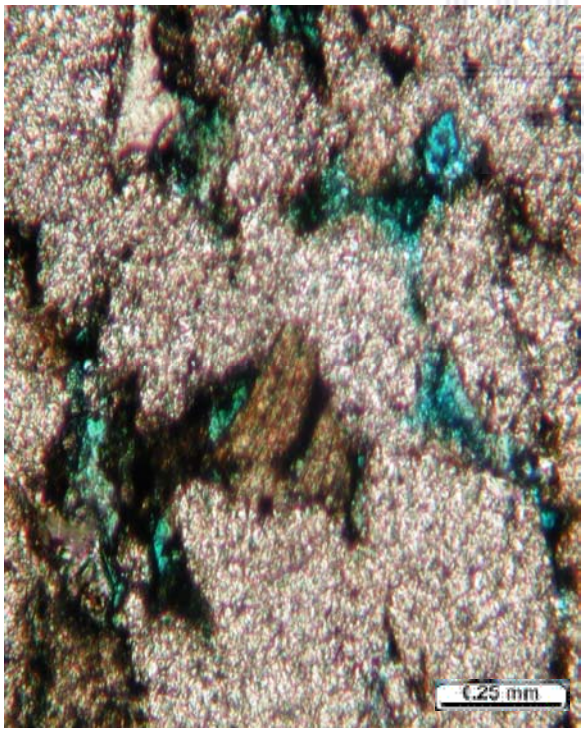

Plate 4.37 (A) PPL

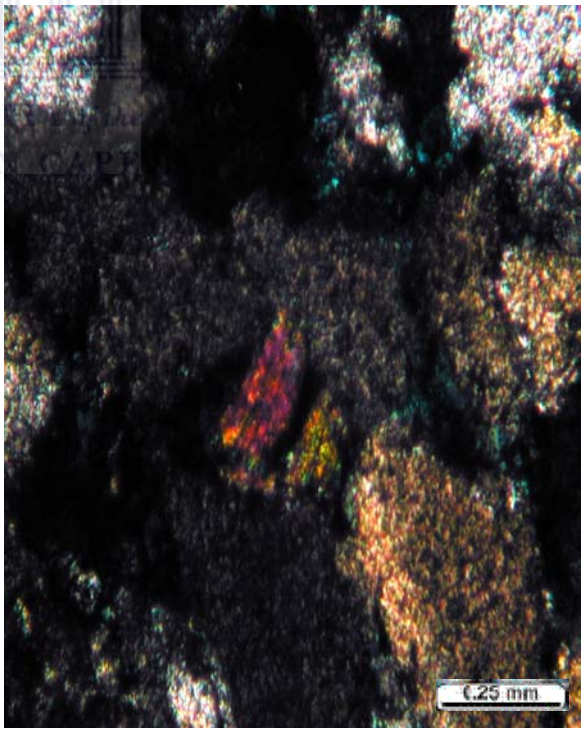

Plate 4.37 (B) XPL

PLATE 4.37 (A & B), E-AO2, 2926.41-.55, X4 MAG.

4.1.1.1.7.3 PLATE 4.38 (A & B), E-AO2, 2978.1, X4 MAG.

It is slightly argillaceous, poorly sorted and very fine to coarse grained, with subangular to rounded grains and slightly loose packing. Glauconite, bivalve fragments, carbonaceous material and litho-clasts are all common. Lithic grains include shelly clasts. Chloritised micas are also present. Poroperm characteristics are poor, due to extensive cementation by quartz overgrowths and dolomite. Detrital clays and authigenic illite also reduce porosity and permeability to a lesser extent. Only minor secondary porosity is observed.

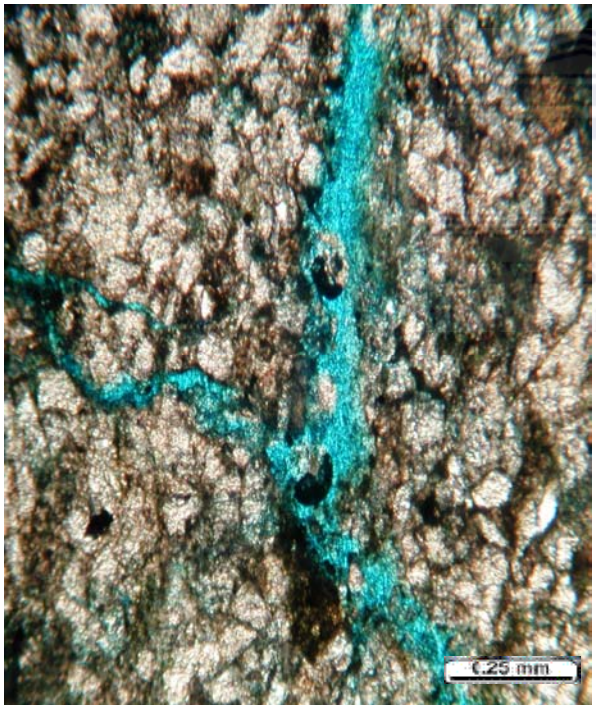

Plate 4.38 (A) PPL

Plate 4.38 (B) XPL

PLATE 4.38 (A & B), E-AO2, 2978.1, X4 MAG.

4.1.1.1.7.4 PLATE 4.39 (A & B), E-AO2, 3048.00, X4 MAG.

The section is poorly sorted and finer grained, ranging from silt to medium grained, with slightly loose packing and rounded grains. Comprises of glauconite, and locally shelly (with bivalve, echinoderm and foraminifera remains). Lithoclasts, mica and carbonaceous material are present. Poroperm characteristics are moderate, 10.5% porosity and 3.54mD permeability, due to their either being argillaceous or pervasively cemented by siderite or poikilotopic calcite.

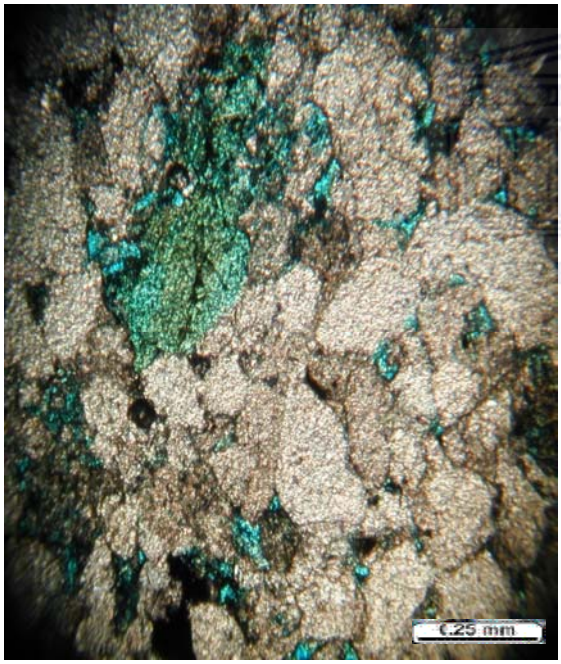

Plate 4.39 (A) PPL

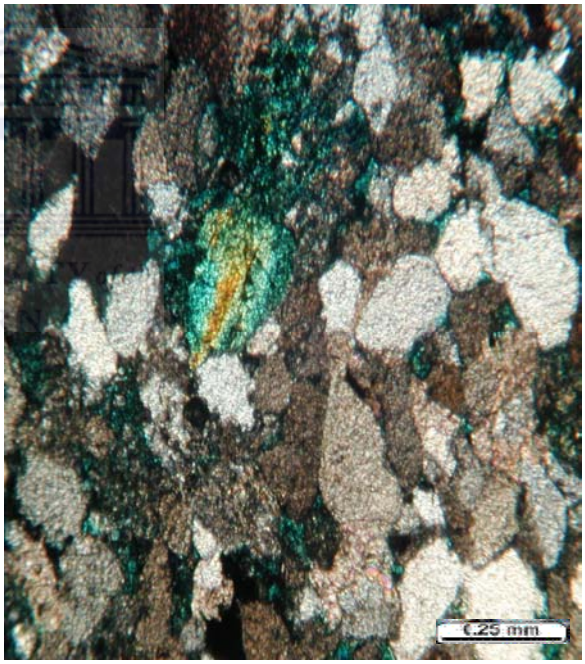

Plate 4.39 (B) XPL

PLATE 4.39 (A & B), E-AO2, 3048.00, X4 MAG.

4.1.1.1.7.5 PLATE 4.40 (A & B), E-AO2, 3076.00, X4 MAG.

A clean, moderately to well sorted and predominantly medium grained, comprising of very loose packing, rounded grains and porous, with high connectivity of pores. It is lithic, slightly feldspathic, and commonly contains minor amounts of carbonaceous material and mica. Glauconite is present, with a few inclusions. The lithic grains comprise mostly, shale and chert clasts, Stylolites are rarely developed. Poroperms are better, 15.5% porosity and 85.08mD permeability, in this section due to the absence of pseudomatrix and, the rarer quartz overgrowths.

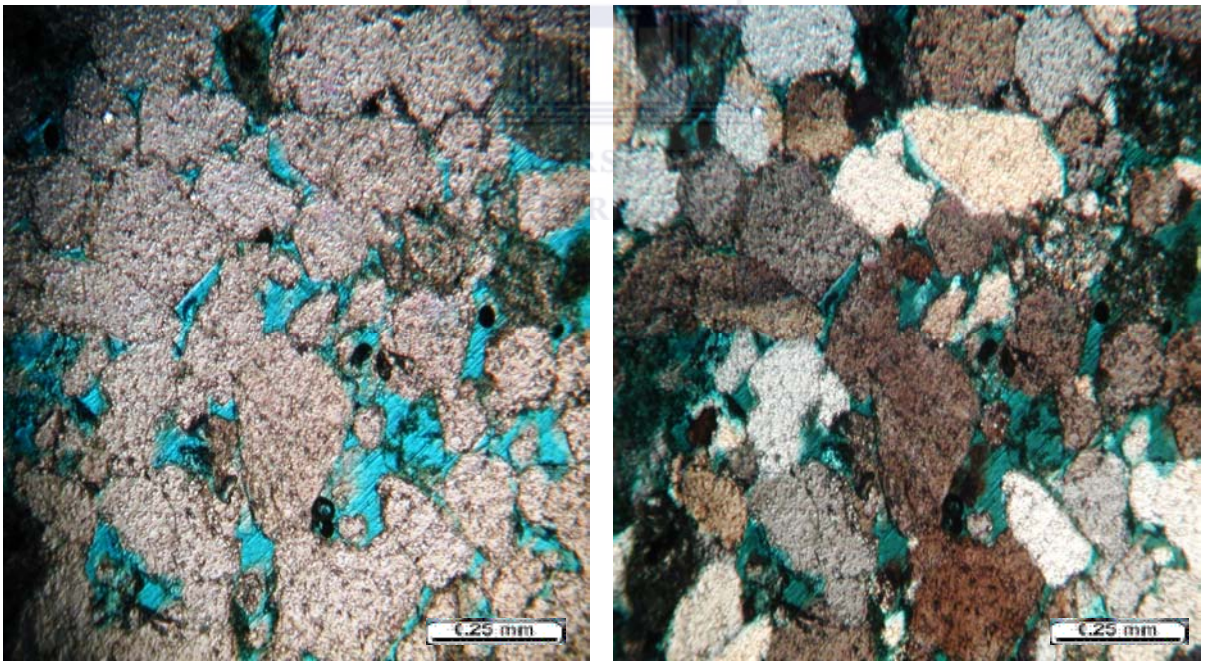

Plate 4.40 (A) PPL Plate 4.40 (B) XPL

PLATE 4.40 (A & B), E-AO2, 3076.00, X4 MAG.

4.1.1.1.8 THIN SECTION PETROGRAPHIC DESCRIPTION FOR WELL E-AD1

4.1.1.1.8.1 PLATE 4.41 (A & B), E-AD1, 2501.18-.32, X4 MAG.

This is a fine grained and poorly sorted section. It is characterised by the presence of lithic material, glauconite, shells and small amounts of dispersed calcareous cement. The presence of abundant illite and kaolinite result in a high proportion of microporosity as well as some secondary porosity. Abundant argillaceous material in the form of clay lamellae and clasts has resulted in silicification and illitization, which together with the fine grain size, contributes to the poor to fair permeability (1.0mD) and poor to moderate porosity (12.6%) results. Secondary pores are probably filled with late stage authigenic clay development (kaolinite). Grain coating illite preserves porosity so where illite is present there isn't much quartz overgrowths.

Plate 4.41 (A) PPL

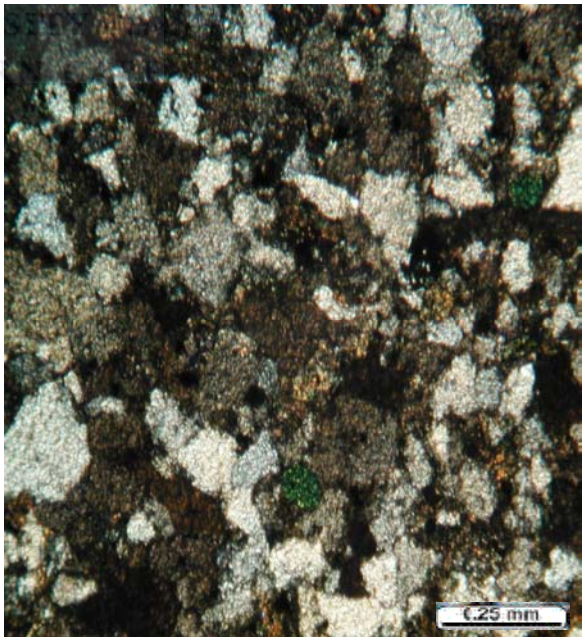

Plate 4.41 (B) XPL

PLATE 4.41 (A & B), E-AD1, 2501.18-.32, X4 MAG.

4.1.1.1.8.2 PLATE 4.42 (A & B), E-AD1, 2503.95-2504.06, X4 MAG.

A very fine to medium grained, poorly sorted, with tight packing. It is very lithic, glauconitic, shelly and calcareous. Poroperm characteristics are poor to fair, with 10.7% porosity and 1.1mD permeability. Abundant grain-coating illite, silica cement and fine grain size result in poor to fair poroperm characteristics. Occasional large pores (secondary pores) are filled with kaolinite, Grain coating illite and occasional pores filled with illite and chlorite

Plate 4.42 (A) PPL

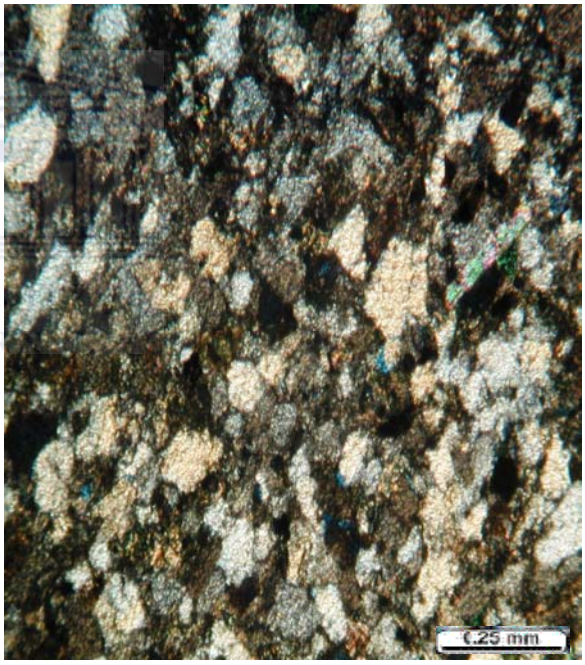

Plate 4.42 (B) XPL

PLATE 4.42 (A & B), E-AD1, 2503.95-2504.06, X4 MAG.

4.1.1.1.8.3 PLATE 4.43 (A & B), E-AD1, 2505.73-2506.02, X4 MAG.

The sample is fine to coarse grained and poorly sorted. Glauconite, shells and pyrite occur but only a small component of Iithic material is present. Occasional claystone clasts are present. The section is generally clean and porous, dominated by secondary porosity, with 15.2% of porosity and 124mD permeability. The only factor adversely affecting porosity is poor sorting. Silica and calcite cements contribute to reduction of pore space to a minor degree. The section is characterised by the presence of argillaceous Lamellae, claystone clasts and a fair proportion of lithic material.

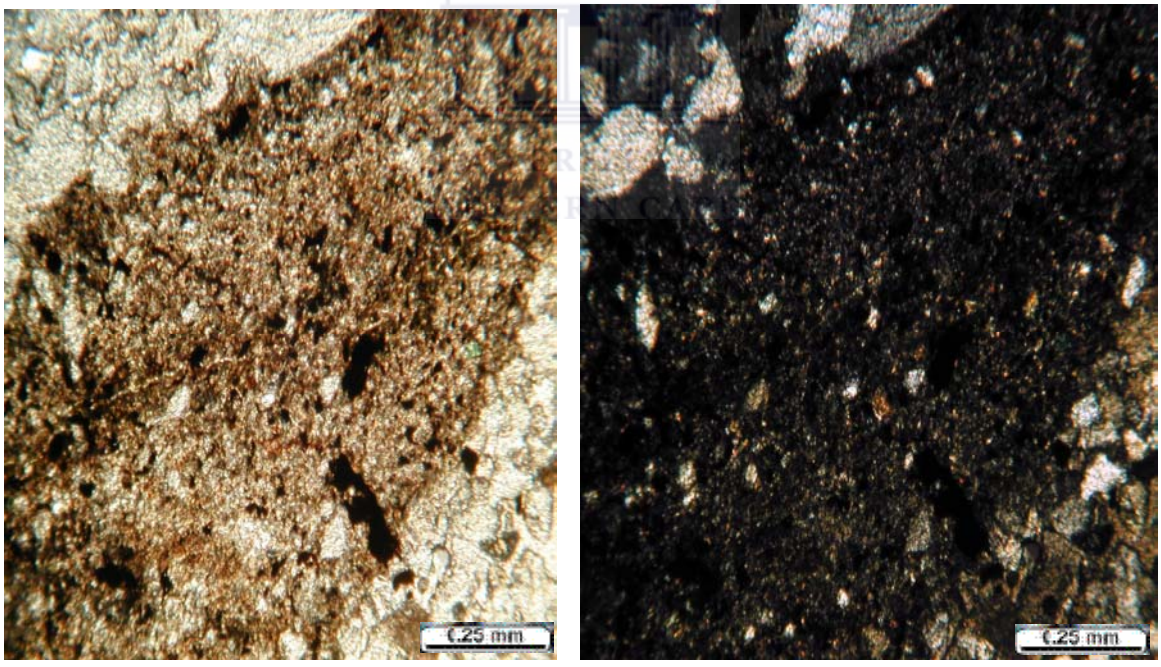

Plate 4.43 (A) PPL Plate 4.43 (B) XPL

PLATE 4.43 (A & B), E-AD1, 2505.73-2506.02, X4 MAG

4.1.1.1.8.4 PLATE 4.44 (A & B), E-AD1, 2506.79-.96, X4 MAG.

A fine grained, argillaceous and siliceous. This section is lithic, glauconitic, shelly, and pyritic. Poroperm characteristics are good, with 15.1% porosity and permeability of 123mD. The main permeability destroyers are fine grain size, poor sorting, silica cement and to a lesser extent, the presence of authigenic, grain—coating illite. Microporosity is associated with the presence of authigenic clay, but secondary porosity is also present.

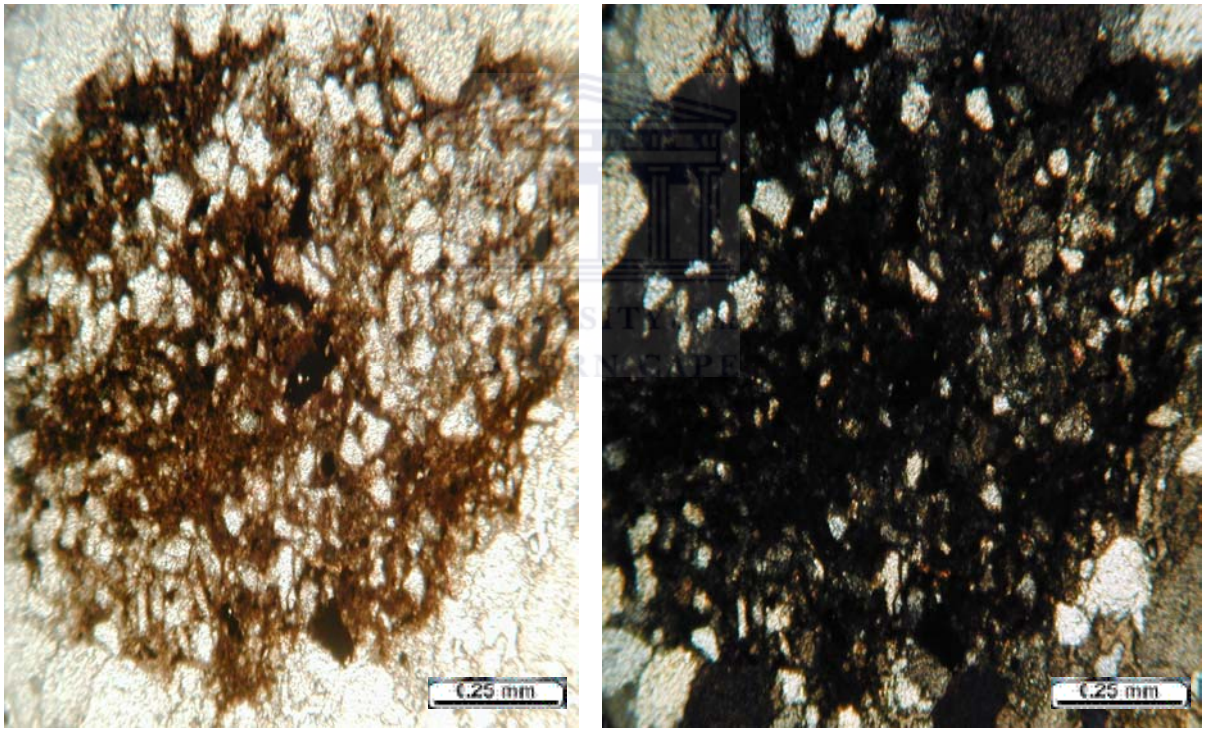

Plate 4.44 (A) PPL Plate 4.44 (B) XPL

PLATE 4.44 (A & B), E-AD1, 2506.79-.96, X4 MAG.

4.1.1.1.8.5 PLATE 4.45 (A & B), E-AD1, 2509.83-.99, X4 MAG.

A coarser grained (fine to coarse, but generally coarse) and clean and is free of authigenic clay. Poor sorting, silica and calcite cement affect pore volume to a small extent and permeability characteristics are good to very good.

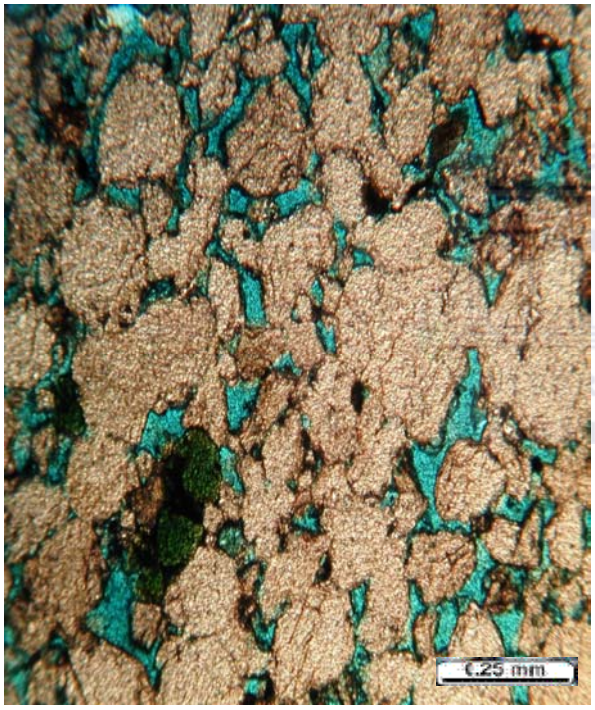

Plate 4.45 (A) PPL

Plate 4.45 (B) XPL

PLATE 4.45 (A & B), E-AD1, 2509.83-.99, X4 MAG.

4.1.1.1.8.6 PLATE 4.46 (A & B), E-AD1, 2868.75-2869.00, X4 MAG.

This section comprises a fine to silty, very argillaceous sandstone. Abundant lithic material, pyrite, minor glauconite and feldspar are present. Poroperm characteristic are poor, with 2.3% porosity and 0.01mD permeability. Poor porosity and permeability values are attributed to the fine to silty nature of the sandstone, a proportion of pseudomatrix and abundant authigenic, grain-coating illite and pore—filling kaolinite.

Illite appears to replace detrital clay (kaolinite) and abundant lithic material.

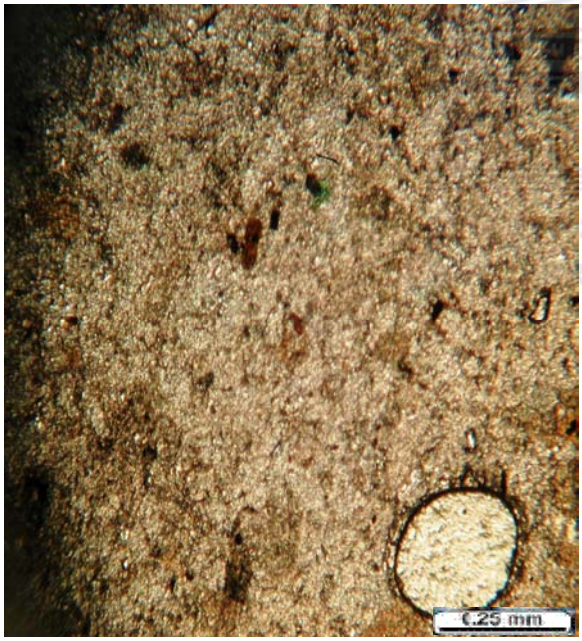

Plate 4.46 (A) PPL

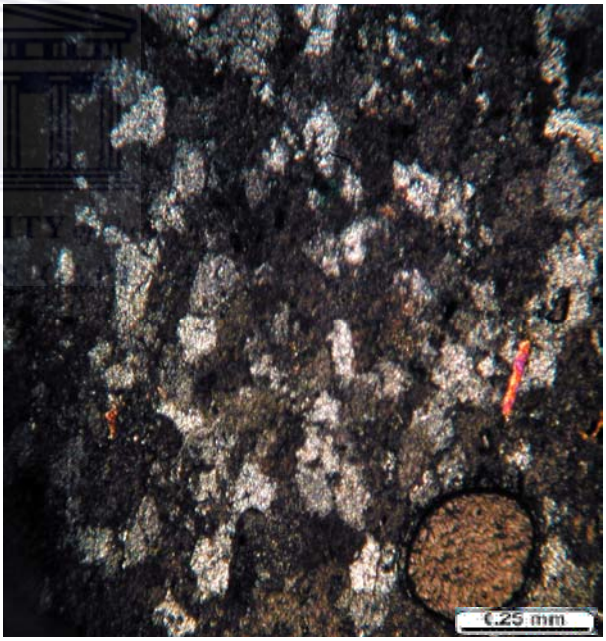

Plate 4.46 (B) XPL

PLATE 4.46 (A & B), E-AD1, 2868.75-2869.00, X4 MAG.

4.1.1.1.8.7 PLATE 4.47 (A & B), E-AD1, 2911.00-.23, X4 MAG.

A good, porous, coarse grained sample well sorted. Lithic material, calcite cement and minor glauconite are present; however the porous sections are generally clean. Poroperm characteristics are very good, with 14.9% porosity and 409mD permeability. The section has good secondary porosity. Occasional small pores are filled with late—stage kaolinite. Calcite cement and to a small degree kaolinite, affects porosity and permeability.

Plate 4.47 (A) PPL

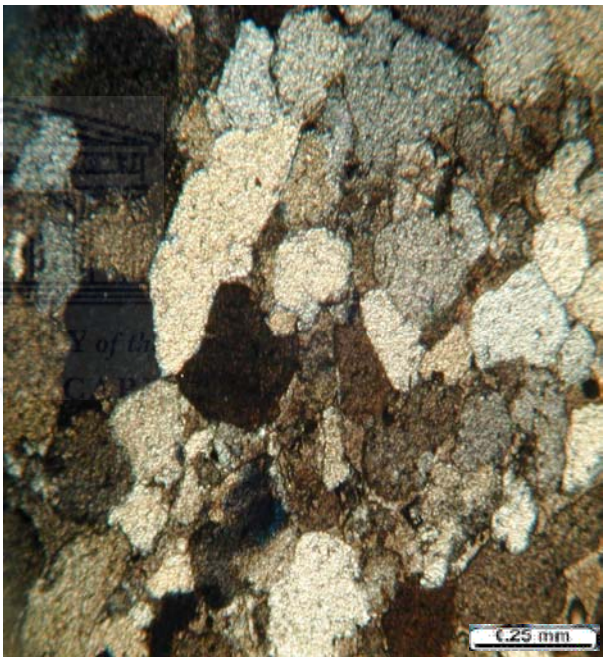

Plate 4.47 (B) XPL

PLATE 4.47 (A & B), E-AD1, 2911.00-.23, X4 MAG.

4.1.1.1.8.8 PLATE 4.48 (A & B), E-AD1, 2954.95-2955.19, X4 MAG.

A fine to medium grained and well sorted. Glauconite and pyrite are present throughout. Generally the section contains a fair proportion of lithic clasts which are altered and replaced by illite and occasionally chlorite. Poroperms are moderate, with 10.1% porosity and 7.0mD permeability, good secondary porosity is present. Poor permeability values are associated with the presence of microporosity. Characteristics of the calcareous cement suggest a composition between calcite and dolomite. The dominant factor in reduction of pore space is pseudomatrix development which results from the lithic content. Porosity is further reduced by calcareous cement and to small degree silica overgrowths. Authigenic grain-coating illite and pore filling kaolinite result in the reduction of permeability by the formation of microporosity.

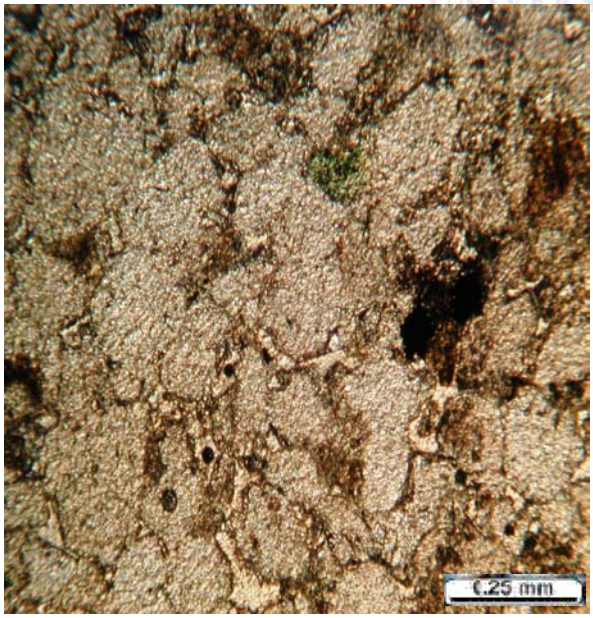

Plate 4.48 (A) PPL

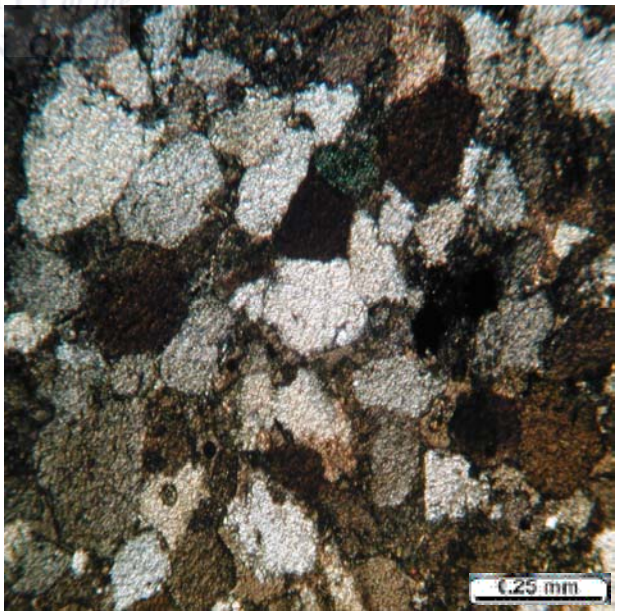

Plate 4.48 (B) XPL

PLATE 4.48 (A & B), E-AD1, 2954.95-2955.19, X4 MAG.

4.1.1.1.8.9 PLATE 4.49 (A & B), E-AD1, 2964.34, X4 MAG.

The section is argillaceous, fine to medium grained, and poorly to moderately sorted. It is very lithic, glauconitic and pyritised. Poroperms are poor, with 7.2% porosity and 0.06mD permeability. Secondary porosity is present. The dominant poroperm destroyer is pseudomatrix which has developed as a result of compaction and diagenesis of sediments containing a high proportion of lithic material. Authigenic illite, late stage, pore filling kaolinite, silica and calcareous cement are present and have an adverse effect on poroperm characterisitics.

Plate 4.49 (A) PPL

Plate 4.49 (B) XPL

PLATE 4.49 (A & B), E-AD1, 2964.34, X4 MAG.

PART TWO

4.1.2 SCANNING ELECTRON MICROSCOPY (SEM) PETROGRAPHY

Scanning electron microscopy (SEM) reveals detailed information on the morphology, distribution and phase relationships of diagenetic minerals and on the shape and distribution of pore systems. SEM is done to provide details of core samples at a microscopic level. Information derived, such as mineralogy, grain size, pore size, clay content and distribution give information relating to the interaction of rock components and fluids. This technique provides a means of high resolution imaging of pore lining clays.

SEM analysis is done on selected depths from each borehole, in order to show the presence of infilled vugs, authigenic cements and authigenic clays and their impact on reservoir quality and/or formation damage. These depths were chosen from three regions of the porosity and permeability distribution scattered plots seen in chapter three, (i.e. good, moderate and poor poroperm areas, in order to identify clay and cement). Good implies 15-20% porosity and permeability of 10-100mD. Moderate implies 10-15% porosity and 1-10mD permeability and poor porosity below 10% and permeability below 1mD.

4.1.2.1 SEM ANALYSIS FOR EACH WELL

4.1.2.1.1 SEM ANALYSIS FOR WELL E-AA1

4.1.2.1.1.1 VUGS

Isolated vugs (plate 4.52A) are infilled with late stage dolomite (plate 4.52B) (post calcite cementation). In plate (4.51A) the vug is partially infilled with kaolinite, which must post date dolomitization. The presence of quartz overgrowth associated with dolomite (plate 4.51 A & B) indicateS that quartz cementation continued until fairly late during the paragenesis. In plate 4.50A, siderite (Fe-rich carbonate) replaces calcite and the resulting reduction in volume contributes towards creating secondary porosity. Plate 4.50B, shows detail of the 'wheatear' siderite crystals.

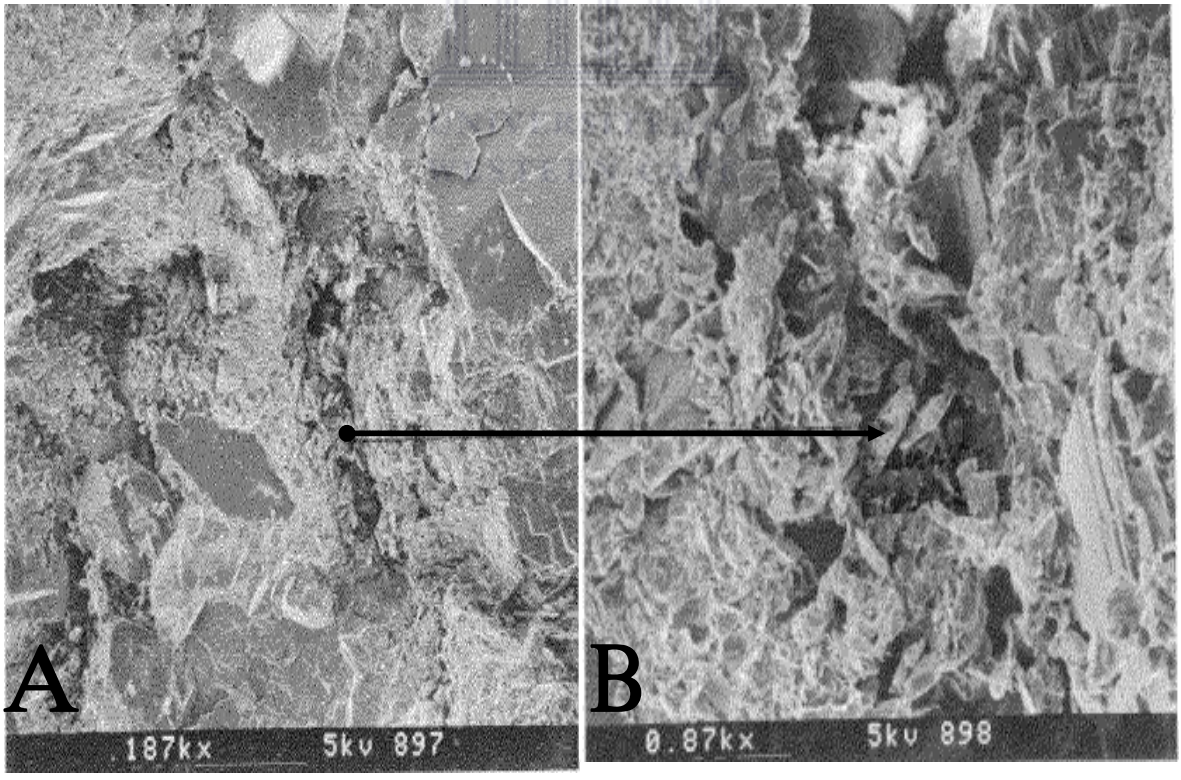

PLATE: 4.50, SEM, E-AA1, 2965.00 ('wheatear' siderite crystals).

(k=0.66mD, Θ=8.8%).

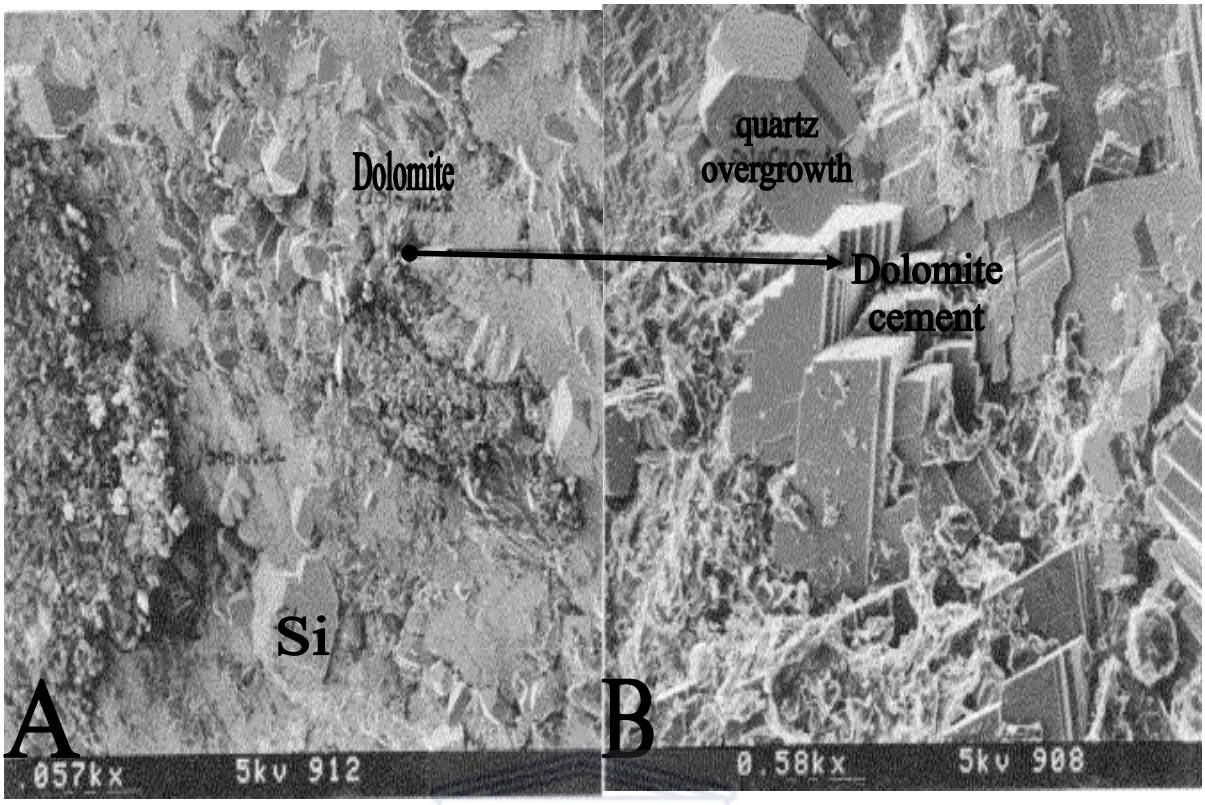

PLATE: 4.51, SEM, E-AA1, 2965.91(quartz overgrowth associated with dolomite)

(k=2.7mD, Θ=10.5%)

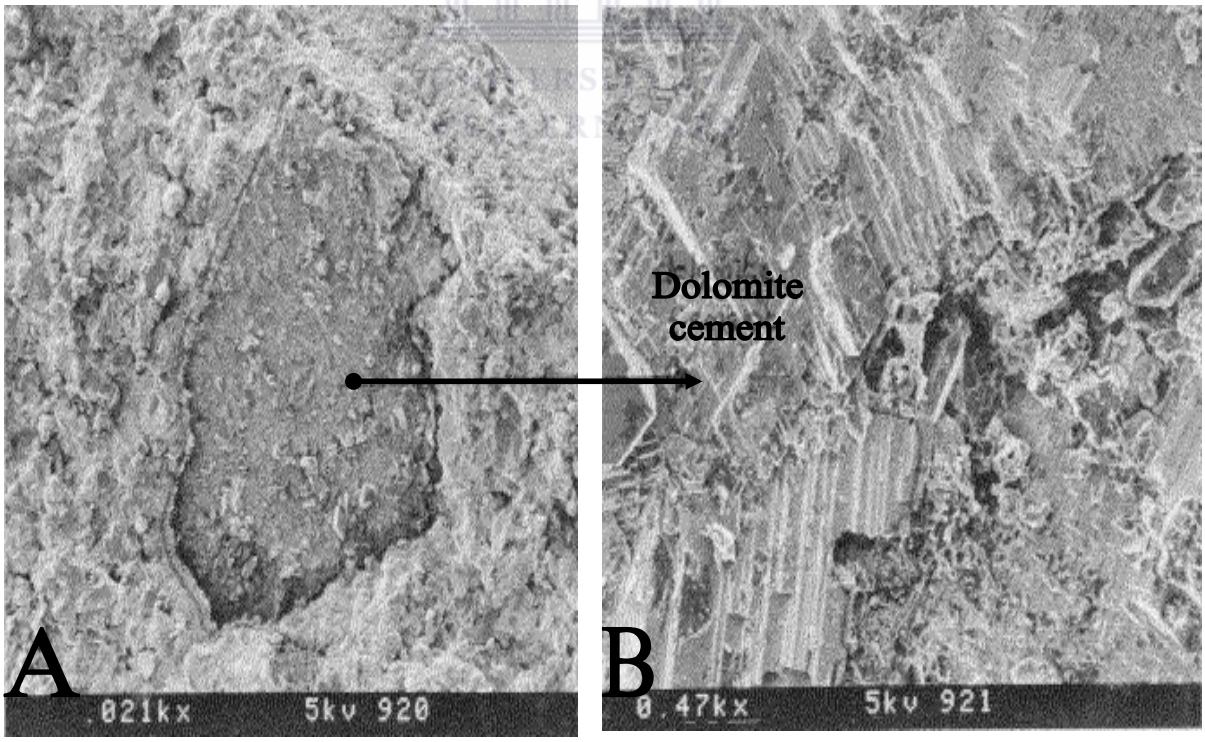

PLATE: 4.52, SEM, E-AA1, 2966.92

(k=0.21mD, Θ=6.9%)

4.1.2.1.1.2 AUTHIGENIC CEMENTS

There is an increase in the degree of silicification from plate 4.53 to 4.57. Plate 4.53 is dominantly calcite cemented, whereas in plate 4.55, calcite cement is patchily observed and plate 4.56 is Silica cemented. Plate 4.54; show an enhancement in porosity which reflects the core analysis records. Plate 4.57 is totally cemented by ferroan carbonate (siderite), and sand grains are floating in the carbonate matrix indicating early cementation.

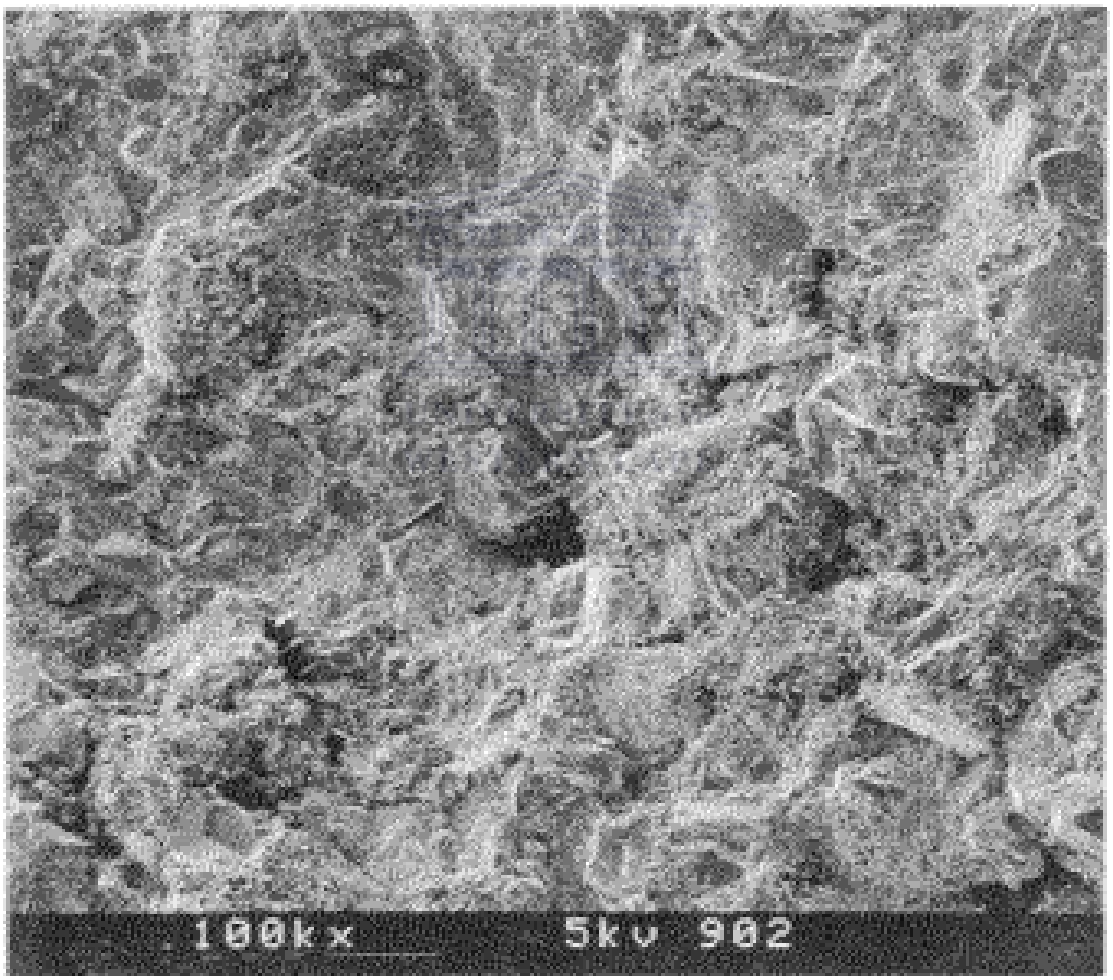

PLATE: 4.53, SEM, E-AA1, 2965.00 (dominantly calcite cemented)

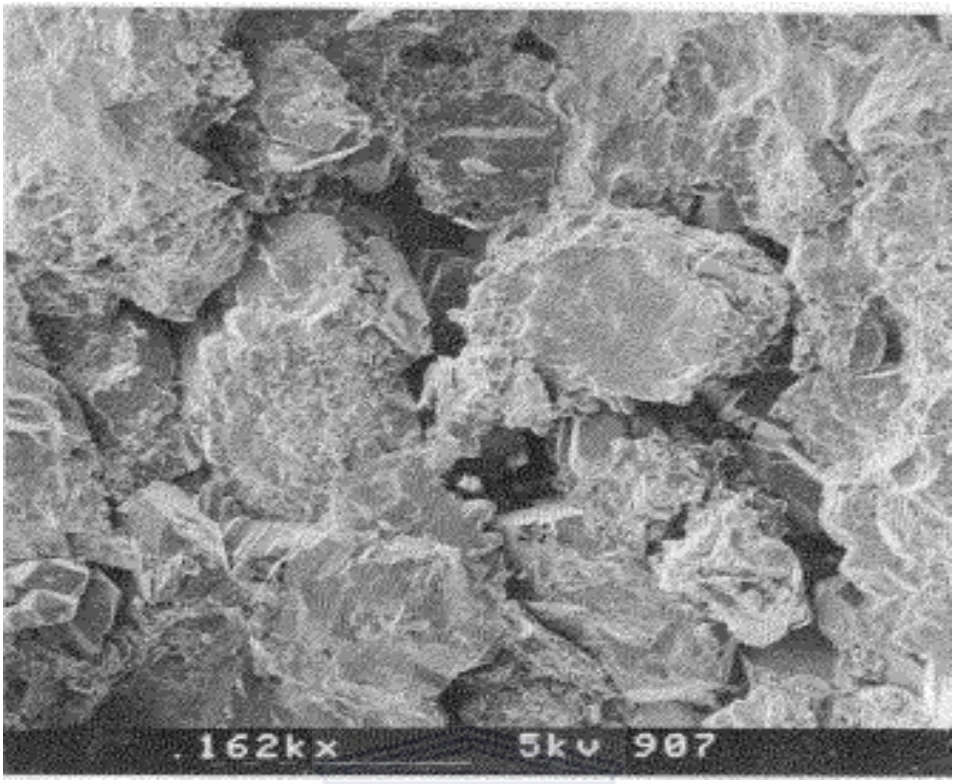

PLATE: 4.54, SEM, E-AA1, 2965.91

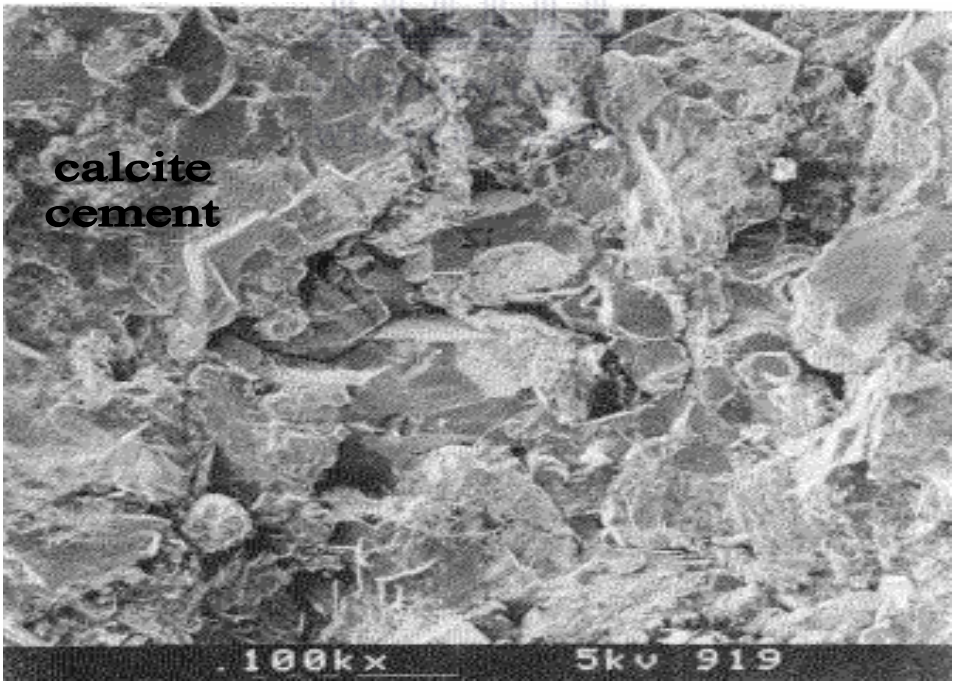

PLATE: 4.55, SEM, E-AA1, 2966.92 (patchy calcite cement)

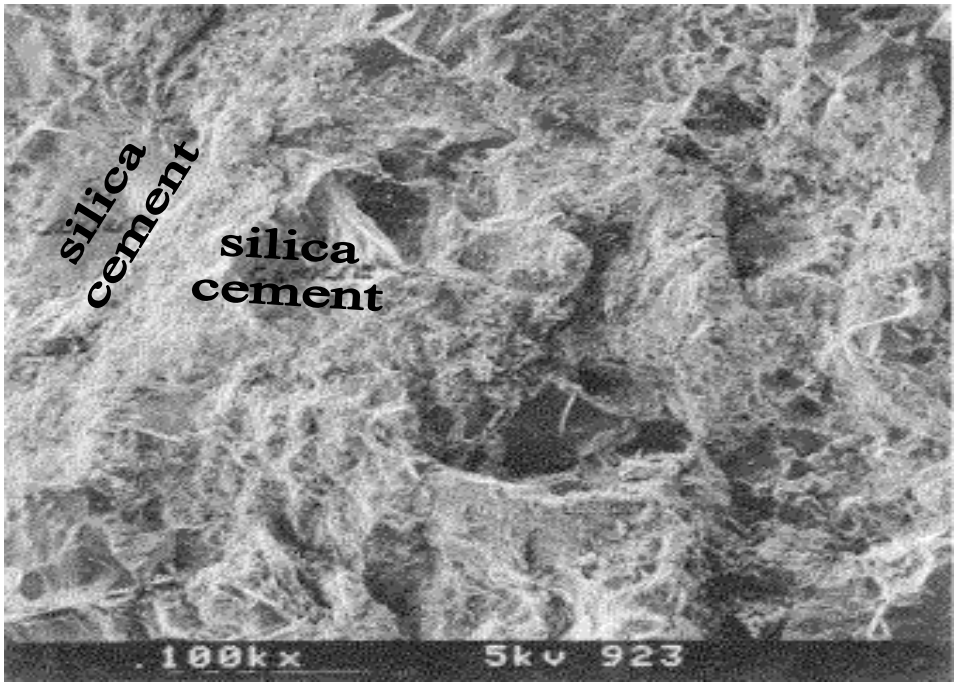

PLATE: 4.56, SEM, E-AA1, 2967.70 (Silica cement)

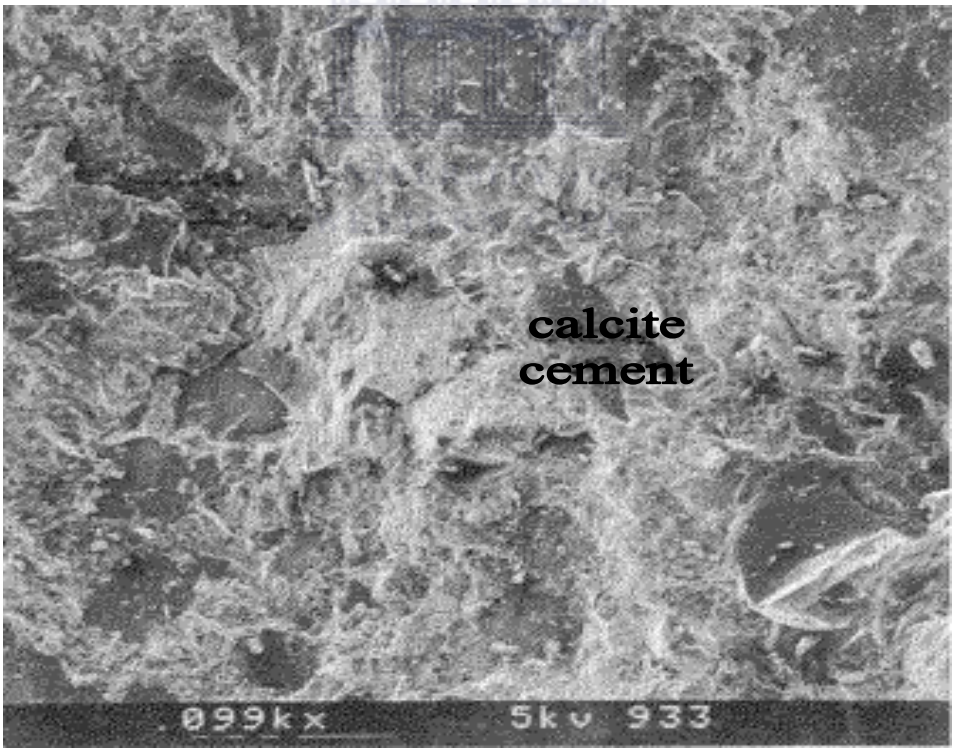

PLATE: 4.57, SEM, E-AA1, 2968.62 (ferroan carbonate cement)

In plate 4.58A, abundant lithic grains have resulted in the formation of pseudomatrix, during burial and compaction, and in the formation of secondary porosity by grain dissolution plate 4.61A. Quartz and calcite cement contribute significantly to low permeability. However, it must be noted that quartz overgrowths do not completely occlude pore space (plate 4.58B, 4.61A & B). The main cause for poor permeabilities in plate 4.59 and plate 4.60 is fine grain size. Calcite and late-stage dolomite cement are present, but affect permeability where poikilotopic calcite cement occur.

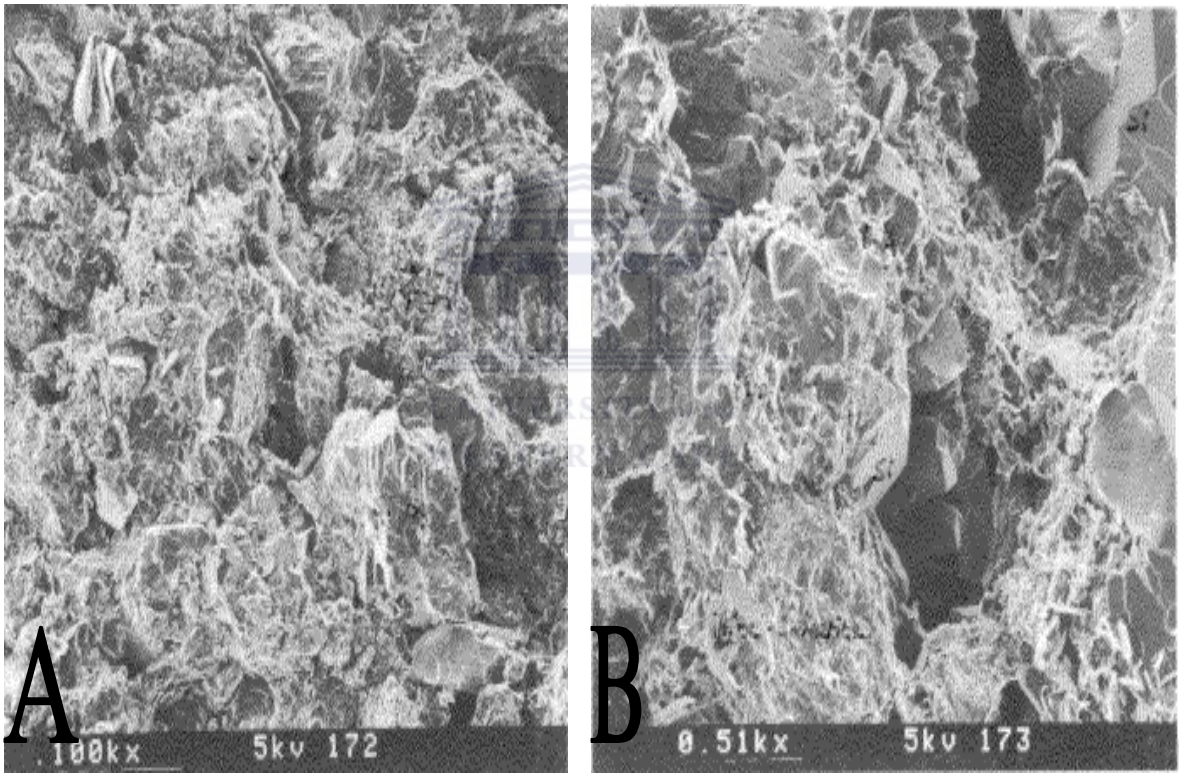

PLATE: 4.58, SEM, E-AA1, 3061.95 (k=1.8mD, Ɵ=11.9%, lithic grains)

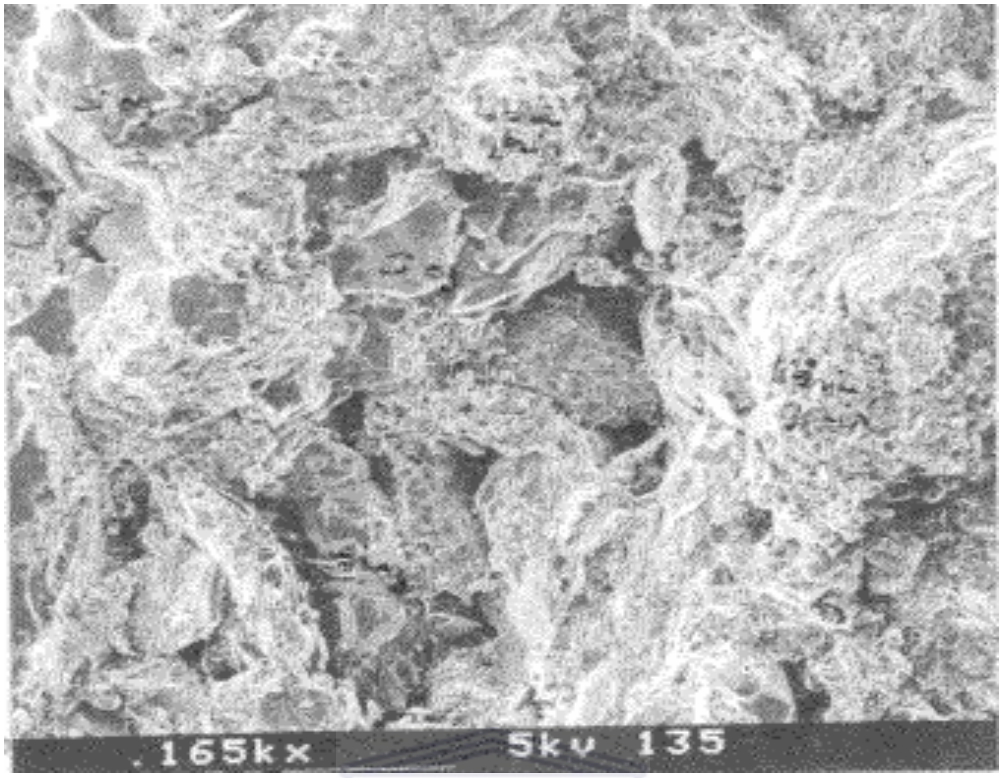

PLATE: 4.59, SEM, E-AA1, 3074.26

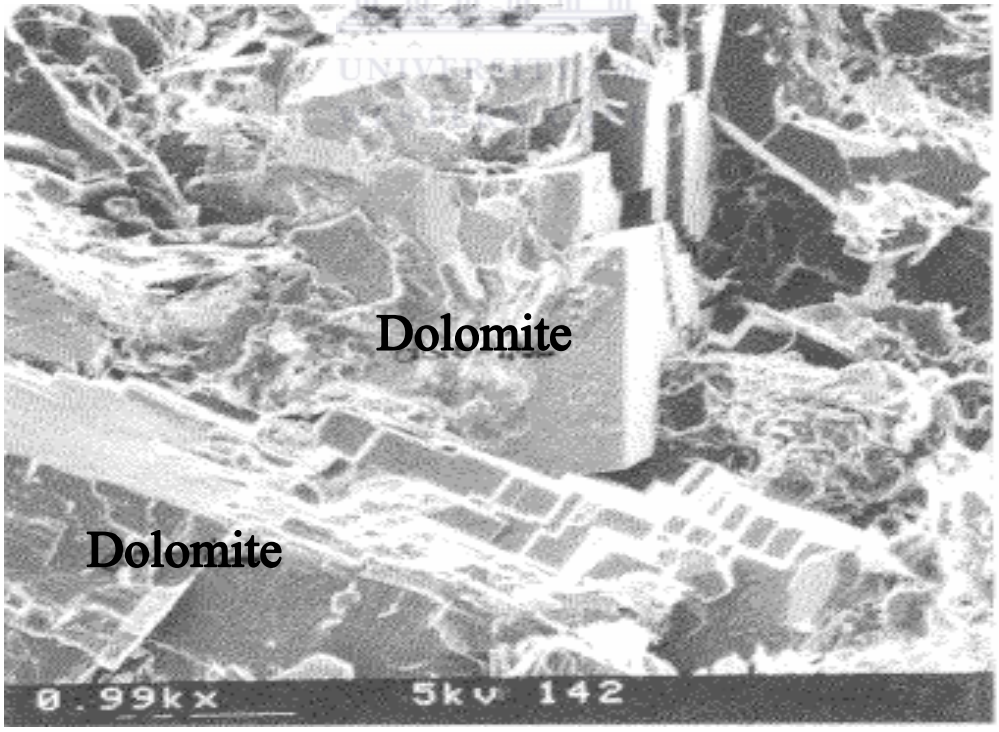

PLATE: 4.60, SEM, E-AA1, 3075.12 (late-stage dolomite cement)

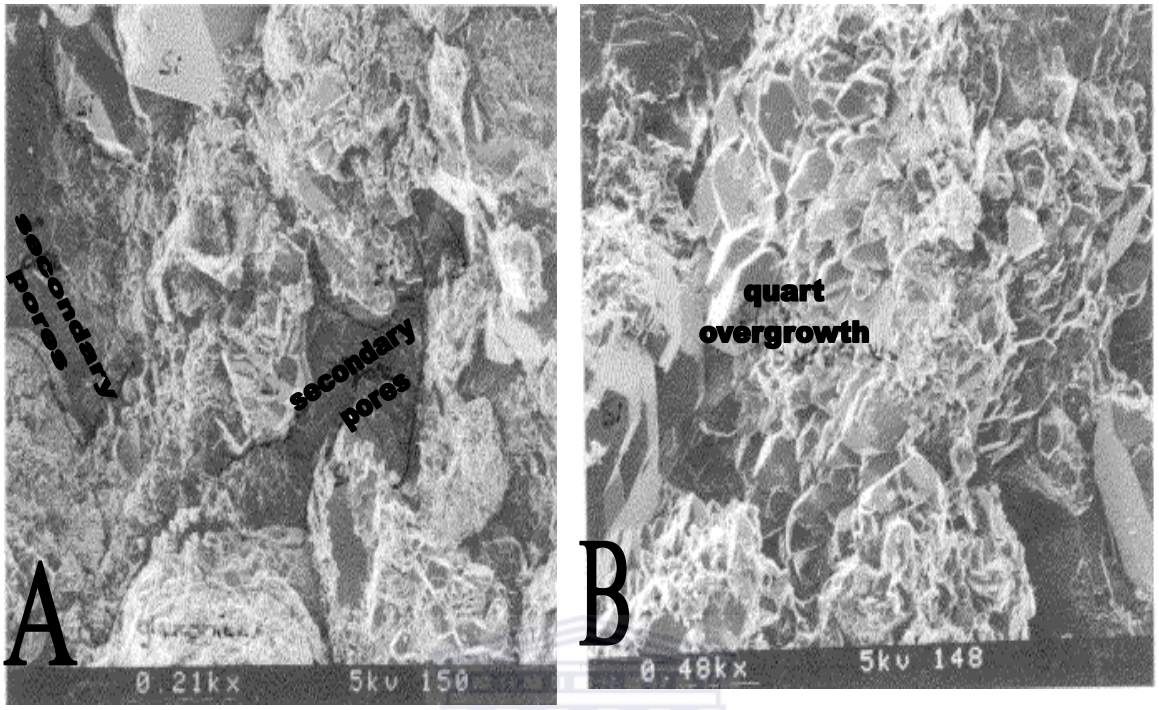

PLATE: 4.61, SEM, E-AA1, 3075.92 (quartz overgrowths and secondary pores)

(k=63.0mD, Θ=16.0%)

4.1.2.1.1.3 AUTHIGENIC CLAYS

Plates 4.63, 4.64A and 4.65B show loosely packed kaolinite infilling pore spaces, and plates 4.62, 4.64B and 4.65A show detail of unaltered kaolinite. The kaolinite is loosely packed and provides microporosity, but also has the potential of becoming dislodged and may cause migration of fines problem.

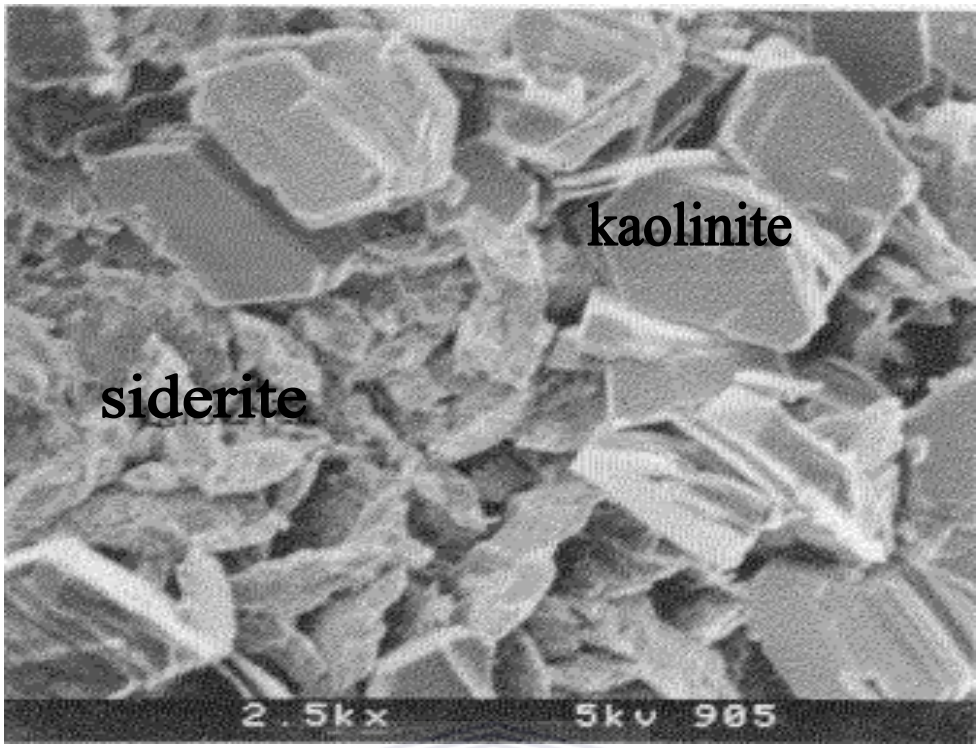

PLATE: 4.62, SEM, E-AA1, 2965.00 (unaltered kaolinite)

(k=0.66mD, Θ=8.8%)

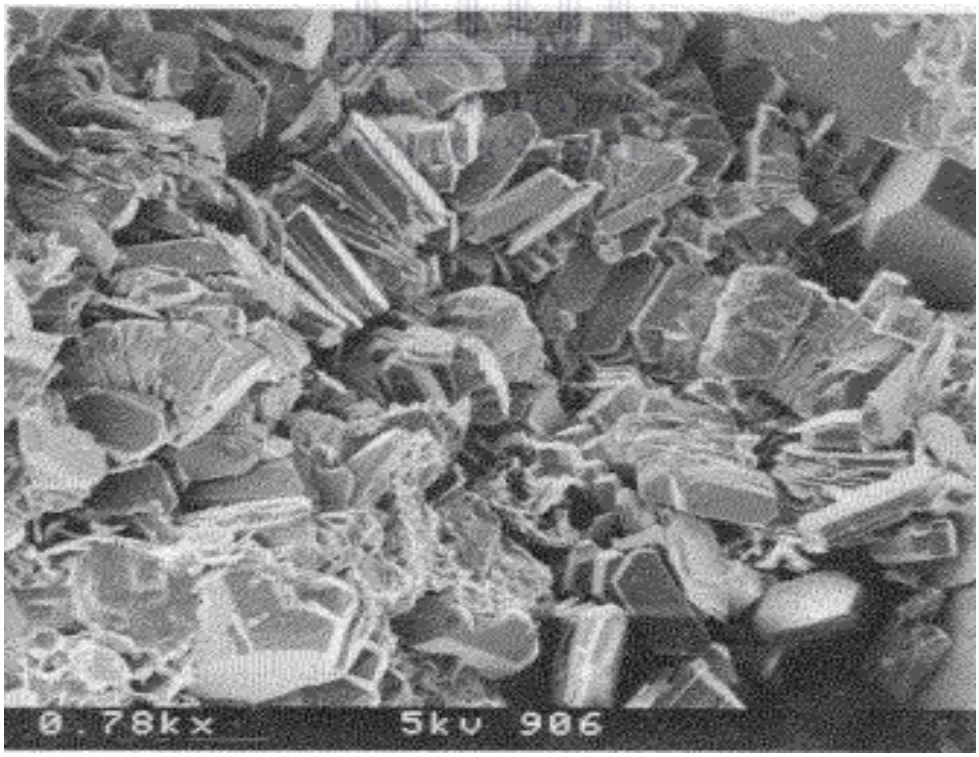

PLATE: 4.63, SEM, E-AA1, 2965.91 (loosely packed kaolinite)

(k=2.70mD, Θ=10.5%)

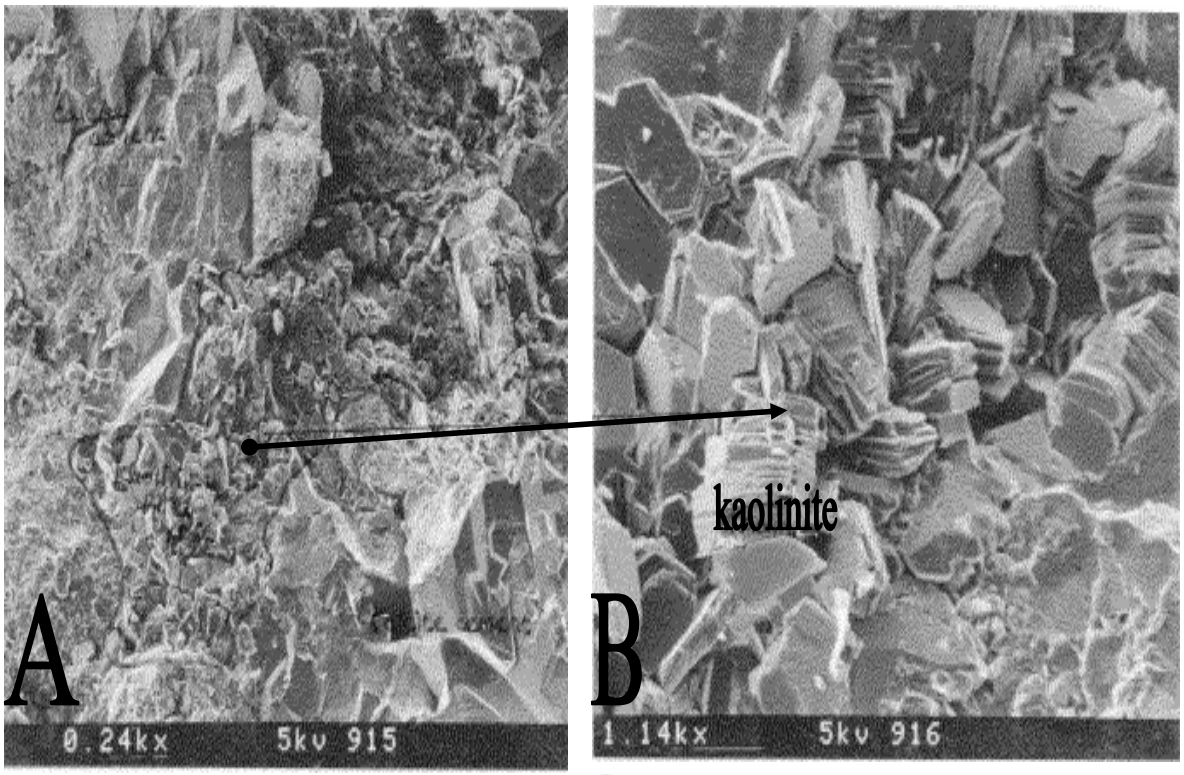

PLATE: 4.64, SEM, E-AA1, 2966.92 (kaolinite is loosely packed and provides microporosity)

(k=0.21mD, Θ=6.9%)

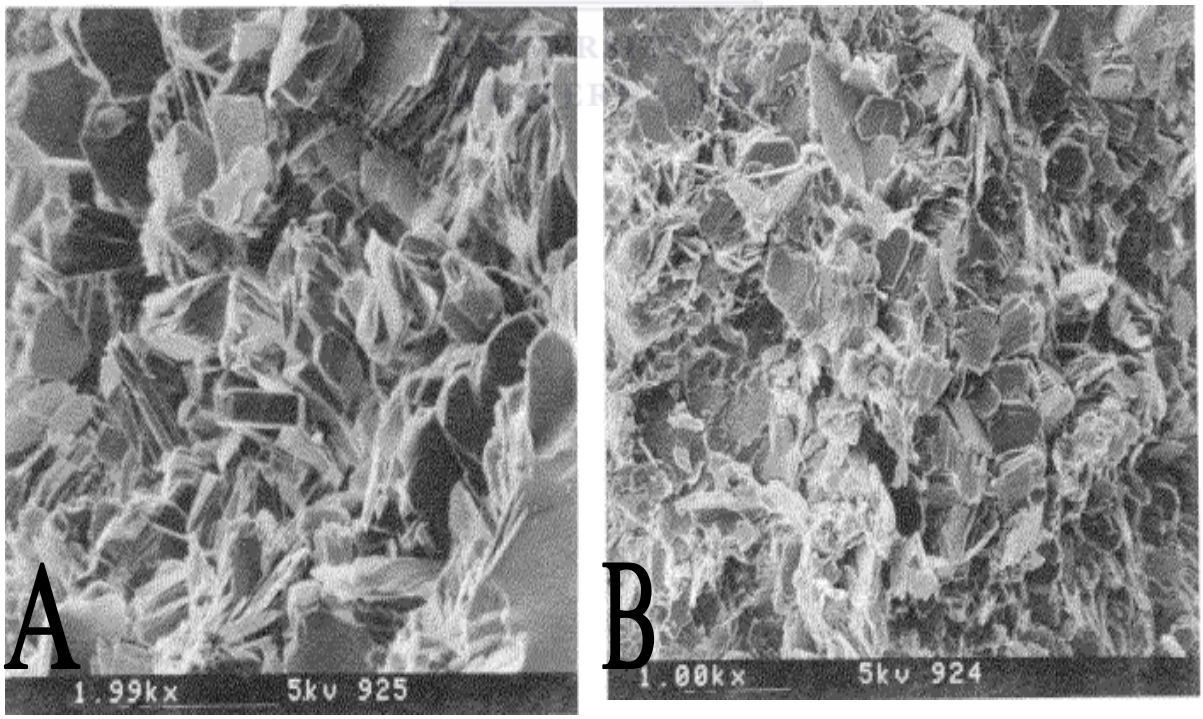

PLATE: 4. 65, SEM, E-AA1, 2967.70 (loosely packed kaolinite infilling pore spaces)

(k=0.38mD, Θ=6.2%)

The breakdown of abundant lithic grains has resulted in the formation of authigenic clays. One of which is kaolinite occur partially infilling pores (plate 4.66A) or totally blocking pore spaces (plate 4.67A and 4.69). Grain coating and pore-bridging illite (plates 4.68 and 4.67B) is also attributed to replacement of precursor detrital clay component. Note that very fresh kaolinite coexists with the illite (plate 4.67A) and is not altered to illite, as commonly occurs. The presence of chlorite locally (plate 4.66A & B) and in minute quantities is attributed to a late stage replacement of lithic grains.

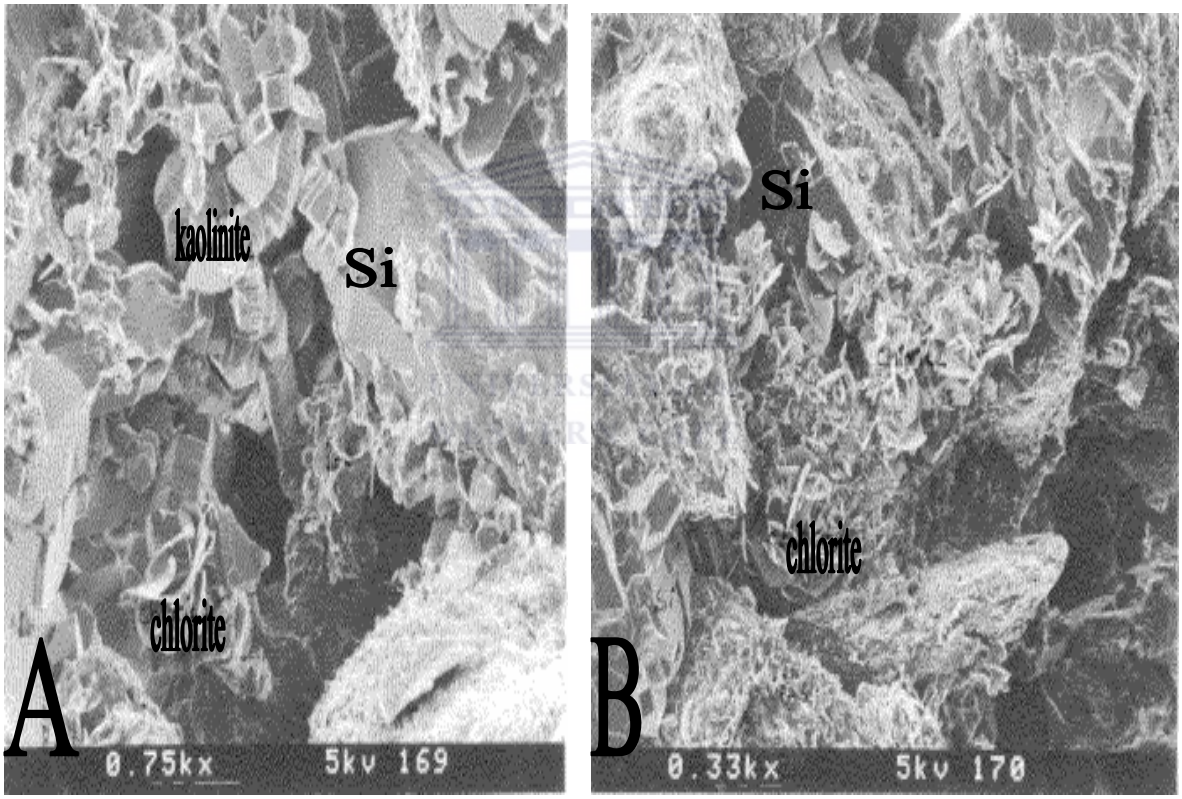

PLATE: 4.66, SEM, E-AA1, 3061.95 (presence of chlorite locally)

(k=1.8mD, Θ=11.9%)

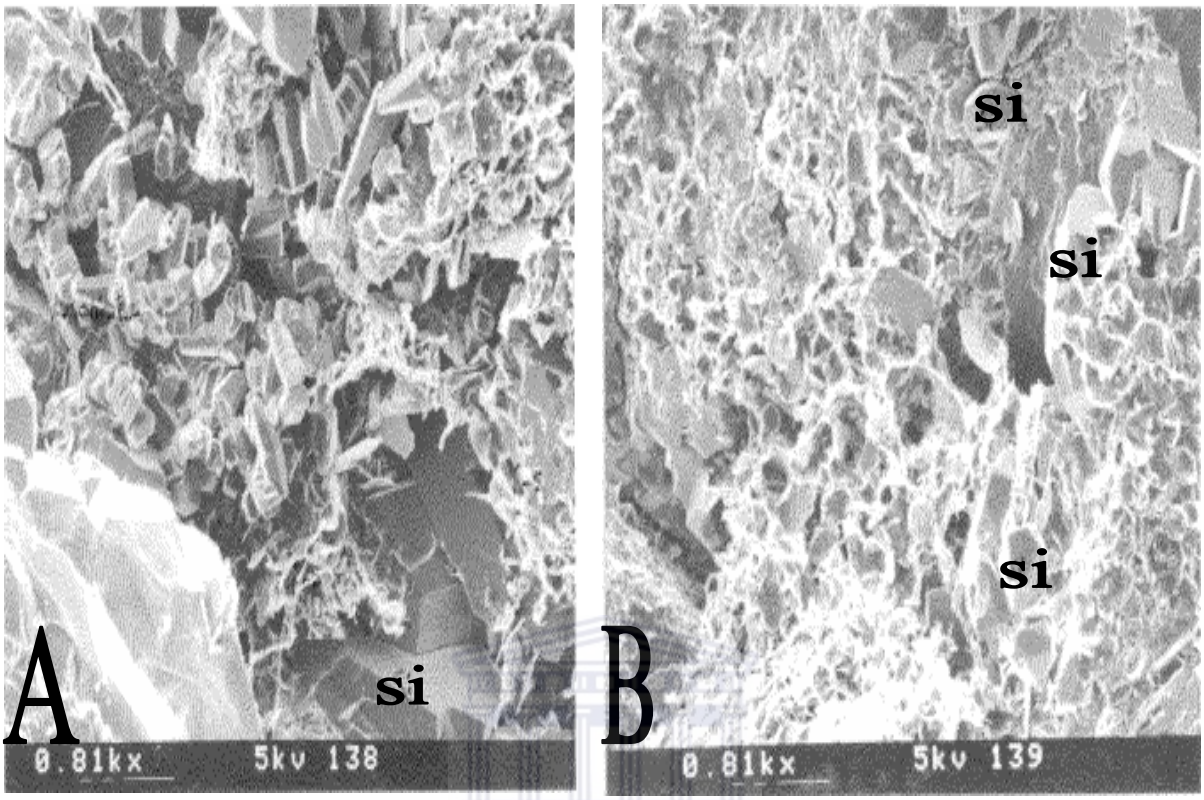

PLATE: 4.67, SEM, E-AA1, 3074.26 (kaolinite coexists with illite)

(k=1.30mD, Θ=11.2%)

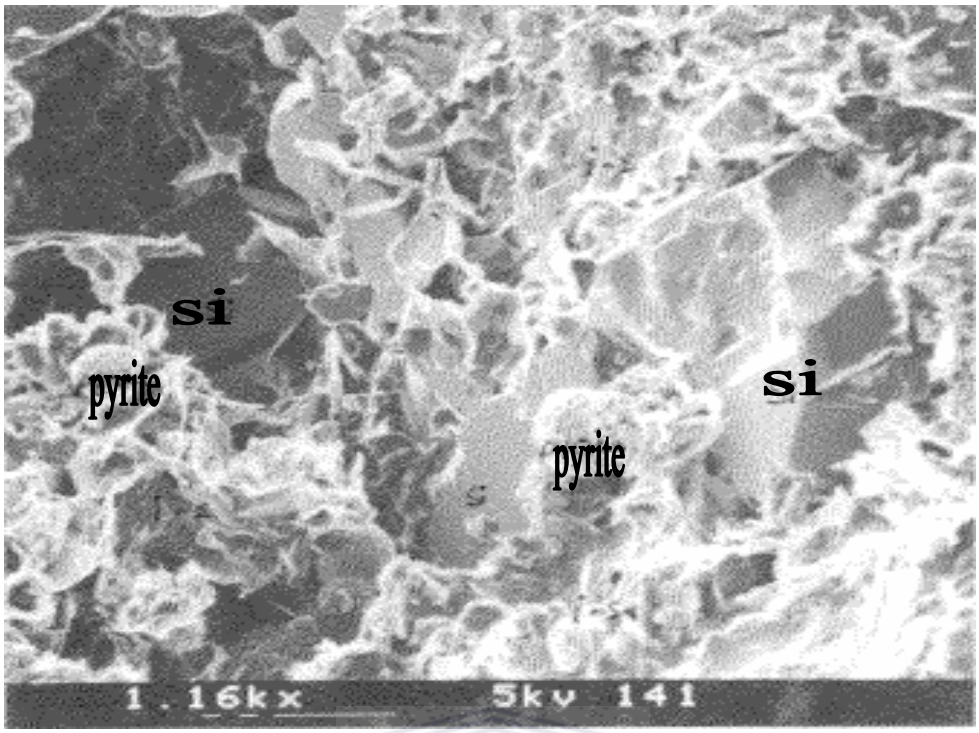

PLATE: 4.68, SEM, E-AA1, 3075.12 (Grain coating and pore-bridging illite)

(k=1.10mD, Θ=9.8%)

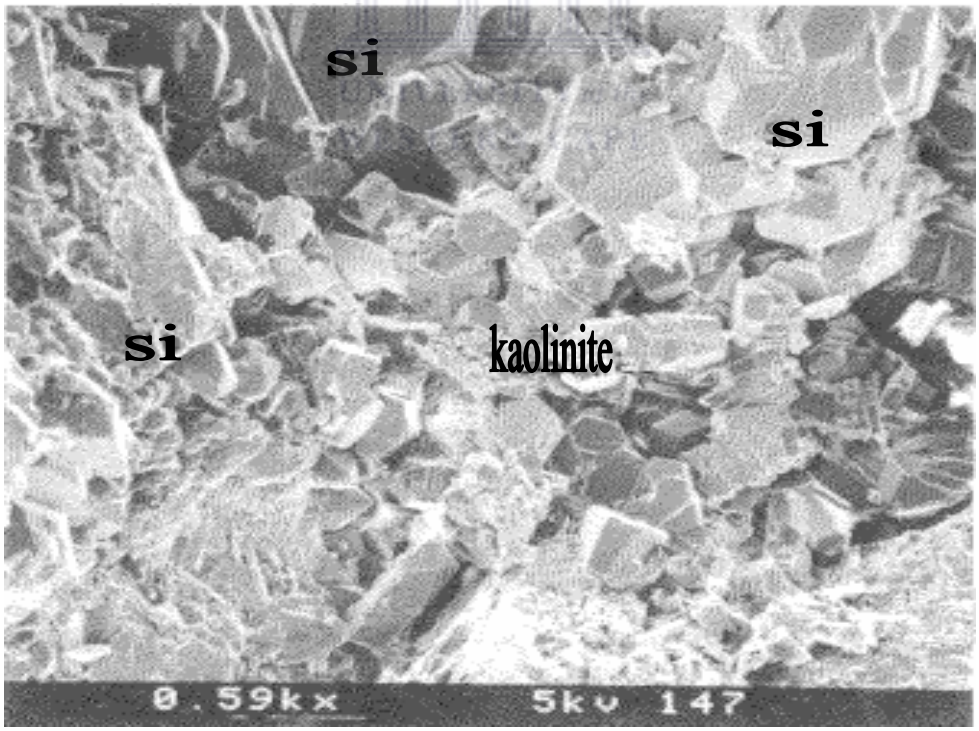

PLATE: 4.69, SEM, E-AA1, 3075.92 (kaolinite totally blocking pore spaces)

(k=63.0mD, Θ=16.0%)

4.1.2.1.2 SEM ANALYSIS FOR WELL E-CA1

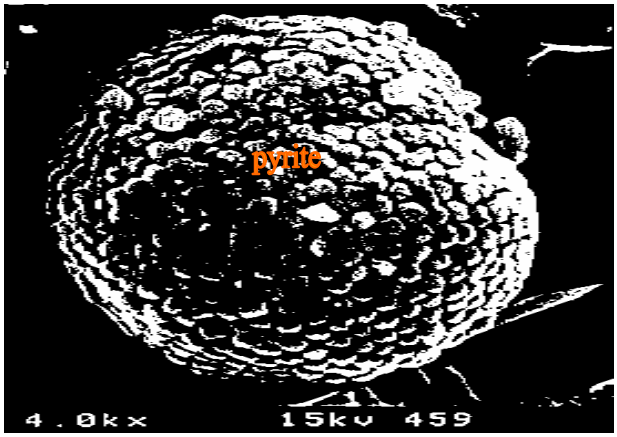

Plate: 4.70, SEM, E-CA1, 2899.12 (k=0.95mD, Θ=10.1%)

Pyrite framboid enveloped by later developed quartz overgrowth.

PLATE: 4.70, SEM, E-CA1, 2899.12 (Pyrite framboid)

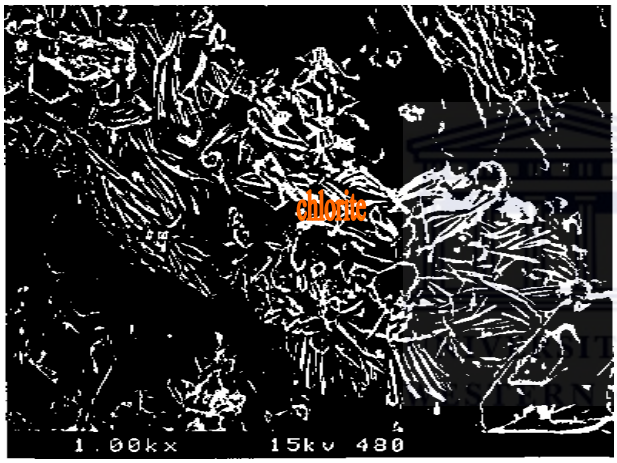

Plate: 4.71, SEM, E-CA1, 2931.86 (k=5.8mD, Θ=9.3%)

Authigenic iron-rich chlorite developed by alteration of detrital grains.

PLATE: 4.71, SEM, E-CA1, 2931.86 (Authigenic iron-rich chlorite)

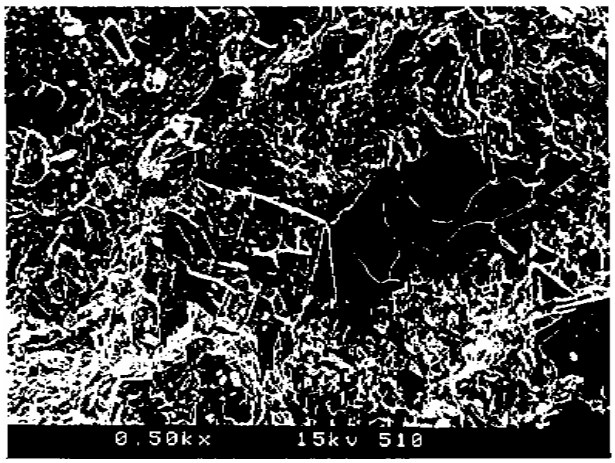

Plate: 4.72, SEM, E-CA1, 3211.63 (k=0.08mD, Θ=7.1%)

Dolomite and quartz overgrowths infill intergranular porosity. Fibrous illite is also developed as a pore filling phase.

PLATE: 4.72, SEM, E-CA1, 3211.63 (Dolomite and quartz overgrowths)

4.1.2.1.3 SEM ANALYSIS FOR WELL E-BA1

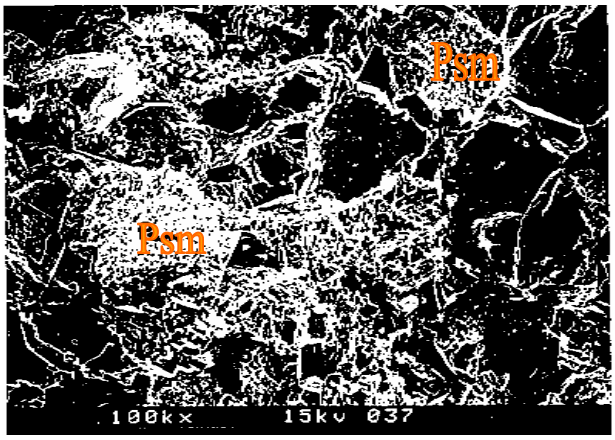

Plate: 4.73, SEM, E-BA1, 2832.92
(k=11.7mD, Θ=11.0%)

Quartz overgrowths and pseudomatrix (psm) reducing intergranular porosity.

PLATE: 4.73, SEM, E-BA1, 2832.92 (Quartz overgrowths and pseudomatrix)

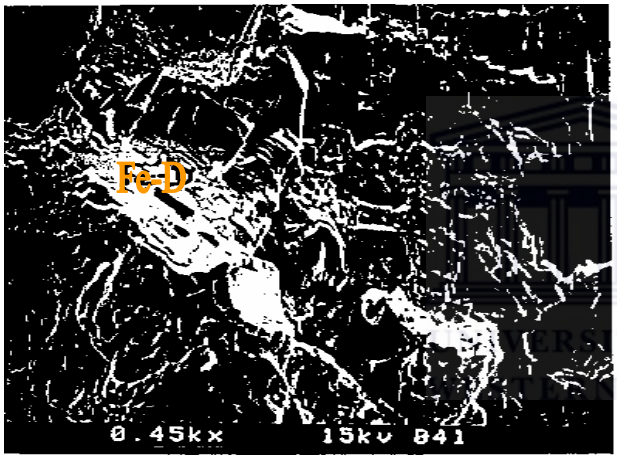

Plate: 4.74, SEM, E-BA1, 2836.01

(k=0.33mD, Θ=9.1%)

Pore-filling Ferroan Dolomite (Fe-D)

PLATE: 4.74, SEM, E-BA1, 2836.01 (Pore-filling Ferroan Dolomite)

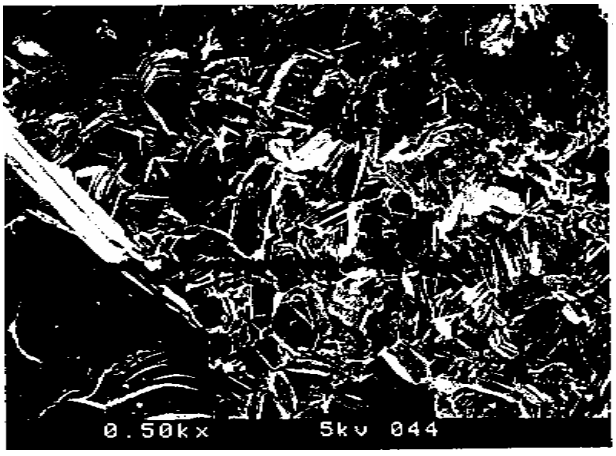

Plate: 4.75, SEM, E-BA1, 2842.10

(k=3.2mD, Θ=10.5%)

Stacked Pseudo-hexagonal kaolinte crystals infill porosity

PLATE: 4.75, SEM, E-BA1, 2842.10 (Stacked Pseudo-hexagonal kaolinite)

4.1.2.1.4 SEM ANALYSIS FOR WELL E-AO1

Plate: 4.76, SEM, E-AO1, 2675.00 (k=83.0mD, Θ=14.6%)

Quartz overgrowths, calcite and dolomite infill intergranular porosity.

PLATE: 4.76, SEM, E-AO1, 2675.00 (calcite and dolomite)

Plate: 4.77, SEM, E-AO1, 2679.84 (k=0.80mD, Θ=11.1%)

Quartz, chlorite and pyrite from alteration of detrital grains.

PLATE: 4.77, SEM, E-AO1, 2679.84 (Quartz, chlorite and pyrite)

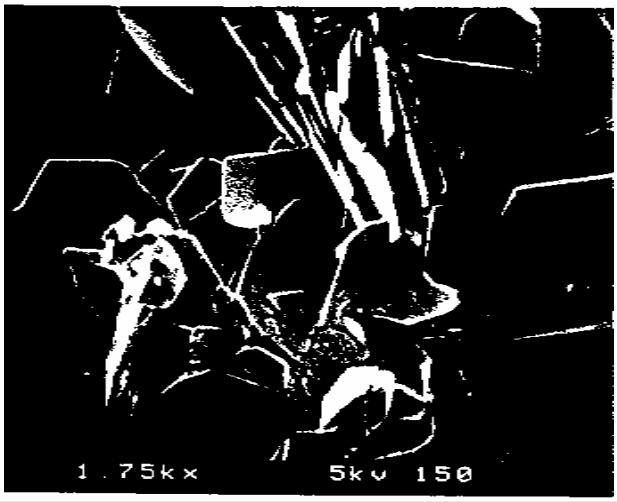

Plate: 4.78, SEM, E-AO1, 3252.00 (k=0.08mD, Θ=7.4%)

Rosettes of authigenic chlorite, partly enveloped by later developed quartz overgrowths

PLATE: 4.78, SEM, E-AO1, 3252.00 (Rosettes of authigenic chlorite)

4.1.2.1.5 SEM ANALYSIS FOR WELL E-BB1

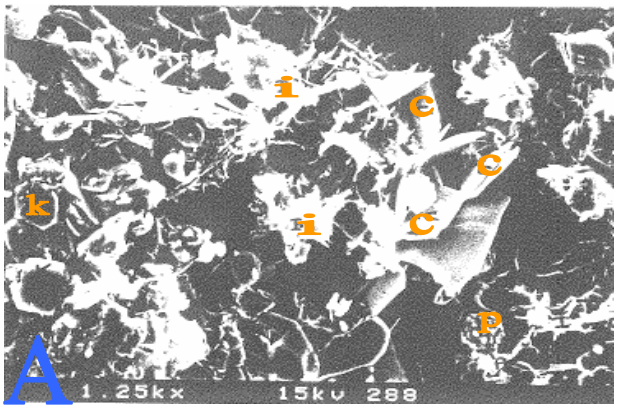

Plate: 4.79, SEM, E-BB1, 3280.00 (k=5.4mD, Θ=0.0%)

Illite (I), chlorite (C), kaolinite (K) and framboidal pyrite (P), from alteration of detrital grains

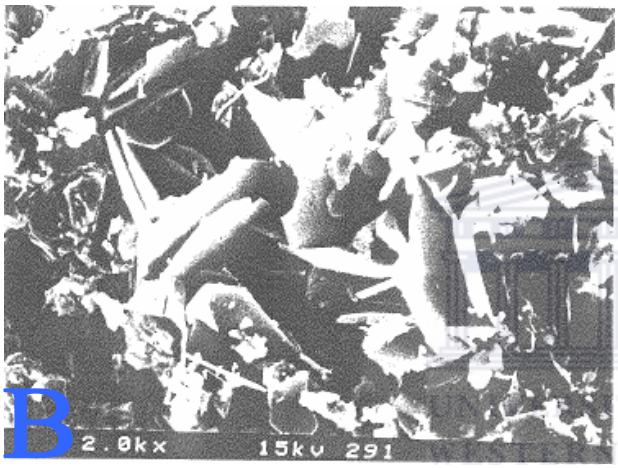

Chlorite rosettes developed on grains surface.

PLATE: 4.79(A & B), SEM, E-BB1, 3280.00 (Chlorite rosettes)

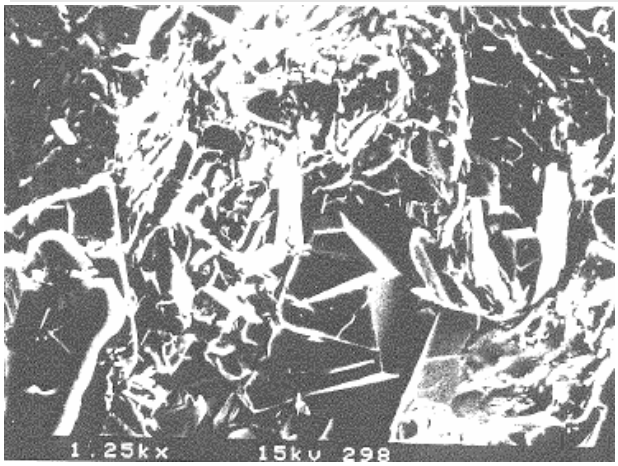

Plate: 4.80, SEM, E-BB1, 3290.00 (k=0.02mD, Θ=10.6%)

Quartz overgrowth and chlorite. The chlorite appears to be etched, and possibly illitised.

PLATE: 4.80, SEM, E-BB1, 3290.00 (Quartz overgrowth and chlorite)

PART THREE

4.1.3 X-RAY DIFFRACTION (XRD) PETROGRAPHY

X-ray diffraction analysis provides relatively precise compositional information, along with phase identification of minerals. Clay analysis is particularly useful in determining the proportions of swelling and non-swelling clays, which is important for potential formation damage. X-ray diffraction is a highly useful method for determining the clay mineralogy and different mineral phases of samples. Identification of damaging clays is very important in the completion and stimulation procedures utilized by field personnel.

4.1.3.1 X-Ray Diffraction Analysis

The analysis started by a search/match process, which tries to identify an unknown scan using a set of reference patterns scaled to take the matched intensities into account. The reference patterns are displayed as stick diagrams. Searching is based on pattern recognition techniques, runs automatically in a few seconds and delivers a list of the best results to check.

Matching is an interactive process: either accept or reject each proposed reference pattern based on graphical compatibility between the unknown scan and the reference pattern and based on compatibility with knowledge of the sample.

XRD analysis is not much different from thin section description and SEM analysis. XRD phase analysis identifies the presence of clay minerals; Kaolinite, illite and chlorite; and cementing materials such as quartz, calcite, dolomite and siderite of ferroan composition. In addition, zeolite; laumontite is identified in a number of samples. Laumontite is thought to have a hydrothermal origin or lining cavities in igneous rocks. It may be formed in thick

sedimentary beds by metamorphism of plagioclase, and may be authigenic, cementing sandstones. Laumontite has a euhedral morphology mainly filling veins, like quartz. It is thought to form associations with calcite, chlorite and quartz. Therefore the occurrence of laumontite as identified from XRD could be linked with decomposition of plagioclase. Also formation of laumontite is thought to occur at temperatures between 100 – 110 degrees Fahrenheit (37.8 – 43.3 degree Centigrade) (Bloch, 1991).

X-ray diffraction patterns for the wells are displayed in appendices eleven to eighteen. The patterns show all the identified clay mineral phases present at selected depths and wells. Analysed plots represent only minerals with maximum number of phases identified are shown, those with single phase are not shown. All 54 X-rayed samples could not be displayed as most of the samples show similar phases.

- X-Ray diffraction patterns for each phase are unique,
- the patterns are produced independently of others, and
- in a mixture, their intensities are proportional to phase concentration.

5. CHAPTER FIVE

5.1 RESULTS AND DISCUSSIONS

Porosity and permeability can be accounted for and evaluated through the direct and indirect parameters which control them. One of the many factors controlling porosity and permeability is cementation, (the process of forming new minerals inside the pores) which leads to diminishing porosity and permeability (negative effect). Various authigenic minerals have been identified in core samples studied in the wells of the central Bredasdorp Basin sediments.

5.1.1 CEMENTATION

The main types of cements identified in the reservoir sandstone samples include quartz, siderite, calcite, dolomite and clays. Inclusions of hydrocarbons are trapped between different phases of the cements. Early cementation of pyrite, siderite nodules, illite and chlorite rims, compaction, quartz overgrowths, could be interpreted to have formed by mobilization of ferrous iron from siderite and pyrite and by precipitation of ferric hydroxide under oxidizing ground-water conditions. Carbonate cement, particularly siderite and calcite, occur in variable amounts in a few samples but generally has little affect on reservoir quality in the majority of samples. Authigenic, pore-filling kaolinite occurs in several samples and is probably related to feldspar/glauconite alteration, and kaolinite degrades reservoir quality.

5.1.1.1 QUARTZ CEMENT

Quartz, in the form of syntaxial rims, is the dominant cement in the reservoir sandstone. Quartz cementation appears to be developed very early in some samples with low ductile rock fragment content. This is indicated by the preservation of the original intergranular volume. Quartz overgrowths grew into the primary pores, largely filling them although the initial intergranular porosity is not completely occluded.

5.1.1.2 CLAYS

SEM of the clays indicated that the clays are dominated by kaolinite and illite and chlorite in some cases. Under the optical/petrographic microscope and SEM, kaolinite occurs as euhedral booklets which infill pore spaces and is intergrown with quartz overgrowths. Kaolinite in the form of pseudo-hexagonal stacked plates is pervasive in nearly the entire reservoir sandstone samples (see SEM photomicrographs).

Genetically, there are two types of authigenic kaolinites in the reservoir sandstones. The first type is formed by the complete replacement of an original or precursor grain. This kind of kaolinite shows the exact margin of the original grains. The second type is precipitated directly from pore fluids. This pore-filling cement alters the intergranular macroporosity to microporosity, which exists among the kaolinite booklets (Plates 4.63, 4.64A and 4.65B). This type of kaolinite, which is coarser-grained, shows less packing, and is also intergrown with the quartz cement (plate 4.66A). Illite is the next most important clay mineral in most of the samples. Its authigenic nature is evident from its fibrous, lath- or lettuce-like habit (plates 4.68 and 4.67B). The mineral is thought to have largely formed as a replacement product of chemically unstable rock fragments. In some rare instances illite occurs as pore bridging cement (plate 4.67A). Laumontite occur in minimal amount as identified from XRD phase analysis.

5.1.2 RESERVOIR QUALITY ANALYSIS RESULTS FOR EACH WELL

5.1.2.1 RESERVOIR QUALITY ANALYSIS RESULTS FOR WELL E-BA1

Porosity and permeability range from very poor to moderate, 6.0-12.15% Porosity and 0.04-42.64mD permeability. Secondary, porosity develops by dissolution of early diagenetic cement (calcite) and detrital grains. Quartz overgrowth and ferroan dolomite are the most abundant pore filling cements. The very abundant of kaolinite has reduced much of the secondary porosity to microporosity, resulting in poor permeability. The development of pseudomatrix and the presence of argillaceous laminae also reduce permeability. Pore filling glauconite may have restricted primary porosity. The best poroperms occur around 2828m, where authigenic cements, particularly kaolinite are less abundant. This suggests that probably migration of hydrocarbons into these sand units halted diagenesis early, hence preserved porosity and permeability.

5.1.2.2 RESERVOIR QUALITY ANALYSIS RESULTS FOR WELL E-CA1

Reservoir quality ranges from poor to good, (7.8-18%) porosity and (4.8-200mD) permeability. Porosity is secondary, after dissolution of early intergranular cement and, to a laser extent, detrital grains. Quartz overgrowths are the major pore-filling cement, and are most abundant in the finer sandstones, resulting in the very poor reservoir quality in these units. Quartz overgrowth, ferroan dolomite and kaolinite are the main porosity reducing phases, with illite also abundant. Laser amounts of authigenic feldspar, siderite, pyrite and pseudomatrix are also developed. The best porosity occurs with more abundant ferroan dolomite cement. This may be due to the dolomite having formed early during diagenesis, thus restricting subsequent quartz cementation by limiting the number of nucleation sites. During late diagenesis the dolomite was leached to form the observed secondary porosity.

5.1.2.3 RESERVOIR QUALITY ANALYSIS RESULTS FOR WELL E-AA1

Reservoir quality of this borehole could be attributed to pervasive calcite and silica cementation that are the main cause of porosity and permeability destruction. Microporosity and the development of secondary porosity are attributed to the formation of authigenic, pore filling kaolinite and partial dissolution of lithic clasts. Poor sorting contribute to the low primary porosity, and fine grain size, argillaceous lamina and silica cement contribute to low permeabilities. Early development of intergranular illite after detrital clay prevented initial silicification and provides microporosity. Kaolinite and minor chlorite development is attributed to lithic clasts and /or feldspar and appears to have formed at a later stage. Dissolution of intergranular kaolinite results in the formation of good, interconnected secondary porosity

5.1.2.4 RESERVOIR QUALITY ANALYSIS RESULTS FOR WELL E-BB1

Reservoir quality characteristics in E-BB1 range from poor to good. Ferroan dolomite and quartz overgrowth cementation, and the development of pseudomatrix (from compaction of clay clasts) have destroyed porosity. These additional pore filling cements may have developed during late diagenesis, after hydrocarbon migration into the reservoir unit. In the argillaceous sections, clays have a more significant porosity and permeability reducing effect, with detrital clays and pseudomatrix infilling much intergranular porosity. SEM analysis indicates that authigenic illite and chlorite are commonly developed by alteration of detrital grains, with associate microporosity. Quartz overgrowths are the most abundant crystalline cement in the argillaceous sections, with minor amounts of ferroan dolomite, pyrite and ferroan calcite.

5.1.2.5 RESERVOIR QUALITY ANALYSIS RESULTS FOR WELL E-AO2

Poroperm characteristics range from very poor to good (4.6%, 0.0lmD to 15.5%, 86.5mD). Secondary porosity is commonly developed by leaching of early calcite cement and detrital grains. The main pore filling phases are quartz overgrowths, dolomite, kaolinite, pseudomatrix and illite. Quartz overgrowths are abundant throughout the samples whereas the other authigenic phases are all present in variable amounts at different depths. Pseudomatrix and illite are developed from deformation and alteration of lithic grains, and hence are most abundant in the more lithic samples (plate 4.37) Kaolinite is most abundant in the less lithic samples (plate 4.40). Pore filling dolomite rhombs developed fairly late during diagenesis, and are generally most abundant in the less siliceous samples (plate 4.40), in which the best secondary porosities have been developed. Minor amounts of feldspar overgrowths, siderite are developed locally.

5.1.2.6 RESERVOIR QUALITY ANALYSIS RESULTS FOR WELL E-AO1

Porosity and permeability are very good (plate 4.25), but tend to deteriorate with depth as grain size decreases and sorting improves. Cementation by quartz, calcite and dolomite becomes more extensive with depth in the sections, as does development of pore – lining authigenic illite and chlorite appear. Hence porosity and permeability are poor as depth increases (plate 4.28). Preserved porosity is secondary, after cement and grain dissolution.

Authigenic chlorite, pyrite and Fe-rich calcite and dolomite may present reactivity problems if the formation is acidised with Hydrochloric acid (Hcl). SEM analysis indicates that authigenic chlorite is common as a grain alteration product, and hence the formation may be sensitive to acidisation.

5.1.2.7 RESERVOIR QUALITY ANALYSIS RESULTS FOR WELL E-AD1

Good secondary porosity is present. The dominant poroperm destroyer is pseudomatrix which has developed as a result of compaction and diagenesis of sediments containing a high proportion of lithic material. Authigenic illite, late stage, pore filling kaolinite, silica and calcareous cements are present and have an adverse effect on poroperm characterisitics. In the argillaceous sections (plate 4.46) abundant detrital clay and silica cement are the dominant poroperm destroyers. Authigenic illite and kaolinite are also present and contribute to reduction in porosity.

5.1.3 GENERAL PETROGRAPHIC SUMMARY

Table 5.0: General petrographic summary (Thin Section, SEM & XRD)

CEMENTS	MORPHOLOGY/POSITION	COMPOSITION
Quartz	Overgrowths on detrital grains	SiO
Calcite	Etched pore filling crystals	$CaCO_3$
Siderite	Microcrystals	
Dolomite	Rhombic pore filling crystals	$Ca(Mg,Fe)(CO_3)_2$
Pyrite	Framboid microcrystals	
AUTHIGENIC CLAYS		
Illite	Fibrous crystals from grain alteration coating grains	$K(AlFe)_2AlSi_3O_{10}(OH)_2H_2O$
Chlorite	Rosettes/Platy crystals from grain alteration coating grains	$Mg_{2.5}Fe_{1.65}Al_{1.5}Si_{2.2}Al_{1.8}O_{10}(OH)_8$
Kaolinite	Pseudo-hexagonal stacked platy crystals infill porosity	$Al_2Si_2O_5(OH)_4$
Pseudomatrix	Compacted clay grains	Mostly illite composition
Detrital clay	Amorphous pore filling, recrystallised to authigenic illite and chlorite	Mostly illite composition
Clay Clasts	Undeformed crystals (possibly glauconite)	
ZEOLITE		
Laumontite		$Ca_4(Al_8Si_{16}O_{48})(H_2O)_{18}$

Table 5.1: Porosity and Permeability Destroyers

DESTROYERS	EFFECT ON POROSITY AND PERMEABILITY
Quartz	Pore coating
Calcite	Pore-filling: fills porosity completely
Illite	Low overall volume: Porosity not reduced much, permeability reduced.
Kaolinite	Greatly reduces porosity but space between layers allows flow: do not reduce permeability
Chlorite	Reduction of both porosity and permeability.

5.1.4 POROSITY AND PERMEABILITY DISTRIBUTION DURING COMPACTION AND DIAGENESIS.

Porosity and permeability is loss due to compaction and diagenesis. Deeply buried sandstones have high intergranular porosities, and consequently high permeabilities, whereas others are completely cemented. The concept of reservoir quality is an evolution in understanding of basic controls on both porosity and permeability. Porosity is created, preserved, or destroyed by a combination of:

(1) Physical (mechanical) compaction of grains, and

(2) Mass transfer processes that supply and remove components required for cementation, grain dissolution, and mineral transformations (Larsen, 1985).

Variation in subsurface permeability reflects the variety of different diagenetic processes that acted to greater or lesser extent on sandstones. Permeability of the sandstones decreases during burial diagenesis, but permeability is reducing in sandstone of different wells more than in others. Mechanical compaction causes sandstones with abundant ductile grains to lose permeability relative to sandstones with few ductile grains. Sandstones with clay laminae or abundant mud clasts are cemented by quartz because of stylotization. Fine-grained sandstone with smaller pores, show greater reduction in permeability due to burial compaction and cementation than coarser grained sandstone. Sandstones having low permeability experiences greater diagenetic loss of reservoir quality, resulting mainly from the loss of porosity by compaction and quartz cementation (Larsen, 1985).

The relationship between porosity and diagenesis is variable and complex. The major diagenetic processes affecting porosity are dissolution, cementation and dolomitization. Dissolution creates and enhances porosity. Dissolution of grains is accompanied by calcite cementation in adjacent primary pores. Cementation is an important diagenetic process because it reduces porosity. The degree of cementation varies from thin cement coatings around the grains that partially fill the pores and alter permeability pattern to calcite that completely fill the pores. Dolomitization may reduce, redistribute and preserve or create porosity. Early dolomitization may preserve porosity by creating a rigid framework that inhibits compaction. Processes such as cementation may reduce porosity, thus porosity preserved through shallow burial may or may not be preserved in the deeper subsurface (Larsen, 1985).

5.1.4.1 DIAGENETIC STAGES AND EVENT SEQUENCES

A combination of thin section petrography, SEM and XRD analysis studies are employed to construct diagenetic stages and event sequences for the studied area. Hydrocarbon migration is linked to the diagenetic events. The early, middle, and late diagenetic stages are shown in Figure 5.0. High initial rates of compaction occurred mainly in muds, and in sands that are not lithified, or supported, by early quartz and/or calcite cementation. The dashed lines are periods of dissolution of grains and cements, which develops secondary porosity and permeability.

5.1.4.1.1 VERY EARLY DIAGENETIC STAGES

The earliest diagenetic event is compaction. This is most significant for sediments with high mud content; sand-sized grains floating in the matrix exhibit minor diagenetic changes. This results from isolation of these grains from pore fluids that affected cementation and dissolution. Compaction of sediments decreases through time; later diagenetic cementation of sandstones by calcite and quartz stabilizes the grain framework; this decreases porosity and permeability loss through rearrangement of grains. Precipitation of pyrite, and alteration of faecal pellets to glauconite results from reducing conditions in marine pore fluids; this occurs soon after burial. Accumulation of bacterial end-products in pore fluids results in precipitation of carbonate minerals (siderite).

5.1.4.1.2 EARLY – MIDDLE DIAGENETIC STAGES

Rims of chlorite grow perpendicular to quartz grain surfaces and appear to be intergrown with the quartz cement, as shown on the plate 4.66 SEM image. Quartz displays well-developed overgrowths. X-ray diffraction analysis indicates that the chlorite is ferroan chlorite. Chlorite and glauconite are found almost exclusively in marine environments. Precipitation of calcite cement prior to cementation by quartz also characterizes this stage.

5.1.4.1.3 MIDDLE – LATE DIAGENETIC STAGES

The late-diagenetic pyrite framboid crystals may probably be associated with dolomite and may result from changes in chemical composition of pore fluids resulting from migration of hydrocarbons into the Bredasdorp basin sandstone. Quartz grains in thin section and SEM display well-developed overgrowths. Overgrowth formation is preceded by precipitation of non-ferroan, poikilotopic, zoned calcite cement (plate 4.35A&B). This was followed by filling of the secondary pore by ferroan dolomite and pyrite. Also glauconite has been slightly altered to illite, and feldspar undergoes extensive late-diagenetic dissolution and recrystallization. Dissolution of the ferroan calcite cements resulted mainly from changes in pore fluid chemistry, primarily organic and carbonic acids associated with hydrocarbon generation and migration into the reservoir. This created secondary porosity, and provided the primary source of chemically reduced iron for pyrite and ferroan dolomite. Migration also resulted in dissolution of feldspar and subsequent precipitation of kaolinite in pores. Dissolution of unstable lithics, chemical compaction by stylolitisation and intergranular pressure solution and other stages are characteristics of middle to late diagenesis. Formation of late kaolinite during late dissolution of feldspar grains by organic acids generated during kerogen maturation.

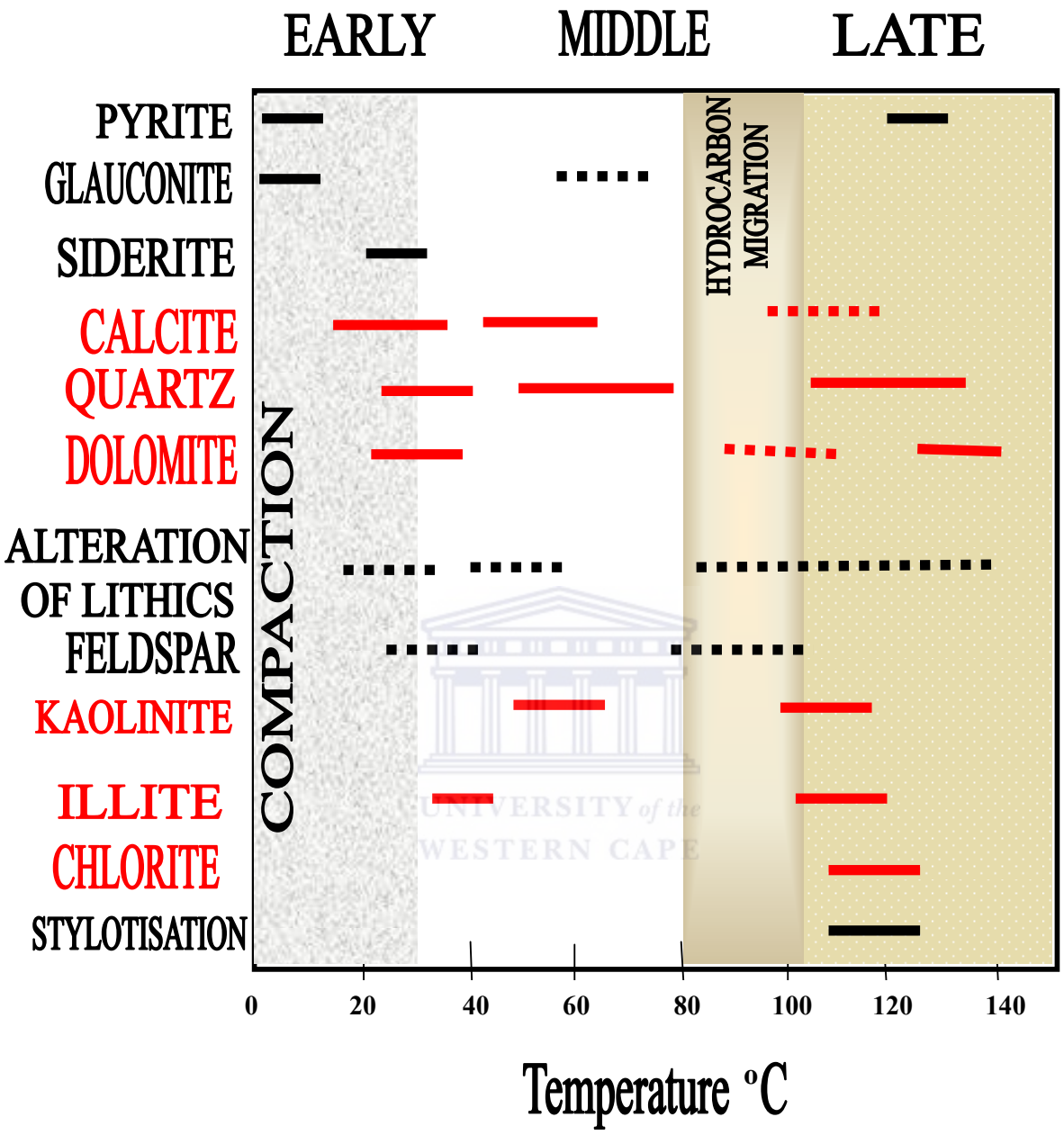

Figure 5.0: Generalized diagenetic stages and event sequences for the Bredasdorp basin.

The interpretation is based on the integration of thin section petrography, SEM, and XRD results. Dashed lines indicate dissolution of cements or lithic grains and cementation (red).

5.1.5 APPROXIMATE RANGES IN CEMENT/CLAY VOLUMES FOR THE DIFFERENT STYLES OF DIAGENESIS.

Table 5.2: Approximate ranges in cement/clay volumes for the different styles of diagenesis.

DIAGENESIS STYLE	VOLUME RANGE OF PRINCIPAL CEMENT/CLAY	VOLUME RANGE OF ANCILLARY CEMENTS
Quartz dominated	10-30% (increase with depth and temperature of burial)	5-10%, late carbonate
Clay dominated	15-25% (illite, chlorite, kaolinite increase with depth and temperature of burial)	≤10% late carbonate
Early Clay/late quartz	5-15% Clay. <10% Quartz	≤5% late carbonate
Early Carbonate	10-20%	
Zeolite	3-5% (increases with increasing lithic content)	≤10% clay, ≤5% late carbonate

6. CHAPTER SIX

6.1 CONCLUSIONS AND RECOMMENDATIONS

6.1.1 CONCLUSIONS

In assessing the reservoir quality in the central Bredasdorp Basin, all the factors controlling reservoir quality do not act in the same way. The various controls on reservoir quality act differently in each borehole and at different depths and sand units.

Quartz overgrowths play an important role in determining the petrophysical properties of sandstones. This cement causes reduction in porosity and permeability. Cement precipitated in limited amounts can probably help the reservoir framework to withstand the destructive effect of overburden pressure and consequent mechanical compaction. However, quartz cementation greatly affects porosity and permeability.

A high argillaceous content is directly responsible for the low permeability obtained in the core analysis. Pervasive calcite and silica cementation are the main cause of porosity and permeability destruction. Dissolution of pore filling intergranular clays may result in the formation of microporosity and interconnected secondary porosity.

Cross- bedded sandstones that are the primary reservoir facies show coarsening-upward sections of laminated clay/siltstones to fine to medium grained sandstones. These thin-bedded sandstone facies have lower reservoir favorability. Poroperm characteristics in these thin sandstones proved to be very poor due to detrital clays and pseudomatrix.

Detrital matrix varies in abundance from one well to another. It is particularly common in many of the Base reservoir samples. The matrix consists predominantly of clay minerals with lesser amounts of detrital cement (derived from weathering and erosion). Clay laminae are common in many of the samples. X-ray diffraction analyses suggest these clays largely consist of illite and kaolinite, with minor amounts of chlorite and laumontite. Because these clays are highly illitic, the matrix could exhibit significant swelling if exposed to fresh sea water, thus further reducing the reservoir quality.

The majority of the samples generally have significant cements; in particular quartz cement occurs abundantly in most samples. The high silica cement is possibly caused by the high number of nucleation sites (high surface area) owing to the relatively high abundance of detrital quartz. The extensive matrix in some of the samples also retards cementation by inhibiting nucleation of overgrowths. Carbonate cement, particularly siderite and calcite, occurs in variable amounts in most samples but generally has little effect on reservoir quality in the majority of samples. Authigenic, pore-filling kaolinite occurs in several samples and is probably related to feldspar/glauconite alteration. Kaolinite seriously degrades reservoir quality. The presence of chlorite locally (plate 4.66A & B) and in minute quantities is attributed to a late stage replacement of lithic grains.

Based on the combination of information derived from thin section petrography, SEM and XRD, diagenetic stages and event sequencesare established for the sandstone in the studied area. Hydrocarbon generation and migration has influenced some diagenetic effects on cements and clays. This includes feldspar dissolution, cement and grain dissolution and late kaolinite precipitation. This study shows that paragenetic sequences and their relation to

hydrocarbon generation and migration can be a valuable tool for oil migration into the reservoir sand units.

To conclude reservoir quality deteriorate with depth, as cementation, grain coating and pore infilling authigenic chlorite, illite, kaolinite become more abundant. Hence, the Top reservoir unit has better quality than the Base reservoir unit. The Top reservoir is oil saturated whereas the Base reservoir could be viewed as gas filled.

6.1.2 RECOMMENDATIONS

Kaolinite is chemically stable, however its lack of attachment to framework grains may cause a migration of fines problem where high fluid flow velocities are introduced into the system. Therefore, a clay stabilising system e.g. polyphydroxy-aluminium compounds or cationic polymer is suggested during the early history of the well.

Large volumes of microporosity are associated with illite and this may result in anomalously low permeabilities where illite is abundant. Fibrous illite may clump together in the presence of freshwater, thus further reducing permeability.

It may be dissolved using an acid mixture consisting of Hydrochloric and hydrofluoric acid.

The paragenetic sequences and their relation to hydrocarbon generation and migration can be a valuable tool for oil migration into the reservoir sand units. This could be reviewed with more data input from the Petroleum Agency South Africa and PetroSA.

XRD has applicability in cements and clay mineralogy (quantitative and qualitative) here it is implemented as a phase identification tool. No quantification measurements are done to know the exact clay mineral amounts, due to lack of quantification software. This aspect could also be reviewed.

REFERENCES

***Adams, A.E, Mackenzie, W.S. and Guilford, C. (1984*)**:* Atlas of Sedimentary Rocks under the Microscope. Longman Group Limited, Longman House, Burnt Mill, Harlow Essex CM20 2JE, England. P.104

Arthur, H. S. and Henderson, N.: Distribution of porosity and permeability in platform dolomites; insight from the Permian of West Texas

AAPG Bulletin; August 1998; v. 82; no. 8; p. 1528-1550.

Atkins, J.E & McBride, E.F., (1992): Porosity and Packing of Holocene river, dune, and beach sands. AAPG Bulletin, Vol. 76. No. 3, p. 339-355.

Bloch, S., (1991): Empirical prediction of porosity and permeability in sandstones: AAPG Bulletin, Vol. 75. No. 7, p. 1145-1160.

Broad, D.S. (2000): Petroleum exploration offshore South Africa: Journal of African Sciences, 31(1), 50-51.

Brown, L.F. (JR.), Benson, J.M., Brink, G.J., Doherty, S., Jollands, A., Jungslager, E.H.A., Keenan, J.H.G., Muntingh, A., and Van Wyk, N.J.S. (1996). Sequence Stratigraphy in Offshore South African Divergent Basins: An Atlas on Exploration for Cretaceous Lowstand Traps, American Association of Petroleum Geologist (AAPG) Studies in Geology, **41**, 184p

Cade, C. A, Evans, I. J & Bryant, S.L, (March, 1994): Analysis of Permeability Controls: A New Approach. Clay Minerals (1994) 29, P. 491-501

Carozzi, A.V., (1960): Microscope Sedimentary Petrography. John Wiley & Sons, Inc. Publishers. P.485

Chilingar, G. V.,(1964): Relationship between Porosity, Permeability and Grain size Distribution of Sands and Sandstones. University of Southern California, Los Angeles, Calif. (USA). P.71-74

De Wit, M.J. & Ransome, I.G.D (Eds) (1992): Inversion tectonics of the Cape Fold Belt, Karoo and Cretaceous Basins of Southern Africa. A.A Balkema/ Rotterdam/Brookfield, 266p.

Dingle, R.V, Siesser, W.G & Newton, A.R (1983): Mesozoic and Tertiary Geology of Southern African. A.A. Balkema/Rotterdam. P.99-106

Dravis, J.J., (1985): Enhanced Carbonate Petrography Using Fluorescence Microscopy. Journal of Sedimentary Petrology. Vol. 55, P.795-804.

Dutton, S.P., & Diggs, T.N., (1992): Evolution of porosity and permeability in the Lower Cretaceous Travis Peak Formation, East Texas: AAPG Bulletin, Vol. 76, No. 2, p.252-269.

Frewin, J., Grobbler, N., & Feddersen, J. (2000): The Oribi and Oryx oil fields: geological characterisation of a deep-marine channel-lobe system, Block 9, Bredasdorp Basin, offshore South Africa. Journal of African Sciences, 31(1), 22.

Georges Millot (1970): Geology of Clays. First English Edition. Masson ET Cie, Paris & Chapman & Hall, London. P.429

Gerald, M. Friedman & Syed A. Ali, (1981): Diagenesis of Carbonate Rocks: Cement-porosity Relationships. Society of Economic Paleontologists and Mineralogists. Reprint Series Number 10. P. 295

Gillott, J.E. (1987): Clay in Engineering Geology. Developments in Geotechnical Engineering. Vol. 41. Elsevier. P.468

Hurtchison C. S., (1974): Laboratory Handbook of Petrographic Techniques. A Wiley-interscience publication. John Wiley & Sons.

Jikelo, N.A. (2000): The natural gas resources of southern Africa: Journal of African Sciences, 31(1), 34.

Larsen, M. J., (April, 1989). Geological Well Completion Report of borehole E-AD1. Petroleum Agency/SoeKor (Pty) Ltd. South Africa.

Larsen G. & Chilingar, G.V. (1985): Diagenesis in sediments and sedimentary rocks. Development in sedimentology-25A. Elsevier Science publishers

Lori L. Summa, (1995): Diagenesis and Reservoir Quality Prediction. Exxon Production Research Company, Houston, Texas. U.S. National Report to IUGG, 1991-1994. Rev. Geophys. Vol 33 Suppl., American Geophysical Union.

MacKenzie, A.E and Guilford, C. (1980): Atlas of Rock-forming Minerals in the thin section. Pearson Education Limited, Edingburgh Gate, Harlow, Essex CM20 2JE, England. P.98

McAloon, W., Barton, K., Egan, J., & Frewin, J. (2000): Pre-development characterisation of a marginal deep-marine channel/lobe-system reservoir: block 9, the Bredasdorp Basin, offshore South Africa. Journal of African Sciences, 31(1), 47.

McLachlan, I.R., & McMillan, I.K (1979): Microfaunal Biostratigrphy, Chronostratigraphy and History of Mesozoic and Cenozoic Deposits on the coastal margin of South Africa. Geocongress 77: Geol. Soc. S. Afr. Spec. Publ. 6 (1979). P.161-181

McLachlan, I.R., & Broad, D.S. (2000): Petroleum exploration offshore South Africa: Journal of African Sciences, 31(1), 50-51.

Moorhouse, W.W. (1959): The study of Rocks in Thin Section. (Harper's Geoscience Series, Carey Croneis, Editor). Harper & Row, Publishers, New York and Evanston. P.514

Petroleum Agency SA Bronchures (2000-2005): South African Exploration Opportunities, p28, published by the South African Agency for Promotion of Petroleum Exploration and Exploitation, Parow, Cape Town. www.petroleumagencysa.com

Philip, A. Allen & John R. Allen, (1990): Basin Analysis – Principles and Applications. Blackwell Scientific Publications.

Philip H. Nelson & Kibler, (2003): A catalog of porosity and permeability from core plugs in siliciclastic rocks. USGS Open-file report 03-420.

http://pubs.usgs.gov/of/2003/ofr-03-420/ofr-03-420.html

Philip H. Nelson, (November 2004): Permeability-porosity data sets for sandstones. USGS, Denver, Colorado, US

Rafdal, J. (1991): Core analysis to calibrate well log interpretation. 2nd SOC CORE ANAL. London, England. 35-51p

Reed S. J. B. (1996): Electron Microprobe Analysis and Scanning Electron Microscope in Geology. Cambridge University Press. P. 201

Rezaee, M.R., (1996): Reservoir Characterization of the Tirrawarra Sandstone, in the Moorari and Fly lake Fields, Cooper Basin, South Australia, University of Adelaide, (unpublished Ph.D. thesis) 189 pp

Rider, M. (2000): The geological interpretation of well logs (2nd Edition). Whittle publishing, Scotland. Printed by interprint Ltd., Malta.

Rocky Reifenstuhl, (2002): Reservoir Characterization Studies in Alaska. Alaska Division of Geological and Geophysical Surveys. Vol. 6. No. 3, Fall 2002.

Saner S. and Sahin A.: Lithological and Zonal Porosity-Permeability Distributions in the Arab-D Reservoir, Uthmaniyah Field, Saudi Arabia: Reply
AAPG Bulletin, September 1, 2000; 84(9): 1368 – 1370

Schlumberger (2005). Schlumberger Oil Field Glossary: Where the Oil Field Meets the Dictionary. URL: http://www.glossary.oilfield.slb.com.

Selley, R.C. (1985): Elements of Petroleum Geology. Freeman, USA.

Serra, O., (1984). Fundamentals of Well-Log Interpretation (Vol. 1): The Acquisition of Logging Data: Dev. Pet. Sci., 15A: Amsterdam (Elsevier).

Shepherd, T.B, Rankin, A.H & Alderton, D.H.M. (1985): A practical Guide to Fluid inclusion Studies. Blackie & Sons Ltd. P.239.

Turner, J.R., Grobbler, N., & Sontundu, S. **(2000).** Geological modelling of the Aptian and Albian sequences within Block 9, the Bredasdorp Basin, offshore South Africa: *Journal of African Sciences*, **31**(1), 80.

USC, April 4, 2006*:* Depositional setting and geometry of carbonate facies. University of South Carolina (USC) sequence stratigraphy web. (www.strata.geol.sc.edu/thinsections/carb-facies.html

Van der Spuy, D. (2000): Potential source rocks and modelled maturity levels in the southern Outeniqua Basin, offshore South Africa.

Weaver, C. E. and Pollard, L. D., (1975): The chemistry of clay minerals. Development in sedimentology -15. Elsevier Scientific publishing company. P.213

Wood, E.M. (1995): Oil and gas development potential in Block 9, the Bredasdorp Basin, offshore South Africa: Oil & Gas Journal.

RELATED WEBSITE

www.ktgeo.com

www.corelab.com/petroleum services/geological/thin.asp

www.people.uncw.edu

www.panterra.nl/geoscienc/geology/reservoir quality.php

www.dog.dnr.state.ak.us/oil/products/publication/akpeninsula/reservoir_quality_report.pdf

http://pubs.usgs.gov/of/2003/ofr-03-420/ofr-03-420.html

www.petroleumagencysa.com

www.petrosa.co.za

APPENDIX

Appendix 1: Porosity and Permeability Values for Borehole E-BA1

Driller's Depth (mbKB)	Boyle's Law Porosity (%)	Klink. Perm. (mD)
2828.05	10.5	42.64
2832	8.9	0.29
2832.34	10.5	1.64
2832.91	11	11.69
2833.14	12.1	14.55
2833.39	11.8	13.94
2833.64	11.8	17.85
2833.93	6	0.05
2834.12	7.8	0.36
2834.33	9.4	0.85
2834.58	9.2	0.69
2834.83	9.7	0.82
2835.1	9	0.63
2835.32	9.6	0.43
2835.57	9.7	0.82
2835.82	8.6	0.15
2836.01	9.1	0.39
2836.28	8.9	0.33
2836.53	10.5	1.76
2836.78	10.5	1.75
2837.01	9.3	1.17
2837.21	9.8	0.58
2837.46	9.8	0.57
2837.71	11	1.81
2838.01	10.3	2.9
2838.3	10.7	1.9
2838.55	10.2	0.59
2838.8	8.2	0.13
2839.05	9.7	0.72
2839.33	10	0.91
2839.58	10	0.81
2839.83	10.1	0.66
2840.05	9.2	0.58
2840.27	9.6	0.53
2840.52	7	0.04
2840.77	8.6	0.15
2841.07	8.7	0.41
2841.36	9.5	0.32
2841.61	11	1.82
2841.86	10.7	4.83
2842.1	10.5	3.21
2842.37	11.2	5.41
2842.58	11.4	11.71
2842.78	11.5	14.89
2843.1	10.1	8.13
2843.39	7.7	0.04

Appendix 2: Porosity And Permeability Values For Borehole E-CA1

Driller's Depth (m)(Kb)	Gas Exp.Porosity (%)	Klink. Perm. (mD)
2783.05	13.3	16.57
2783.23	13.5	20.51
2783.49	14.1	29.58
2783.74	12.1	7.37
2784.03	12.8	11.81
2784.25	13.5	21.87
2784.5	13.7	46.81
2784.71	12.6	13.21
2784.98	10.4	0.19
2785.26	8.4	0.74
2785.49	9.2	0.23
2787.13	5.3	0.01
2788.05	7.1	0.01
2788.35	7.9	0.16
2788.67	6.4	0.04
2789.07	7.4	0.02
2789.29	7.1	0.03
2789.53	6.6	0.08
2789.79	8.3	0.04
2790.11	9.4	0.23
2790.32	9.7	0.57
2790.57	10.1	0.61
2790.82	10.1	0.45
2791.03	9.9	0.82
2791.24	9.2	1.21
2791.48	8.3	0.07
2792.31	6	0.02
2792.56	7.9	0.03
2793.02	3.4	0.01
2891.05	12.1	19.36
2891.25	9.2	0.69
2891.54	7.4	0.08
2891.79	9.3	0.57
2892.06	10.8	3.47
2892.3	11.3	7.78
2892.55	9.9	1.53
2892.8	10.6	2.17
2893.02	12.5	7.09
2893.25	11.4	3.37
2893.48	9	0.47
2893.73	9.6	1.2
2894.03	12	5.46
2894.25	11.9	8.24
2894.5	11.8	8.91
2894.77	12.1	9.97
2895.04	10.4	2.61

Appendix 2: Continued

2895.28	11.3	5.01
2895.53	10.2	2.55
2895.78	10	2.02
2896.06	10.3	2.19
2896.3	10.9	3.84
2896.55	12.5	9.04
2896.8	12.6	10.7
2897.04	9.2	0.36
2897.26	9.2	0.29
2897.76	7.4	0.07
2898.12	9.4	0.45
2898.35	9.3	0.46
2898.6	8.5	0.21
2898.86	9.8	0.72
2899.12	10.1	0.95
2899.35	10.8	2.54
2899.6	10.4	1.16
2899.85	9.3	0.34
2900.13	8.4	0.1
2900.38	8	0.1
2900.63	8.5	0.11
2900.87	9.3	0.31
2901.13	7.9	0.07
2901.38	9.9	0.31
2901.63	11.6	2.24
2901.88	10.9	1.32
2902.23	9.7	0.14
2902.48	9.8	0.25
2902.73	9.4	0.18
2902.98	9.2	0.15
2903.25	9.5	0.16
2903.54	7.6	0.13
2906.11	8.6	0.09
2906.3	8.3	0.06
2906.55	4.7	0.01
2925.05	11.3	27.68
2925.28	11	26.18
2925.53	12.1	38.42
2925.81	11	22.05
2926.1	9.8	8.2
2926.32	6.1	3.3
2926.57	11.6	48.49
2926.82	11.3	48.2
2927.08	9.9	10.15
2927.31	12.7	100.08
2927.56	14.9	120.91
2927.81	15.5	167.89
2928.05	16	146.84
2928.3	17.5	257.68
2928.55	17.8	285.62

Appendix 2: Continued

2928	16.6	218.58
2929.06	15.8	206.89
2929.29	16.1	263.65
2929.54	13	100.59
2929.79	8.9	25.62
2930.04	8.9	4.79
2930.28	10.4	17.23
2930.53	9.2	4.17
2930.78	11.3	25.44
2931.05	12.2	45.97
2931.33	12.1	39.07
2931.58	11.6	36.48
2931.86	9.3	5.81
2952.55	6.7	0.01
2952.77	6.7	0.02
2953.02	6.7	0.02
2953.27	6.1	0.01
2953.55	8.2	0.07
2953.78	8.5	0.11
2954.03	8.7	0.17
2954.28	9	0.41
2954.53	9.2	0.21
2954.81	8.6	0.14
2956.55	3.7	0.01
2979.05	14.2	27.51
2980.03	15.3	38.38
2981.01	10.3	2.48
2981.29	7	0.1
2981.79	9.9	1.31
2982.04	9.7	0.93
2982.53	10.5	4.84
2982	8	0.24
2983.95	9.8	1.2
2984.44	10.6	1.7
2984.69	11.3	2.88
2984.92	11	3.64
2985.16	9.4	0.98
2985.4	9.6	0.94
2985.66	8.8	0.41
2985.87	10.4	1.13
2986.11	10.6	1.69
2986.36	11	2.76
2986.61	11.4	3.4
2986.9	11.2	3.35
3209.05	9.1	0.04
3209.44	8.7	0.04
3209.96	8.2	0.01
3210.22	7.8	0.01
3210.67	8.1	0.02
3210.88	8.4	0.03

Appendix 2: Continued

3211.62	7.1	0.03
3211.87	9.8	0.06
3212.02	9.3	0.18
3212.61	10.5	0.02

Appendix 3: Porosity And Permeability Values For Borehole E-AA1

Driller's Depth (m)(Kb)	Gas Exp.Porosity (%)	Liq.Perm. (mD)
2509	3.7	0.02
2511.56	6.3	0.03
2512	6.5	0.03
2514.13	6.1	0.06
2516.3	6.5	0.05
2519.12	4.3	0.03
2520.98	4.2	0.05
2965	8.8	0.66
2965.55	9.9	5.5
2965.87	9.8	2.7
2965.91	10.5	2.7
2966.45	9.1	1.4
2966.75	4.3	0.03
2966.92	6.9	0.21
2967.1	10	1.6
2967.7	6.2	0.38
2968.02	5.3	0.02
2968.62	1.3	0.01
3060.5	3.3	0.04
3061.29	1.5	0.01
3061.88	17.6	6.5
3061.95	11.9	1.8
3062.36	10.9	0.05
3074.14	11.7	0.71
3074.26	11.2	1.3
3074.69	14.3	8
3074.92	12.6	3.5
3075.12	9.8	1.1
3075.5	14.5	3.5
3075.88	17.2	51
3075.92	16	60
3076.41	14.9	12
3076.67	12.6	8.2
3076.91	1.1	0.02
3077.24	2.9	0.01

Appendix 4: Porosity And Permeability Values For Borehole E-AD1

Driller's Depth (m)(Kb)	Gas Exp. Por. (%)	Liq. Perm. (mD)
2500	15.8	34
2500.44	14.4	29
2500.55	12.8	22
2500.75	11.8	8
2501.18	12.6	1
2501.45	9.4	28
2501.85	8.3	0.07
2502.5	9.2	0.13
2503.05	4.8	0.08
2503.87	8.2	0.52
2503.95	10.7	1.1
2504.45	12	10
2504.85	13.7	31
2505	14.9	15
2505.73	15.2	124
2505.85	15.2	163
2506.02	15.1	145
2506.3	15.2	121
2506.5	14.4	89
2506.6	14.7	49
2506.79	15.1	123
2507	14.6	122
2507.25	14.4	96
2507.5	14.3	44
2507.75	14.2	129
2507.87	14	93
2508.23	14.4	138
2508.48	14.1	141
2508.73	14.1	136
2508.76	13.8	76
2509.3	17.3	117
2509.65	17.3	299
2509.83	17	129
2509.9	16.8	283
2510.25	15.6	174
2510.5	15.1	161
2510.55	15.2	61
2510.75	15.7	104
2511.3	15.3	123
2511.55	15.2	156
2511.8	15.1	132
2512	13.7	80
2512.15	13.1	85
2512.4	13.7	102

Appendix 4: Continued

2512.82	13.9	43
2518	14.3	34
2518.53	12.6	31
2518.77	13.9	42
2519	14.4	31
2519.04	13.9	54
2519.71	16.9	49
2519.94	15	43
2520.19	15.2	37
2520.22	15.4	61
2520.65	15.1	33
2520.9	14.8	31
2521	14.8	42
2521.43	14.8	35
2521.68	15.2	49
2521.92	14.4	42
2522.15	13.8	46
2522.18	14.1	53
2522.67	13.9	18
2523.06	14.8	59
2523.54	14.7	36
2523.88	15	87
2846.77	4.8	0.12
2868	9.6	0.01
2868.75	2.3	0.01
2869.97	1.9	0.01
2911	14.9	409
2911.15	14.9	354
2911.44	13.2	280
2911.62	13.2	274
2911.74	12.3	226
2911.83	11.5	251
2911.95	11.8	168
2912.26	12.2	31
2912.42	10.3	9.2
2912.59	7.1	0.48
2912.7	7.7	0.13
2913.16	11.2	41
2913.4	3.5	0.08
2943	8.1	0.16
2943.93	2.3	0.01
2944.3	2.2	0.01
2944.4	3.7	0.03
2944.61	0.09	0.01
2945	2.5	0.01
2945.35	2.1	0.02
2945.8	7.3	0.06
2946.01	4	0.07
2946.14	6.3	0.12
2946.9	6.3	0.04

Appendix 4: Continued

2947.28	4.9	0.08
2947.5	6.6	0.32
2947.7	7.4	0.21
2947.9	7.9	1.4
2947.93	7.9	1.3
2948.39	7.9	1
2948.59	6.8	0.15
2948	7.5	0.56
2948.92	8.1	1.9
2949.73	9.9	4.9
2949.82	10.7	12
2950.28	10.1	10
2950.53	10.4	8
2950.75	10.3	8.9
2950.91	10.8	14
2951.34	11.4	16
2951.59	11.1	14
2951.78	10.4	9.3
2952.28	10.9	14
2952.53	9.6	4.8
2952.74	11.2	17
2953.24	10.6	13
2953.49	9.7	6.7
2953.74	10.1	9
2953.93	10	7
2954.46	9.9	7.7
2954.71	10.5	11
2954.93	10.1	8.2
2954.95	10.1	7
2955.5	10.7	14
2955.75	10.2	8.8
2955.98	11	16
2956.25	10.8	16
2956.49	10.4	13
2956.52	11.3	17
2956.88	10.8	17
2957.13	9.7	16
2957.38	8.4	2.5
2957.46	8.2	1.3
2957.82	2	0.01
2958.06	1.4	0.01
2958.11	6.4	0.16
2958.54	8	0.83
2963.12	10.5	1.1
2963.24	10.4	1.4
2963.56	11.5	2.2
2963.81	9.3	0.34
2964.09	8.6	0.21
2964.29	7.1	0.06
2964.34	7.2	0.06

Appendix 4: Continued

2964.56	8.5	0.22
2964.81	8.5	0.22
2965.06	6.9	0.03
2965.18	5.5	0.01
2978.27	7.3	0.01
2978.52	7.6	0.05
2978.77	6.9	0.05

Appendix 5: Porosity And Permeability Values For Borehole E-BB1

Driller's Depth (m)(Kb)	Boyle's LawPorosity (%)	Klink. Perm.(mD)
2537.25	13.1	2.74
2538.05	12.3	1.49
2539.1	12.5	3.08
2540.05	13.7	3.21
2541.05	13.1	1.04
2542.05	14.2	3.65
2543.05	11.5	1.76
2544.05	13.2	2.78
2545.05	13.3	2.04
2546	13.9	0.3
2547.05	10.3	0.07
2552.51	10.1	0.05
2553.51	11.6	0.48
2554.4	11.7	0.28
2555.44	12	0.22
2556.21	8.2	0.03
2659.05	11.6	0.93
2660.05	10.2	0.1
2660.93	8.2	0.02
2661.72	2.9	0.01
2663.16	2.8	0.01
2719.55	14.2	6.82
2720.55	14.3	11.23
2721.55	11.8	0.77
2722.55	13.2	1.31
2846.05	13.7	26.44
2847.05	13	23.67
2848.03	11.3	9.02
2849.05	12.6	28.08
2850.05	12	14.57
2851.05	11.8	7.79
2852.03	8	0.09
2853.11	13.7	16.64
2854.05	12.4	9.85
2855.05	11.3	4.65
2856.05	11	2.62
2872.05	11.9	16.5
2894.05	10.9	7.7
3281.5	5.6	0.01
3282.62	12.4	0.25
3283.87	11.3	0.18
3284.87	11.3	1.18
3286.04	10.4	0.07
3286.83	9.7	0.02
3287.9	11.5	0.23
3289	9.2	0.02
3290.31	10.6	0.02

Appendix 6: Porosity And Permeability Values For Borehole E-BB2

Driller's Depth (m)(Kb)	Boyle's Law Porosity (%)	Air Perm. (mD)
2542.2	20.1	7
2557.3	21.9	12
2569	18.8	3
2579	23.7	25
2611	22.9	20
2696.5	20.2	9
2830.6	22.3	18
2848.5	24	40
2854	23	30
2859.5	23.6	35
2868	24.4	50
2872	24.2	60
2876.5	24.9	55
2926.8	22.3	25
2947.5	20.2	7
2949.5	19.3	5
2970.5	20.3	8
2973.6	20.6	9
2975.5	21.3	13
2977.3	22.1	15
2990.5	20.5	11
2994.5	22.8	19
3004.6	23.7	45
3006.3	22.3	17
3011.6	23.6	25
3019.5	22.1	16
3024.5	22.9	20
3029	19	5

Appendix 7: Porosity And Permeability Values For Borehole E-AO1

Driller's Depth (m)(Kb)	Gas Exp. Por. (%)	Liq. Perm. (mD)
2674	16.1	106.44
2674	15.7	99.75
2674.3	15	1.06
2674.3	14	9.97
2674.55	14	7.38
2674.55	14	6.93
2674.8	15	6.28
2674.8	14	8.74
2675	14.6	83.34
2675	14.2	78.43
2675.25	13	5.29
2675.25	13	4.97
2675.5	13	3.44
2675.5	13	3.24
2675.75	12	8.95
2675.75	12	8.31
2675.85	14.8	4.09
2675.85	14.3	3.79
2676.19	14	1.13
2676.19	13	9.12
2676.44	11	1.2
2676.44	11	1.02
2676.69	12	1.63
2676.69	12	1.36
2676.91	14	1.1
2676.91	14.1	0.85
2677.3	10	8.37
2677.3	9	4.06
2677.55	12	4.5
2677.55	11	3.73
2677.8	12	1.16
2677.8	11	9.55
2677.92	12.9	1.14
2677.92	12.4	0.87
2678.25	11	1.8
2678.25	10	9.76
2678.5	12	9.36
2678.5	11	6.96
2678.75	5	1.7
2678.75	5	2.5
2678.88	11.1	0.8
2678.88	10.6	0.62
2679.14	11	9.17
2679.14	11	7.72
2679.38	11	8.3
2679.38	11	6.77

Appendix 7: Continued

2679.64	11	9.43
2679.64	11	7.8
2679.84	11.5	0.95
2679.84	11.1	0.82
2680.19	10	1.48
2680.19	10	9.99
2680.44	10	2.1
2680.44	9	1.46
2680.69	9	9.13
2680.69	9	6.22
2680.84	7	5.13
2680.84	6	2.82
2681.15	7	3.06
2681.15	6	1.2
3014.7	10	2.12
3014.7	9	1.59
3014.95	10	1.44
3014.95	10	1.25
3015.2	11	2.42
3015.2	10	2.14
3015.41	12	2.26
3015.41	11	1.94
3015.75	11	4.26
3015.75	10	3.85
3016	11	3.62
3016	11	3.31
3016.25	12	7.43
3016.25	11	6.76
3016.6	11	8.01
3016.6	10	7.3
3016.85	11	5.58
3016.85	10	5.03
3017.1	10	3.05
3017.1	10	2.72
3017.26	11	1.49
3017.26	10	1.25
3018.08	7	6.1
3018.08	7	2.94
3252	7	8.15
3252	6	5.39

Appendix 8: Porosity And Permeability Values For Borehole E-AO2

Driller's Depth (m)(Kb)	Gas Exp.Porosity (%)	Liq. Perm. (mD)
2912	9.7	2.11
2914	8	0.77
2916	8.6	1.56
2919	8.6	1.32
2924	6.6	0.04
2925.25	9.7	8.7
2925.37	8.2	0.98
2925.81	4.6	0.01
2926.21	5.1	0.02
2926.46	5	0.03
3028	7.2	0.12
3031	9.7	2.03
3033	7.5	0.03
3035	6.4	0.04
3037	9.3	0.41
3040	10.2	2.23
3046	5.2	0.02
3048	10.5	3.54
3072	13.1	21.51
3074	12.9	21.05
3076	15.5	85.08
3078	10.9	2.02
3080	10.5	2.49

Appendix 9: Porosity And Permeability Values For Borehole E-AR1

Drillers Depth (m)(Kb)	Gas Exp.Porosity. (%)	Klink.Perm. (mD)
2455	18.5	448
2455.25	18	169
2455.73	14.3	129
2455.91	16.6	272
2456.15	18.8	274
2456.23	18.4	306
2456.4	20	557
2456.46	19.3	379
2456.59	19.3	417
2456.8	19.9	328
2456.88	17.7	263
2457.12	17.1	531
2457.25	19.9	571
2457.4	20.5	566
2457.56	18.3	393
2457.82	17	171
2458.07	16.2	140
2458.31	15.2	59
2458.55	16.2	64
2458.6	13.6	82
2459.1	13.2	43
2459.2	14.7	28
2459.31	13	21
2459.48	15.1	115
2459.58	17.5	387
2459.69	17.7	632
2459.82	18.1	630
2460.05	17.7	457
2460.23	16.4	224
2460.38	16.8	209
2460.63	18	142
2460.92	18.5	512
2461.08	16.5	95
2461.39	15.8	35
2461.67	17.9	109
2461.89	18.5	49
2462.13	16.9	44
2462.31	15.8	35
2462.63	15.8	70
2462.7	16.4	13.6
2462.83	16.4	74
2463.03	17	66
2463.23	17.2	63
2463.43	17.3	38
2463.83	15.1	48

Appendix 9: Continued

2464.1	15.5	75
2464.35	15.2	48
2464.61	16.4	52
2464.7	16.7	85
2464.85	15.1	55
2465.1	15.1	43
2465.35	16	55
2465.6	15.2	61
2465.83	12.8	15
2466.59	10.3	11
2466.84	11	5.1
2467.12	18.6	183
2467.27	19.1	237
2467.6	17.8	368
2467.85	18.2	460
2468.1	17.3	376
2468.36	16.7	320
2468.61	17.2	416
2468.87	16.6	277
2469.12	16.4	147
2469.38	15.7	81
2469.62	15.9	53
2469.86	16.2	51
2470.11	15.6	53
2470.35	15.9	56
2470.59	18	53
2470.83	16.3	101
2471.08	17.3	77
2471.32	17.5	76
2471.57	16.8	72
2471.82	17.5	274
2472.08	17.9	104
2472.43	17.8	136
2472.66	16.9	155
2472.89	16.4	133
2473.09	16.1	119
2473.22	16.3	102
2849.1	3	0.01
2849.35	2.6	0.01
2849.4	2.2	0.01
2849.57	1	0.01
2849.63	1.9	0.01
2849.96	1.6	0.01
2850	2	0.01
2850.18	1.2	0.01
2850.3	2.4	0.01
2850.35	1.8	0.01
3116.24	2.6	0.01
3116.46	2.1	0.01
3116.68	1.5	0.01

Appendix 9: Continued

3116.97	3.7	0.01
3118.19	2.7	0.01
3118.79	4.3	0.01
3119.02	6.9	0.01
3119.32	4.5	0.01
3119.64	5.4	0.01
3119.89	5.6	0.01
3120.31	4	0.01
3120.64	4.9	0.02
3121.01	5.4	0.01
3121.43	3.7	0.01
3121.54	2.2	0.01
3121.94	5.1	0.01
3122.22	5.3	0.01
3122.43	4.8	0.01
3122.68	6.7	0.01
3122.94	7.5	0.01
3123.22	9.3	0.01
3123.51	7.8	0.01
3123.82	6.9	0.01
3124.07	6.6	0.01
3124.32	2.5	0.01
3124.55	6.5	0.02
3124.8	6.4	0.01
3125.25	7.4	0.01
3125.54	6.8	0.01
3125.78	7.3	0.01
3126	6.9	0.01
3126.13	4.5	0.01
3126.3	6.9	0.01
3126.5	5.5	0.01
3126.95	1.5	0.01
3127.18	2.3	0.01
3127.5	5.2	0.01
3127.75	7	0.01
3128.02	5.8	0.01
3128.22	3.3	0.01
3128.96	5.1	0.02
3129.33	6.1	0.02
3129.56	6.2	0.02
3129.81	4.7	0.01
3130.09	2.4	0.01
3130.39	2.9	0.01
3130.77	4.8	0.01
3131.08	3.9	0.01
3131.48	3.3	0.01
3131.97	3.6	0.01
3212	6.8	0.01
3212.3	7.4	0.01
3212.95	8.7	0.02

Appendix 9: Continued

3213.67	3.8	0.02
3214.08	5.4	0.02
3214.34	6	0.01
3215.09	8.2	0.05
3215.28	7.8	0.01
3215.67	10.1	0.07
3215.92	9	0.06
3216.07	7.4	0.01
3217.72	0.7	0.01
3217.78	3.9	0.01
3218.38	1.4	0.01

APPENDIX 10

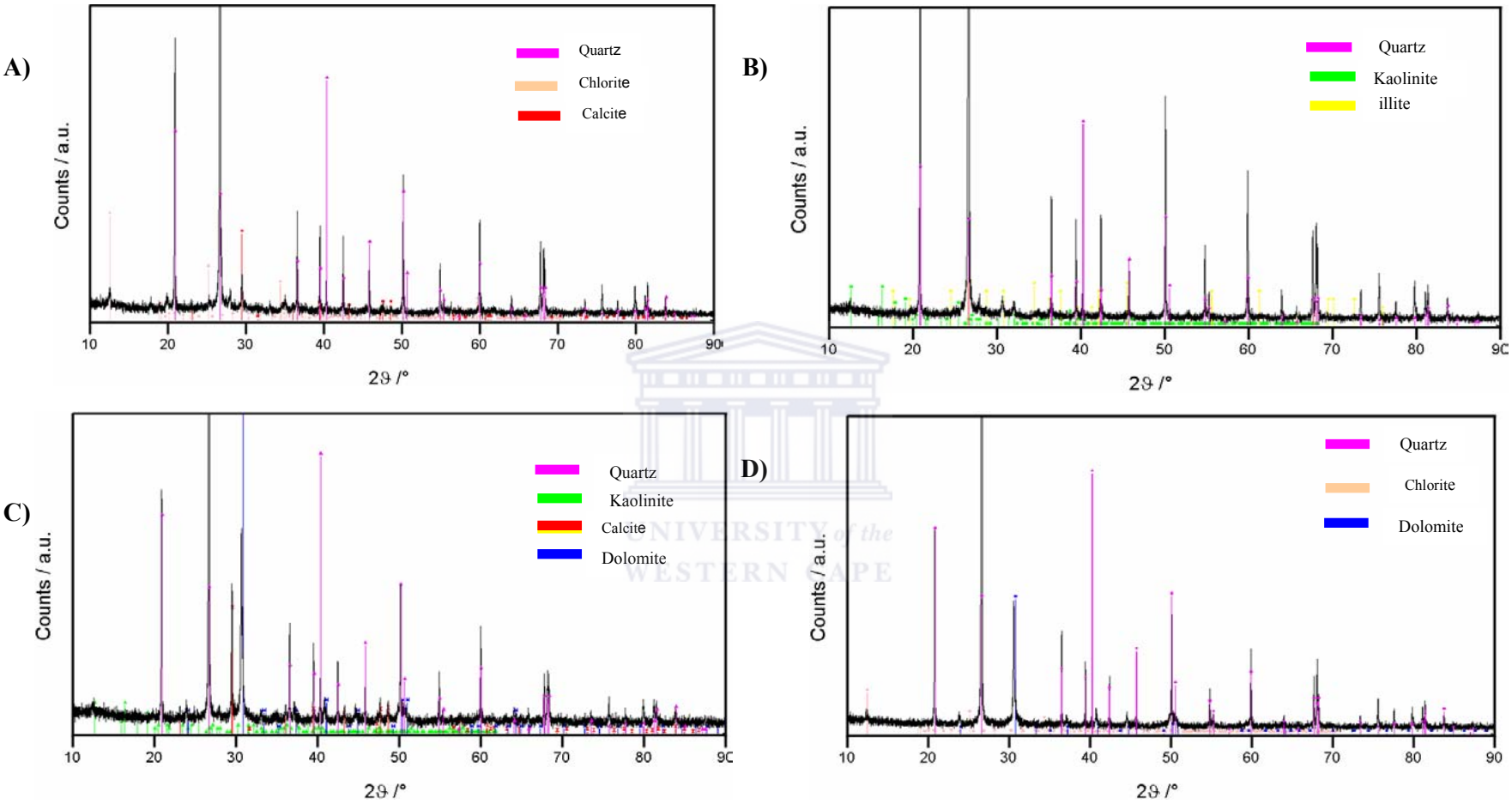

Appendix 10: XRD plots for well E-AA1;

Plot A) at depth of 2520.98m, B) at 3075.95m, C) at 3076.91m and D) at 2966.92m.

APPENDIX 11

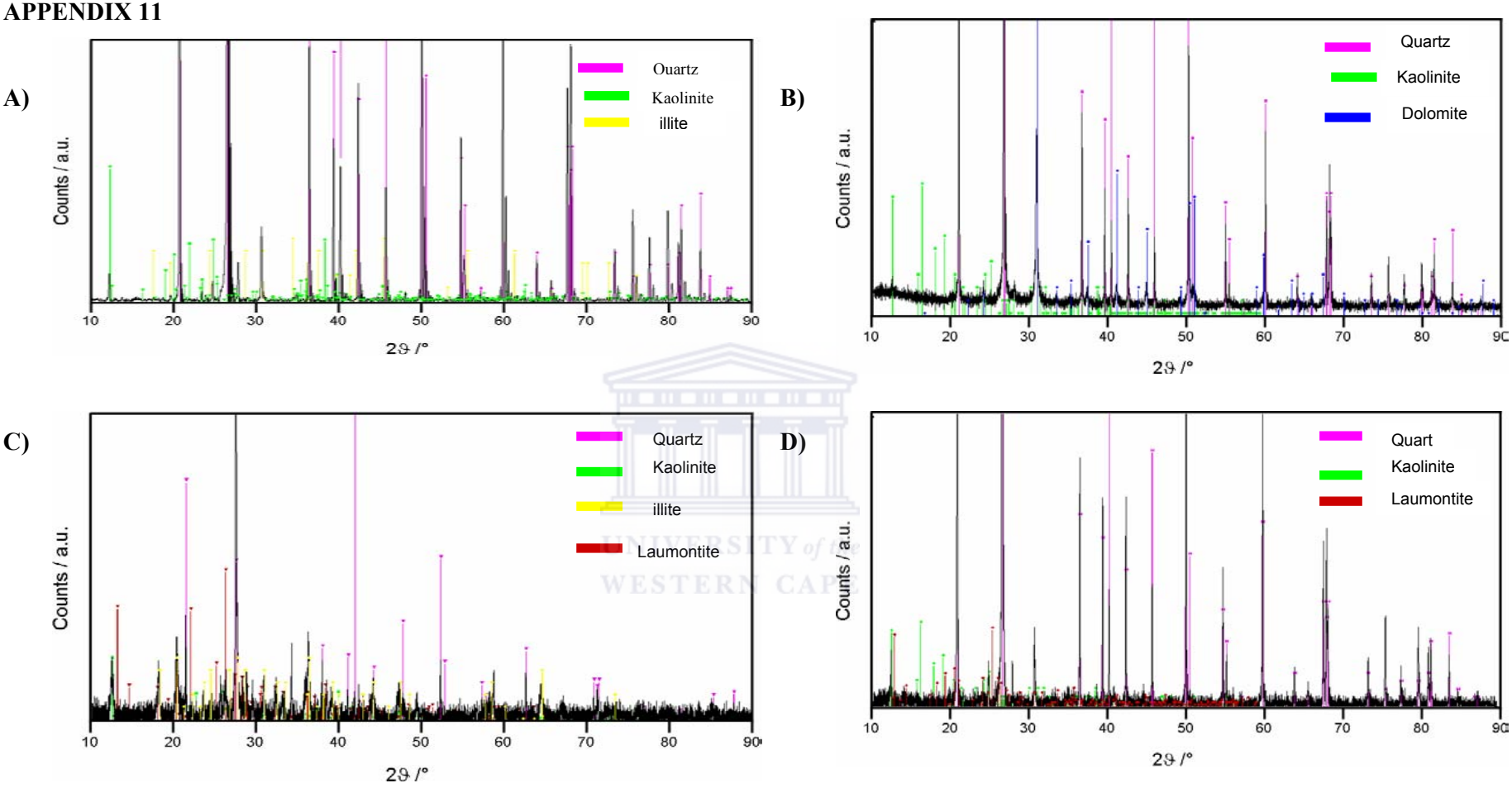

Appendix 11: XRD plots for well E-BA1;

Plot A) at depth of 2842.05m, B) at 2842.96m, C) at 2828.00m and D) at 2833.89m.

APPENDIX 12

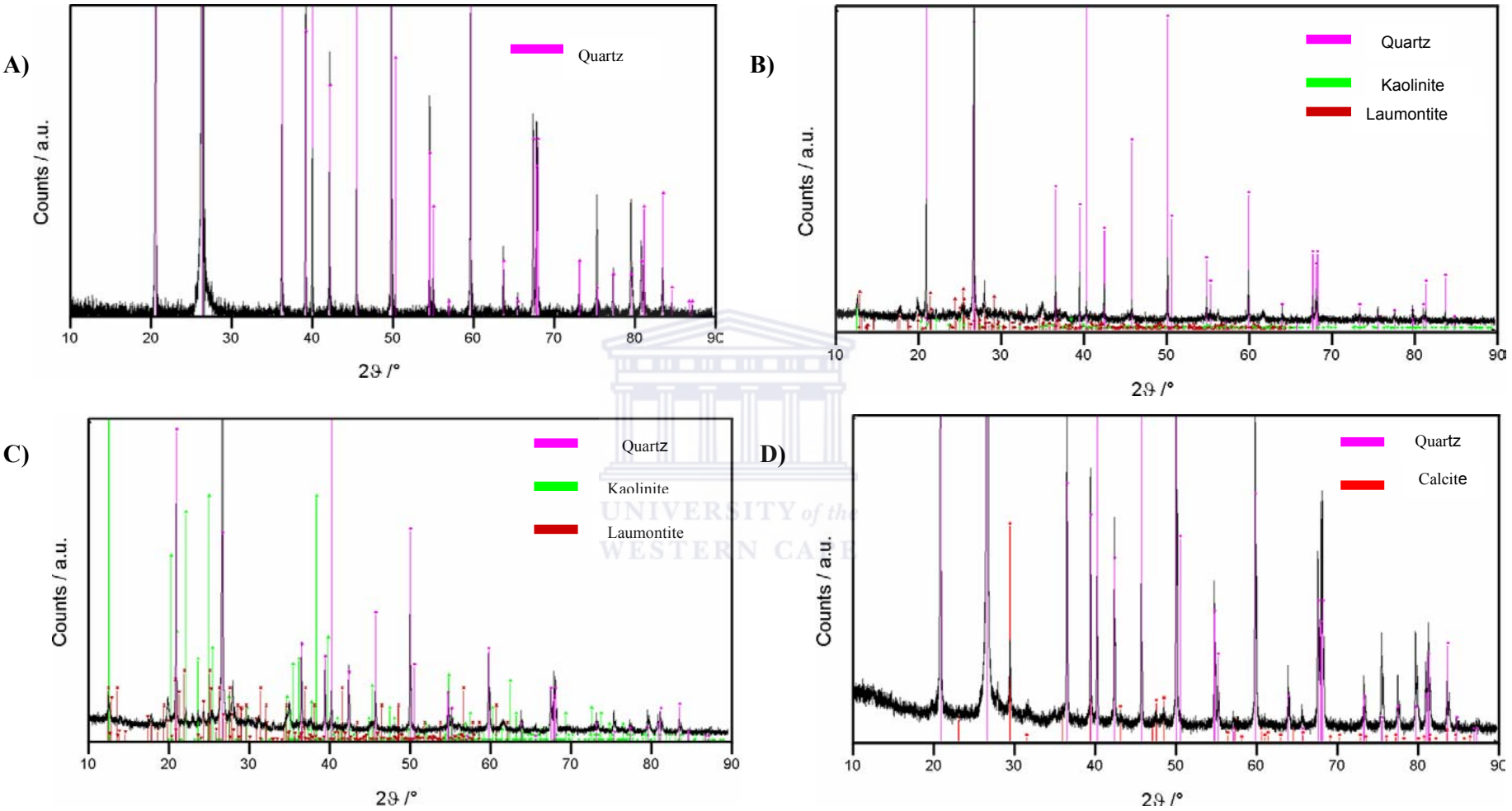

Appendix 12: XRD plots for well E-AR1;

Plot A) at depth of 2457.25-.38m, B) at 3215.28m, C) at 3214.45m and D) at 2465.30-.31m.

APPENDIX 13

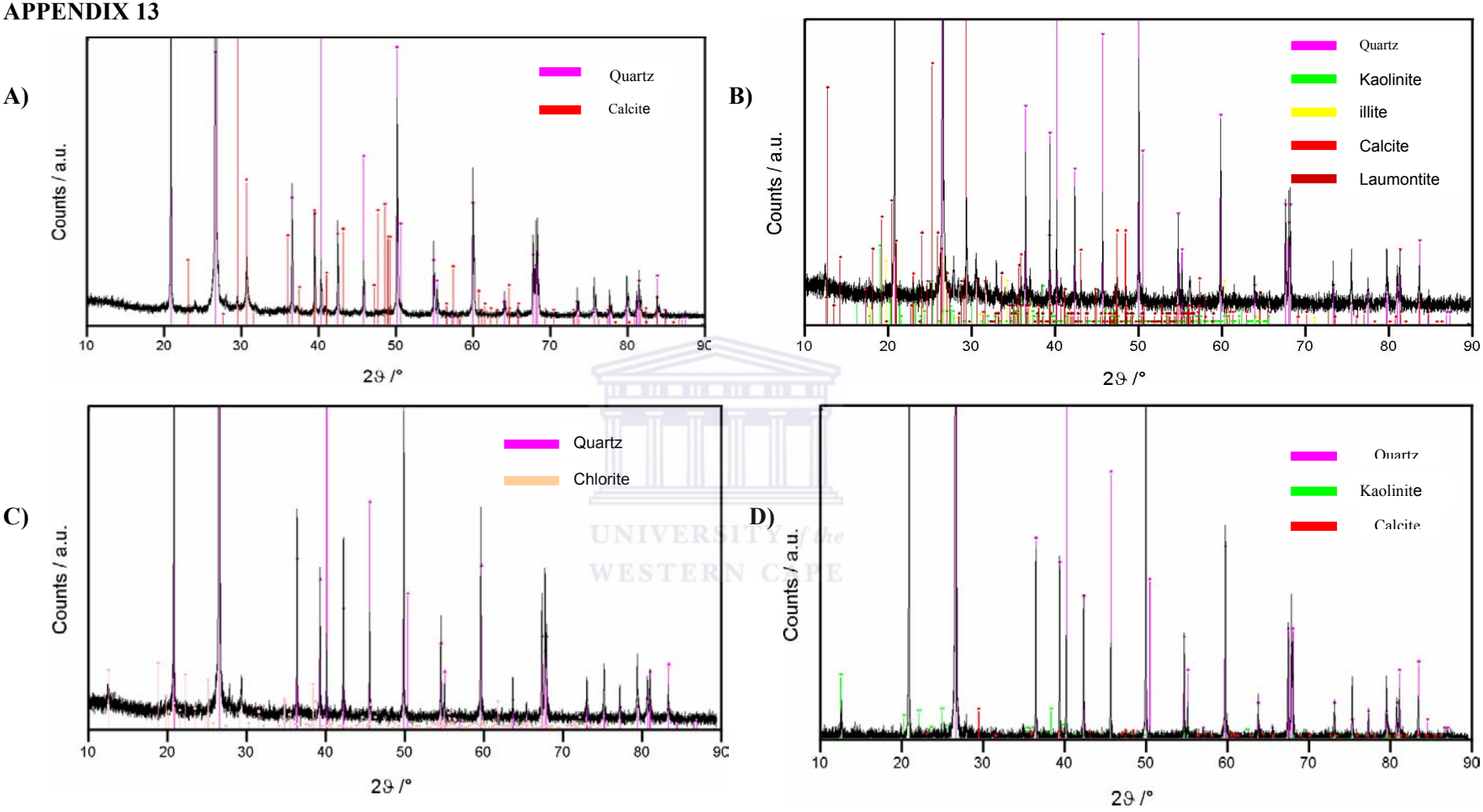

Appendix 13: XRD plots for well E-AO1;

Plot A) at depth of 2675.00m, B) at 2678.88m, C) at 2676.91m and D) at 3252.00m.

APPENDIX 14

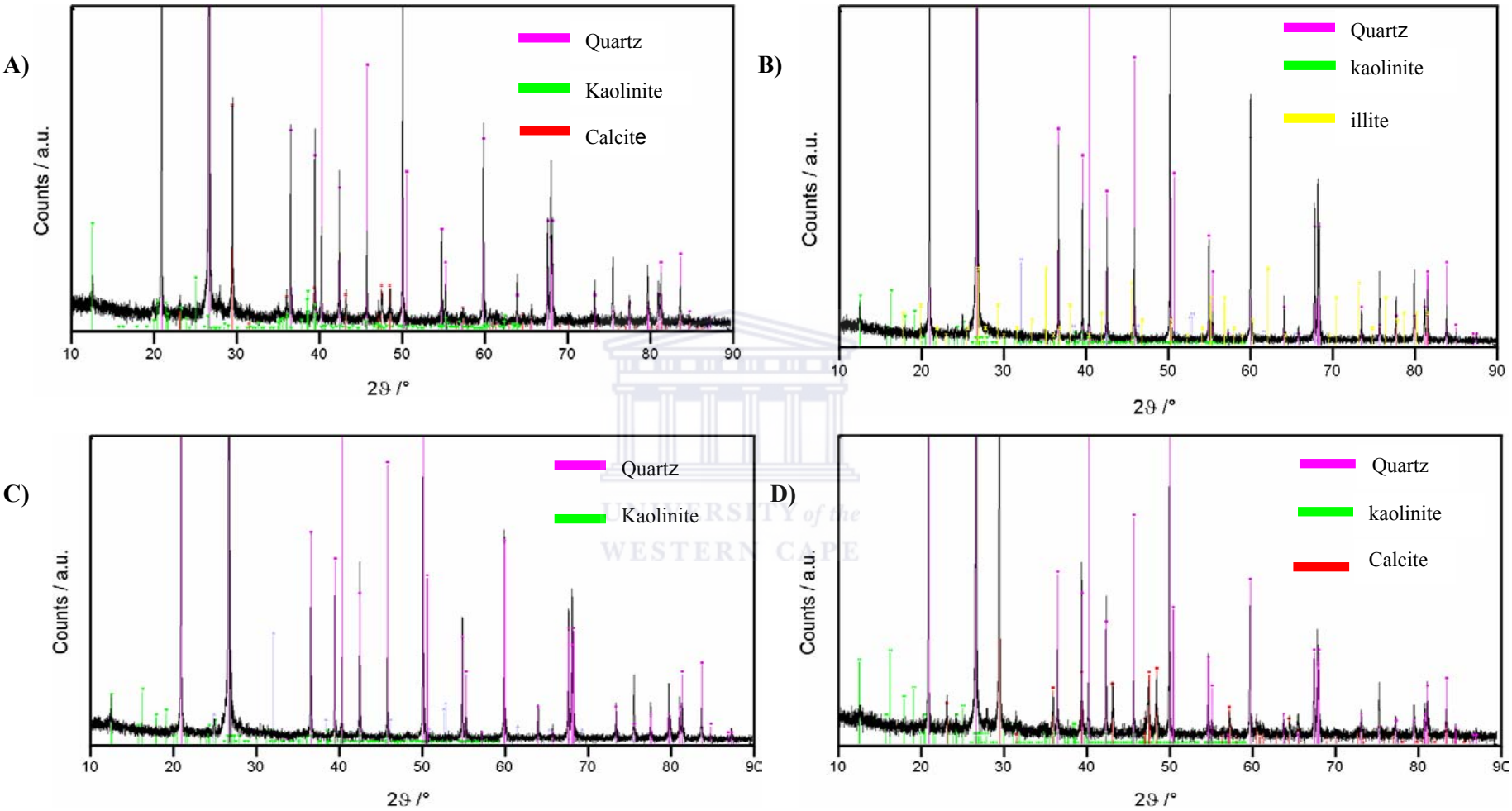

Appendix 14: XRD plots for well E-BB1;

Plot A) at depth of 2552.51m, B) at 2853.00m, C) at 2849.00m and D) at 2660.05m.

APPENDIX 15

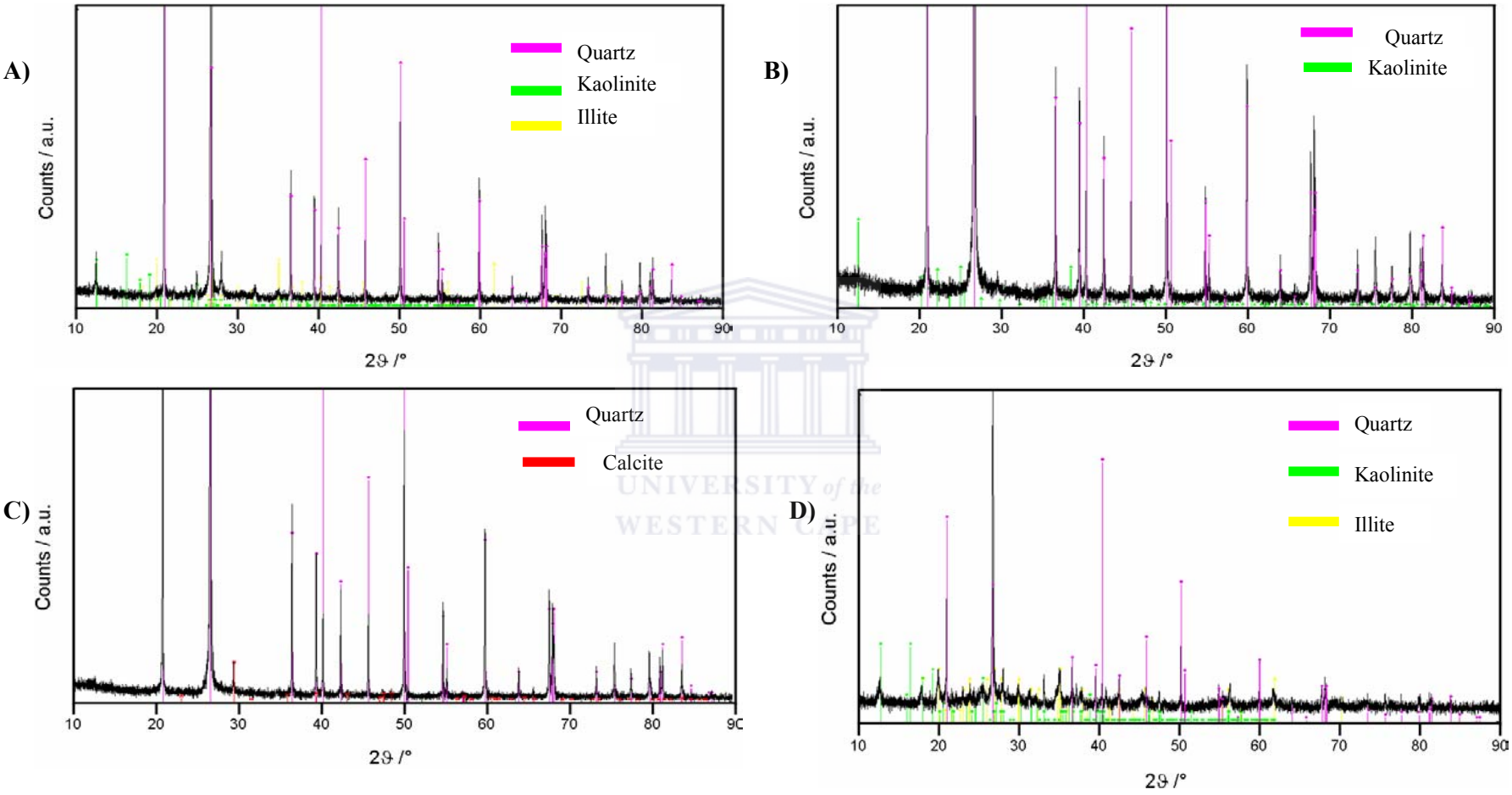

Appendix 15: XRD plots for well E-AD1;

Plot A) at depth of 2964.32m, B) at 2503.87m, C) at 2505.85m and D) at 2868.75m.

APPENDIX 16

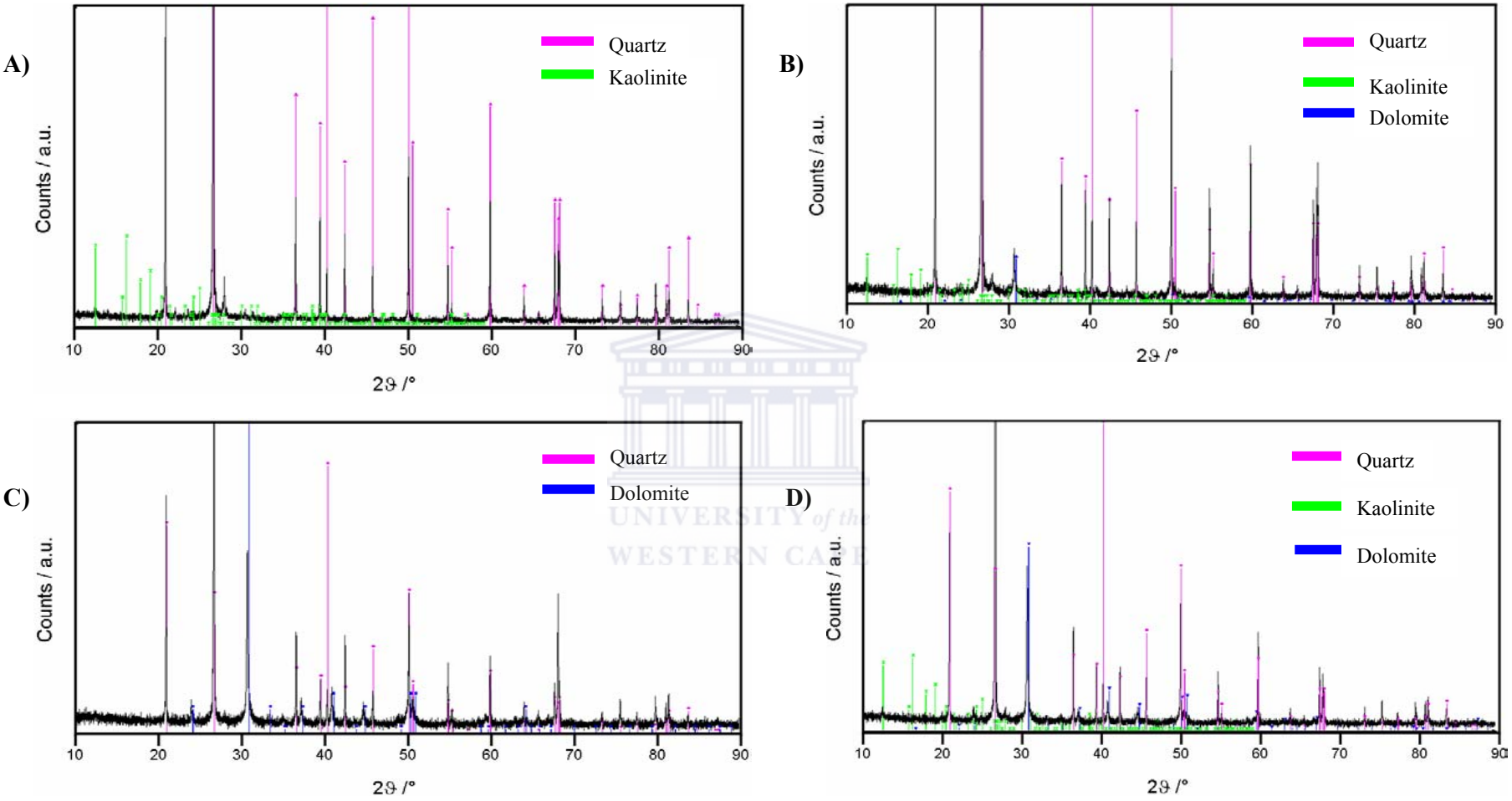

Appendix 16: XRD plots for well E-CA1;

Plot A) at depth of 2784.03m, B) at 2930.04m, C) at 2927.08m and D) at 2980.03m.

APPENDIX 17

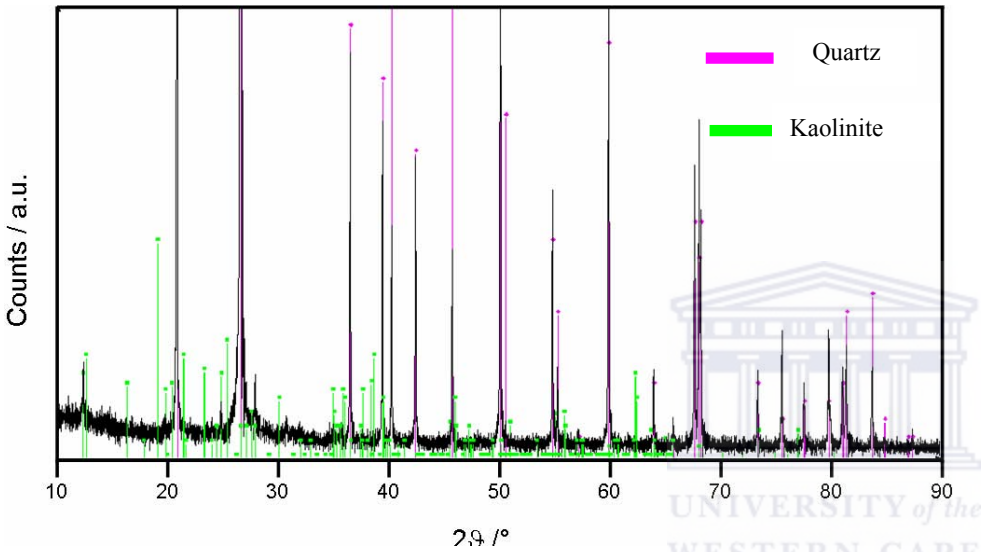

Appendix 17: XRD plots for well E-AO2;

Plot at depth of 2926.41m

UNIVERSITY of the
WESTERN CAPE

UNIVERSITY of the
WESTERN CAPE

UNIVERSITY of the
WESTERN CAPE

UNIVERSITY of the
WESTERN CAPE